



January 2012

# Formal Insertion Reactions Of Stannylenes And Germylenes Into Phosphorus-Halogen Bonds: A Structural And Mechanistic Investigation

Joseph Kent West

Follow this and additional works at: <https://commons.und.edu/theses>

---

## Recommended Citation

West, Joseph Kent, "Formal Insertion Reactions Of Stannylenes And Germylenes Into Phosphorus-Halogen Bonds: A Structural And Mechanistic Investigation" (2012). *Theses and Dissertations*. 1327.  
<https://commons.und.edu/theses/1327>

This Dissertation is brought to you for free and open access by the Theses, Dissertations, and Senior Projects at UND Scholarly Commons. It has been accepted for inclusion in Theses and Dissertations by an authorized administrator of UND Scholarly Commons. For more information, please contact [zeinebyousif@library.und.edu](mailto:zeinebyousif@library.und.edu).

FORMAL INSERTION REACTIONS OF STANNYLENES AND GERMYLENES  
INTO PHOSPHORUS–HALOGEN BONDS: A STRUCTURAL AND MECHANISTIC  
INVESTIGATION

by

Joseph Kent West

Bachelor of Science, Southwestern Oklahoma State University, 2005

A Dissertation

Submitted to the Graduate Faculty

of the

University of North Dakota

in partial fulfillment of the requirements

for the degree of

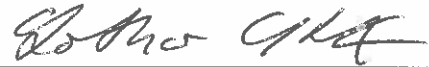
Doctor of Philosophy

Grand Forks, North Dakota

August

2012

This dissertation, submitted by Joseph Kent West in partial fulfillment of the requirements for the degree of Doctor of Philosophy from the University of North Dakota, has been read by the Faculty Advisory Committee under whom the work has been done and is hereby approved.



Chairperson









This dissertation meets the standards for appearance, conforms to the style and format requirements of the Graduate school of the University of North Dakota, and is hereby approved.

  
Dean of the Graduate School

  
Date

## PERMISSION

Title                      Formal Insertion Reactions of Stannylenes and Germylenes into  
Phosphorus–Halogen Bonds: A Structural and Mechanistic  
Investigation

Department              Chemistry

Degree                     Doctor of Philosophy

In presenting this dissertation in partial fulfillment of the requirements for a graduate degree from the University of North Dakota, I agree that the library of this University shall make it freely available for inspection. I further agree that permission for extensive copying for scholarly purposes may be granted by the professor who supervised my dissertation work or, in his absence, by the chairperson of the department or dean of the Graduate School. It is understood that any copying or publication or other use of this dissertation or part thereof for financial gain shall not be allowed without my written permission. It is also understood that due recognition shall be given to me and to the University of North Dakota in any scholarly use which may be made of any material in my dissertation.

Joseph West

---

Signature

August 3, 2012

---

Date

## TABLE OF CONTENTS

LIST OF FIGURES.....	vi
LIST OF TABLES.....	viii
LIST OF CHARTS.....	xi
LIST OF SCHEMES.....	xii
LIST OF ABBREVIATIONS.....	xvii
ACKNOWLEDGEMENTS.....	xix
ABSTRACT.....	xx
CHAPTER	
I. INTRODUCTION.....	1
I.1. Metal-based Reduction of P–Cl Bonds.....	2
I.2. Insertion of Group 14 Species into E–X Bonds (E = C, Si, and P; X = Cl, Br, and I).....	15
Insertions into C–X Bonds.....	15
Insertions into Si–X Bonds.....	23
Insertions into P–X Bonds.....	25
I.3. Syntheses and Isolation of Stable Phosphenium Ions.....	31
II. RESULTS AND DISCUSSION.....	35
II.1. Reactions of Stannylenes and Germylenes with Alkyl- and Arylchlorophosphines.....	35
Insertion reactions of cyclic stannylenes and germylenes.....	35

Insertion reactions of acyclic stannylenes and germylenes.....	58
Reactions with bis(dichlorophosphino)methane.....	72
Reactions with phosphorus trichloride.....	79
II.2. Mechanistic Investigations.....	83
Kinetic studies and comparisons of reactions rates.....	83
P-lone pair “occupation” studies.....	86
Reactions of amino(chloro)phosphines.....	101
Steric effects of non-halide substituents on phosphorus.....	116
II.3. Mechanistic Hypotheses.....	121
Proposed insertion mechanisms.....	121
Mechanistic hypotheses for the decomposition of insertion products.....	132
II.4. Conclusions.....	138
III. EXPERIMENTAL.....	140
III.1. Starting Materials and General Procedures.....	140
III.2. Syntheses.....	141
III.3. X-ray Crystallography.....	155
REFERENCES.....	156

## LIST OF FIGURES

Figure	Page
1. Crystal structure of <b>186</b> showing the two independent molecules in the unit cell....	27
2. Crystal structure of <b>4</b> .....	36
3. $^{31}\text{P}\{^1\text{H}\}$ NMR spectrum of stannylene insertion product <b>5</b> .....	39
4. $^{31}\text{P}\{^1\text{H}\}$ NMR spectrum of cyclic oligophosphines <b>6–10</b> obtained from the breakdown of <b>5</b> .....	40
5. Crystal structure of <b>15</b> .....	41
6. Crystal structure of <b>17</b> .....	44
7. Crystal structure of <b>18</b> .....	48
8. $^{31}\text{P}\{^1\text{H}\}$ NMR spectrum of <b>17</b> and its monoinsertion intermediate.....	51
9. Crystal structure of <b>20</b> .....	52
10. Crystal structure of <b>21</b> .....	54
11. Crystal structure of <b>26</b> .....	60
12. Crystal structure of <b>27</b> .....	64
13. Crystal structure of <b>29</b> .....	69
14. $^{31}\text{P}\{^1\text{H}\}$ NMR spectrum of tri- <i>tert</i> -butylcyclotriposphine <b>31</b> .....	71
15. $^{31}\text{P}\{^1\text{H}\}$ NMR spectrum for reaction mixture of stannylene <b>23</b> with chlorophosphine <b>19</b> displaying three separate, yet similar, products.....	72
16. Crystal structure of <b>33</b> .....	74
17. $^{31}\text{P}\{^1\text{H}\}$ NMR spectrum of reaction mixture from Scheme 51.....	77
18. Crystal structure of <b>44</b> .....	81

19.	Kinetics data for addition of carbenoids <b>2</b> , <b>22</b> , and <b>23</b> to <sup>t</sup> Bu(Ph)PCl <b>45</b> .....	86
20.	Crystal structure of <b>49</b> .....	87
21.	Crystal structure of <b>50</b> .....	90
22.	Crystal structure of <b>53</b> .....	94
23.	Crystal structure of <b>54</b> .....	97
24.	Crystal structure of <b>60</b> .....	102
25.	Crystal structure of <b>62</b> .....	106
26.	Crystal structure of <b>65</b> .....	110
27.	Crystal structure of <b>66</b> .....	113
28.	<sup>31</sup> P{ <sup>1</sup> H} NMR spectrum of the reaction mixture containing cyclic stannylene <b>2</b> and dichlorophenylphosphine <b>3</b> (see Scheme 43 for reaction).....	118



## LIST OF TABLES

Table	Page
1. Isolated diphosphene-bridged compounds and yields from Scheme 6.....	7
2. Isolated phosphinidene-bridged compounds and yields from Scheme 6.....	8
3. Yields of diphenylphosphine <b>47</b> obtained from the metal reduction of chlorodiphenylphosphine <b>46</b> with reaction conditions.....	10
4. Isolated phosphanediide salts from Scheme 12.....	13
5. Kinetic data for reaction of stannylene <b>79</b> with organic halides <b>74</b> , and <b>80–93</b> .....	17
6. Crystal data for compound <b>4</b> .....	37
7. Selected bond lengths and angles for compound <b>4</b> .....	38
8. Crystal data for compound <b>15</b> .....	42
9. Selected bond lengths and angles for compound <b>15</b> .....	43
10. Crystal data for compound <b>17</b> .....	46
11. Selected bond lengths and angles for compound <b>17</b> .....	47
12. Crystal data for compound <b>18</b> .....	49
13. Selected bond lengths and angles for one of two independent molecules in the unit cell of compound <b>18</b> .....	50
14. Crystal data for compound <b>20</b> .....	53
15. Selected bond lengths and angles for compound <b>20</b> .....	54
16. Crystal data for compound <b>21</b> .....	56
17. Selected bond lengths and angles for compound <b>21</b> .....	57
18. Crystal data for compound <b>26</b> .....	62

19.	Selected bond lengths and angles for compound <b>26</b> .....	63
20.	Crystal data for compound <b>27</b> .....	66
21.	Selected bond lengths and angles for compound <b>27</b> .....	67
22.	Crystal data for compound <b>29</b> .....	70
23.	Selected bond lengths and angles for compound <b>29</b> .....	71
24.	Crystal data for compound <b>33</b> .....	75
25.	Selected bond lengths and angles for compound <b>33</b> .....	76
26.	Crystal data for compound <b>44</b> .....	82
27.	Selected bond lengths and angles for compound <b>44</b> .....	83
28.	Approximate completion times for insertion reactions.....	85
29.	Crystal data for compound <b>49</b> .....	88
30.	Selected bond lengths and angles for compound <b>49</b> .....	89
31.	Comparison of Pd–P and Pd–Cl bond lengths for various <i>trans</i> bis(phosphine)palladium dichloride complexes.....	89
32.	Crystal data for compound <b>50</b> .....	91
33.	Selected bond lengths and angles for compound <b>50</b> .....	92
34.	Crystal data for compound <b>53</b> .....	95
35.	Selected bond lengths and angles for compound <b>53</b> .....	96
36.	Crystal data for compound <b>54</b> .....	98
37.	Selected bond lengths and angles for compound <b>54</b> .....	99
38.	Crystal data for compound <b>60</b> .....	103
39.	Selected bond lengths and angles for compound <b>60</b> .....	104
40.	Crystal data for compound <b>62</b> .....	107
41.	Selected bond lengths and angles for compound <b>62</b> .....	108

42.	Crystal data for compound <b>65</b> .....	111
43.	Selected bond lengths and angles for compound <b>65</b> .....	112
44.	Crystal data for compound <b>66</b> .....	114
45.	Selected bond lengths and angles for compound <b>65</b> .....	115
46.	Summary of relative completion times of stannylene <b>2</b> with monochlorophosphines.....	123

## LIST OF CHARTS

Chart	Page
1. Proposed structures for oligophosphanides of alkali metals.....	4
2. Structural variety observed for reported phosphenium ions.....	32

## LIST OF SCHEMES

Scheme	Page
1. First reported reductions of dichlorophenylphosphine <b>1</b> using metals.....	3
2. Reduction of <b>1</b> using Li or Mg.....	4
3. Synthesis of the first diphosphene <b>13</b> .....	5
4. Preparation of 1,2-dibromo-1,2-diphenyldiphosphine <b>15</b> .....	5
5. Preparation of <b>13</b> using tin- and germanium-based reductants.....	6
6. Syntheses of diphosphene- and phosphinidene-ligated metal carbonyls.....	7
7. FVP studies on <i>n</i> -alkyldichlorophosphines.....	8
8. FVP studies of aryldichlorophosphine <b>12</b> and aminodichlorophosphine <b>42</b> .....	9
9. C–C bond insertion of a Mg-generated phosphinidene.....	9
10. Reduction of chlorodiphenylphosphine <b>46</b> to diphenylphosphine <b>47</b> .....	10
11. Preparation of cyclopentaphosphanide <b>50</b> and diphosphene–Ni complex <b>52</b> .....	12
12. Synthesis of alkaline metal phosphanediides.....	13
13. Varying binding modes of phosphanediides.....	14
14. Titanocene-mediated reduction of dichlorophosphines <b>68</b> and <b>69</b> .....	15
15. Oxidative addition of methyl iodide <b>74</b> to stannocene <b>73</b> .....	16
16. Reaction template for kinetic experiments.....	16
17. Proposed mechanism of insertion of stannylene into C–X bonds.....	18
18. Attempt to obtain chiral stannane from prochiral stannylene <b>109</b> .....	18
19. Insertion of silylene <b>112</b> into the C–I bond of <b>74</b> .....	18

20.	Syntheses of disilanes <b>119–124</b> from silylene <b>114</b> and organochlorides <b>88</b> and <b>115–118</b> .....	19
21.	Proposed mechanism for the formation of disilane <b>120</b> from silylene <b>114</b> and chloroform <b>116</b> .....	19
22.	Range of observed products following rearrangement of cyclopropyl radical.....	20
23.	C–H activation of ethers and alkanes by iodophenylgermane <b>134</b> .....	21
24.	C–H activation of ethers and alkanes by iodophenylstannane <b>141</b> .....	22
25.	Recent reports of insertions of heterocarbenoids into C–X bonds.....	23
26.	Addition of SiCl <sub>4</sub> to germylene <b>159</b> and stannylene <b>160</b> .....	23
27.	Insertion of silylene <b>164</b> into Si–Cl bonds of chlorosilanes.....	24
28.	Possible mechanistic routes for insertion into Si–Cl bonds.....	25
29.	Two synthetic routes for trichlorogermlyphosphine <b>180</b> .....	26
30.	Insertion of GeCl <sub>2</sub> into P–Cl bonds of dichlorophosphines.....	26
31.	Insertion of GeCl <sub>2</sub> and “SiCl <sub>2</sub> ” into P–Cl bond of phosphalkene <b>187</b> .....	27
32.	Reactions of stannylene <b>16</b> with PCl <sub>3</sub> <b>49</b> and PhPCl <sub>2</sub> <b>1</b> .....	28
33.	Addition of germylene <b>195</b> plumbylene <b>196</b> to PCl <sub>3</sub> <b>49</b> .....	29
34.	Addition of heterocarbenoids to aryldichlorophosphines.....	29
35.	Addition of bulky stannylene <b>205</b> to dichlorophenylphosphine <b>1</b> .....	30
36.	Amine exchange observed for addition of <b>208</b> to <b>49</b> .....	30
37.	Amine exchange formation of phosphonium ion <b>211</b> .....	31
38.	Generation of phosphonium ion <b>213</b> .....	32
39.	Addition of NHC <b>222</b> to dichlorophenylphosphine <b>1</b> .....	33
40.	New synthetic method for carbene-stabilized phosphonium ions.....	33
41.	Preparation of phosphonium triflate salt <b>231</b> .....	34

42.	Synthesis of phosphonium trication <b>235</b> .....	34
43.	Reactions of carbenoids <b>1</b> and <b>2</b> with dichlorophenylphosphine <b>3</b> .....	35
44.	Reactions of carbenoids <b>1</b> and <b>2</b> with chlorodiphenylphosphine <b>11</b> .....	40
45.	Reactions of carbenoids <b>1</b> and <b>2</b> with <i>tert</i> -butyldichlorophosphine <b>16</b> .....	43
46.	Reactions of carbenoids <b>1</b> and <b>2</b> with di- <i>tert</i> -butylchlorophosphine <b>19</b> .....	51
47.	Reactions of acyclic carbenoids <b>22</b> and <b>23</b> to dichlorophenylphosphine <b>3</b> .....	59
48.	Reactions of acyclic carbenoids <b>22</b> and <b>23</b> with chlorodiphenylphosphine <b>11</b> ....	64
49.	Reactions of carbenoids <b>22</b> and <b>23</b> with <i>tert</i> -butyldichlorophosphine <b>16</b> .....	68
50.	4:1 addition of germylene <b>1</b> with tetrachlorobisphosphine <b>32</b> .....	73
51.	2:1 addition of germylene <b>1</b> to bis(dichlorophosphine)methane <b>32</b> .....	77
52.	4:1 addition of stannylene <b>2</b> to tetrachlorobisphosphine <b>32</b> .....	78
53.	2:1 addition of germylene <b>22</b> to tetrachlorobisphosphine <b>32</b> .....	79
54.	Reactions of carbenoids <b>1</b> and <b>2</b> with phosphorus trichloride <b>39</b> .....	80
55.	Reactions of acyclic carbenoids <b>22</b> and <b>23</b> with phosphorus trichloride <b>39</b> .....	80
56.	Synthesis of <i>tert</i> -butyliodophenylphosphine <b>47</b> from its chloro analogue <b>45</b> .....	84
57.	Kinetic experiments for insertions of carbenoids <b>1</b> , <b>2</b> , <b>22</b> , and <b>23</b> with chlorophosphine <b>45</b> and iodophosphine <b>47</b> .....	84
58.	Syntheses of <i>trans</i> -bisphosphine palladium dichloride complexes <b>49</b> and <b>50</b> .....	86
59.	Reactions of cyclic stannylene <b>2</b> with Pd <sup>II</sup> complexes <b>49</b> and <b>50</b> .....	93
60.	Reaction of stannylene <b>2</b> with Pd <sup>II</sup> complex <b>52</b> to give 3:1 and 1:1 addition products <b>53</b> and <b>54</b> .....	93
61.	Preparation of thiophosphine <b>56</b> and its reaction with stannylene <b>2</b> .....	100
62.	Sulfur oxidation of <b>21</b> providing thiophosphine <b>58</b> .....	100
63.	Reaction of stannylene <b>2</b> with cyclic bis(amino)chlorophosphine <b>59</b> .....	101

64.	Reactions of carbenoids <b>1</b> and <b>2</b> with bis(amido)chlorophosphine <b>61</b> .....	105
65.	Reactions of carbenoids <b>1</b> and <b>2</b> with amidodichlorophosphine <b>64</b> .....	109
66.	Synthesis of chlorobis(pyrrolyl)phosphine <b>70</b> .....	116
67.	Reaction of stannylene <b>2</b> with monochlorophosphine <b>70</b> .....	116
68.	Reactions of carbenoids <b>1</b> , <b>2</b> , <b>22</b> , and <b>23</b> with chlorodiethylphosphine <b>73</b> .....	117
69.	Two conformations, <i>syn s</i> and <i>anti a</i> , of dimeric <b>79</b> .....	119
70.	Reactions of cyclic carbenoids <b>1</b> and <b>2</b> the aryldichlorophosphine <b>80</b> .....	120
71.	Reaction of cyclic stannylene <b>2</b> with the chlorodiarylphosphine <b>86</b> .....	120
72.	Radical-based mechanism for insertion of carbenoid <b>Q</b> into phosphine <b>Z</b> .....	121
73.	S <sub>N</sub> P mechanism for halide substitution by a metal fragment.....	122
74.	Two alternative routes for P→M coordination-initiated mechanistic hypothesis.....	125
75.	Synthesis of the stannylene-phosphine adduct <b>90</b> .....	126
76.	Phosphenium ion generation <b>Q-Z<sup>+</sup></b> and stabilization <b>Q<sup>-</sup>Z<sup>+</sup></b> by carbenoid species <b>Q</b> .....	128
77.	Attempted reactions of <b>17</b> with stannylene <b>2</b> and NHC <b>88</b> .....	128
78.	Coordination-initiated pathway for the reaction of carbenoid <b>Q</b> with bis(amido)chlorophosphine <b>S</b> resulting in the ligand-exchange product <b>QS</b> .....	131
79.	Phosphenium ion pathway for formation of complex <b>QS</b> .....	131
80.	Breakdown of insertion product <b>MP</b> by homolytic cleavage (radical mechanism).....	133
81.	Radical-based mechanism for the breakdown of diinsertion products <b>A</b> eventually yielding phosphacycles <b>6–8</b> , <b>31</b> , and <b>83–85</b> (NO = “not observed”).....	134
82.	Complexation-elimination route for decomposition of monoinsertion <b>MP</b> yielding <b>M<sub>2</sub></b> and <b>P<sub>2</sub></b> .....	136



83. Complexation-elimination mechanism for the decomposition of diinsertion product **A** eventually yielding phosphacycles (NO = “not observed”).....137

## LIST OF ABBREVIATIONS

Ph	phenyl
THF	tetrahydrofuran
<sup>t</sup> Bu	<i>tert</i> -butyl
Me	methyl
FVP	flash vacuum pyrolysis
Et	ethyl
<sup>i</sup> Pr	<i>iso</i> -propyl
DMF	dimethylformamide
DMA	dimethylamine
DMI	1,5-dimethylimidazole
NMP	<i>N</i> -methylpyrrolidinone
TMEDA	tetramethylethylenediamine
DETA	diethylenetriamine
mes	mesityl
btmsa	bis(trimethylsilyl)acetylene
Cp	cyclopentadienyl
<sup>n</sup> Pr	propyl
<sup>n</sup> Bu	butyl
adm	adamantyl
NMR	nuclear magnetic resonance

Ar	aryl
NHC	<i>N</i> -heterocyclic carbene
OTf	triflate
GooF	goodness of fit
EW	electron-withdrawing
ED	electron-donating
EPR	electron paramagnetic resonance spectroscopy

## ACKNOWLEDGEMENTS

I am grateful to my advisor, Dr. Lothar Stahl, and my graduate advisory committee for their guidance and support throughout my pursuit of this degree. I am thankful to the UND Chemistry Department and the Graduate School and for the financial support they have provided.

I also thank my wife for all the encouragement and confidence she has given me, and for her insights and ideas.

## ABSTRACT

Insertion reactions of Group 14 carbenoids, divalent species of the form  $(R_2N)_2M$  ( $M = Ge$  or  $Sn$ ) into the P–halogen bond of halophosphines have been known for some time. However, very few examples have been reported and no evidence has been presented regarding the mechanism by which these reactions take place. Comparatively, insertion of the same or analogous carbenoid species into C–halogen bonds have been thoroughly explored for scope and application, and the mechanism has been investigated multiple times.

In this dissertation, numerous new examples of insertion products of Group 14 carbenoids into P–halogen bonds are presented. This array of products has been characterized by  $^{31}P\{^1H\}$  and  $^1H$  NMR spectroscopy and single-crystal X-ray diffraction analysis. In addition, purity of the obtained compounds has been confirmed by elemental analyses.

In concert with a diverse group of products, kinetic experiments were employed to examine the possible mechanistic pathways. All reasonable pathways for these reactions are discussed, analyzed and compared. Additionally, as most tin-containing insertion products are unstable, the likely mechanisms for their decomposition are discussed in detail.

## CHAPTER I

### INTRODUCTION

Insertions and oxidative additions have been demonstrated countless times with transition metals and main-group metals. This type of reactivity can be a means to activating species in new, interesting, and valuable ways and it can be a poison for homogeneous catalyst systems. In other cases, oxidative addition is an important step preceding reductive elimination to provide a new compound. Insertion chemistry is an important aspect of chemistry due to its prevalence and role in numerous reaction pathways involving transition and main group metal systems.

While the ability of a metal to insert into a bond has been demonstrated for nearly every metal in the periodic table, divalent species of Group 14 (C, Si, Ge, Sn, and Pb) have exhibited a particular penchant for the phenomenon, often opening new avenues to interesting structures and useful compounds. Carbenoids, as they are often called, have been shown to insert into P–P,<sup>1</sup> S–S/Se–Se,<sup>2</sup> Fe–Fe,<sup>3</sup> O–H,<sup>4–8</sup> N–H,<sup>9,10</sup> and even H–H<sup>11</sup> bonds. Additionally, insertions into C–X and Si–X bonds have been reported and bear a significant resemblance and relevance to this study.

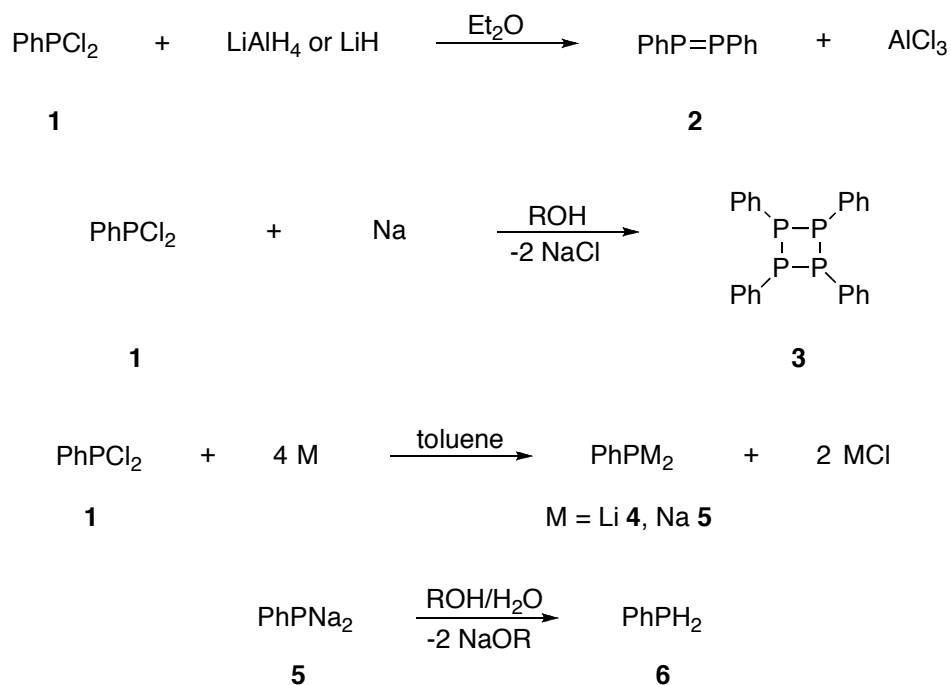
The work described herein was an investigation into the relatively unexplored reactions of mono-, di-, and tri-halophosphines with stannylenes and germylenes, divalent species of tin and germanium. These systems can be discussed primarily in three different ways: 1) metal reduction of P–X bonds, 2) oxidative insertion of divalent Group 14 species into P–X bonds, or 3) ligand substitution of chloride by Sn<sup>II</sup> or Ge<sup>II</sup>. The

obtained results do not appear to adhere to one specific interpretation and thus reactions will be discussed in the context of all three perspectives. Additionally, the introduction will cover these three areas separately.

### I.1. Metal-based Reduction of P–Cl Bonds

The reduction of carbon–halogen bonds by metals is a common and useful method for providing carbanion sources or new C–C bonds. These reductions are often carried out using lithium or magnesium due to the isolable nature of their reduced products, their low relative cost, and the generality of their conversions. However, these metals also present significant drawbacks, specifically their lack of selectivity, low stability, and strong reducing ability. Alternatives in the realm of organic transformations often utilize other metals such as Zn, Cd, Hg, and Al. These systems often ameliorate the problems associated with Li and Mg, but bring their own issues (e.g., high toxicity for Hg).

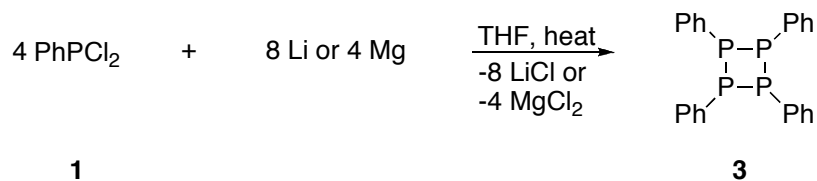
Similar approaches have been taken to reduce phosphorus–halogen bonds providing a metal phosphide. Compared to carbon analogues, significantly fewer examples of varying reductive metals systems have been reported. Additionally, fewer metal phosphide systems appear to be stable (e.g., Mg + R<sub>2</sub>PCl) relative to analogous carbon-based systems, often providing diphosphines, (R<sub>2</sub>P)<sub>2</sub>, or cyclic oligophosphines, (RP)<sub>n</sub>, n = 3–5. Early work in the field investigated the simple reduction of PhPCl<sub>2</sub> and Ph<sub>2</sub>PCl by alkali metals and hydride sources (Scheme 1).<sup>12–15</sup> It was reported that P=P double bonds were produced, though this could never be confirmed by structural analysis, and subsequent studies made it seem unlikely that such a product was obtained.



Scheme 1. First reported reductions of dichlorophenylphosphine **1** using metals.

Additional studies on cyclic polyphosphines expanded the range of metals, which could lead to reductive P–P coupling to include magnesium (Scheme 2).<sup>16</sup> Little understanding and no observation of any intermediates could be gained as these studies predated commonly available access to NMR (nuclear magnetic resonance) spectroscopy and the air-/moisture-sensitivity of any meta-stable intermediates and products would have disallowed structural determination by X-ray diffraction at the time. Breakthroughs in these areas allowed for a resurgence of interest in the field in the late 1960s. Independent investigations led by Issleib, Baudler and Caulton provided the first detailed <sup>31</sup>P NMR data giving insight into the intermediate structures of alkali- and alkaline-earth phosphides. Oligomerization was shown to occur by reaction of phosphides with the starting chlorophosphine(s).





Scheme 2. Reduction of **1** using Li or Mg.

Disagreements surfaced in the literature on the solution state structures of these metal phosphides (Chart 1). In the case of potassium phenylphosphide, Issleib<sup>17</sup> favored a three-membered cyclic phosphorus ring, Caulton<sup>18</sup> believed it to be a five-membered metallacycle containing four phosphorus atoms and potassium, and Baudler<sup>19,20</sup> found it to be a more complex bimetallacycle.

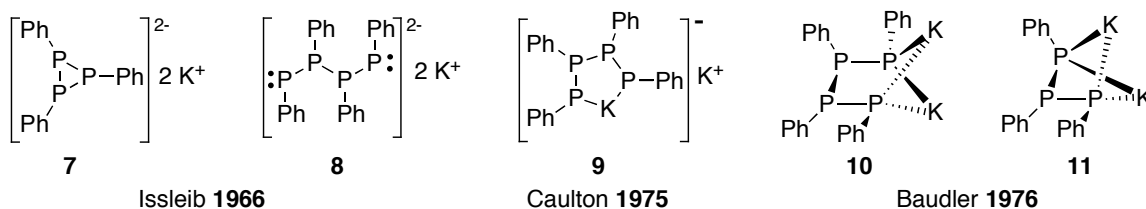
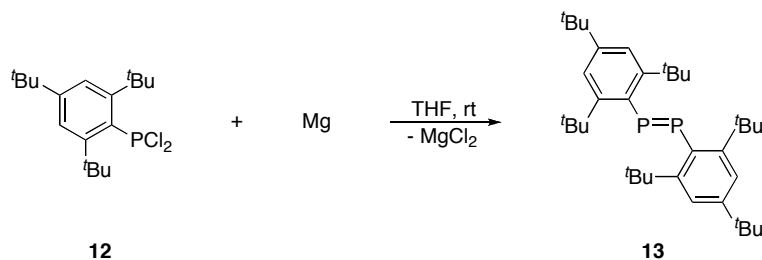


Chart 1. Proposed structures for oligophosphanides of alkali metals.

It later became understood that many factors can contribute to the solution state structure of these phosphides. Not only do the obvious factors of concentration, solvent, and temperature influence them, but additionally, the metal (Li, Na, K), the source of phosphide ( $\text{RPhCl}_2$ ,  $\text{RPhH}_2$ , cyclic  $(\text{RP})_n$ , and other metal phosphides) also play significant roles in affecting the intermediate structures. None of these structures was ever isolated and characterized by X-ray analysis, and all gave the same eventual end product, a mixture of cyclic polyphosphines,  $(\text{RP})_n$ .

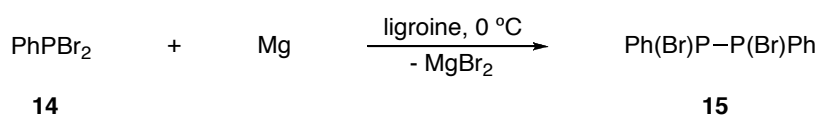
In the early 1980s, the belief that phosphinidenes—highly reactive, neutral  $\text{P}^{\text{I}}$  species, isoelectronic with carbenes and nitrenes—were possibly being generated for some of these reductions gained momentum and thus interest. A major breakthrough in

this vein was the first synthesis of a stable diphosphene, a species with a P=P bond, which was reported by Yoshifuji in 1981 (Scheme 3).<sup>21</sup>



Scheme 3. Synthesis of the first diphosphene **13**.

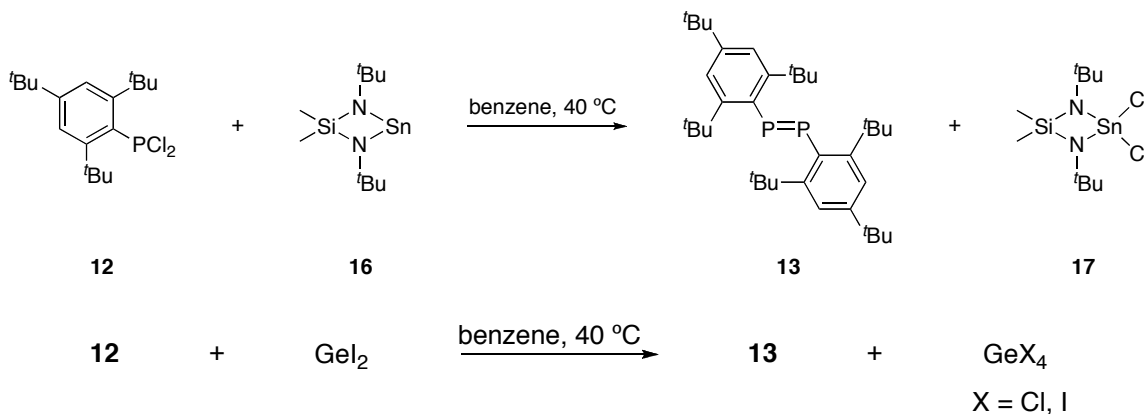
In general, it was believed that metal reduction of  $\text{RPCl}_2$  generates a diphosphene which subsequently undergoes a 2+2 cycloaddition; however, no such species was ever isolated and structurally verified before Yoshifuji's accomplishment. This example utilized steric shielding to prevent any cyclizations. Following this discovery, the first 1,2-dihalodiphosphine was isolated. Under carefully controlled stoichiometric conditions several, compounds of the general structure  $\text{R}(\text{Br})\text{P}-\text{P}(\text{Br})\text{R}$  were prepared by reduction with magnesium (Scheme 4).<sup>22</sup> A variety of conformational of **15** isomers were identified in the reaction mixture along with remaining starting materials and some  $(\text{RP})_n$ .



Scheme 4. Preparation of 1,2-dibromo-1,2-diphenyldiphosphine **15**.

Following Yoshifuji's synthesis of a diphosphene, studies followed two major pathways: 1) syntheses of new, stable diphosphenes and 2) the development of new methods for their syntheses. Approximately twenty structures of new diphosphenes were reported over the next 20 years, a selected few of which are cited herein. While exploring new methods for the syntheses of diphosphenes, a relative breakthrough relevant to the

work herein was the discovery of the ability of divalent Group 14 species to reduce dichlorophosphines. Bertrand and Veith reported<sup>23</sup> the synthesis of Yoshifuji's diphosphene **13** via the cyclic tin diamide **16** and germanium diiodide (Scheme 5) instead of the originally reported magnesium reduction.

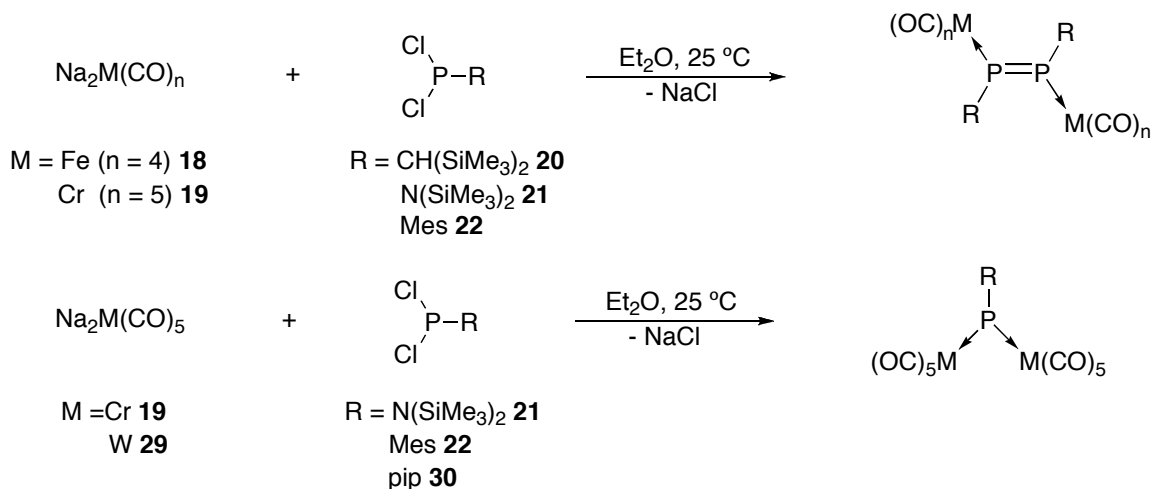


Scheme 5. Preparation of **13** using tin- and germanium-based reductants.

Cowley and Atwood provided a somewhat more comprehensive investigation into reduction methods to produce diphosphenes.<sup>24</sup> They found the synthesis of Yoshifuji's diphosphene **13** to be reproducible by his Mg reduction method, but they obtained higher yields and fewer side products using a Na/naphthalenide reducing system. This method also proved to be preferable to the <sup>t</sup>BuLi approach reported by Escudié and Satgé for the synthesis of (Me<sub>3</sub>SiP)<sub>2</sub>.<sup>25</sup>

Interest in these diphosphenes as ligands closely followed their initial isolation and syntheses. Power *et al.* developed<sup>26–30</sup> the first method for producing diphosphenes *in situ* and forming a transition metal complex immediately thereafter. Huttner<sup>31</sup> also released a report concurrent with Power's studies, using Group 6 carbonyl metallates to reduce a dichlorophosphine substituted with a cyclic amide (Scheme 6). These are also the first and only reports of transition metal reductions of halophosphines. Using salts of

the type  $\text{Na}_2\text{M}(\text{CO})_n$  ( $\text{M} = \text{Fe}$  or  $\text{Cr}$ ,  $n = 4$  or  $5$ ), reduction of the dichlorophosphines and formation of di-adducts with metal carbonyl centers was achieved. Unfortunately, these reactions also provided numerous side products and thus gave low yields as shown in Tables 1 and 2.



Scheme 6. Syntheses of diphosphene- and phosphinidene-ligated metal carbonyls.

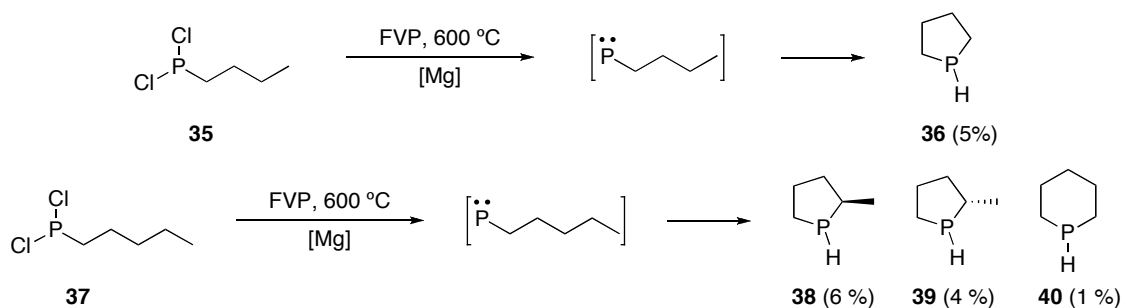
Table 1. Isolated diphosphene-bridged compounds and yields from Scheme 6.

<u>M</u>	<u>n</u>	<u>R</u>	<u>Product</u>	<u>Yield (%)</u>
Fe	4	CH(SiMe <sub>3</sub> ) <sub>2</sub>	<b>23</b>	50
Fe	4	N(SiMe <sub>2</sub> ) <sub>2</sub>	<b>24</b>	45
Fe	4	Mes	<b>25</b>	35
Cr	5	CH(SiMe <sub>3</sub> ) <sub>2</sub>	<b>26</b>	12
Cr	5	N(SiMe <sub>2</sub> ) <sub>2</sub>	<b>27</b>	18
Cr	5	Mes	<i>trans</i> - <b>28</b>	21
Cr	5	Mes	<i>cis</i> - <b>28</b>	38

Table 2. Isolated phosphinidene-bridged compounds and yields from Scheme 6.

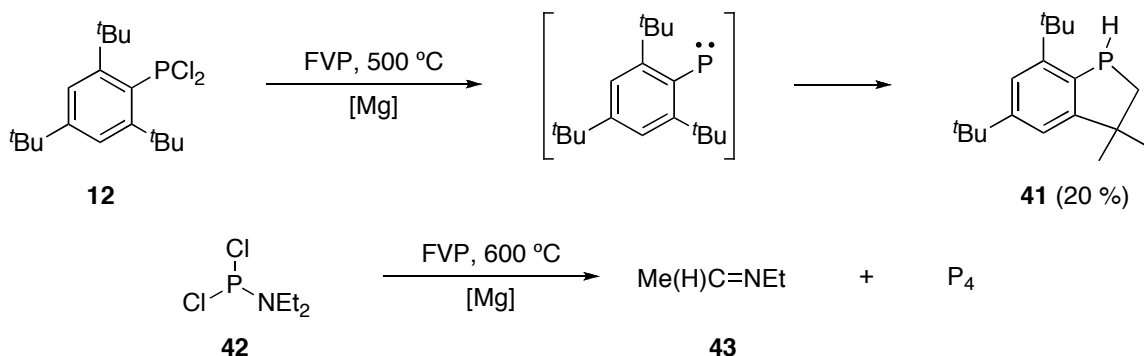
<u>M</u>	<u>R</u>	<u>Product</u>	<u>Yield (%)</u>
Cr	N(SiMe <sub>2</sub> ) <sub>2</sub>	<b>31</b>	45
Cr	Mes	<b>32</b>	5
Cr	piperidyl	<b>33</b>	22
W	piperidyl	<b>34</b>	17

The first of several intermittent studies into the possible phosphinidene intermediacy of metal-based reductions was reported by Bock (Scheme 7).<sup>32</sup> In an attempt to generate MeP=PMe, MePCl<sub>2</sub> was passed over Mg powder via flash vacuum pyrolysis (FVP) and monitored by photoelectron spectroscopic real-time gas analysis. The range of isolated products suggested that phosphinidene intermediates were chemisorbed to the Mg surface (Scheme 7). This was followed<sup>33</sup> by substantiating evidence displaying cyclizations for <sup>n</sup>BuPCl<sub>2</sub> **35** and *n*-pentyldichlorophosphine **37**. Following reduction, the “free” phosphinidene is then believed to insert into a C–H bond of the organic substituent attached to phosphorus. In the case of **35**, phosphole **36** is yielded and, when **37** is used, the three isomers **38–40** are obtained.



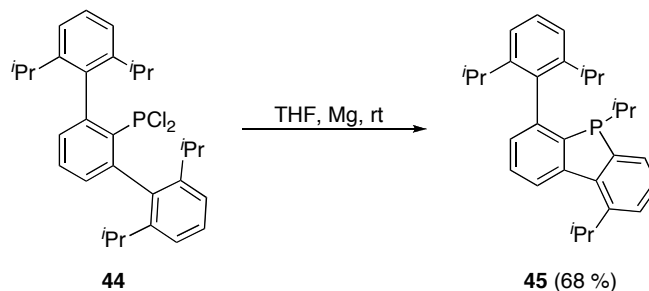
Scheme 7. FVP studies on *n*-alkyldichlorophosphines.

As shown in Scheme 8, insertion into a methyl C–H bond on the ortho *tert*-butyl group of 2,4,6-*t*Bu<sub>3</sub>PhPCl<sub>2</sub> **12** providing phosphole **41** was also displayed. Attempts to produce a heterocycle by similar methodology using Et<sub>2</sub>NPCl<sub>2</sub> **42** furnished only imine **43** and white phosphorus.<sup>33</sup>



Scheme 8. FVP studies of aryldichlorophosphine **12** and aminodichlorophosphine **42**.

In a single-case example, Power reported a C–C insertion (no other report has shown this type of action) by a probable phosphinidene intermediate following dehalogenation by magnesium (Scheme 9).<sup>34</sup> Again, displaying the ambiguity of these reductions, reaction with potassium produced little if any insertion product and instead gave only the diphosphene.

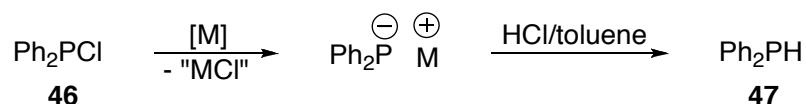


Scheme 9. C–C bond insertion of a Mg-generated phosphinidene.

Following his report<sup>35</sup> of Mg reduction of dichloro-(2,6-dimesitylphenyl)phosphine to the diphosphene, Protasiewicz focused on the potential of phosphinidene production via metal reduction of dihalophosphines.<sup>36</sup> They reiterated the

importance of the identity of the metal on the product outcome. Moreover, they determined that certain preparatory methods of the metal can have a significant impact on product distribution and yield.

Kawashima,<sup>37</sup> compared reducing abilities of several p-block and transition metals using Ph<sub>2</sub>PCl as a substrate (Scheme 10). The study was thorough, but very specific to the substrate and no follow-up was ever produced. As shown in Table 3, activated Zn in THF proved to be the most effective, with Sn and Mn also providing respectable yields in dimethylformamide (DMF). Nickel, vanadium, and titanium were found to be the least effective, as was SnCl<sub>2</sub>, the only metal chloride tested. Additionally, Devarda's alloy composed of Cu/Al/Zn was tested with average results.



Scheme 10. Reduction of chlorodiphenylphosphine **46** to diphenylphosphine **47**.

Table 3. Yields of diphenylphosphine **47** obtained from the metal reduction of chlorodiphenylphosphine **46** with reaction conditions. DMF = dimethylformamide, DMA = dimethylamine, NMP = *N*-methylpyrrolidinone, and DMI = 1,5-dimethylimidazole.

<u>Reductant</u>	<u>Molar Equivalents</u>	<u>Solvent</u>	<u>Time (h)</u>	<u>Yield of Ph<sub>2</sub>PH (%)</u>
Zn, powder	1.1	DMF	1	55
Zn, powder	1.5	DMF	1	63
Activated Zn	1.5	DMF	1	63
Zn, powder	1.5	DMF	20	63
Zn, powder	3.0	DMF	1	45
Zn, powder	1.5	DMA	1	59

Table 3 cont.

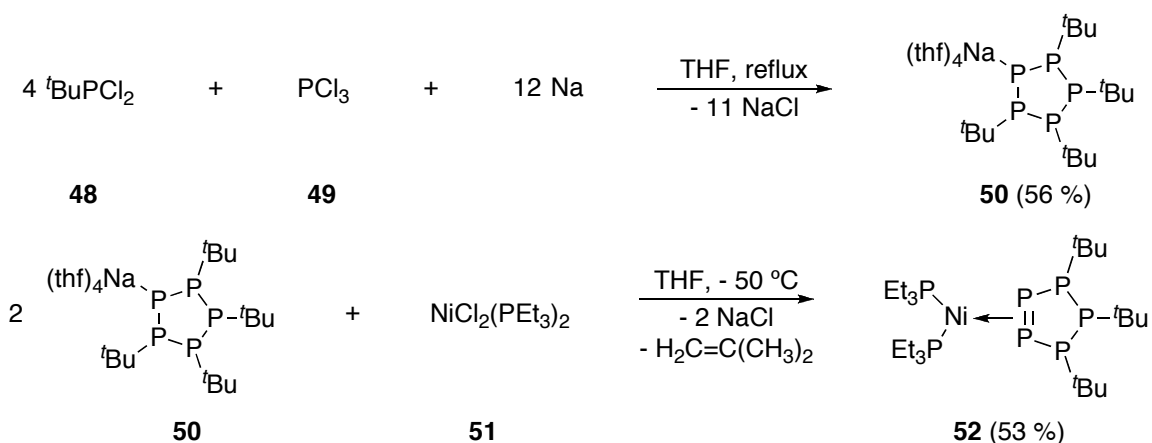
<u>Reductant</u>	<u>Molar Equivalents</u>	<u>Solvent</u>	<u>Time (h)</u>	<u>Yield of Ph<sub>2</sub>PH (%)</u>
Zn, powder	1.5	NMP	1	49
Zn, powder	1.5	DMI	1	45
Zn, powder	1.5	THF	1	62
Activated Zn	1.5	THF	1	84
Zn, powder	1.5	Toluene	1	35
Mg, turnings	1.5	DMF	1	46
Mg, turnings	1.5	DMF	20	68
Mg, turnings	1.5	THF	20	68
Al, foil	1.5	DMF	20	56
Al, foil	0.67	DMF	20	49
Sn, powder	1.5	DMF	20	72
Sn, powder	0.5	DMF	20	75
SnCl <sub>2</sub>	1.0	DMF	20	8
Ti, powder	1.5	DMF	20	19
Ti, powder	0.5	DMF	20	8
V, turnings	1.5	DMF	20	7
V, turnings	0.5	DMF	20	5
Cr, powder	1.5	DMF	20	23
Cr, powder	0.5	DMF	20	34
Mn, powder	1.5	DMF	20	48
Mn, powder	0.67	DMF	20	67



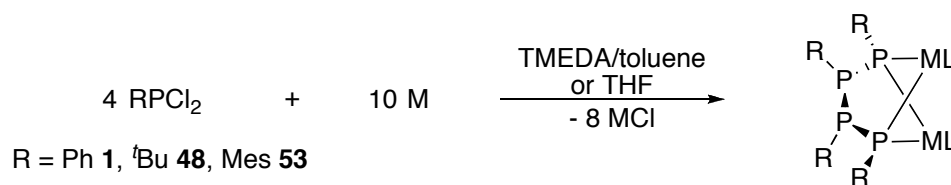
Table 3 cont.

<u>Reductant</u>	<u>Molar Equivalents</u>	<u>Solvent</u>	<u>Time (h)</u>	<u>Yield of Ph<sub>2</sub>PH (%)</u>
Mn, powder	0.5	DMF	20	72
Fe, powder	1.5	DMF	20	30
Fe, powder	0.67	DMF	20	36
Co, powder	1.5	DMF	20	19
Ni, powder	1.5	DMF	20	8
Cu, powder	1.5	DMF	20	16
Devarda's alloy	1.5	DMF	20	58

Coincidental with this work, another burgeoning area of phosphorus chemistry was being developed. The first example of a cyclic phosphanide **50** was produced by a one-pot reduction of <sup>t</sup>BuPCl<sub>2</sub> **48** and PCl<sub>3</sub> **49** using sodium metal (Scheme 11).<sup>38</sup> This product, **50**, was shown to form an end-on diphosphene complex **52** when two equivalents were added to NiCl<sub>2</sub>(PEt<sub>3</sub>)<sub>2</sub> **51**, displacing the chlorides and producing an alkene and cyclopentaphosphine in the process.

Scheme 11. Preparation of cyclopentaphosphanide **50** and diphosphene–Ni complex **52**.

Following this example numerous reports have surfaced on other acyclic phosphanides and phosphanediides.<sup>39-42</sup> These systems have seen a resurgence from their initial discovery and investigation in the 1960s and 1970s. With the greater availability and ease of X-ray and NMR methods numerous substituent/metal/ligand combinations were studied (Scheme 12 and Table 4). Structurally, they hold well to the model put forth by Baudler (Chart 1) and they have provided interesting new possibilities, both synthetically and structurally. Now that these phosphides are fairly well understood, interest in these species as ligands is slowly growing.

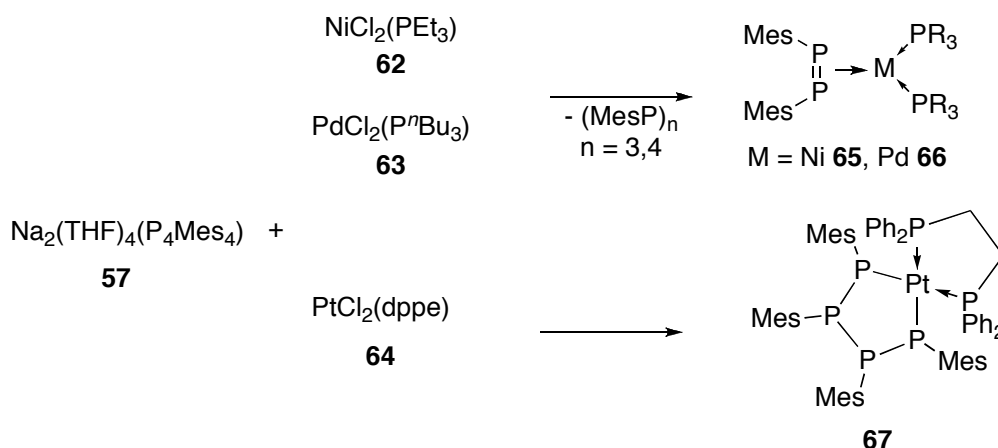


Scheme 12. Synthesis of alkaline metal phosphanediides.

Table 4. Isolated phosphanediide salts from Scheme 12.

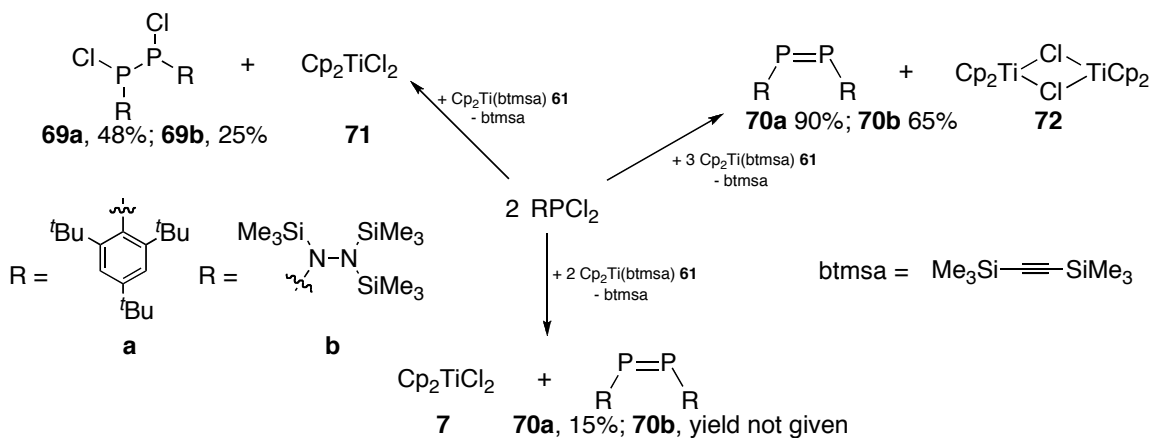
<u>M</u>	<u>R</u>	<u>L</u>	<u>#</u>	<u>Yield (%)</u>
Li	Ph	TMEDA	<b>54</b>	87
Na	Ph	TMEDA	<b>55</b>	73
Na	Ph	(THF) <sub>2</sub>	<b>56</b>	48
Na	Mes	(THF) <sub>2</sub>	<b>57</b>	27
Na	<sup>t</sup> Bu	(THF) <sub>2</sub>	<b>58</b>	43
K	Ph	(THF) <sub>3</sub>	<b>59</b>	54
K	Mes	(THF) <sub>3</sub>	<b>60</b>	43
K	<sup>t</sup> Bu	DETA	<b>61</b>	55

Reports as continuations of previous studies are still being generated, but their numbers appear to be on the decline. A few of the more recent examples, reported by Hey-Hawkins (Scheme 12), broadens the scope of phosphanediides to transition metal ligands.<sup>43,44</sup> These species have demonstrated an interesting variability in their reactivity with divalent Group 9 metals. Addition of the mesityl-substituted sodium phosphanediide to the bisphosphine palladium and nickel chloride complexes **62** and **63**, respectively, resulted in the side-bound diphosphenes complexes **65** and **66**. However, addition to a similar platinum chloride complex **64** provided the bisphosphide complex **67**.



Scheme 13. Varying binding modes of phosphanediides.

Another transition-metal route to reduction of dichlorophosphines was reported using a stabilized titanocene,  $\text{Cp}_2\text{Ti}(\text{btmsa})$  (btmsa = bis(trimethylsilyl)acetylene) (Scheme 14).<sup>45</sup> This  $\text{Ti}^{\text{II}}$  species readily reacted with the bulky dichlorophosphines **68** and **69** at low temperature to provide diphosphenes, 1,2-dichlorodiphosphines and titanocene dichloride.



Scheme 14. Titanocene-mediated reduction of dichlorophosphines **68** and **69**.

As could be inferred by its absence above, no systematic study has been done on Group 14 metal reduction products of halophosphines, though several examples of “happence” products were reported.

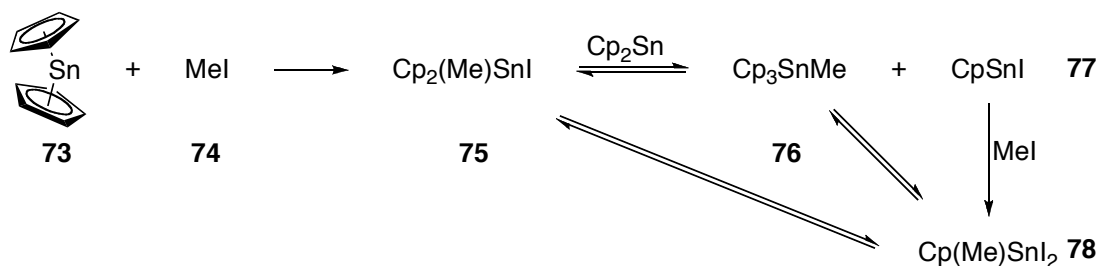
### I.2. Insertion of Group 14 Species into E–X Bonds (E = C, Si, and P; X = Cl, Br, and I)

Reports of insertion reactions for divalent Group 14 metals are numerous and varied, lending to this class of molecules diverse reactivity. It has been demonstrated that divalent species from this group have the ability to insert into C–X (X = Cl, Br, and I), Si–Cl, and P–Cl bonds. No reports have given complete attention or evidence towards the mechanism of insertion, although many researchers have conjectured on the possible pathways. The most popular view is that insertions take place via a radical-based mechanism.<sup>5,7</sup> Because they bear the most in common with the work herein, reported insertions into C–X, Si–Cl, and P–Cl bonds are discussed in detail.

#### *Insertions into C–X Bonds*

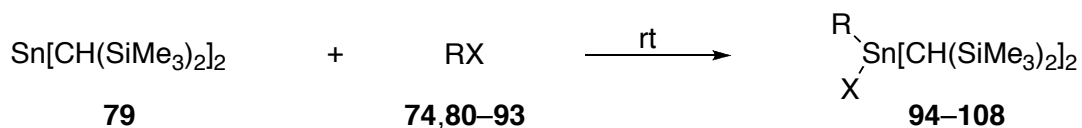
Studies of insertions into C–X bonds began with a rise in the interest and ability to isolate divalent tin species. Initially, dicyclopentadienyltin **73** was shown to oxidatively insert into the C–I bond of methyl iodide **74** (Scheme 15).<sup>46</sup> However, it was

discovered that this insertion product, **75**, was unstable. First, it would disproportionate into the Sn<sup>IV</sup> species tris(cyclopentadienyl)methyltin **76** and the Sn<sup>II</sup> compound cyclopentadienyltin iodide **77**. The latter would undergo a subsequent insertion with the remaining starting material forming an equilibrium between **75**, **76** and **77**, and **78**.



Scheme 15. Oxidative addition of methyl iodide **74** to stannocene **73**.

Lappert's extensive investigations into bulky, acyclic stannylenes, specifically Sn[CH(SiMe<sub>3</sub>)<sub>2</sub>]<sub>2</sub> **79**, led to a more thorough study of their reactivities with alkyl and aryl halides (Scheme 16, Table 2). Kinetic studies gauging relative rates of reactions were conducted for the addition of Sn[CH(SiMe<sub>3</sub>)<sub>2</sub>]<sub>2</sub> to R-X (R = <sup>t</sup>Bu, <sup>i</sup>Pr, Ph, <sup>n</sup>Bu, <sup>n</sup>Pr, Et, and Me; X = Cl, Br, and I).<sup>5</sup>



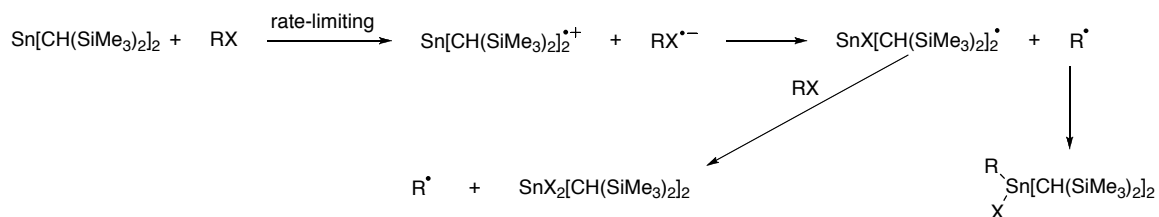
Scheme 16. Reaction template for kinetic experiments.

They concluded that most likely these insertions proceed via a radical mechanism, the rate-limiting step being the electron transfer from the stannylene to the organic halide (Scheme 17). Their argument for this mechanism was a lack of significant variability in reaction times for different alkyl/aryl groups for a given halide. Monitoring of the reaction mixture containing stannylene **79** and alkyl halide **87** by electron paramagnetic resonance (EPR) spectroscopy, showed a large signal attributed to the radical species

•Sn(Br)[CH(SiMe<sub>3</sub>)<sub>2</sub>]<sub>2</sub>. Furthermore, attempts to obtain an enantiopure post-insertion product from the addition of (+)-C<sub>6</sub>H<sub>13</sub>(Me)CHCl to Sn[CH(SiMe<sub>3</sub>)<sub>2</sub>]<sub>2</sub> were unsuccessful, only a racemate was obtained.

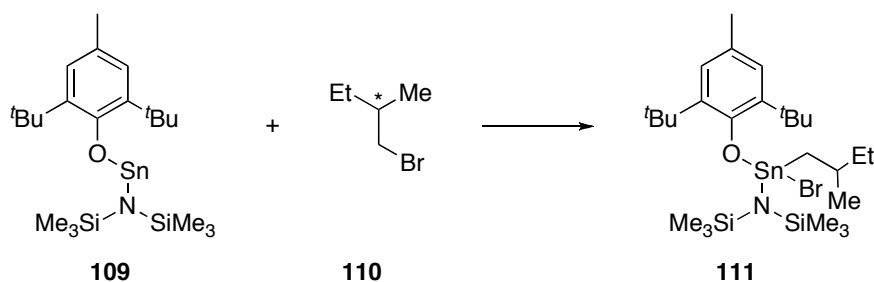
Table 5. Kinetic data for reaction of stannylenes **79** with organic halides **74**, and **80–93**.

<u>RX</u>	<u>#</u>	<u>Solvent</u>	<u>~ Time (h)</u>	<u>Yield (%)</u>	<u>Prod. #</u>
MeI	<b>74</b>	hexanes	< 0.1	83	<b>94</b>
EtI	<b>80</b>	hexanes	< 0.1	81	<b>95</b>
<sup>i</sup> PrI	<b>81</b>	hexanes	< 0.1	71	<b>96</b>
<sup>n</sup> BuI	<b>82</b>	hexanes	< 0.1	72	<b>97</b>
PhI	<b>83</b>	toluene	< 0.1	62	<b>98</b>
MeBr	<b>84</b>	hexanes	1	86	<b>99</b>
EtBr	<b>85</b>	hexanes	1	81	<b>100</b>
<sup>n</sup> PrBr	<b>86</b>	hexanes	1	65	<b>101</b>
<sup>t</sup> BuBr	<b>87</b>	hexanes	1	82	<b>102</b>
PhBr	<b>88</b>	toluene	10	63	<b>103</b>
<sup>i</sup> PrCl	<b>89</b>	hexanes	4	57	<b>104</b>
<sup>n</sup> BuCl	<b>90</b>	hexanes	4	68	<b>105</b>
<sup>t</sup> BuCl	<b>91</b>	hexanes	4	54	<b>106</b>
(Me <sub>3</sub> Si) <sub>2</sub> CHCl	<b>92</b>	hexanes	2	89	<b>107</b>
PhCl	<b>93</b>	toluene	80	49	<b>108</b>



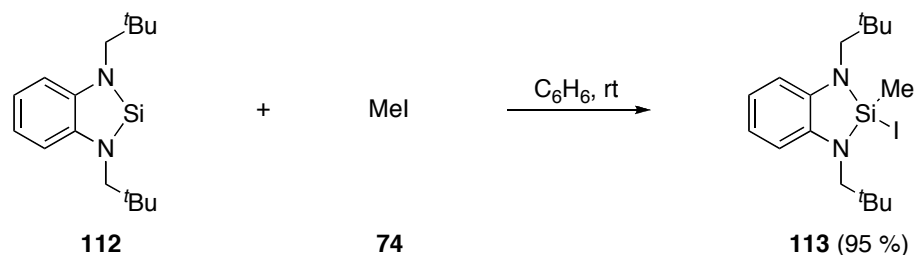
Scheme 17. Proposed mechanism of insertion of stannylene into C–X bonds.

Further attempts to obtain an enantio-enriched insertion product were undertaken<sup>7</sup> by adding the prochiral stannylene **109**, Sn[O(2,6-(*t*Bu)<sub>2</sub>-4-MeC<sub>6</sub>H<sub>2</sub>)] [N(SiMe<sub>3</sub>)<sub>2</sub>], to (+)-EtCH(Me)CH<sub>2</sub>Br (Scheme 18). Again, only a racemate was obtained which was attributed to insufficient steric demands from the C-centered radical to cause preference in reacting with either the *R* or *S* Sn<sup>III</sup> radicals.



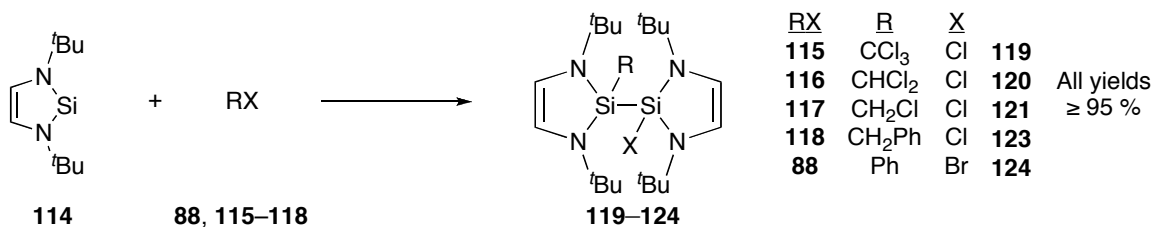
Scheme 18. Attempt to obtain chiral stannane from prochiral stannylene **109**.

Next, attention shifted towards silylenes as the first stable species had only been recently isolated.<sup>47</sup> Initial studies showed similar insertion products. When the diamino silylene **112** was combined with methyl iodide **74**, the iododisilane **113** was obtained (Scheme 19).<sup>48,49</sup>



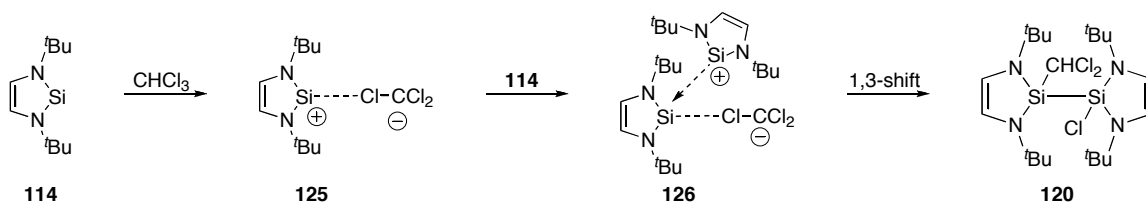
Scheme 19. Insertion of silylene **112** into the C–I bond of **74**.

When West's Arduengo-type silylene **114** was combined with various alkyl and aryl chlorides, a new type of product featuring a Si–Si bond was formed (Scheme 20).<sup>50</sup>



Scheme 20. Syntheses of disilanes **119–124** from silylene **114** and organochlorides **88** and **115–118**.

In the proposed mechanism for these insertions, shown in Scheme 21, the initiating step is the formation of a weak Lewis acid-base adduct between the organic chloride **125** and the Lewis acidic silylene **114**. Subsequent attack at the ligated silicon by another silylene molecule provides complex **126**. Finally, a 1,3-shift by the chloride yields the disilane **120**. This proposed mechanism was supported by a theoretical study, which explained the preference for insertion into a C–Cl bond over a C–Br bond as a thermodynamic phenomenon and quantified the small stabilization energy achieved from the formation of the acid-base complex at  $\sim 0.3$ – $3.1$  kcal/mol.<sup>51</sup>

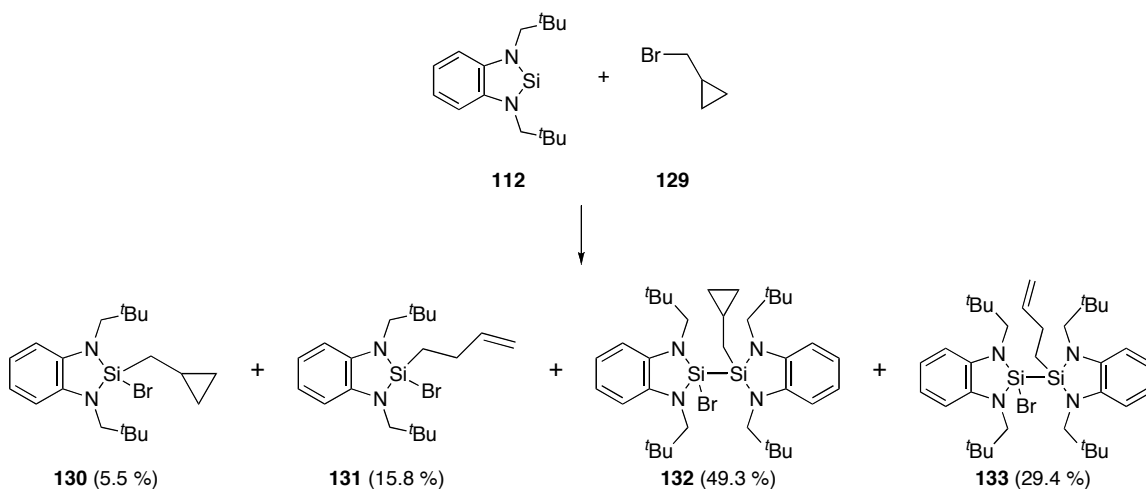


Scheme 21. Proposed mechanism for the formation of disilane **120** from silylene **114** and chloroform **116**.

A follow-up<sup>52</sup> to these reports demonstrated that the abnormal Si–Si bond-containing products were actually meta-stable intermediates towards the “standard”



insertion products. By combining silylene **112** with numerous haloalkanes at low temperature the disilane products were formed. Subsequent heating gave the halosilanes of previously reported form. Also in this work Hitchcock *et al.* furthered the case for a radical mechanism. Addition of silylene **112** to 1-bromo-1-cyclopropylmethane **129**, shown in Scheme 22, provided the expected insertion product **130** and disilane **132**, but also the butenyl silane **131** and disilane **133**. The latter two compounds could only have been formed if the cyclopropyl radical is present and undergoes subsequent rearrangement to the 1-butenyl isomer, which is a more stable form.

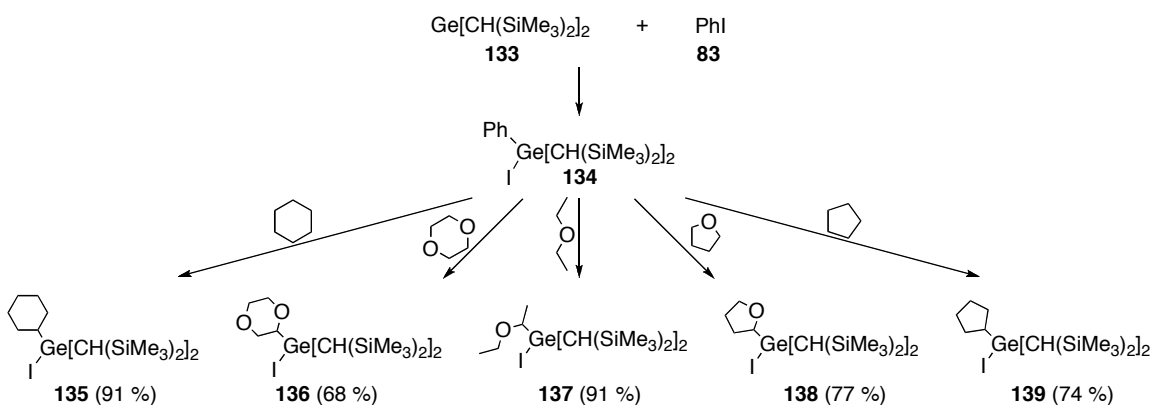


Scheme 22. Range of observed products following rearrangement of cyclopropyl radical.

The most recent analysis<sup>53</sup> of these silylene insertions conceded that a radical mechanism was perhaps more likely due to the findings of small amounts of radical coupling products and the nearly insignificant energy gain stemming from the formation of the Lewis acid-base complex. Considering that no Lewis acid-base adduct had ever been isolated (e.g.,  $R_2Si-NEt_3$ ), the authors concluded that the Lewis acidity of the silylene was likely quite low. They believed that the silylenes' nucleophilicities or

pendant for radical formation (via a modest singlet-triplet energy gap) would have a greater impact on their reactivities than would their Lewis acidities.

Currently, the most attractive results stemming from insertions of divalent Group 14 compounds, in terms of direct application, are those reported by Miller *et al.* claiming C–H activation following the insertion of a germylene or stannylene into the C–I bond of phenyl iodide. Using a method developed by Fouquet,<sup>55</sup> involving a one-pot approach in the synthesis of monoorganotin reagents followed by Pd<sup>0</sup>-catalyzed Stille coupling, studies from the Banaszak Holl group focused on the C–H activation of ethers and cyclic alkanes by Ph(I)Ge[CH(SiMe<sub>3</sub>)<sub>2</sub>]<sub>2</sub> **134** (Scheme 23).<sup>54</sup>

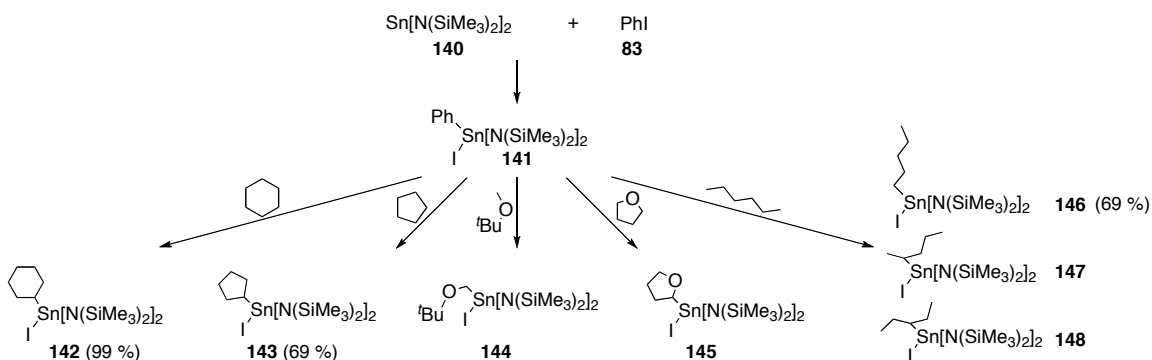


Scheme 23. C–H activation of ethers and alkanes by iodophenylgermane **134**.

Regioselectivities consistent with a radical mechanism were observed; however, when a germyl radical anion was generated using Na metal, no C–H activation was observed. This could indicate that the radicals do not play a significant role in these reactions or simply that the germyl radical is not responsible for activation of the C–H bond and thus the phenyl radical is.

These findings were promising, but there are few transformations utilizing Ge–C bonds in C–C bond forming reactions. Several reports followed<sup>56,57</sup> using the analogous stannylenes to bring about the same C–H activations (Scheme 24). These Sn–C bond-

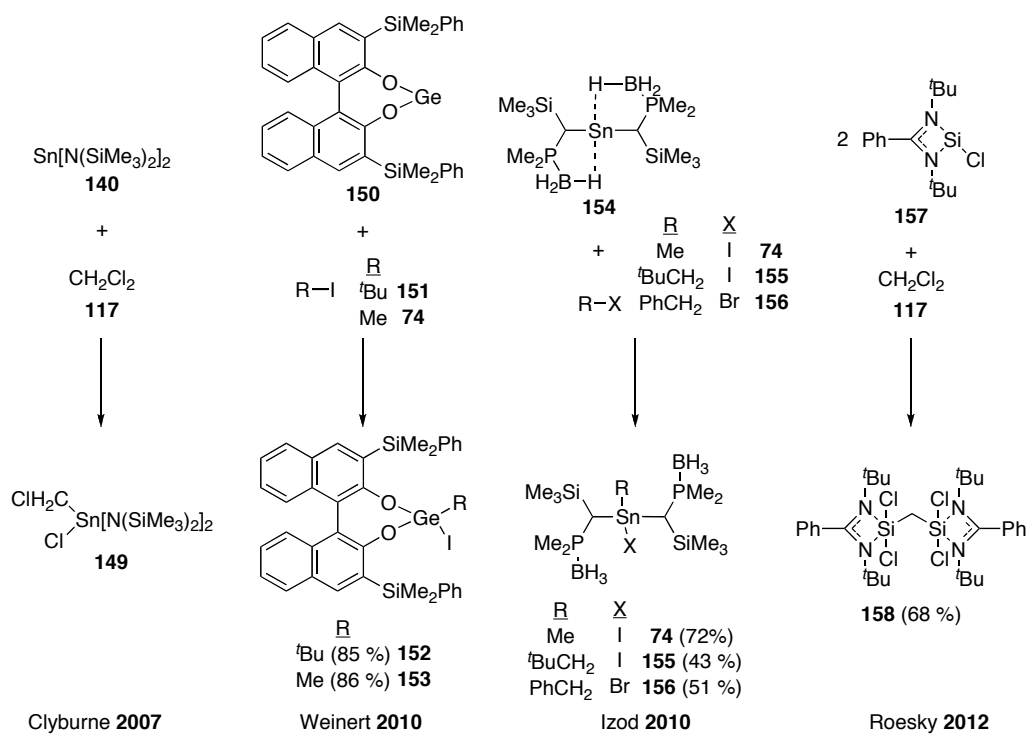
containing compounds were seen as vastly superior to their germanium analogues due to the greater utility. Numerous C–C bond forming reactions utilize organostannanes as a starting reagent (e.g. Stille couplings).



Scheme 24. C–H activation of ethers and alkanes by iodophenylstannane **141**.

To counter problems with amide transfer (a competing side reaction), the authors repeated their previously reported experiments, substituting a cyclic dialkyl stannylene for the bis(amino)tin compound **140**.<sup>57</sup> However, this new stannylene showed somewhat unexpected reactivity by causing C–C bond formation when added to some alkenes. Additionally, the Banaszak Holl group demonstrated that by switching the aryl halide to mesityl iodide, product distribution was significantly altered. These types of encountered frustrations have shown the wide scope of possibilities for these reactive divalent heterocarbenoids. However, due to their general unpredictability through various substituents, they continue to receive limited attention.

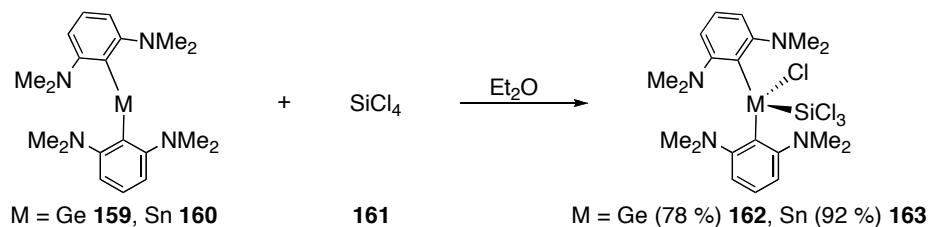
Oxidative additions have been consistently used as a benchmark reaction for newly reported silylenes, germylenes and stannylenes, as demonstrated in four recent reports by Clyburne,<sup>58</sup> Izod,<sup>59</sup> Weinert,<sup>60</sup> and Roesky,<sup>61</sup> (Scheme 25) though no systematic investigation into the full scope and likely mechanism has been attempted since Lappert's initial studies in the mid to late 1970s.



Scheme 25. Recent reports of insertions of heterocarbenoids into C–X bonds.

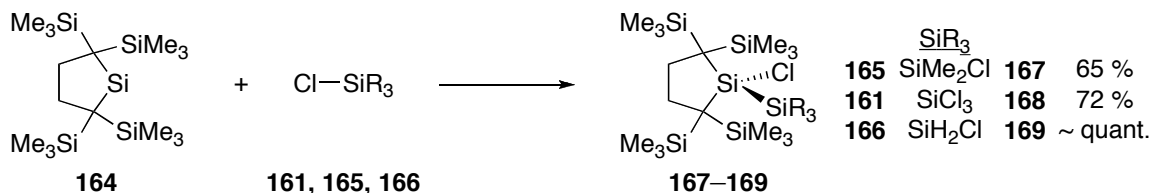
### Insertions into Si–X Bonds

Insertions into Si–X bonds are an important case comparison and “stepping stone” between the well-studied C–X insertions and the poorly studied P–X insertions. There have been only two experimental reports regarding the insertion of divalent Group 14 compounds into Si–Cl bonds. Initially, Lappert *et al.* reported the insertion of [2,6-(NMe<sub>2</sub>)<sub>2</sub>Ph]<sub>2</sub>M (M = Ge, **159** or Sn, **160**) into a Si–Cl bond of SiCl<sub>4</sub>, **161**, and MeSiCl<sub>3</sub> (Scheme 26).<sup>62</sup> No multiple insertion products were mentioned or even conjectured as possible.



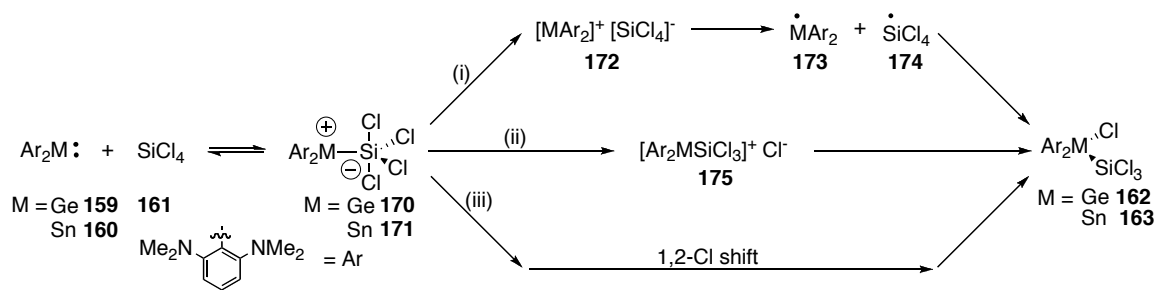
Scheme 26. Addition of SiCl<sub>4</sub> to germylene **159** and stannylene **160**.

The second report came from the Kira group providing data regarding the insertion of the dialkyl, cyclic silylene **164** into  $\text{Me}_2\text{SiCl}_2$  **165**,  $\text{SiCl}_4$  **161**, and  $\text{H}_2\text{SiCl}_2$  **166** including a diinsertion into  $\text{H}_2\text{SiCl}_2$ .<sup>63</sup> The silylene was found to preferentially insert into the Si–H bond rather than the Si–Cl bond of  $\text{Me}_2\text{Si}(\text{H})\text{Cl}$  and no insertion occurred when the silylene was combined with  $\text{Me}_3\text{SiCl}$  (Scheme 27).



Scheme 27. Insertion of silylene **164** into Si–Cl bonds of chlorosilanes.

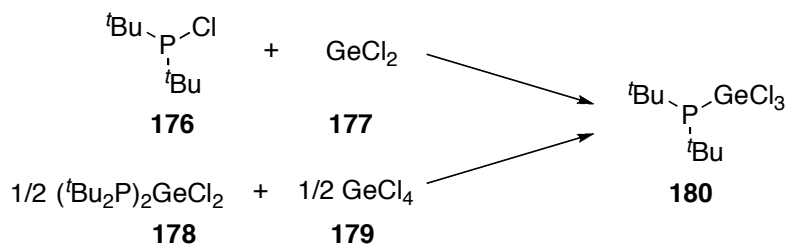
The Si–X bond insertions share an important commonality with the P–X insertions, namely hypervalency. Due to the ability of Si and P to accommodate more than four ligands and/or substituents, in contrast to carbon, the number of mechanistic pathways increases significantly. Only in the former report<sup>62</sup> were possible mechanisms discussed in some detail (Scheme 26). The authors believed that the most likely initial intermediate is a five-coordinate silicon complex. Three possible pathways were proposed (Scheme 28) based on this hypothesis: i) homolytic cleavage of the Si–M (M = Ge, Sn) bond providing the two radical species **173** and **174**, ii) transfer of the chloride from the inner to the outer coordination sphere providing the  $\text{Si}^{\text{IV}}$  complex **175**, and iii) a 1,2-chloride shift from silicon to M. While Lappert *et al.* have been the major proponents of a radical pathway for the C–X insertions, in this case they favored the third pathway with a  $\text{Cl}^-$  migration.



Scheme 28. Possible mechanistic routes for insertion into Si–Cl bonds.

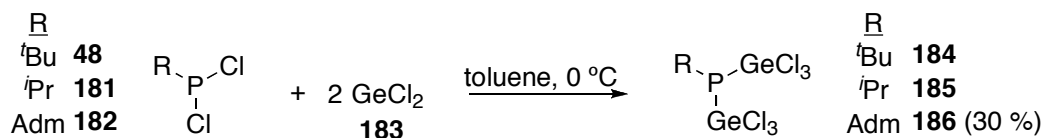
### *Insertions into P–X Bonds*

Insertion into P–X bonds have received considerably less attention than their carbon counterparts. While C–C bond forming reactions have wide applicability, formation of P–C bonds are important in their own right, for example in the formation of tertiary phosphine ligands. The first example of an insertion of a  $\text{M}^{\text{II}}$  species ( $\text{M} = \text{Si}, \text{Ge},$  or  $\text{Sn}$ ) into a P–X bond was reported by du Mont *et al.*<sup>65</sup> Previously, the authors had reported several chlorostannyl- and germyl-substituted phosphines synthesized by the thermodynamically driven formation of a Si–Cl bond.<sup>64–71</sup> Many of the structures within these papers, while obtained by different routes, are very similar to the new compounds produced in this work. The lack of stability of the tin-containing products was demonstrated from the beginning, with  $\text{Me}_2\text{Sn}(\text{Cl})\text{P}^t\text{Bu}_2$ ,  $\text{MeSn}(\text{Cl})_2\text{P}^t\text{Bu}_2$  and  $\text{MeSn}(\text{Cl})(\text{P}^t\text{Bu}_2)_2$  being the only isolable examples. Attempting to obtain the chlorophosphino dichlorogermanium complex instead resulted in the isolation of di-*tert*-butyl trichlorogermylphosphine **180** (Scheme 29).<sup>65</sup> The authors were also able to synthesize this same product by comproportionation of the bisphosphinodichlorogermane **178** with  $\text{GeCl}_4$  **179**.



Scheme 29. Two synthetic routes for trichlorogermylphosphine **180**.

After two decades, du Mont reinvestigated these reactions and reported a more detailed analysis of the observed intermediates and products.<sup>72,73</sup> Directly addressing the insertion chemistry previously observed, the dichlorophosphines **48**, **181**, and **182** were combined with  $\text{GeCl}_2$  **183** providing the insertion products **184–186** (Scheme 30). The adamantyl-substituted phosphine **186** was the only stable insertion species, while the others yielded cyclic polyphosphines [e.g.  $(\text{}^i\text{PrP})_4$ ].



Scheme 30. Insertion of  $\text{GeCl}_2$  into P–Cl bonds of dichlorophosphines.

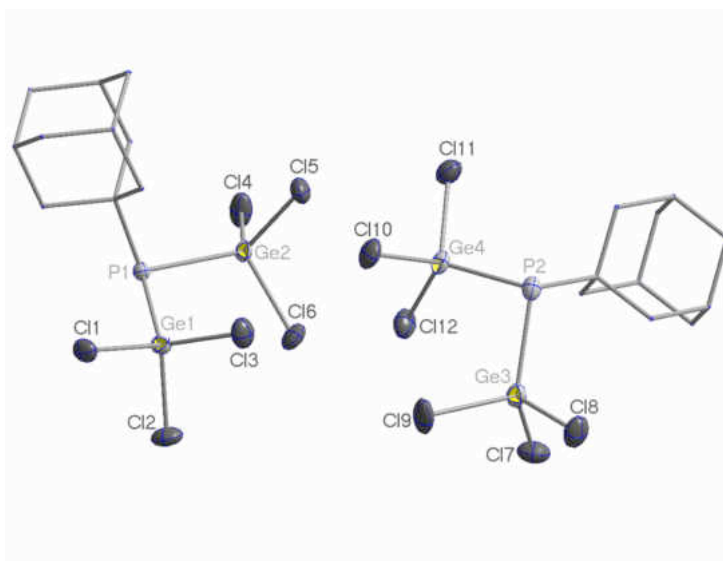
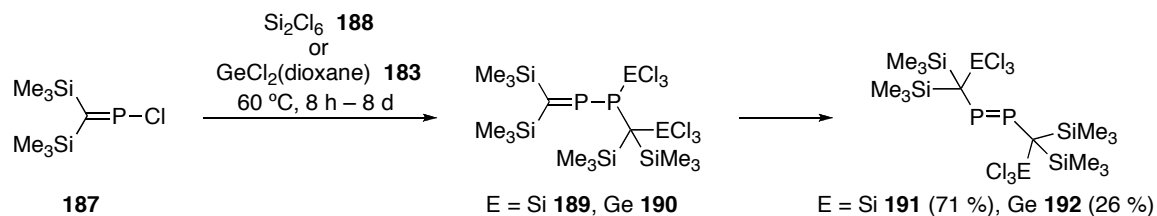


Figure 1. Crystal structure of **186** showing the two independent molecules in the unit cell. Ellipsoids are given at 50% probability. Hydrogens have been omitted and the adamantyl groups are drawn as wireframes for clarity. Average bond lengths (Å) and angles (°): Ge–P = 2.304, P–C = 1.884, Ge–Cl = 2.128; C–P–Ge = 105.38, and Ge–P–Ge = 97.21.

A detailed report<sup>74</sup> from du Mont in the interim showed the use of  $\text{GeCl}_2$  **183** and  $\text{Si}_2\text{Cl}_6$  **188** to reduce the *P*-chlorophosphaalkene **187** to the diphosphenes **191** and **192**. They proposed an intermediate with an insertion into the P–Cl bond providing **189** and **190** (Scheme 31). A subsequent rearrangement led to a diphosphene with a trichlorogermyl- or silyl-substituent on the neighboring carbon.

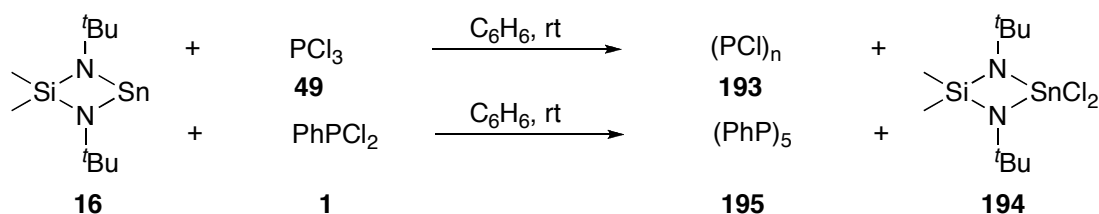


Scheme 31. Insertion of  $\text{GeCl}_2$  and “ $\text{SiCl}_2$ ” into P–Cl bond of phosphalkene **187**.

Initial studies into the oxidative addition of stannylenes and germylenes to P–Cl bonds were led by Veith and Bertrand<sup>23</sup> with the goal of mildly reducing



dichlorophosphines to obtain diphosphenes, *vide supra*. As shown in Scheme 32, addition of the cyclic stannylene **16** to  $\text{PCl}_3$  **49**, in equimolar amounts, yielded an insoluble powder of the form  $(\text{PCl})_n$  **193**, along with the dichlorostannane **194**. The latter was identified by  $^1\text{H}$  NMR and elemental analysis. When the same stannylene was combined with  $\text{PhPCl}_2$  **1**, the same dichlorostannane was obtained along with  $(\text{PhP})_5$  **195**. The authors hypothesized that, since  $\text{P}^{\text{I}}$  products were obtained transient phosphinidenes,  $\text{RP}^{\text{I}}$ , were the likely intermediates and that these were formed from the intermediate insertion products.

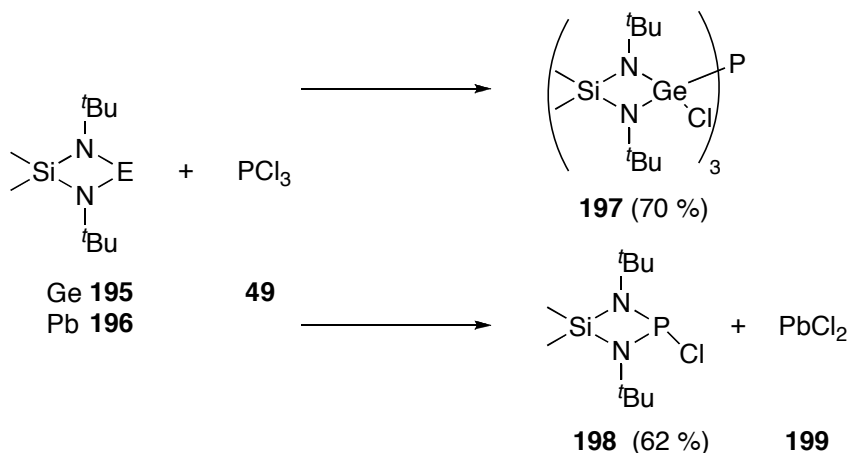


Scheme 32. Reactions of stannylene **16** with  $\text{PCl}_3$  **49** and  $\text{PhPCl}_2$  **1**.

As was described earlier (Scheme 5), the goal of providing a mild reducing agent was realized when it was shown that the previously reported diphosphene **13** could be obtained from (2,4,6-tri-*tert*-butylphenyl)dichlorophosphine and either stannylene **16** or germanium diiodide. The isolation of stable insertion products was also a goal of this study in order to prove their role as intermediates. Unfortunately, that goal was not realized.

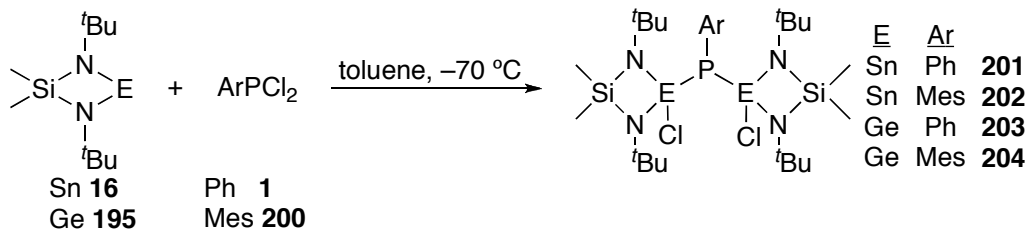
Following these results, Veith directly studied the direct addition of the analogous germylene and plumbylene  $\text{Me}_2\text{Si}(\mu\text{-N}^t\text{Bu})_2\text{E}$  [ $\text{E} = \text{Ge}$  (**195**) and  $\text{Pb}$  (**196**)] to  $\text{PCl}_3$  **49**.<sup>75</sup> A diverse range of products were obtained, exemplifying not only the scope of possible products which could be obtained, but also the complexity of these interactions (Scheme 33). The reaction between three equivalents of germylene **195** and  $\text{PCl}_3$  **49** furnished the

triinsertion product,  $[\text{Me}_2\text{Si}(\mu\text{-N}^t\text{Bu})_2\text{Ge}(\text{Cl})]_3\text{P}$  **197**, while the plumbylene **196** yielded exclusively the ligand exchange product  $\text{Me}_2\text{Si}(\mu\text{-N}^t\text{Bu})_2\text{P}(\text{Cl})$  **198** and  $\text{PbCl}_2$  **199**.



Scheme 33. Addition of germylene **195** and plumbylene **196** to  $\text{PCl}_3$  **49**.

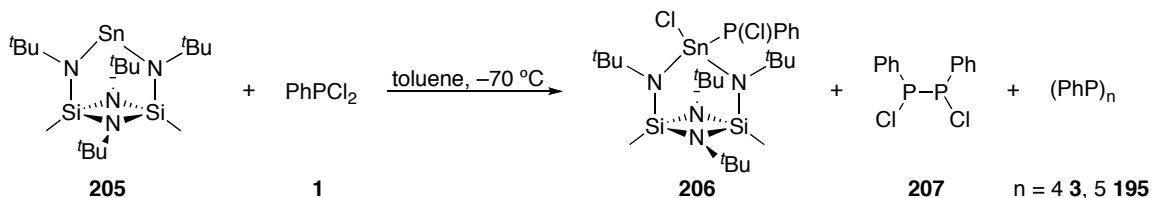
A final follow-up study was conducted to attempt to ascertain any intermediates in these reactions and to hopefully isolate another stable insertion product.<sup>76</sup> The same stannylene and germylene were combined with  $\text{PhPCl}_2$  **1** and  $\text{MesPCl}_2$  **200**, now in a 2:1 ratio (Scheme 34).  $^{31}\text{P}\{^1\text{H}\}$  NMR spectroscopic studies allowed the intermediate monoinsertions (for the germylene **195**) and the unstable diinsertion (for the stannylene **16**) to be identified. The characterization was neither completed, nor were yields reported for any of the few stable species.



Scheme 34. Addition of heterocarbenoids to aryldichlorophosphines.

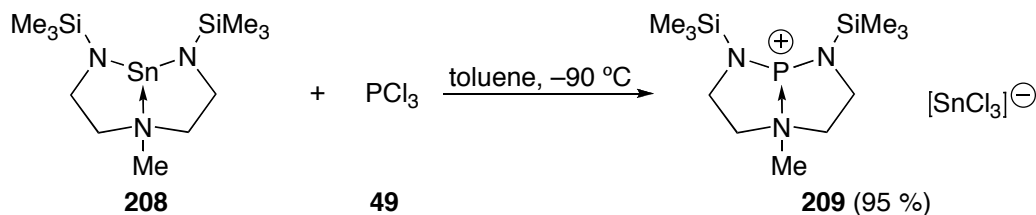
Attempting to slow reaction processes or to shield unstable intermediates, the bulkier stannylene  $(\text{Me}_2\text{Si})_2(\mu\text{-N}^t\text{Bu})_4\text{Sn}$  **205** was combined with  $\text{PhPCl}_2$  **1** in equimolar

amounts (Scheme 35). The resulting mixture gave numerous, identifiable  $^1\text{H}$  and  $^{31}\text{P}$  signals, which were attributed to two isomeric dichlorodiphosphines, the dichlorostannane, the polyphosphine(s)  $(\text{PhP})_n$ , and excess  $\text{PhPCl}_2$ . It is noteworthy that the identification of  $(\text{PhP})_n$  was incomplete.



Scheme 35. Addition of bulky stannylene **205** to dichlorophenylphosphine **1**.

No subsequent studies of divalent Group 14 species with P–X bonds were reported. One happenstance report, from Bertrand,<sup>77</sup> displayed a type of product not previously reported for the addition of a stannylene to a chlorophosphine. Stannylene **208**, stabilized by a tridentate, dianionic triamine ligand, was combined with  $\text{PCl}_3$  **49** in a 1:1 ratio. Instead of the anticipated polyphosphine  $(\text{PCl})_n$ , a phosphonium ion, a  $\text{P}^{\text{III}}$ -centered cation **209**, with associated trichlorostannate anion was obtained (Scheme 36).

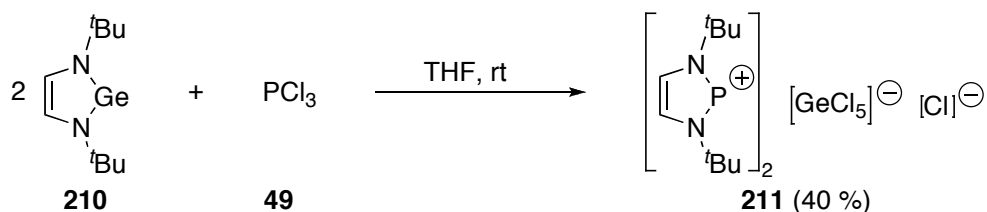


Scheme 36. Amine exchange observed for addition of **208** to **49**.

This product type more closely resembles the amide exchange product obtained from the plumblylene reported earlier (Scheme 33).<sup>75</sup> This final report demonstrates the effect the carbenoid's ligand can have on the product structure.

Somewhat similarly, several groups<sup>78–80</sup> have utilized the tendency of germynes and stannylenes to reduce  $\text{PCl}_3$  as a means to generate  $\text{P}^{\text{I}}$  cations, which are subsequently

trapped. Addition of the Arduengo-type germylene **210** to  $\text{PCl}_3$  **49** (Scheme 37) gave not an insertion product but resulted in a ligand exchange,<sup>79</sup> again similar to reactions of Veith's plumbylene<sup>75</sup> and Bertrand's stannylene.<sup>77</sup> The germanium was oxidized to  $\text{Ge}^{\text{IV}}$  and it crystallized with the phosphonium ion **211** as a pentachlorogermanate anion.



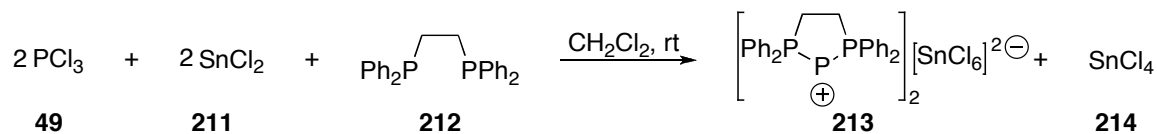
Scheme 37. Amine exchange formation of phosphonium ion **211**.

Excluding these few mentions in the literature, no other report has appeared discussing the addition of a heavier divalent Group 14 species (Si, Ge, Sn, and Pb) to a halophosphine. However, with the rise in popularity of *N*-heterocyclic carbenes (NHCs), the addition of  $\text{C}^{\text{II}}$  species to compounds containing P–Cl bonds has begun to surface, and these give starkly different results.

### 1.3. Syntheses and Isolation of Stable Phosphonium Ions

Recent investigations into reactions of *N*-heterocyclic carbenes with halophosphines have opened a different perspective to the aforementioned insertions. Addition of an NHC to a halophosphine results not in a formal oxidative addition, but in the formation of an NHC-stabilized phosphonium salt, a  $\text{P}^{\text{III}}$ -centered cation. Stable, isolable examples have been reported<sup>81–84</sup> since the early 1970s and are comprised of four components: 1) a di-/tri-halophosphine, 2) a reducing agent, 3) a stabilizer (generally a Lewis base), and 4) an acceptor for the halide ions (generally a Lewis acid). Not all systems contain four clear-cut components because frequently one species fills more than one role in the system.

One of the first unequivocal (i.e., ion is not just a possible resonance form) phosphonium ions was generated by the addition of  $\text{PCl}_3$  to  $\text{SnCl}_2$  in the presence of 1,2-bis(diphenylphosphino)ethane (Scheme 38).<sup>85</sup>



Scheme 38. Generation of phosphonium ion **213**.

Schmidpeter<sup>86</sup> followed this study with an acyclic variant utilizing  $\text{AlCl}_3$  as the halide acceptor. Since this time myriad examples<sup>87-94</sup> of cyclic and acyclic phosphonium ions have been reported often using a Group 13 metal halide as a halide acceptor (Chart 2).

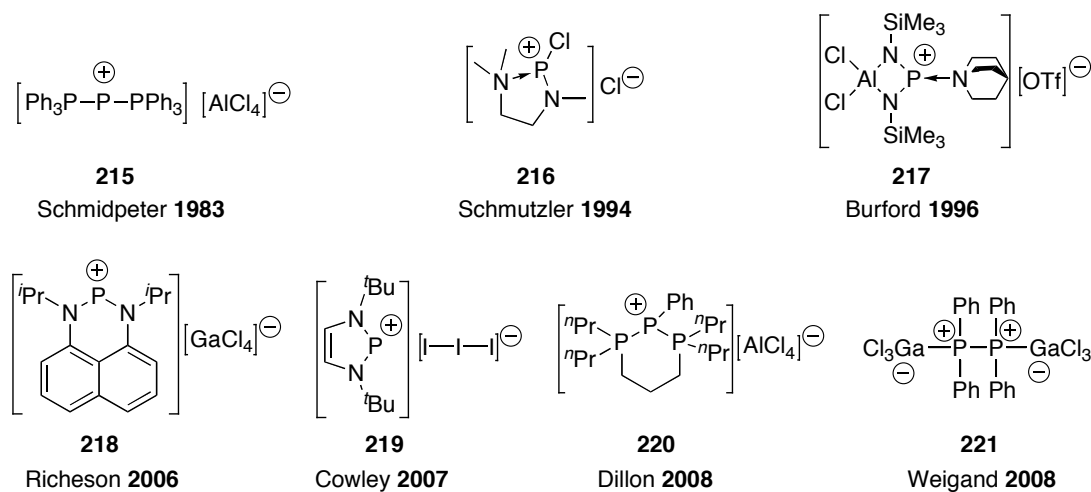
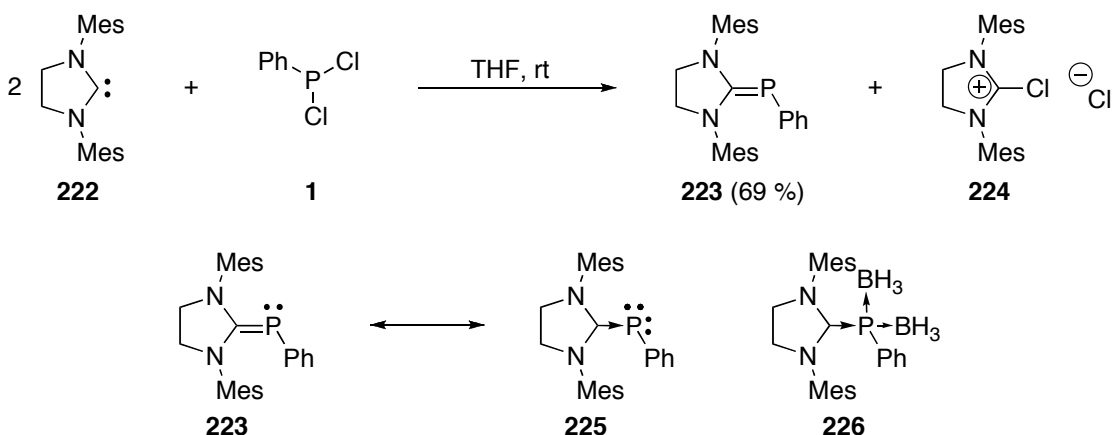


Chart 2. Structural variety observed for reported phosphonium ions.

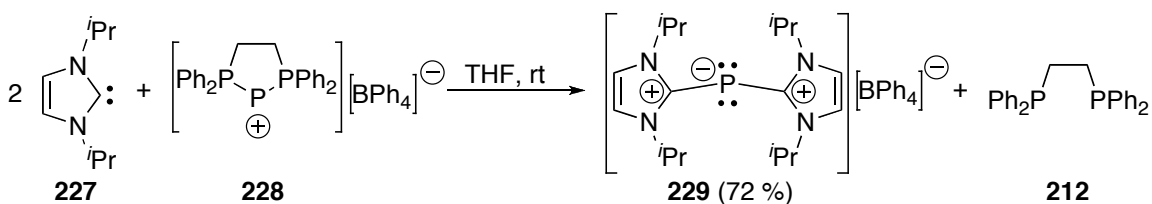
More recently, *N*-heterocyclic carbenes (important examples, given their analogy to germylenes and stannylenes) have been shown to cause the same kind of displacement of halide ions from a  $\text{P}^{\text{III}}$  center (Scheme 39). Since their first isolation by Arduengo and Cowley,<sup>95,96</sup> they have been treated as stabilized phosphinidenes **225** and as phosphalkenes **223**. In many respects they are both phosphinidenes and phosphalkenes,

as the two forms are related by resonance. However, addition of borane to a solution of **223/225** led solely to the bisborane adduct **226**.<sup>96</sup> This indicates that **225** is the dominant form of these two possible resonance species.



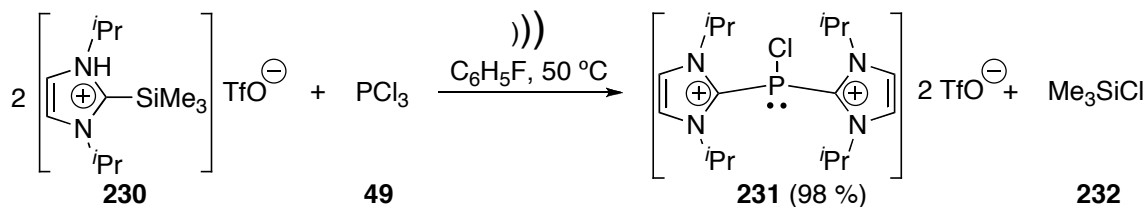
Scheme 39. Addition of NHC **222** to dichlorophenylphosphine **1**.

Once discovered, however, they remained virtually untouched (one report from Kuhn<sup>97</sup> in 1999 slightly expanded the study) until 2005. Macdonald and coworkers<sup>98</sup> developed two further methods for the syntheses of NHC-stabilized phosphonium ions, adding the unsaturated NHC **227** to the chelated phosphonium cation **228**, and delved further into the nature of the electronic structure of these species (Scheme 39).



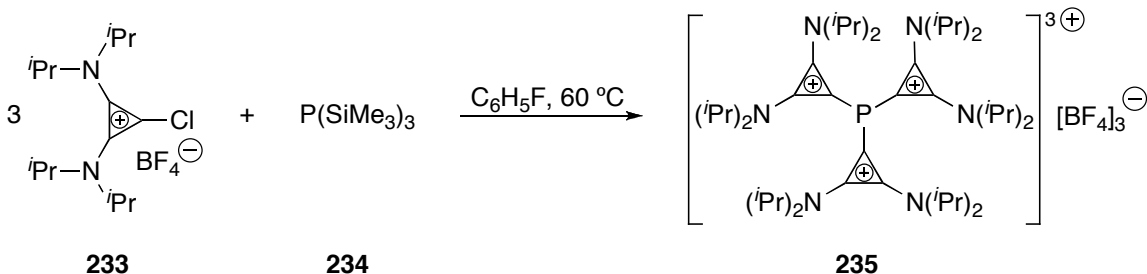
Scheme 40. New synthetic method for carbene-stabilized phosphonium ions.

Once again, no reports on these types of compounds were published for several years. In 2010, Weigand *et al.* produced mono- and dicationic forms **231** (as triflate salts), substituting chlorides from PCl<sub>3</sub> **49** and producing Me<sub>3</sub>SiCl **232** as a by-product (Scheme 41).<sup>99</sup>



Scheme 41. Preparation of phosphonium triflate salt **231**.

Since this time, several more have been published,<sup>100–102</sup> most notably the synthesis of a tris(cyclopropenyl)phosphonium trication **235** (Scheme 42) and complexes thereof with Pd<sup>II</sup> and Pt<sup>II</sup> chloride salts.<sup>103</sup> Calculations showed that this phosphonium trication, when employed as a ligand, is a poor  $\sigma$ -donor and an excellent  $\pi$ -acceptor.



Scheme 42. Synthesis of phosphonium trication **235**.

The entirety of the reactions discussed above: i) metal reduction of P–X bonds, ii) insertion into E–X bonds (E = C, Si, P), and iii) generation of phosphonium cations using NHCs, give insight into the difficulty and ambiguity faced in our investigations of the reactions of cyclic and acyclic germlyenes and stannylenes with halophosphines. There is substantial leeway for interpretation of mechanistic possibilities and reactivity implications of the products' structures. These three motifs will be employed when it is deemed suitable to interpret and to explain the obtained results.

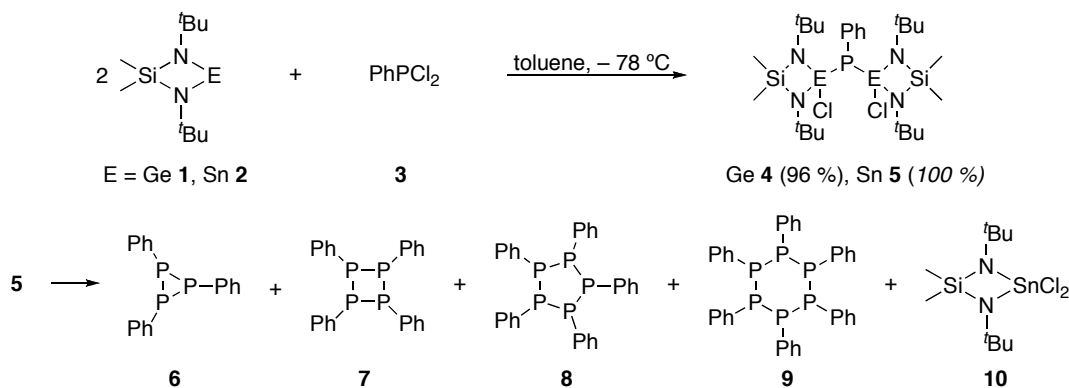
## CHAPTER II

### RESULTS AND DISCUSSION

#### II.1. Reactions of Stannylenes and Germylenes with Alkyl- and Arylchlorophosphines\*

##### *Insertion reactions of cyclic stannylenes and germylenes*

Early experimental endeavors focused on reinvestigating those reactions already reported by the Veith *et al.* Addition of  $\text{Me}_2\text{Si}(\mu\text{-N}^t\text{Bu})_2\text{M}$  (M = Ge **1** or Sn **2**) to  $\text{PhPCl}_2$  **3** was shown to provide the diinsertion product **4** for M = Ge and cyclic oligophosphines **6–9** for M = Sn (Scheme 43).



Scheme 43. Reactions of carbenoids **1** and **2** with dichlorophenylphosphine **3**.

These results matched earlier reports, though greater details of these reactions are now available. The reactions appear to proceed extremely rapidly, requiring < 1 h at  $-78 \text{ }^\circ\text{C}$ . Isolation of crystalline samples of  $[\text{Me}_2\text{Si}(\mu\text{-N}^t\text{Bu})_2\text{Ge}]_2\text{PPh}$  **4** and subsequent single-crystal X-ray analysis provided the structure shown in Figure 2.

The diinsertion product **4** crystallized from toluene as clear rods in the monoclinic space group  $P2_1/n$  with  $Z = 4$ . Additional crystallographic data for **4**

\* Numbering of compounds will begin anew in this chapter.



can be found in Table 6. The Ge–P bond lengths of 2.3315(8) and 2.3226(8) Å are normal for Ge–P bonds and can be classified as single bonds. Additional selected bond lengths and angles can be found in Table 7. The Ge–P bond distances are comparable to the 2.329(4), 2.319(4), and 2.298(3) Å found in  $[\text{Me}_2\text{Si}(\mu\text{-N}^t\text{Bu})_2\text{Ge}]_3\text{P}$  and the 2.304 Å average observed in  $(\text{adm})\text{P}(\text{GeCl}_3)_2$  (**186** in Introduction, page 27).<sup>72,75</sup> The rings are non-coplanar and align to allow interaction with H atoms from the phenyl group on phosphorus (for Cl1) and from the  $t$ Bu group on N2 (for Cl2). There are no H-bonds, thus only van der Waals forces are responsible for the molecule's orientation in the unit cell.

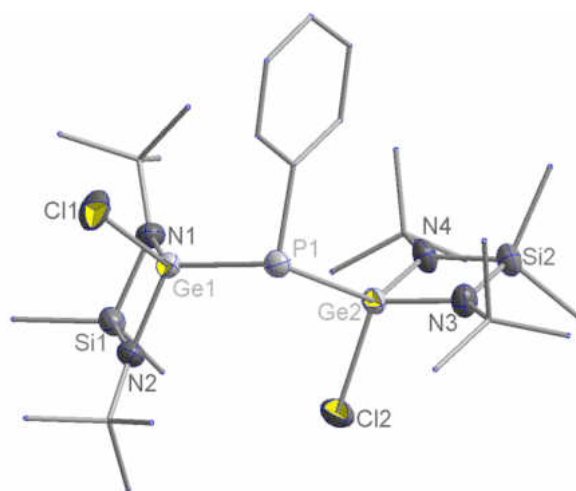


Figure 2. Crystal structure of **4**. Thermal ellipsoids are drawn at 50 % probability.

Hydrogen atoms have been omitted and *tert*-butyl, phenyl and methyl groups are drawn as wireframes for clarity.

Table 6. Crystal data for compound 4.

Molecular Formula	C <sub>26</sub> H <sub>47</sub> Cl <sub>2</sub> Ge <sub>2</sub> N <sub>4</sub> PSi <sub>2</sub>
Formula Weight (g/mol)	718.91
Crystal System	monoclinic
Space Group	<i>P</i> 2 <sub>1</sub> / <i>n</i> (No. 14)
<i>a</i> , Å	17.330(3)
<i>b</i> , Å	10.0397(16)
<i>c</i> , Å	22.406(4)
$\alpha$ , °	90
$\beta$ , °	107.715(2)
$\gamma$ , °	90
<i>V</i> , Å <sup>3</sup>	3713.5(10)
<i>Z</i>	4
F(000)	1512
$\rho_{\text{calcd}}$ , g cm <sup>-3</sup>	1.286
$\lambda$ , Å	0.71073
Temperature, K	173
<i>h</i> , min/max	-23/22
<i>k</i> , min/max	-13/13
<i>l</i> , min/max	-29/29
2 $\theta$ maximum, °	56.46
$\mu$ , mm <sup>-1</sup>	1.891
# Reflections Collected	30238
# Unique Reflections ( <i>R</i> <sub>int</sub> )	8071 (0.0242)
<i>R</i> (F) <sup>a</sup>	0.0273
<i>R</i> <sub>w</sub> (F <sup>2</sup> ) <sup>b</sup>	0.0834
Goof	0.990

$${}^a R = \sum |F_o - F_c| / \sum |F_o| \quad {}^b R_w = \{[\sum w(F_o - F_c)^2 / [\sum w(F_o^2)^2]\}^{1/2}; w = 1/[\sigma^2(F_o)^2 + (xP)^2 + yP],$$

where P = (F<sub>o</sub><sup>2</sup> + 2F<sub>c</sub><sup>2</sup>)/3.

Table 7. Selected bond lengths and angles for compound **4**.

Bond Lengths (Å)			
Ge(1)–N(1)	1.828(2)	Ge(2)–P(1)	2.3326(8)
Ge(1)–N(2)	1.826(2)	Ge(2)–Si(2)	2.6105(11)*
Ge(1)–Cl(1)	2.1977(8)	Si(1)–N(1)	1.759(3)
Ge(1)–P(1)	2.3315(8)	Si(1)–N(2)	1.742(3)
Ge(1)–Si(1)	2.6029(9)*	Si(2)–N(3)	1.743(3)
Ge(2)–N(3)	1.831(3)	Si(2)–N(4)	1.746(3)
Ge(2)–N(4)	1.837(3)	P(1)–C(50)	1.837(3)
Ge(2)–Cl(2)	2.1906(8)		
Bond Angles (°)			
N(1)–Ge(1)–N(2)	84.32(11)	Cl(2)–Ge(2)–P(1)	100.33(3)
Cl(1)–Ge(1)–N(1)	111.86(9)	C(50)–P(1)–Ge(2)	105.29(11)
Cl(1)–Ge(1)–N(2)	111.79(8)	C(50)–P(1)–Ge(1)	103.85(10)
N(2)–Ge(1)–P(1)	119.43(8)	Ge(2)–P(1)–Ge(2)	108.78(3)
N(1)–Ge(1)–P(1)	130.17(9)	N(2)–Si(1)–N(1)	88.93(11)
Cl(1)–Ge(1)–P(1)	99.34(3)	N(4)–Si(2)–N(3)	88.97(13)
N(3)–Ge(2)–N(4)	83.34(11)	Si(1)–N(1)–Ge(1)	93.02(11)
N(3)–Ge(2)–Cl(2)	112.45(9)	Si(1)–N(2)–Ge(1)	93.67(12)
N(4)–Ge(2)–Cl(2)	112.42(8)	Si(2)–N(3)–Ge(2)	94.14(12)
N(3)–Ge(2)–P(1)	114.15(8)	Si(2)–N(4)–Ge(2)	93.52(12)
N(4)–Ge(2)–P(1)	133.51(9)		

\*non-bonding distance

The 2:1 addition of  $\text{Me}_2\text{Si}(\mu\text{-N}^t\text{Bu})_2\text{Sn}$  to  $\text{PhPCl}_2$  provides the unstable  $[\text{Me}_2\text{Si}(\mu\text{-N}^t\text{Bu})_2\text{Sn}]_2\text{PPh}$  **5**, identified by its  $^{31}\text{P}\{^1\text{H}\}$  NMR signal at  $\delta$  –61.0 ppm. As is typical of Sn- and P-containing compounds, coupling of  $^{117}\text{Sn}$  and  $^{119}\text{Sn}$  to  $^{31}\text{P}$  was observed and coupling constants of  $^1J_{^{119}/^{117}\text{SnP}} = 1524/1462$  Hz were measured.

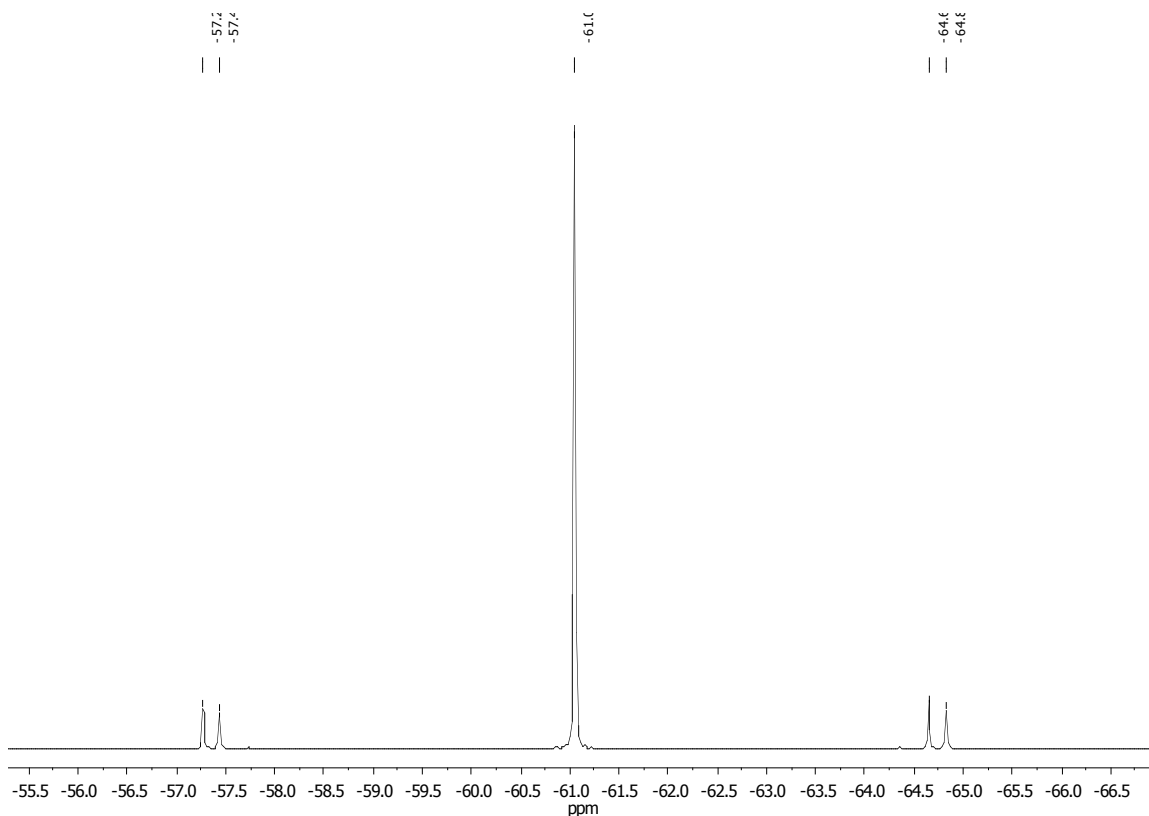


Figure 3.  $^{31}\text{P}\{^1\text{H}\}$  NMR spectrum of stannylene insertion product **5**.

Stirring of  $[\text{Me}_2\text{Si}(\mu\text{-N}^t\text{Bu})_2\text{Sn}(\text{Cl})]\text{PPh}$  **5** at ambient conditions resulted in the formation of the cyclic oligophosphines  $(\text{PhP})_3$  **6**,  $(\text{PhP})_4$  **7**, and  $(\text{PhP})_5$  **8** (with trace amounts of the six-membered ring **9**) in the approximate ratio of 1:6:13, respectively.

In order to determine if the lack of stability of the Sn-based diinsertions stemmed from the fact that there are two chlorostannyl units attached to the phosphorus center,  $\text{Me}_2\text{Si}(\mu\text{-N}^t\text{Bu})_2\text{Sn}$  **2** was added to  $\text{Ph}_2\text{PCl}$  **11**. A reaction with the analogous germylene **1** was also conducted, as shown in Scheme 44. Again, these reactions proceeded fairly rapidly even at low temperatures, but the overall rates for  $\text{Ph}_2\text{PCl}$  appeared to be slightly slower than for  $\text{PhPCl}_2$ . In addition, a disparity between insertion rates of the analogous germylene and stannylene began to appear, with the stannylene reaction reaching completion significantly quicker than the germylene reaction.

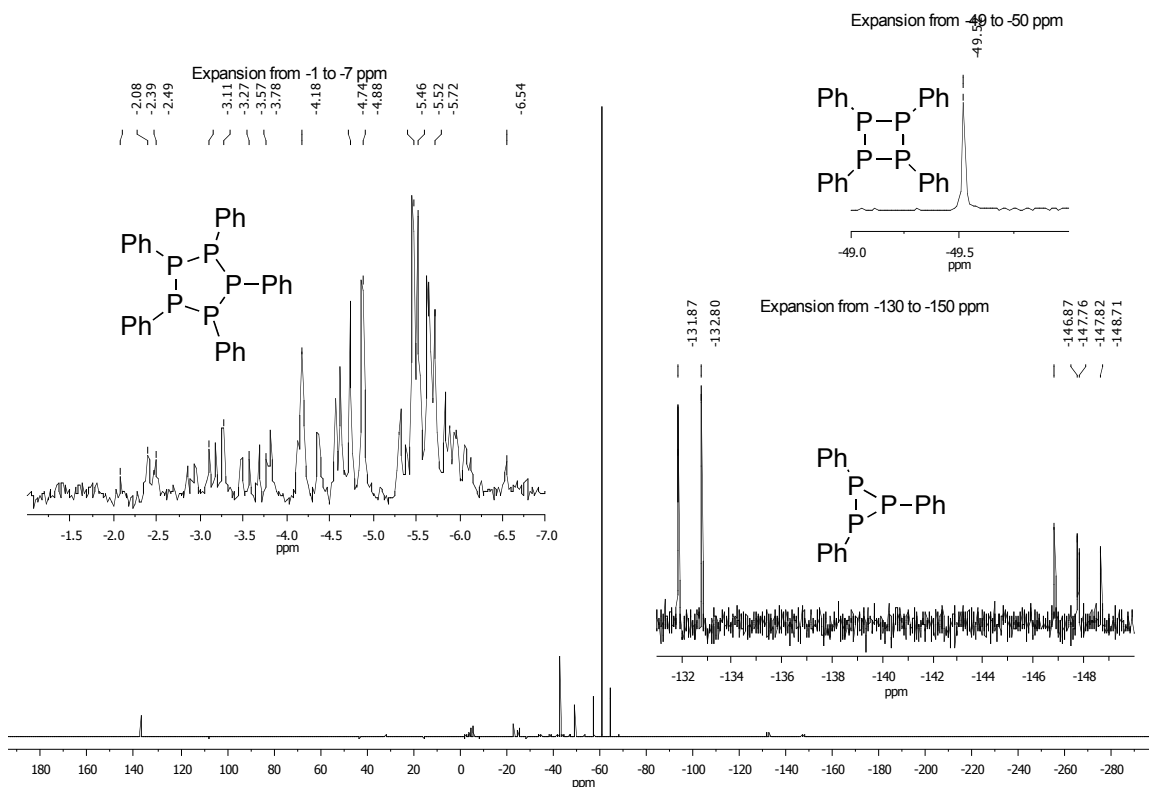
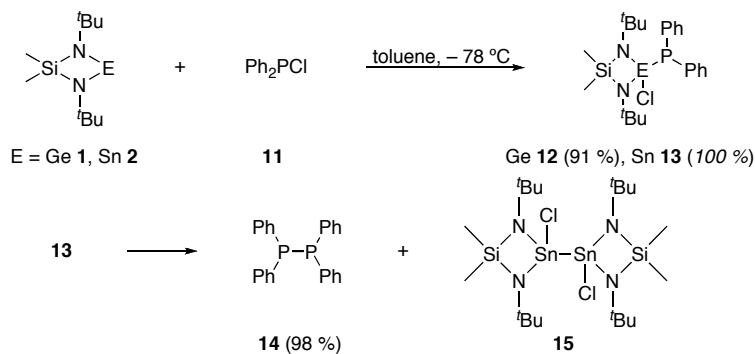


Figure 4.  $^{31}\text{P}\{^1\text{H}\}$  NMR spectrum of cyclic oligophosphines **6–10** obtained from the breakdown of **5**.



Scheme 44. Reactions of carbenoids **1** and **2** with chlorodiphenylphosphine **11**.

Once again, the gerylene insertion product **12** proved stable while the stannylene insertion product **13**, was not. Breakdown of  $\text{Me}_2\text{Si}(\mu\text{-N}^t\text{Bu})_2\text{Sn}(\text{Cl})\text{PPh}_2$ , **13**, resulted in the formation of the diphosphine  $\text{Ph}_2\text{PPPPh}_2$  **14**, identified by its  $^{31}\text{P}\{^1\text{H}\}$  signal at  $\delta -16.0$  ppm in  $\text{C}_6\text{D}_6$  (in accord with literature data),<sup>104</sup> and the newly obtained and

structurally characterized distannane **15**. No other products or intermediates were observed.

These results led to no real conclusion on the insertion mechanism. Decomposition of stannylene insertion products were previously proposed to proceed via a radical pathway, although this was based solely on the weakness of Sn–P bonds.<sup>75,76</sup> The first evidence supporting this theory was given by the isolation of the distannane  $[\text{Me}_2\text{Si}(\mu\text{-N}^t\text{Bu})_2\text{Sn}(\text{Cl})]_2$  **15** (Figure 5).

The distannane **15** crystallized from toluene, after having been stored for several weeks at  $-5\text{ }^\circ\text{C}$ , as orange, rectangular prisms in the monoclinic space group  $P2_1/c$  with  $Z = 4$ . Additional crystallographic data for **15** can be found in Table 8. The Sn–Sn distance of  $2.7797(12)\text{ \AA}$  is shorter than would be expected given the covalent radius of tin.<sup>105</sup> The rings are non-coplanar and the chloride atoms display a gauche-type conformation with a Cl–Sn–Sn–Cl torsion angle of  $68.59(8)^\circ$ . There are no interactions to favor the chlorides taking a true anti conformation (i.e., Cl–Sn–Sn–Cl equal to  $180^\circ$ ) other than electronic repulsion. No H-bonding was observed and only van der Waals forces were responsible for the intermolecular arrangement within the crystal.

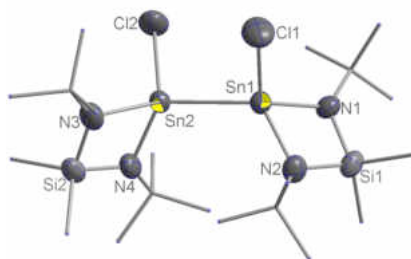


Figure 5. Crystal structure of **15**. Thermal ellipsoids are drawn at 50 % probability.

Hydrogen atoms have been omitted and *tert*-butyl and methyl groups are drawn as

wireframes for clarity.

Table 8. Crystal data for compound **15**.

Molecular Formula	C <sub>20</sub> H <sub>48</sub> Cl <sub>2</sub> N <sub>4</sub> Si <sub>2</sub> Sn <sub>2</sub>
Formula Weight (g/mol)	709.08
Crystal System	monoclinic
Space Group	<i>P</i> 2 <sub>1</sub> / <i>c</i> (No. 14)
<i>a</i> , Å	16.175(10)
<i>b</i> , Å	12.434(7)
<i>c</i> , Å	17.246(10)
$\alpha$ , °	90
$\beta$ , °	108.827(9)
$\gamma$ , °	90
<i>V</i> , Å <sup>3</sup>	3283(3)
<i>Z</i>	4
F(000)	1432
$\rho_{\text{calcd}}$ , g cm <sup>-3</sup>	1.435
$\lambda$ , Å	0.71073
Temperature, K	173
<i>h</i> , min/max	-21/21
<i>k</i> , min/max	-15/16
<i>l</i> , min/max	-22/21
2 $\theta$ maximum, °	56.66
$\mu$ , mm <sup>-1</sup>	1.771
# Reflections Collected	22017
# Unique Reflections ( <i>R</i> <sub>int</sub> )	6175 (0.0346)
<i>R</i> (F) <sup>a</sup>	0.0336
<i>R</i> <sub>w</sub> (F <sup>2</sup> ) <sup>b</sup>	0.1462
Goof	1.138

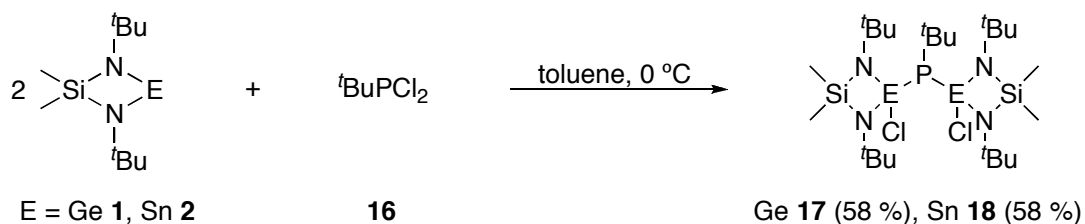
$${}^a R = \sum |F_o - F_c| / \sum |F_o|, \quad {}^b R_w = \{[\sum w(F_o - F_c)^2 / [\sum w(F_o^2)^2]\}^{1/2}; \quad w = 1/[\sigma^2(F_o)^2 + (xP)^2 + yP],$$

where  $P = (F_o^2 + 2F_c^2)/3$ .

Table 9. Selected bond lengths and angles for compound **15**.

Bond Lengths (Å)			
Sn(1)–N(1)	2.005(5)	Sn(2)–Cl(2)	2.3562(17)
Sn(1)–N(2)	2.008(5)	Si(1)–N(2)	1.742(5)
Sn(1)–Cl(1)	2.3695(19)	Si(1)–N(1)	1.745(5)
Sn(1)–Sn(2)	2.7799(12)	Si(2)–N(4)	1.723(5)
Sn(2)–N(3)	2.005(5)	Si(2)–N(3)	1.743(6)
Sn(2)–N(4)	2.026(5)		
Bond Angles (°)			
N(1)–Sn(1)–N(2)	77.1(2)	Cl(2)–Sn(2)–N(3)	111.06(16)
Cl(1)–Sn(1)–N(1)	114.48(15)	Cl(2)–Sn(2)–N(4)	113.20(15)
Cl(1)–Sn(1)–N(2)	113.57(16)	N(3)–Sn(2)–Sn(1)	125.64(16)
N(1)–Sn(1)–Sn(2)	124.16(14)	N(4)–Sn(2)–Sn(1)	121.30(14)
N(2)–Sn(1)–Sn(2)	122.63(15)	Cl(1)–Sn(1)–Sn(2)	106.62(6)
Cl(1)–Sn(1)–Sn(2)	103.89(7)	N(1)–Si(1)–N(2)	91.6(2)
N(3)–Sn(2)–N(4)	76.7(2)	N(3)–Si(2)–N(4)	92.4(2)

In an effort to study the both the electronic and steric effects of the substituents on phosphorus, the slightly electron-withdrawing and sterically smaller phenyl group was replaced with the strongly electron-donating and bulky *tert*-butyl group. Me<sub>2</sub>Si( $\mu$ -N<sup>*t*</sup>Bu)<sub>2</sub>M (M = Ge **1** and Sn **2**) were added to <sup>*t*</sup>BuPCl<sub>2</sub> **16** in a 2:1 ratio (Scheme 45).

Scheme 45. Reactions of carbenoids **1** and **2** with *tert*-butyldichlorophosphine **16**.



To our surprise, both the germylene diinsertion product,  $[\text{Me}_2\text{Si}(\mu\text{-N}^t\text{Bu})_2\text{Ge}(\text{Cl})]_2\text{P}^t\text{Bu}$  **17** (Figure 6), and stannylene diinsertion,  $[\text{Me}_2\text{Si}(\mu\text{-N}^t\text{Bu})_2\text{Sn}(\text{Cl})]_2\text{P}^t\text{Bu}$  **18** (Figure 7), were found to be stable and isolable. This is the first example of a stable insertion product resulting from the addition of a stannylene to a halophosphine.

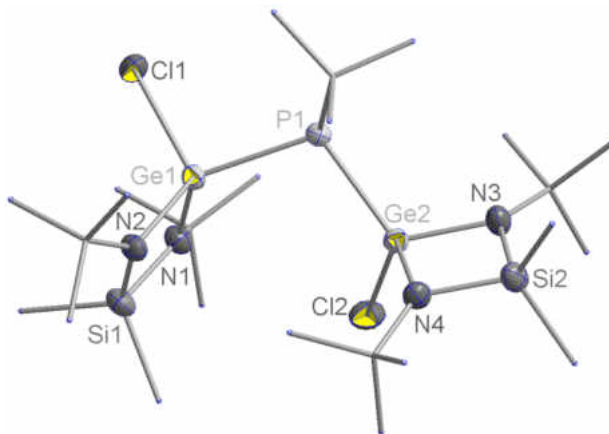


Figure 6. Crystal structure of **17**. Thermal ellipsoids are drawn at 50 % probability. Hydrogen atoms have been omitted and *tert*-butyl and methyl groups are drawn as wireframes for clarity.

The diinsertion product **17** crystallized from toluene at 3 °C as colorless chunk crystals in the monoclinic space group  $P2_1/c$  with  $Z = 4$ . Additional crystallographic data for **17** can be found in Table 11. The Ge–P distances of 2.3365(5) and 2.3286(5) Å are nearly identical to the Ge–P bond lengths of the analogous phenyl-substituted diinsertion **4** with bond lengths of 2.3315(8) and 2.3226(8) Å. All other bonds in **17** are similarly close to their corresponding bonds in **4**, with the exception of the lone P–C bond. In **17**, the P–C bond of 1.906(2) Å is significantly longer than its counterpart in **4** at 1.837(3). This can mostly be attributed to the difference in P–C lengths for  $sp^3$  versus  $sp^2$  carbons.

Surprisingly, the Ge–P–Ge bond angle is only slightly smaller in **17** at 107.67(2)° versus 108.78(3) in **4**, implying a small repulsive effect for the *tert*-butyl compared to the phenyl group. However, the C–P–Ge angles of 104.52(7) and 113.38(7)° for **17** versus 103.85(10) and 105.29(11)° indicate that the *tert*-butyl group's repulsive effect is likely significant, but the P-center lost a significant degree of its pyramidal character. This is displayed in the angle sum around P for **17** of 325.51(16)° versus 317.92(24)° for **4**.

Table 10. Crystal data for compound **17**.

Molecular Formula	C <sub>24</sub> H <sub>57</sub> Cl <sub>2</sub> Ge <sub>2</sub> N <sub>4</sub> PSi <sub>2</sub>
Formula Weight (g/mol)	704.97
Crystal System	monoclinic
Space Group	<i>P</i> 2 <sub>1</sub> / <i>c</i> (No. 14)
<i>a</i> , Å	16.782(3)
<i>b</i> , Å	18.699(3)
<i>c</i> , Å	11.7227(19)
$\alpha$ , °	90
$\beta$ , °	100.186(2)
$\gamma$ , °	90
<i>V</i> , Å <sup>3</sup>	3620.7(10)
<i>Z</i>	4
F(000)	1480
$\rho_{\text{calcd}}$ , g cm <sup>-3</sup>	1.293
$\lambda$ , Å	0.71073
Temperature, K	173
<i>h</i> , min/max	-21/21
<i>k</i> , min/max	-24/24
<i>l</i> , min/max	-15/15
2 $\theta$ maximum, °	56.48
$\mu$ , mm <sup>-1</sup>	1.937
# Reflections Collected	29782
# Unique Reflections ( <i>R</i> <sub>int</sub> )	7862 (0.0242)
<i>R</i> (F) <sup>a</sup>	0.0238
<i>R</i> <sub>w</sub> (F <sup>2</sup> ) <sup>b</sup>	0.0659
Goof	0.944

$${}^a R = \sum |F_o - F_c| / \sum |F_o| \quad {}^b R_w = \{[\sum w(F_o - F_c)^2 / [\sum w(F_o^2)^2]\}^{1/2}; w = 1/[\sigma^2(F_o)^2 + (xP)^2 + yP],$$

where  $P = (F_o^2 + 2F_c^2)/3$ .

Table 11. Selected bond lengths and angles for compound **17**.

Bond Lengths (Å)			
Ge(1)–N(1)	1.8323(17)	Ge(2)–Cl(2)	2.1844(6)
Ge(1)–N(2)	1.8455(17)	Ge(2)–P(1)	2.3294(6)
Ge(1)–Cl(1)	2.2056(6)	Si(1)–N(1)	1.7375(18)
Ge(1)–P(1)	2.3358(6)	Si(1)–N(2)	1.7462(19)
Ge(1)–Si(1)	2.6062(7)*	Si(2)–N(3)	1.7404(19)
Ge(2)–N(3)	1.8336(17)	Si(2)–N(4)	1.7454(19)
Ge(2)–N(4)	1.8338(17)	P(1)–C(5)	1.906(2)
Bond Angles (°)			
N(1)–Ge(1)–N(2)	83.69(8)	Cl(2)–Ge(2)–P(1)	104.52(2)
N(1)–Ge(1)–Cl(1)	111.15(6)	C(5)–P(1)–Ge(2)	104.52(7)
N(2)–Ge(1)–Cl(1)	111.44(5)	C(5)–P(1)–Ge(1)	113.38(7)
N(1)–Ge(1)–P(1)	115.23(5)	Ge(2)–P(1)–Ge(1)	107.67(2)
N(2)–Ge(1)–P(1)	133.88(6)	N(1)–Si(1)–N(2)	89.54(8)
Cl(1)–Ge(1)–P(1)	100.49(2)	N(3)–Si(2)–N(4)	88.81(8)
N(3)–Ge(2)–N(4)	83.38(8)	Si(1)–N(1)–Ge(1)	93.75(8)
N(3)–Ge(2)–Cl(2)	111.27(6)	Si(1)–N(2)–Ge(1)	93.00(8)
N(4)–Ge(2)–Cl(2)	111.56(6)	Si(2)–N(3)–Ge(2)	93.93(8)
N(3)–Ge(2)–P(1)	114.85(6)	Si(2)–N(4)–Ge(2)	93.75(8)
N(4)–Ge(2)–P(1)	129.72(6)		

\* non-bonding distance

The diinsertion product **15** crystallized as yellow, irregularly-shaped crystals from hexanes at rt in the triclinic space group  $P\bar{1}$  with  $Z = 4$ . Two independent molecules were found in the unit cell. Additional crystallographic data for **15** can be found in Table 12. The Sn–P bonds are typical at 2.5083(8) and 2.4937(8) Å. The stannylene insertion product **18** is quite similar to its germanium analogue **17**: the P–C bond length of 1.901(3) Å in **18** is nearly identical to the 1.906(2) Å found in **17**. Any extra bulk from

the size of tin versus germanium (van der Waals radii of 2.17 and 2.00 Å, respectively) is ameliorated by the longer Sn–P versus Ge–P bond lengths. This effect can be observed by the greater pyramidal character of phosphorus in **18** versus **17** with total angle sums of 320.18(23)° and 325.51(16)°, respectively.

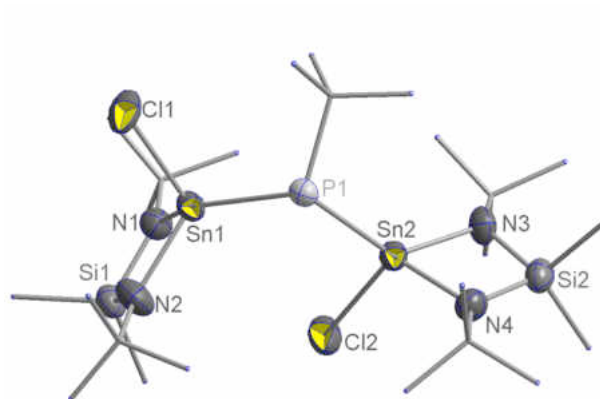


Figure 7. Crystal structure of **18**. Thermal ellipsoids are drawn at 50 % probability. Hydrogen atoms have been omitted and *tert*-butyl and methyl groups are drawn as wireframes for clarity.

Table 12. Crystal data for compound **18**.

Molecular Formula	C <sub>24</sub> H <sub>57</sub> Cl <sub>2</sub> N <sub>4</sub> PSi <sub>2</sub> Sn <sub>2</sub>
Formula Weight (g/mol)	797.17
Crystal System	triclinic
Space Group	<i>P</i> -1 (No. 2)
<i>a</i> , Å	12.4363(14)
<i>b</i> , Å	16.8886(19)
<i>c</i> , Å	19.353(2)
$\alpha$ , °	93.611(2)
$\beta$ , °	106.664(2)
$\gamma$ , °	100.286(2)
<i>V</i> , Å <sup>3</sup>	3803.3(7)
<i>Z</i>	4
F(000)	1588
$\rho_{\text{calcd}}$ , g cm <sup>-3</sup>	1.392
$\lambda$ , Å	0.71073
Temperature, K	173
<i>h</i> , min/max	-16/15
<i>k</i> , min/max	-22/21
<i>l</i> , min/max	-24/25
2 $\theta$ maximum, °	56.62
$\mu$ , mm <sup>-1</sup>	1.577
# Reflections Collected	29902
# Unique Reflections ( <i>R</i> <sub>int</sub> )	14842 (0.0167)
<i>R</i> (F) <sup>a</sup>	0.0316
<i>R</i> <sub>w</sub> (F <sup>2</sup> ) <sup>b</sup>	0.0853
Goof	1.016

$${}^a R = \sum |F_o - F_c| / \sum |F_o| \quad {}^b R_w = \{[\sum w(F_o - F_c)^2 / [\sum w(F_o^2)^2]\}^{1/2}; w = 1/[\sigma^2(F_o)^2 + (xP)^2 + yP],$$

where  $P = (F_o^2 + 2F_c^2)/3$ .

Table 13. Selected bond lengths and angles for one of two independent molecules in the unit cell of compound **18**.

Bond Lengths (Å)			
Sn(1)–N(1)	2.024(3)	Sn(2)–P(1)	2.4937(8)
Sn(1)–N(2)	2.031(2)	Sn(2)–Si(2)	2.7886(9)*
Sn(1)–Cl(1)	2.3837(9)	Si(1)–N(1)	1.733(3)
Sn(1)–P(1)	2.5082(8)	Si(1)–N(2)	1.734(3)
Sn(1)–Si(1)	2.7882(9)*	Si(2)–N(3)	1.748(3)
Sn(2)–N(3)	2.032(2)	Si(2)–N(4)	1.730(3)
Sn(2)–N(4)	2.020(3)	P(1)–C(5)	1.901(3)
Sn(2)–Cl(2)	2.3570(9)		
Bond Angles (°)			
N(2)–Sn(1)–N(1)	76.48(11)	Cl(2)–Sn(2)–P(1)	103.38(3)
N(2)–Sn(1)–Cl(1)	109.41(10)	C(1)–P(1)–Sn(2)	106.47(10)
N(1)–Sn(1)–Cl(1)	109.53(8)	C(1)–P(1)–Sn(1)	109.66(10)
N(2)–Sn(1)–P(1)	119.30(9)	Sn(2)–P(1)–Sn(1)	104.05(3)
N(1)–Sn(1)–P(1)	140.56(8)	N(1)–Si(1)–N(2)	92.75(13)
Cl(1)–Sn(1)–P(1)	99.03(3)	N(3)–Si(2)–N(4)	92.65(13)
N(4)–Sn(2)–N(3)	76.74(11)	Si(1)–N(1)–Sn(1)	95.26(12)
N(4)–Sn(2)–Cl(2)	112.39(8)	Si(1)–N(2)–Sn(1)	95.51(13)
N(3)–Sn(2)–Cl(2)	111.85(8)	Si(2)–N(3)–Sn(2)	94.78(12)
N(4)–Sn(2)–P(1)	115.76(8)	Si(2)–N(4)–Sn(2)	95.76(13)
N(3)–Sn(2)–P(1)	134.31(8)		

\* non-bonding distance

Both the stannylene and germylene reactions again proceeded at low temperature, though they were significantly slower than reactions with the phenyl analogue. Action of the germylene on the dichlorophosphine could even be easily tracked through both insertion steps (Figure 8).

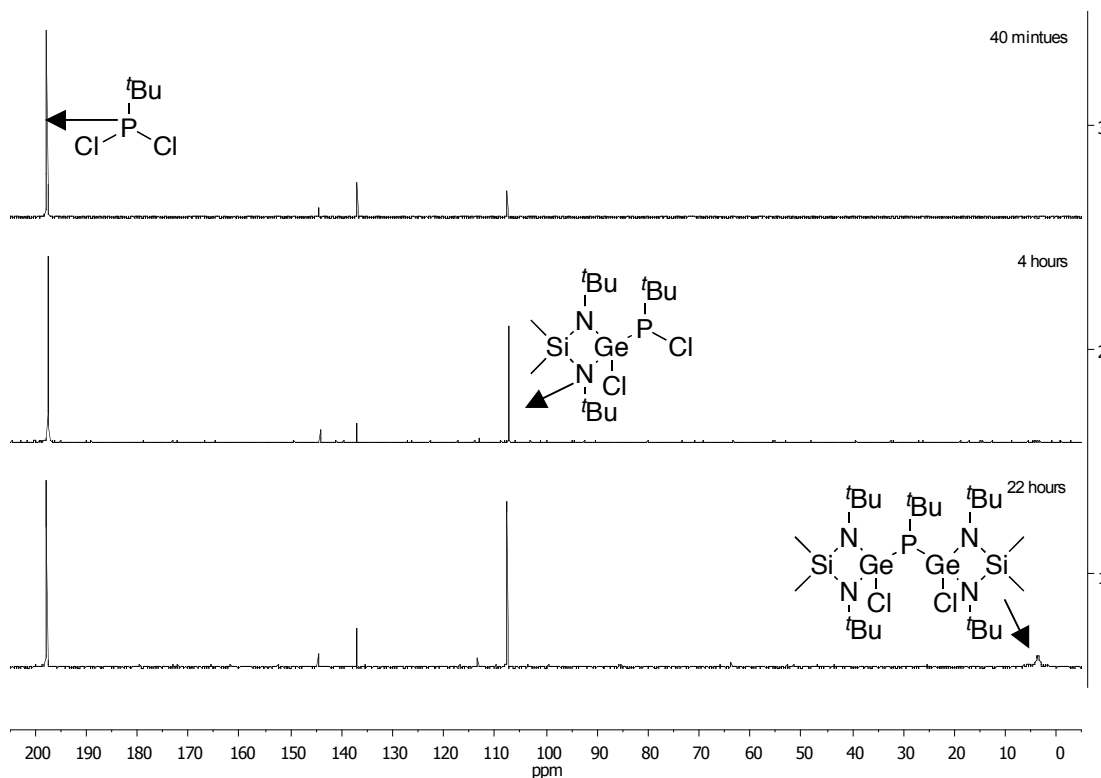
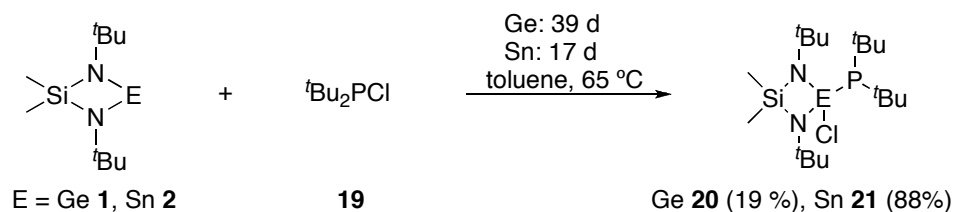


Figure 8.  $^{31}\text{P}\{^1\text{H}\}$  NMR spectra of **17** and its monoinsertion intermediate.

Due to the stability of the tin insertion product **18**, we set out to determine if this was intrinsic to this phosphine only and/or if only dihalophosphines insertion products are stable. Addition of  $\text{Me}_2\text{Si}(\mu\text{-N}^t\text{Bu})_2\text{M}$  ( $\text{M} = \text{Ge}$  **1** and  $\text{Sn}$  **2**) to  $^t\text{Bu}_2\text{PCl}$  **19** was used to test these postulates. Both germylene and stannylene insertion products, **20** and **21**, respectively, were found to be stable and isolable (Scheme 46) and single-crystal X-ray analyses were conducted for both products (shown in Figures 9 and 10, respectively).



Scheme 46. Reactions of carbenoids **1** and **2** with di-*tert*-butylchlorophosphine **19**.



The insertion product,  $[\text{Me}_2\text{Si}(\mu\text{-N}^t\text{Bu})_2\text{Ge}(\text{Cl})]\text{P}^t\text{Bu}_2$  **20**, crystallized as colorless, irregularly-shaped crystals from toluene after the solution had been stored for several weeks at 5 °C in toluene. The crystals were monoclinic, crystallizing in the space group  $P2_1/c$  with  $Z = 4$ . Additional crystallographic data for **20** can be found in Table 14. The Ge–P bond of 2.3425(4) Å is slightly longer than those in previous examples. Ge–P lengths of 2.3365(5) and 2.3286(5) Å were observed in the *tert*-butyl-substituted germylene diinsertion product **17** and 2.3315(8) and 2.3226(8) Å were observed in the phenyl-substituted compound **4**. Surprisingly, the P–C bond lengths of 1.9016(15) and 1.8885(15) in **20** are very close to the lone P–C bond in **17** at 1.906(2) Å despite the bulk of two *tert*-butyl groups. However, the repulsion of these groups can be observed in the reduced pyramidalization around phosphorus, which shows an angle sum of 329.18(17)° versus 325.51(23)° in **17**.

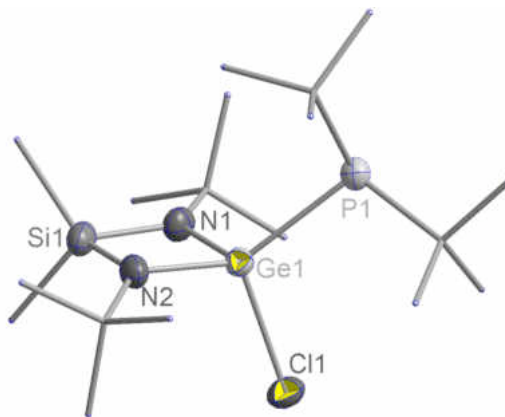


Figure 9. Crystal structure of **20**. Thermal ellipsoids are drawn at 50 % probability. Hydrogen atoms have been omitted and *tert*-butyl and methyl groups are drawn as wireframes for clarity.

Table 14. Crystal data for compound **20**.

Molecular Formula	C <sub>18</sub> H <sub>42</sub> ClGeN <sub>2</sub> PSi
Formula Weight (g/mol)	453.64
Crystal System	monoclinic
Space Group	<i>P</i> 2 <sub>1</sub> / <i>c</i> (No. 14)
<i>a</i> , Å	11.2153(12)
<i>b</i> , Å	11.8227(13)
<i>c</i> , Å	18.439(2)
$\alpha$ , °	90
$\beta$ , °	93.948(2)
$\gamma$ , °	90
<i>V</i> , Å <sup>3</sup>	2439.2(5)
<i>Z</i>	4
F(000)	968
$\rho_{\text{calcd}}$ , g cm <sup>-3</sup>	1.235
$\lambda$ , Å	0.71073
Temperature, K	173
<i>h</i> , min/max	-14/14
<i>k</i> , min/max	-15/14
<i>l</i> , min/max	-24/24
2 $\theta$ maximum, °	56.48
$\mu$ , mm <sup>-1</sup>	1.215
# Reflections Collected	19840
# Unique Reflections ( <i>R</i> <sub>int</sub> )	5315 (0.0188)
<i>R</i> (F) <sup>a</sup>	0.0256
<i>R</i> <sub>w</sub> (F <sup>2</sup> ) <sup>b</sup>	0.0742
Goof	1.064

$${}^a R = \sum |F_o - F_c| / \sum |F_o|, \quad {}^b R_w = \{[\sum w(F_o - F_c)^2 / [\sum w(F_o^2)^2]\}^{1/2}; \quad w = 1/[\sigma^2(F_o)^2 + (xP)^2 + yP],$$

where  $P = (F_o^2 + 2F_c^2)/3$ .

Table 15. Selected bond lengths and angles for compound **20**.

Bond Lengths (Å)			
Ge(1)–N(1)	1.8365(12)	P(1)–C(30)	1.8885(15)
Ge(1)–N(2)	1.8365(12)	P(1)–C(40)	1.9016(15)
Ge(1)–Cl(1)	2.2172(4)	Si(1)–N(1)	1.7369(13)
Ge(1)–P(1)	2.3427(4)	Si(1)–N(2)	1.7450(14)
Bond Angles (°)			
N(1)–Ge(1)–N(2)	83.22(6)	Cl(1)–Ge(1)–P(1)	109.117(17)
N(1)–Ge(1)–Cl(1)	109.09(4)	C(30)–P(1)–Ge(1)	108.41(5)
N(2)–Ge(1)–Cl(1)	107.45(4)	C(40)–P(1)–Ge(1)	104.79(5)
N(1)–Ge(1)–P(1)	111.93(4)	C(30)–P(1)–C(40)	111.66(7)
N(2)–Ge(1)–P(1)	132.23(4)	N(1)–Si(1)–N(2)	89.21(6)

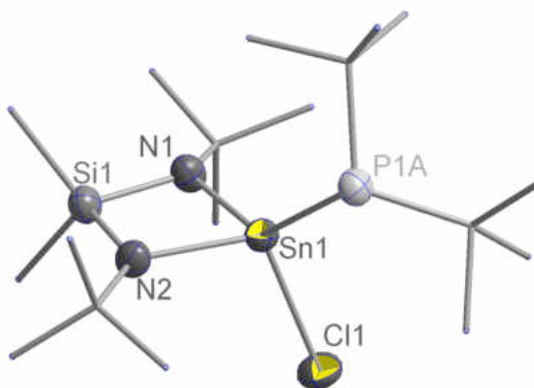


Figure 10. Crystal structure of **21**. Thermal ellipsoids are drawn at 50 % probability.

Hydrogen atoms have been omitted and *tert*-butyl and methyl groups are drawn as wireframes for clarity.

$[\text{Me}_2\text{Si}(\mu\text{-N}^t\text{Bu})_2\text{Sn}(\text{Cl})]\text{P}^t\text{Bu}_2$  **21** also crystallized from toluene at 3 °C and, like its germanium counterpart, in the space group  $P2_1/c$  with four molecules in the unit cell. Additional crystallographic data for **21** can be found in Table 16. The Sn–P bond is

slightly shorter at 2.4718(10) Å compared to the Sn–P distances in the *tert*-butyl-substituted diinsertion **18** at 2.5083(8) and 2.4937(8) Å. The tin monoinsertion product shows similar trends to its germanium analogue **20**. A reduction in pyramidal character of phosphorus from 320.18(23)° in **18** to 321.58(16)° in **21** is observed following replacement of a chlorostannyl group with a *tert*-butyl. This difference of 3.40° is nearly identical to the difference observed of 3.67° for the analogous germanium compounds **17** and **20**.

Table 16. Crystal data for compound **21**.

Molecular Formula	C <sub>18</sub> H <sub>42</sub> ClN <sub>2</sub> PSiSn
Formula Weight (g/mol)	499.74
Crystal System	monoclinic
Space Group	<i>P</i> 2 <sub>1</sub> / <i>c</i> (No. 14)
<i>a</i> , Å	16.0010(14)
<i>b</i> , Å	9.0520(8)
<i>c</i> , Å	18.8509(16)
$\alpha$ , °	90
$\beta$ , °	110.2880(10)
$\gamma$ , °	90
<i>V</i> , Å <sup>3</sup>	2561.0(4)
<i>Z</i>	4
F(000)	1040
$\rho_{\text{calcd}}$ , g cm <sup>-3</sup>	1.296
$\lambda$ , Å	0.71073
Temperature, K	173
<i>h</i> , min/max	-20/21
<i>k</i> , min/max	-11/11
<i>l</i> , min/max	-25/23
2 $\theta$ maximum, °	56.48
$\mu$ , mm <sup>-1</sup>	1.215
# Reflections Collected	20788
# Unique Reflections ( <i>R</i> <sub>int</sub> )	5543 (0.0164)
<i>R</i> (F) <sup>a</sup>	0.0249
<i>R</i> <sub>w</sub> (F <sup>2</sup> ) <sup>b</sup>	0.0676
Goof	1.050

$${}^a R = \sum |F_o - F_c| / \sum |F_o|, \quad {}^b R_w = \{[\sum w(F_o - F_c)^2 / [\sum w(F_o^2)^2]\}^{1/2}; \quad w = 1/[\sigma^2(F_o)^2 + (xP)^2 + yP],$$

where  $P = (F_o^2 + 2F_c^2)/3$ .

Table 17. Selected bond lengths and angles for compound **21**.

Bond Lengths (Å)			
Sn(1)–N(1)	2.0372(16)	Si(1)–N(1)	1.7386(17)
Sn(1)–N(2)	2.0314(17)	P(1A)–C(30)	1.846(2)
Sn(1)–Cl(1)	2.3879(5)	P(1A)–C(40A)	1.883(10)
Sn(1)–P(1A)	2.4716(9)	P(1B)–C(30)	1.882(3)
Sn(1)–P(1B)	2.5942(10)	P(1B)–C(40B)	1.892(11)
Si(1)–N(2)	1.7322(18)		
Bond Angles (°)			
N(1)–Sn(1)–N(2)	76.34(7)	N(2)–Si(1)–N(1)	92.85(8)
N(1)–Sn(1)–Cl(1)	107.46(5)	Si(1)–N(2)–Sn(1)	95.59(8)
N(2)–Sn(1)–Cl(1)	107.73(5)	Si(1)–N(1)–Sn(1)	95.19(7)
N(2)–Sn(1)–P(1A)	112.14(5)	C(30)–P(1A)–C(40A)	110.5(4)
N(1)–Sn(1)–P(1A)	136.13(5)	C(30)–P(1A)–Sn(1)	108.93(9)
Cl(1)–Sn(1)–P(1A)	109.84(3)	C(40A)–P(1A)–Sn(1)	102.8(3)
N(2)–Sn(1)–P(1B)	136.57(6)	C(30)–P(1B)–C(40B)	116.5(4)
N(1)–Sn(1)–P(1B)	113.53(5)	C(30)–P(1B)–Sn(1)	103.06(9)
Cl(1)–Sn(1)–P(1B)	108.80(3)	C(40B)–P(1B)–Sn(1)	102.2(4)
P(1A)–Sn(1)–P(1B)	31.53(3)		

In stark contrast to the aforementioned reactions, both insertions proceeded exceptionally slowly. A reaction temperature of 60 °C was used with the stannylene insertion requiring ca. 2 weeks to achieve an 88 % yield and the germylene insertion requiring a staggering 5 weeks to achieve a meager 19 % yield.

The significant increase in time required for insertion into *tert*-butyl-substituted chlorophosphines versus their phenyl counterparts, seemed to indicate that the insertion mechanism was more likely proceeding through an S<sub>N</sub>2-like pathway as opposed to a

radical-based one. Were a radical pathway in play, the added bulk of the *tert*-butyl group should be more shielding than the phenyl substituent and thus the reaction should proceed more rapidly for the former. Additionally, the electronic effects of *tert*-butyl group would seem to be preferable to the phenyl moiety in terms of stabilizing a radical in the same way that  $(\text{CH}_3)_3\text{C}\cdot$  is more stable than the phenyl radical ion. Since observations were contrary to that, we began to favor an  $\text{S}_{\text{N}}2$ -like mechanism over a radical mechanism.

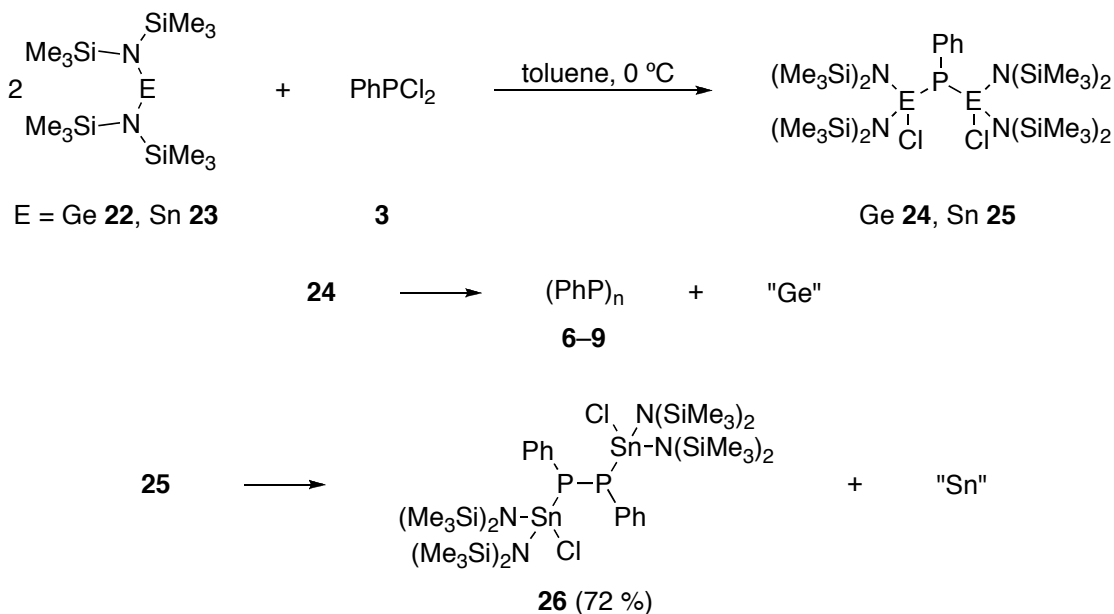
Perhaps more interesting was the isolation of two stannylene insertion products. With the data obtained to this point, we conjectured that a radical mechanism may not be at work for the decomposition of stannylene insertion products. For the same reasons mentioned above, formation of the di-*tert*-butylphosphine radical ion should be more favorable than that of its phenyl counterpart. However, given the fact that both the steric effects and electronic effects were significantly different between the two substituents, no further inferences could be made regarding the decomposition mechanism.

#### *Insertion reactions of acyclic stannylenes and germylenes*

Utilizing the acyclic stannylene and germylene  $[(\text{Me}_3\text{Si})_2\text{N}]_2\text{M}$  (M = Ge **22** and Sn **23**), we decided to test reactivities with all of the previously used chlorophosphines. We felt that the lack of ring strain and added bulk of the bis(trimethylsilyl)amide substituents might favor stable insertion products in the same way as the *tert*-butyl group did when attached to the phosphorus center.

Addition of  $[(\text{Me}_3\text{Si})_2\text{N}]_2\text{M}$  (M = Ge **22**, Sn **23**) to  $\text{PhPCl}_2$  **3** in a 2:1 ratio provided very unusual results (Scheme 47). First, the germylene insertion product **24** was not observed to be stable (no other germylene-halophosphine combination has ever been found to behave in this way). It decomposed to provide the same cyclic oligophosphines

observed for the decomposition of  $[\text{Me}_2\text{Si}(\mu\text{-N}^t\text{Bu})_2\text{Sn}(\text{Cl})_2]\text{PPh}$  **5** though in a ratio of 3:5:8 for  $(\text{PhP})_3$  **6**,  $(\text{PhP})_4$  **7**, and  $(\text{PhP})_5$  **8**. Additionally, the  $^{31}\text{P}$  NMR signal associated with the germylene insertion product was shifted considerably downfield compared to its cyclic counterpart at  $\delta$  67.7 ppm versus  $-55.2$  ppm for **4**. We believed that this could be due to only a single insertion occurring, but, with no observable Ge–P couplings, this could not be confirmed. Based on this result, it was expected that addition of the acyclic stannylene **23** to  $\text{PhPCl}_2$  should fall in line with other observed results and also provide the oligophosphines **6–10** shown in Scheme 1. To our surprise, the product **26**, displaying a Sn–P–P–Sn motif, was obtained in nearly quantitative yield. Attempts to prove the hypothesized meta-stability of **26** failed when heating to reflux in toluene for 8 h did not cause decomposition.



Scheme 47. Reactions of acyclic carbenoids **22** and **23** with dichlorophenylphosphine **3**.



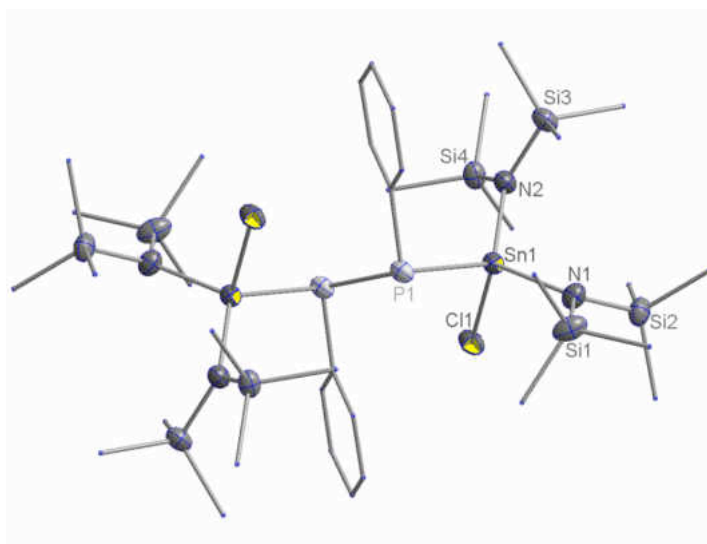


Figure 11. Crystal structure of **26**. Thermal ellipsoids are drawn at 50 % probability.

Hydrogen atoms have been omitted and phenyl and methyl groups are drawn as wireframes for clarity.

Product **26** has an interesting structure; it is unlike any other compound we had previously obtained. It crystallized from toluene at 3 °C as yellow rhomboids in the triclinic space group  $P\bar{1}$ , but with only one molecule in the unit cell ( $Z = 1$ ). This indicates the asymmetric unit is half of the molecule. Additional crystallographic data for **26** can be found in Table 18. The P–P distance of 2.2360(10) Å is consistent with a P–P single bond, thus **26** is cannot be interpreted as a stabilized diphosphene, although it could be viewed as a “trapped” one. Also, the presence of an inversion center at the center of the P–P bond renders both halves of the molecule metrically equivalent to one another, with every metric (bond lengths and angles) equivalent. The Sn–P bond length of 2.5706(6) Å is significantly longer than any previously observed. For comparison, the next longest examples are the 2.4718(10) Å displayed in the monoinsertion product **21** and 2.5083(8) and 2.4937(8) Å in the diinsertion **18**. This observation is attributable to the bulk of the substituents on tin. The P–C distances of 1.839(2) Å are nearly identical to

the phenyl-substituted germylene diinsertion product **4** with a P–C bond length of 1.837(3) Å. The phosphorus centers in **26** show greater pyramidalization than any previously discussed structure with a total angle sum of 300.17(16)°. This is likely due to the increased Sn–P bond length and the effective implementation of a phosphide as a substituent. Overall, this structure shares the most similarity to the acyclic diphosphorus dication (structure **221**, as shown in Chart 4 of the Introduction) reported by Weigand.<sup>94</sup> The P–P bond length of **221** of 2.2400(9) Å is nearly identical to that of **26**, 2.2360(10) Å. The P–C distances of 1.806(2) and 1.814(2) Å in **221** are also quite similar to P–C bond length of 1.8392(2) Å found for **26**.

Table 18. Crystal data for compound **26**.

Molecular Formula	C <sub>36</sub> H <sub>82</sub> Cl <sub>2</sub> N <sub>4</sub> P <sub>2</sub> Si <sub>8</sub> Sn <sub>2</sub>
Formula Weight (g/mol)	1166.00
Crystal System	triclinic
Space Group	<i>P</i> -1 (No. 2)
<i>a</i> , Å	9.5087(10)
<i>b</i> , Å	10.5988(16)
<i>c</i> , Å	15.3895(15)
$\alpha$ , °	75.362(2)
$\beta$ , °	78.652(2)
$\gamma$ , °	70.7470(10)
<i>V</i> , Å <sup>3</sup>	1405.7(2)
<i>Z</i>	1
F(000)	602
$\rho_{\text{calcd}}$ , g cm <sup>-3</sup>	1.377
$\lambda$ , Å	0.71073
Temperature, K	173
<i>h</i> , min/max	-12/12
<i>k</i> , min/max	-13/13
<i>l</i> , min/max	-18/20
2 $\theta$ maximum, °	56.54
$\mu$ , mm <sup>-1</sup>	1.239
# Reflections Collected	11738
# Unique Reflections ( <i>R</i> <sub>int</sub> )	5976 (0.0166)
<i>R</i> (F) <sup>a</sup>	0.0248
<i>R</i> <sub>w</sub> (F <sup>2</sup> ) <sup>b</sup>	0.0685
Goof	1.067

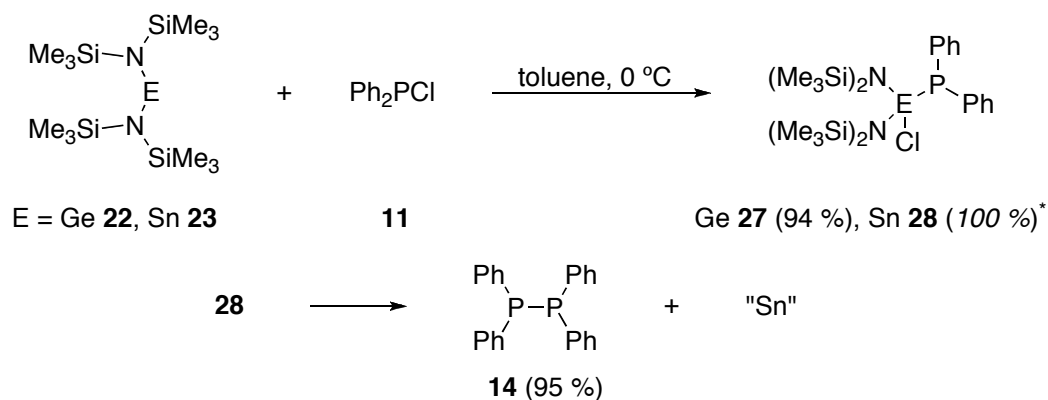
$${}^a R = \sum |F_o - F_c| / \sum |F_o| \quad {}^b R_w = \{[\sum w(F_o - F_c)^2 / [\sum w(F_o^2)^2]\}^{1/2}; w = 1/[\sigma^2(F_o)^2 + (xP)^2 + yP],$$

where  $P = (F_o^2 + 2F_c^2)/3$ .

Table 19. Selected bond lengths and angles for compound **26**.

Bond Lengths (Å)			
Sn(1)–N(2)	2.0449(16)	C(13)–P(1)	1.839(2)
Sn(1)–N(1)	2.0478(16)	Si(1)–N(1)	1.7511(18)
Sn(1)–Cl(1)	2.3653(5)	Si(2)–N(1)	1.7514(18)
Sn(1)–P(1)	2.5706(6)	Si(3)–N(2)	1.7608(17)
P(1)–P(1)	2.2361(10)	Si(4)–N(2)	1.7648(17)
Bond Angles (°)			
N(2)–Sn(1)–N(1)	113.85(7)	Cl(1)–Sn(1)–P(1)	103.631(17)
N(2)–Sn(1)–Cl(1)	105.79(5)	C(13)–P(1)–P(1)	100.26(7)
N(1)–Sn(1)–Cl(1)	101.87(5)	C(13)–P(1)–Sn(1)	99.34(6)
N(2)–Sn(1)–P(1)	119.35(5)	P(1)–P(1)–Sn(1)	100.57(3)
N(1)–Sn(1)–P(1)	110.14(5)		

Following these tests, [(Me<sub>3</sub>Si)<sub>2</sub>N]<sub>2</sub>M (M = Ge **22**, Sn **23**) were combined with Ph<sub>2</sub>PCl (Scheme 48). These reactions appeared to behave much more similarly to those of their cyclic counterparts. The germylene insertion product **27** was found to be isolable and was subsequently characterized by X-ray diffraction studies (Figure 12). The stannylene insertion product, identified by its <sup>31</sup>P{<sup>1</sup>H} NMR signal at δ –8.1 ppm (<sup>1</sup>J<sub>119/117SnP</sub> = 1557/1490 Hz), was observed to decompose, providing the diphosphine Ph<sub>2</sub>PPPh<sub>2</sub> **14** and a tin-containing by-product.



Scheme 48. Reactions of acyclic carbenoids **22** and **23** with chlorodiphenylphosphine **11**.

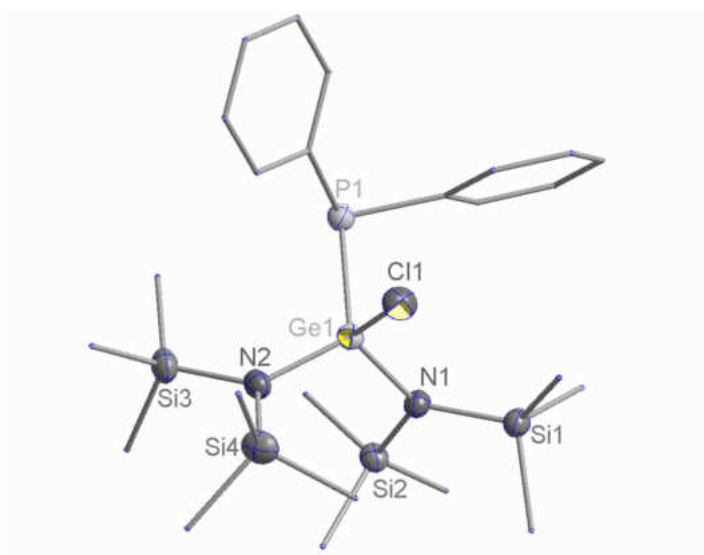


Figure 12. Crystal structure of **27**. Thermal ellipsoids are drawn at 50 % probability.

Hydrogen atoms have been omitted and phenyl and methyl groups are drawn as wireframes for clarity.

Monoinsertion product **27** crystallized from toluene at 3 °C in the triclinic space group  $P\bar{1}$  with  $Z = 2$ . Additional crystallographic data for **27** can be found in Table 20. The Ge–P bond length of 2.3432(7) Å is nearly identical to the 2.3427(4) Å observed for the di-*tert*-butyl-substituted monoinsertion **20** and slightly longer than the 2.3365(5) and

\* Yields given in *italics* are based on NMR observations, and do not represent isolated yields.

2.3286(5), and 2.3315(8) and 2.3226(8) Å for the *tert*-butyl-substituted diinsertion **17** and for the phenyl-substituted diinsertion **4**, respectively. This can be attributed to the bulk of substituents on germanium. Other bond lengths and angles are in normal ranges for the respective contributing atoms, but the total angle sum for the phosphorus center, 330.64(25)°, is larger than that of any previous structure showing even greater planarity and less pyramidal character.

Table 20. Crystal data for compound **27**.

Molecular Formula	C <sub>24</sub> H <sub>46</sub> ClGeN <sub>2</sub> PSi <sub>4</sub>
Formula Weight (g/mol)	614.00
Crystal System	monoclinic
Space Group	<i>P</i> -1 (No. 2)
<i>a</i> , Å	9.0100(10)
<i>b</i> , Å	11.5526(13)
<i>c</i> , Å	17.337(2)
$\alpha$ , °	89.039(2)
$\beta$ , °	78.051(2)
$\gamma$ , °	67.828(2)
<i>V</i> , Å <sup>3</sup>	1631.2(3)
<i>Z</i>	2
F(000)	648
$\rho_{\text{calcd}}$ , g cm <sup>-3</sup>	1.250
$\lambda$ , Å	0.71073
Temperature, K	173
<i>h</i> , min/max	-11/11
<i>k</i> , min/max	-15/15
<i>l</i> , min/max	-22/22
2 $\theta$ maximum, °	56.52
$\mu$ , mm <sup>-1</sup>	1.232
# Reflections Collected	12778
# Unique Reflections ( <i>R</i> <sub>int</sub> )	6335 (0.0186)
<i>R</i> (F) <sup>a</sup>	0.0342
<i>R</i> <sub>w</sub> (F <sup>2</sup> ) <sup>b</sup>	0.0922
Goof	1.051

$${}^a R = \sum |F_o - F_c| / \sum |F_o|, \quad {}^b R_w = \{[\sum w(F_o - F_c)^2 / [\sum w(F_o^2)^2]\}^{1/2}; \quad w = 1/[\sigma^2(F_o)^2 + (xP)^2 + yP],$$

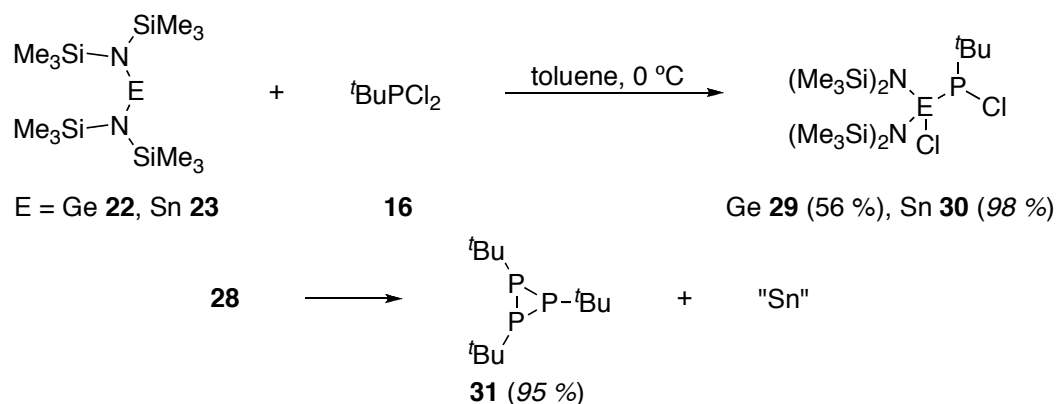
where  $P = (F_o^2 + 2F_c^2)/3$ .

Table 21. Selected bond lengths and angles for compound **27**.

Bond Lengths (Å)			
Ge(1)–N(1)	1.8448(18)	P(1)–C(7)	1.840(2)
Ge(1)–N(2)	1.8497(18)	Si(1)–N(1)	1.7694(19)
Ge(1)–Cl(1)	2.1921(6)	Si(2)–N(1)	1.7709(19)
Ge(1)–P(1)	2.3435(6)	Si(3)–N(2)	1.763(2)
P(1)–C(1)	1.838(2)	Si(4)–N(2)	1.780(2)
Bond Angles (°)			
N(1)–Ge(1)–N(2)	112.26(8)	Cl(1)–Ge(1)–P(1)	103.35(2)
N(1)–Ge(1)–Cl(1)	110.05(6)	C(1)–P(1)–C(7)	103.14(11)
N(2)–Ge(1)–Cl(1)	103.09(6)	C(1)–P(1)–Ge(1)	98.61(7)
N(1)–Ge(1)–P(1)	110.84(6)	C(7)–P(1)–Ge(1)	102.18(7)
N(2)–Ge(1)–P(1)	116.45(6)		

Similar to the reactions with  $\text{PhPCl}_2$ , 2:1 additions of  $[(\text{Me}_3\text{Si})_2\text{N}]_2\text{M}$  ( $\text{M} = \text{Ge}$  **22**,  $\text{Sn}$  **23**) to  ${}^t\text{BuPCl}_2$  **16** again provided unexpected results, but in different ways (Scheme 49). It was anticipated that both reactions should yield isolable diinsertion products like their cyclic analogues; however, the germylene product **29** provided the first observed stable monoinsertion into a dihalophosphine (Figure 12), and the stannylene insertion product **30** decomposed exclusively to the cyclotriphosphine,  $({}^t\text{BuP})_3$  **31**. This nearly exclusive formation of the three-membered phosphorus ring was observed by its interesting  $\text{AB}_2$ -patterned NMR spectrum (Figure 14).





Scheme 49. Reactions of carbenoids **22** and **23** with *tert*-butylidichlorophosphine **16**.

The monoinsertion product **29** crystallized as colorless plates from hexanes at  $-5^\circ\text{C}$  in the triclinic space group  $P\bar{1}$  with  $Z = 2$ . Additional crystallographic data for **29** can be found in Table 22. The Ge–P bond distance, at 2.3992(4) Å (the next closest being 2.3432(7) Å observed in the diphenyl-substituted monoinsertion **27**) is longer than all other Ge–P distances found in this study. The observation can be attributed to the bulk of the substituents on both phosphorus and germanium. The P–C bond at 1.8827(15) Å is comparable to those observed in the di-*tert*-butyl-substituted monoinsertion **20** at 1.8885(15) and 1.9016(15) Å and in the *tert*-butyl-substituted diinsertion **17** at 1.906(2) Å. The significantly longer Ge–P bond is likely responsible for the significantly greater pyramidal character of the phosphorus center in **29** with an angle sum of  $316.26(12)^\circ$  compared to  $330.64(25)^\circ$  in **27**,  $329.18(17)^\circ$  in **20**, and  $325.51(23)^\circ$  in **17**.

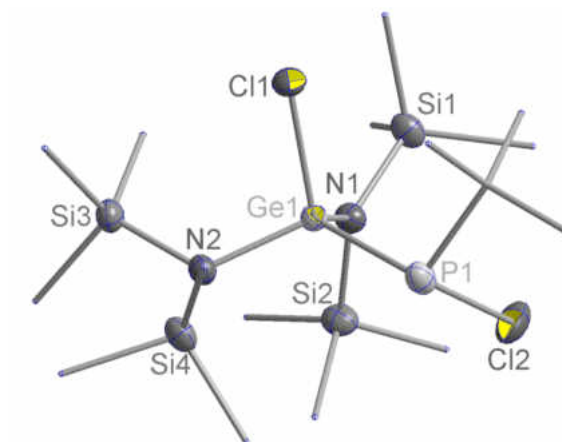


Figure 13. Crystal structure of **29**. Thermal ellipsoids are given at 50 % probability. Hydrogen atoms have been omitted and *tert*-butyl and methyl groups drawn as wireframe for clarity.

Table 22. Crystal data for compound **29**.

Molecular formula	C <sub>16</sub> H <sub>45</sub> Cl <sub>2</sub> GeN <sub>2</sub> PSi <sub>4</sub>
Formula Weight (g/mol)	552.36
Crystal System	triclinic
Space Group	<i>P</i> -1 (No. 2)
<i>a</i> , Å	10.6676(9)
<i>b</i> , Å	11.8453(10)
<i>c</i> , Å	12.1007(11)
$\alpha$ , °	77.3000(10)
$\beta$ , °	89.9670(10)
$\gamma$ , °	76.1580(10)
<i>V</i> , Å <sup>3</sup>	1446.1(2)
<i>Z</i>	2
F(000)	584
$\rho_{\text{calcd}}$ , g cm <sup>-3</sup>	1.269
$\lambda$ , Å	0.71073
Temperature, K	173
<i>h</i> , min/max	-14/14
<i>k</i> , min/max	-15/14
<i>l</i> , min/max	-16/15
2 $\theta$ maximum, °	56.52
$\mu$ , mm <sup>-1</sup>	1.471
# Reflections Collected	12177
# Unique Reflections ( <i>R</i> <sub>int</sub> )	6172 (0.0130)
<i>R</i> (F) <sup>a</sup>	0.0266
<i>R</i> <sub>w</sub> (F <sup>2</sup> ) <sup>b</sup>	0.0655
Goof	1.064

$${}^a R = \sum |F_o - F_c| / \sum |F_o| \quad {}^b R_w = \{[\sum w(F_o - F_c)^2 / [\sum w(F_o^2)^2]\}^{1/2}; w = 1/[\sigma^2(F_o)^2 + (xP)^2 + yP],$$

where P = (F<sub>o</sub><sup>2</sup> + 2F<sub>c</sub><sup>2</sup>)/3.

Table 23. Selected bond lengths and angles for compound **29**.

Bond Lengths (Å)			
Ge(1)–N(1)	1.8411(11)	P(1)–C(13)	1.8827(15)
Ge(1)–N(2)	1.8467(11)	Si(1)–N(1)	1.7714(12)
Ge(1)–Cl(1)	2.1868(4)	Si(2)–N(1)	1.7755(12)
Ge(1)–P(1)	2.3991(4)	Si(3)–N(2)	1.7767(12)
P(1)–Cl(2)	2.0794(6)	Si(4)–N(2)	1.7655(12)
Bond Angles (°)			
N(1)–Ge(1)–N(2)	112.08(5)	Cl(1)–Ge(1)–P(1)	104.428(15)
N(1)–Ge(1)–Cl(1)	111.55(4)	C(13)–P(1)–Cl(2)	100.00(5)
N(2)–Ge(1)–Cl(1)	101.56(4)	C(13)–P(1)–Ge(1)	109.82(5)
N(1)–Ge(1)–P(1)	114.68(4)	Cl(2)–P(1)–Ge(1)	97.14(2)
N(2)–Ge(1)–P(1)	111.49(4)		

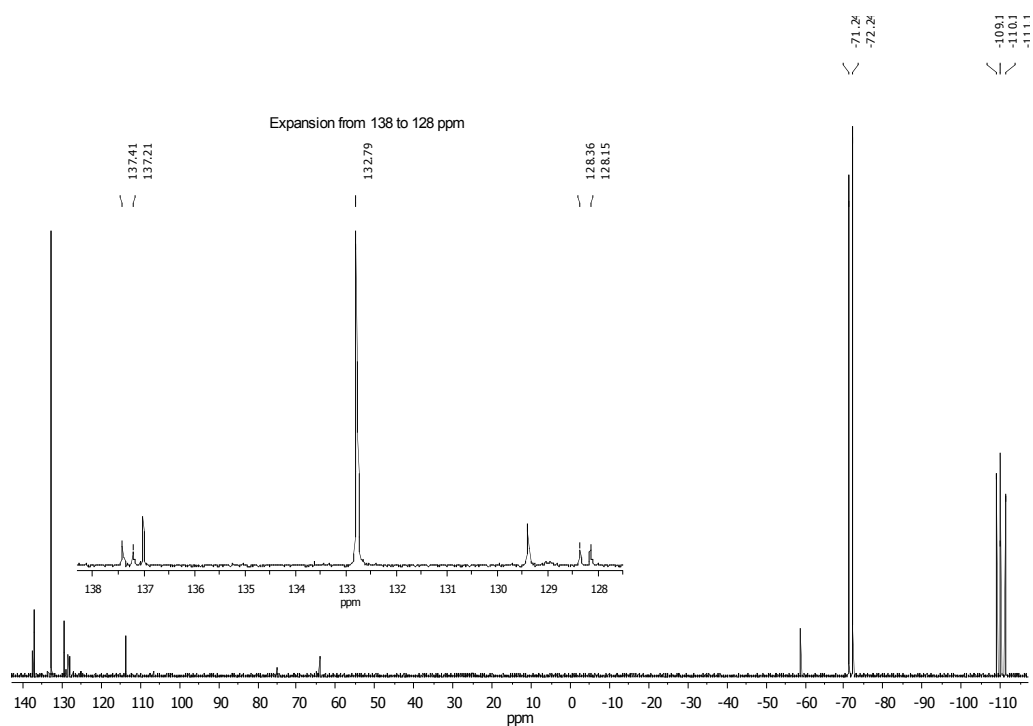


Figure 14.  $^{31}\text{P}\{^1\text{H}\}$  NMR spectrum of tri-*tert*-butylcyclotriphosphine **31**.

Investigation of the reactions of  $[(\text{Me}_3\text{Si})_2\text{N}]_2\text{M}$  ( $\text{M} = \text{Ge}$  **22**,  $\text{Sn}$  **23**) with  ${}^t\text{Bu}_2\text{PCl}$  **19** proved fruitless. The  ${}^{31}\text{P}\{^1\text{H}\}$  NMR spectrum (Figure 15) for the reaction of the stannylene with  ${}^t\text{Bu}_2\text{PCl}$  displayed an interesting mixture of only three products. All of these products displayed Sn–P coupling and all signals appeared fairly close to one another. However, this reaction was very slow, requiring 4–5 weeks at elevated temperatures to achieve any appreciable yield, and no identifiable product could ever be obtained.

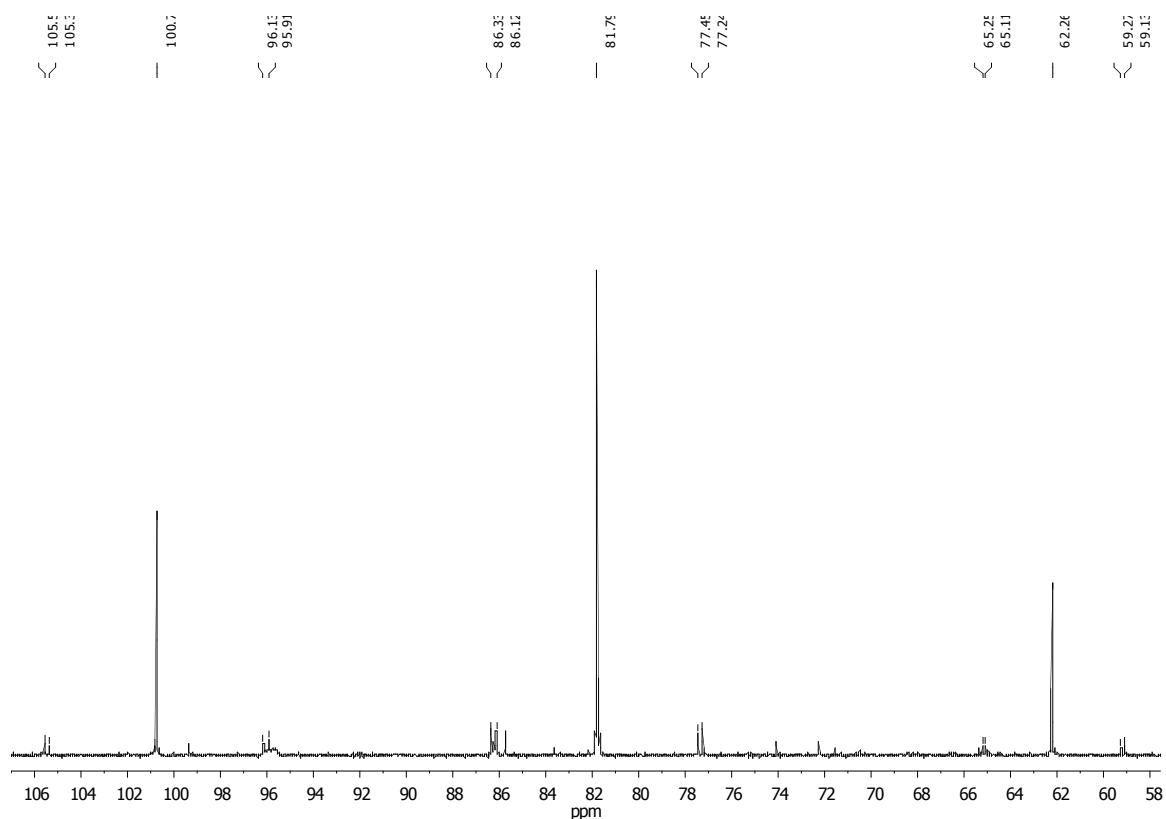
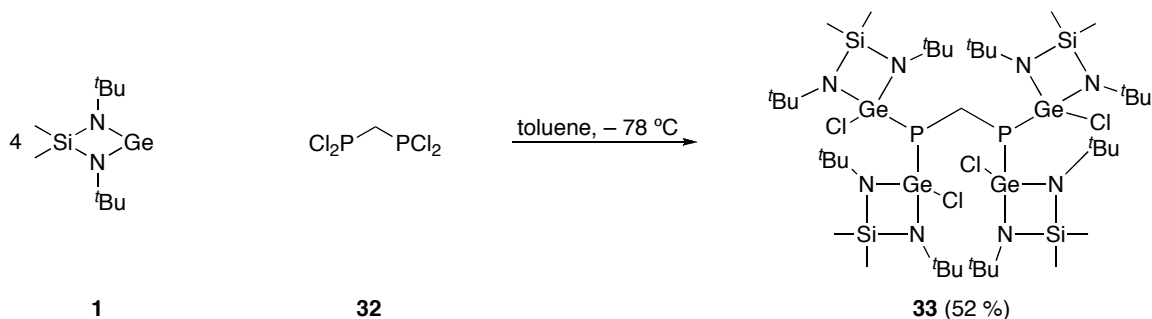


Figure 15.  ${}^{31}\text{P}\{^1\text{H}\}$  NMR spectrum for reaction mixture of stannylene **23** with chlorophosphine **19** displaying three separate, yet similar, products.

#### *Reactions with bis(dichlorophosphine)methane*

Finally, in an attempt to determine the degree to which insertion can occur for a completely non-crowded phosphine, the cyclic germylene **1** and stannylene **2** were added

in a 4:1 ratio to bis(dichlorophosphino)methane **32** (Scheme 50). In the case of **1**, the tetrainsertion product **33** was isolated with ease and found to be quite stable.



Scheme 50. 4:1 addition of germylene **1** with tetrachlorobisphosphine **32**.

The tetrainsertion product **33** crystallized from toluene at  $-5\text{ }^{\circ}\text{C}$  in the tetragonal space group  $P-4$  with  $Z = 2$ , indicating that half a molecule constitutes the asymmetric unit. Additional crystallographic data for **33** can be found in Table 24. A two-fold rotation axis, passing through C5 in the PCP plane, renders the bis(chlorogermyl)phosphine moieties crystallographically equivalent. The Ge–P bonds of 2.3306(5) and 2.3347(5) Å are nearly identical to those previously observed for insertions products with germylene **1**, indicating there is not significant crowding around the phosphorus centers. Germanium–phosphorus distances of 2.3425(4) Å in **20**, 2.3365(5) and 2.3286(5) Å in **17**, and 2.3315(8) and 2.3226(8) Å in **4** were observed. Furthermore, the central carbon (C5) is nearly perfectly tetrahedral with a P–C–P bond angle of  $108.99(14)^{\circ}$ . Surprisingly, the phosphorus centers in **33** show a high degree of pyramidal character with total angle sums of  $315.62(27)^{\circ}$ .

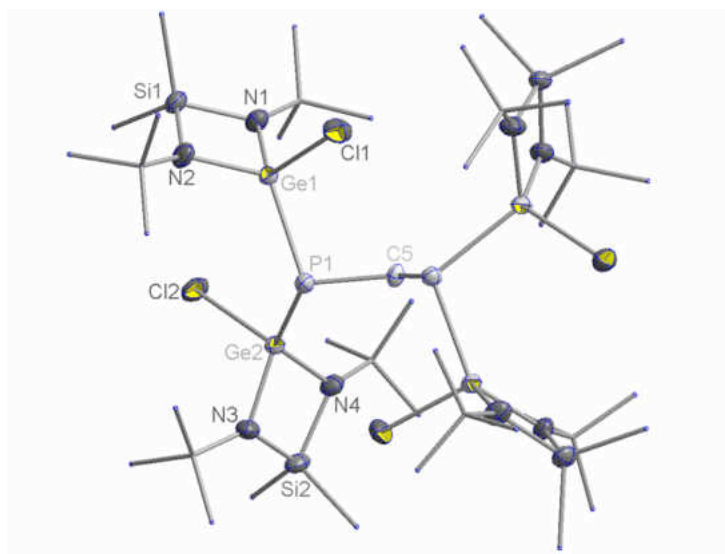


Figure 16. Crystal structure of **33**. Thermal ellipsoids are drawn at 50 % probability.

Hydrogen atoms are omitted and the *tert*-butyl and methyl groups are drawn as wireframes for clarity.

Table 24. Crystal data for compound **33**.

Molecular Formula	C <sub>41</sub> H <sub>98</sub> Cl <sub>4</sub> Ge <sub>4</sub> N <sub>8</sub> P <sub>2</sub> Si <sub>4</sub>
Formula Weight (g/mol)	1309.73
Crystal System	tetragonal
Space Group	<i>P</i> -4 (No. 81)
<i>a</i> , Å	17.6548(7)
<i>b</i> , Å	17.6548(7)
<i>c</i> , Å	10.5683(8)
$\alpha$ , °	90
$\beta$ , °	90
$\gamma$ , °	90
<i>V</i> , Å <sup>3</sup>	3294.1(3)
<i>Z</i>	2
F(000)	1364
$\rho_{\text{calcd}}$ , g cm <sup>-3</sup>	1.320
$\lambda$ , Å	0.71073
Temperature, K	173
<i>h</i> , min/max	-23/23
<i>k</i> , min/max	-23/23
<i>l</i> , min/max	-14/14
2 $\theta$ maximum, °	57.56
$\mu$ , mm <sup>-1</sup>	2.124
# Reflections Collected	45380
# Unique Reflections ( <i>R</i> <sub>int</sub> )	8131 (0.0212)
<i>R</i> (F) <sup>a</sup>	0.0218
<i>R</i> <sub>w</sub> (F <sup>2</sup> ) <sup>b</sup>	0.0600
Goof	1.039

$${}^a R = \sum |F_o - F_c| / \sum |F_o| \quad {}^b R_w = \{[\sum w(F_o - F_c)^2 / [\sum w(F_o^2)^2]\}^{1/2}; w = 1/[\sigma^2(F_o)^2 + (xP)^2 + yP],$$

where  $P = (F_o^2 + 2F_c^2)/3$ .



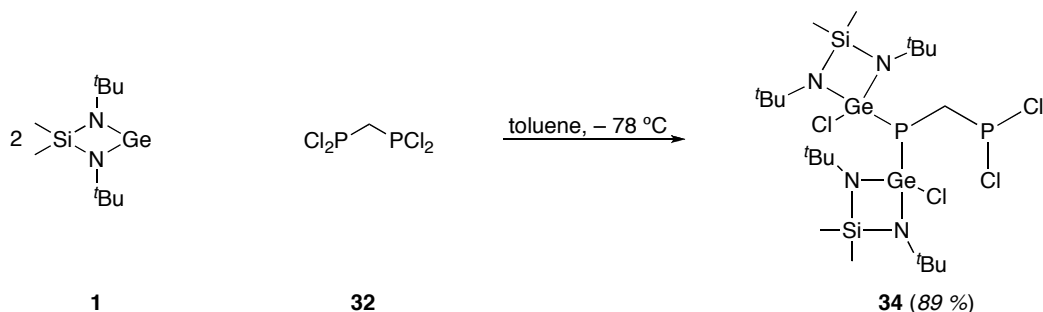
Table 25. Selected bond lengths and angles for compound **33**.

Bond Lengths (Å)			
Ge(1)–N(2)	1.8222(17)	Ge(2)–P(1)	2.3357(5)
Ge(1)–N(1)	1.8276(16)	Ge(2)–Si(2)	2.6056(6)*
Ge(1)–Cl(1)	2.2075(5)	Si(1)–N(1)	1.7416(18)
Ge(1)–P(1)	2.3306(5)	Si(1)–N(2)	1.743(2)
Ge(1)–Si(1)	2.6081(5)*	Si(2)–N(3)	1.7381(18)
Ge(2)–N(3)	1.8303(17)	Si(2)–N(4)	1.7494(18)
Ge(2)–N(4)	1.8373(16)	P(1)–C(5)	1.8699(17)
Ge(2)–Cl(2)	2.1979(5)		
Bond Angles (°)			
N(2)–Ge(1)–N(1)	83.56(8)	Cl(2)–Ge(2)–P(1)	105.166(19)
N(2)–Ge(1)–Cl(1)	112.89(6)	C(5)–P(1)–Ge(1)	102.89(2)
N(1)–Ge(1)–Cl(1)	110.12(5)	C(5)–P(1)–Ge(2)	104.31(6)
N(2)–Ge(1)–P(1)	118.95(6)	Ge(1)–P(1)–Ge(2)	108.422(19)
N(1)–Ge(1)–P(1)	136.09(6)	N(1)–Si(1)–N(2)	88.53(8)
Cl(1)–Ge(1)–P(1)	95.654(19)	N(3)–Si(2)–N(4)	88.98(8)
N(3)–Ge(2)–N(4)	83.57(8)	Si(1)–N(1)–Ge(1)	93.86(9)
N(3)–Ge(2)–Cl(2)	109.61(6)	Si(1)–N(2)–Ge(1)	94.02(9)
N(4)–Ge(2)–Cl(2)	115.07(6)	Si(2)–N(3)–Ge(2)	93.77(8)
N(3)–Ge(2)–P(1)	116.08(6)	Si(2)–N(4)–Ge(2)	93.15(8)
N(4)–Ge(2)–P(1)	125.65(6)		

\*non-bonding distance

Attempts to isolate a 2:1 addition product with **32** were unsuccessful, but a surprising discovery was that, when two germylene (**1**) molecules were added to **32**, they added asymmetrically, as confirmed by the  $^{31}\text{P}\{^1\text{H}\}$  NMR spectrum of the reaction mixture (Figure 17). Considering the additional steric congestion caused by the addition of the first germyl unit, it seems counterintuitive that the second unit should add at the

same phosphorus center. Currently, the only explanation for this phenomenon is that substitution of a chloride for a germanium (considerably less electronegative) causes the basicity of phosphorus to increase driving it to coordinate the Lewis acidic site preferentially versus the dichlorophosphine.



Scheme 51. 2:1 addition of germylene **1** to bis(dichlorophosphine)methane **32**.

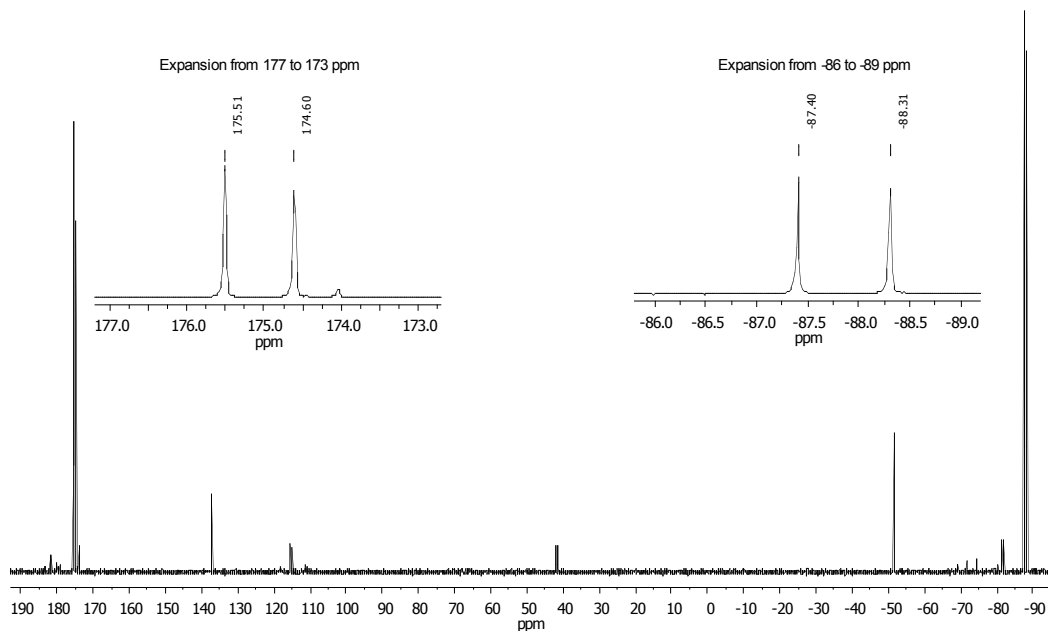
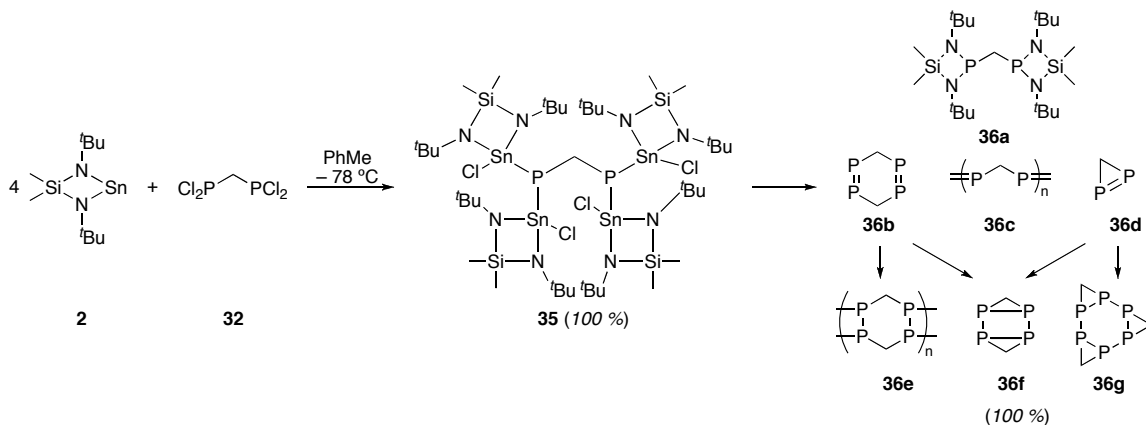


Figure 17.  $^{31}\text{P}\{^1\text{H}\}$  NMR spectrum of reaction mixture from Scheme 51.

The stannylene insertion product **35**, while observable by  $^{31}\text{P}\{^1\text{H}\}$  NMR, was not stable and decomposed quite rapidly. The final product gave only one singlet in the

phosphorus spectrum at  $\delta -136.3$  ppm, but determining the exact nature of this structure has proven elusive. Several different possible structures may be proposed, **36a–g**, based on the observed spectra.

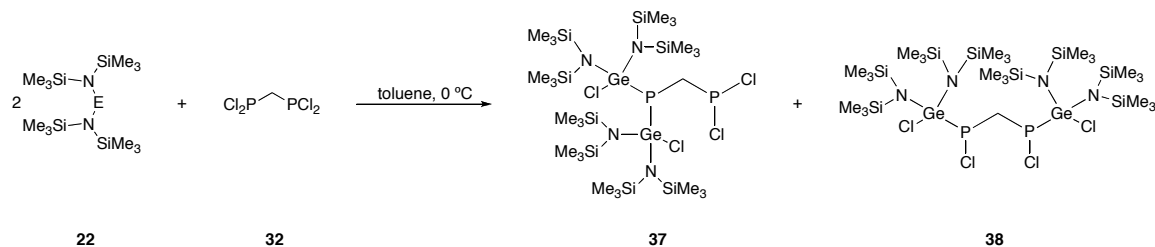


Scheme 52. 4:1 addition of stannylene **2** to tetrachlorobisphosphine **32**.

Of the predicted products, several can be ruled out for various reasons. The ethane-bridged analogue of compound **36a** had been previously reported<sup>106</sup> by Lief *et al.* (synthesized from 1,2-bis(dichlorophosphino)ethane and the lead analogue of **2** in an amide exchange reaction). Its phosphorus signal is located at 143.9 ppm (in C<sub>6</sub>D<sub>6</sub>), significantly different from the observed  $-136.3$  ppm for **36**. Compounds **36b** and **36d**, while possible given the tendency of these systems to form diphosphenes, are unlikely as diphosphenes tend to undergo 2+2 cycloadditions. Accounting for this, **36b** could lead to the polymeric **36e** or **36f** (via intramolecular addition) and **36d** could lead to **36f** or **36g**. Compounds **36f** and **36g** have significant ring strain and thus seem unlikely as well. The obtained product forms a thick precipitate in non-polar solvents (including THF), thus the two polymeric forms **36c** and **36e** seem most likely at this time.

Addition of the bulkier, acyclic germylene **22** to **32** gave only 2:1 addition products (Scheme 53). Compound **37**, the analogue of **34**, was observed but the

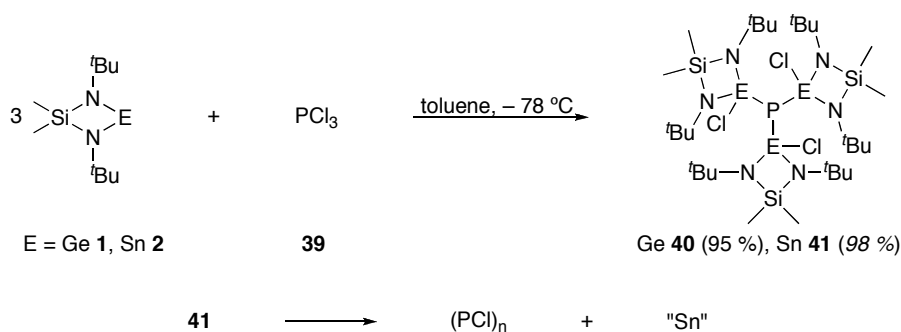
symmetric addition product **38** was actually found to be the major product. These products were identified by their  $^{31}\text{P}\{^1\text{H}\}$  NMR signals. Neither of these could be isolated, but this observation gave further mechanistic insight. It shows the competition between the increased basicity of the monosubstituted phosphine and its repulsion of any incoming germylene moiety due to steric congestion.



Scheme 53. 2:1 addition of germylene **22** to tetrachlorobisphosphine **32**.

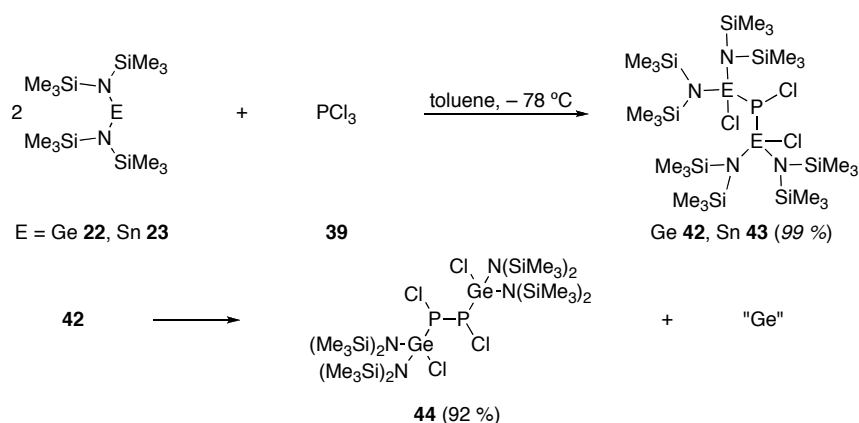
#### *Reactions with phosphorus trichloride*

Although additions of the cyclic germylene and stannylene  $\text{Me}_2\text{Si}(\mu\text{-N}^t\text{Bu})_2\text{M}$  ( $\text{M} = \text{Ge}$  **1** and  $\text{Sn}$  **2**) to  $\text{PCl}_3$  **39** had been previously explored,<sup>75</sup> we felt a reinvestigation of these reactions could prove informative given the new information gained and the new methodology developed to this point. Confirming previous reports, when the cyclic germylene **2** was added to  $\text{PCl}_3$  in a 3:1 ratio, the stable triinsertion product  $[\text{Me}_2\text{Si}(\mu\text{-N}^t\text{Bu})_2\text{Ge}(\text{Cl})]_3\text{P}$  **40** was obtained. The previously unreported  $^{31}\text{P}\{^1\text{H}\}$  NMR signal at  $\delta -78.0$  ppm was observed. Also in accord with the mentioned report,<sup>75</sup> the 3:1 addition of the cyclic stannylene **2** to  $\text{PCl}_3$  resulted in an unidentifiable mixture of compounds, stemming from decomposition of the NMR-observable triinsertion product **41** at  $\delta -114.6$  ppm,  $^1J_{119/117\text{SnP}} = 1541/1472$  Hz.



Scheme 54. Reactions of carbenoids **1** and **2** with phosphorus trichloride **39**.

The additions of the acyclic germylene and stannylene had different outcomes (Scheme 55). Initially, 3:1 additions were conducted in an attempt to obtain triinsertion products. The  $^{31}\text{P}\{^1\text{H}\}$  NMR spectrum showed only the diinsertion product **43** for the stannylene addition at  $\delta$  64.6 ppm ( $^1J_{119/117\text{SnP}} = 1693/1620$  Hz) indicating the bulk of two chlorostannyl groups on phosphorus prohibited a third insertion. A secondary, but quite important, finding was that this diinsertion product **43** only very slowly decomposed; however, it could never be isolated. Following the observed diinsertion for the stannylene addition to  $\text{PCl}_3$ , a 2:1 addition of the germylene to  $\text{PCl}_3$  was attempted resulting in the isolation of the stable product with a Ge–P–P–Ge motif, **44**.



Scheme 55. Reactions of acyclic carbenoids **22** and **23** with phosphorus trichloride **39**.

Product **44** crystallized from toluene at 3 °C as pale pink plates in the triclinic space group  $P\bar{1}$  with  $Z = 2$ . Additional crystallographic data for **44** can be found in

Table 26. Compound **44**, with its “Ge–P–P–Ge” motif is isostructural to **26**, resulting from the addition of [(Me<sub>3</sub>Si)<sub>2</sub>N]<sub>2</sub>Sn **23** to PhPCl<sub>2</sub> **3**. The P–P distance of 2.2175(10) Å is only slightly smaller than the 2.2360(10) Å observed in **26**. Just as in **26**, the presence of an inversion center in the middle of the P–P bond renders both halves of the molecule metrically equivalent. The Ge–P bond length of 2.4087(6) Å is longer than any previously observed, including the 2.3991(4) Å in **29**. In contrast, the P–Cl distances of 1.839(2) Å are significantly shorter than the P–Cl bond length of 2.0794(6) Å, also observed in **29**. This is likely due to less bulk around phosphorus exchanging the *tert*-butyl in **29** for a phosphine moiety. The phosphorus centers in **44** show greater pyramidalization than any previously discussed structure with a total angle sum of 293.86(10)°, the next closest being 300.17(16)° observed in **26**. Similar to **26**, this is likely due to the increased Ge–P bond length and the effective implementation of a phosphide as a substituent.

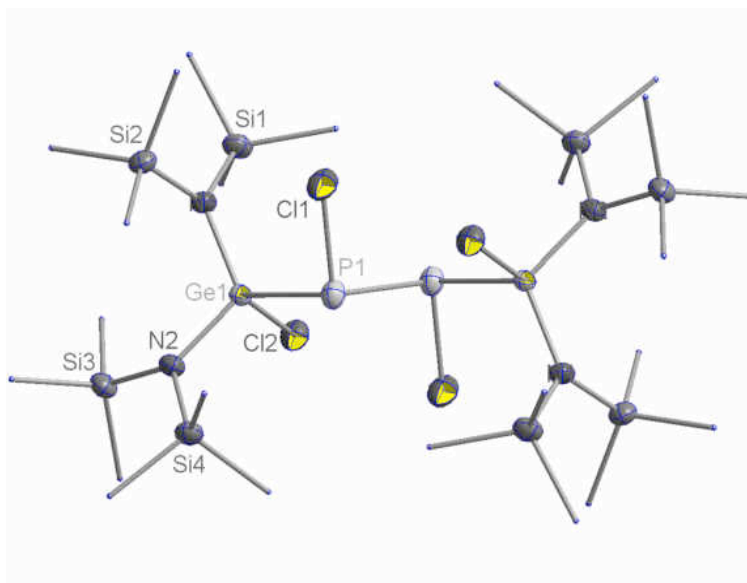


Figure 18. Crystal structure of **44**. Thermal ellipsoids are drawn at 50 % probability.

Hydrogen atoms are omitted and the methyl groups are drawn as wireframes for clarity.

Table 26. Crystal data for compound **44**.

Molecular Formula	C <sub>12</sub> H <sub>36</sub> Cl <sub>4</sub> Ge <sub>2</sub> N <sub>4</sub> P <sub>2</sub> Si <sub>8</sub>
Formula Weight (g/mol)	495.24
Crystal System	triclinic
Space Group	<i>P</i> -1 (No. 2)
<i>a</i> , Å	10.0430(6)
<i>b</i> , Å	11.6131(7)
<i>c</i> , Å	13.8927(13)
$\alpha$ , °	108.69(3)
$\beta$ , °	102.262(3)
$\gamma$ , °	104.771(2)
<i>V</i> , Å <sup>3</sup>	1405.58(18)
<i>Z</i>	1
F(000)	581
$\rho_{\text{calcd}}$ , g cm <sup>-3</sup>	1.170
$\lambda$ , Å	0.71073
Temperature, K	173
<i>h</i> , min/max	-13/12
<i>k</i> , min/max	-15/13
<i>l</i> , min/max	0/18
2 $\theta$ maximum, °	55.00
$\mu$ , mm <sup>-1</sup>	1.536
# Reflections Collected	6336
# Unique Reflections ( <i>R</i> <sub>int</sub> )	5976 (0.0232)
<i>R</i> (F) <sup>a</sup>	0.0353
<i>R</i> <sub>w</sub> (F <sup>2</sup> ) <sup>b</sup>	0.0968
Goof	1.077

$${}^a R = \sum |F_o - F_c| / \sum |F_o| \quad {}^b R_w = \{[\sum w(F_o - F_c)^2 / [\sum w(F_o^2)^2]\}^{1/2}; w = 1/[\sigma^2(F_o)^2 + (xP)^2 + yP],$$

where  $P = (F_o^2 + 2F_c^2)/3$ .

Table 27. Selected bond lengths and angles for compound **44**.

Bond Lengths (Å)			
Ge(1)–N(1)	1.8363(16)	Cl(1)–P(1)	2.0547(8)
Ge(1)–N(2)	1.8375(15)	Si(1)–N(1)	1.7786(18)
Ge(1)–Cl(2)	2.1855(5)	Si(2)–N(1)	1.7690(17)
Ge(1)–P(1)	2.4087(6)	Si(3)–N(2)	1.7695(17)
P(1)–P(1)	2.2175(10)	Si(4)–N(2)	1.7699(17)
Bond Angles (°)			
N(2)–Ge(1)–N(1)	114.40(7)	Cl(2)–Ge(1)–P(1)	105.15(2)
N(1)–Ge(1)–Cl(2)	108.11(5)	Cl(1)–P(1)–P(1)	96.85(4)
N(2)–Ge(1)–Cl(1)	105.34(5)	Cl(1)–P(1)–Ge(1)	96.43(3)
N(1)–Ge(1)–P(1)	113.43(5)	P(1)–P(1)–Ge(1)	100.58(3)
N(2)–Ge(1)–P(1)	109.67(5)		

## II. 2. Mechanistic Investigations

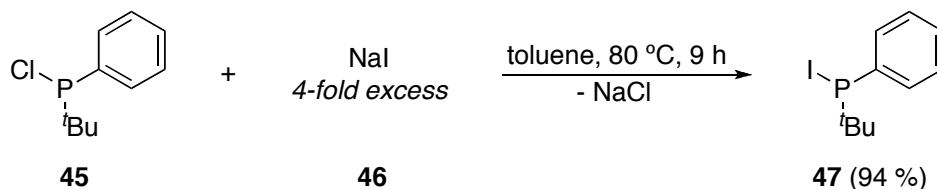
### *Kinetic studies and comparisons of reaction rates*

Following these studies, our primary beliefs remained that the insertions proceed via an S<sub>N</sub>2-type mechanism and the decomposition via an unknown, non-radical mechanism. The isolation of M–P–P–M type products (e.g. **26** and **44**) seemed to be connected to the decomposition pathway rather than the insertion pathway. This along with the fact that, for the most part, only Sn-based products were unstable and products with bulkier substituents break down more slowly, we inferred that the lone pair of phosphorus might be important to the pathway of these observed decompositions.

To gain further insight, the “mixed” alkyl-/aryl-chlorophosphine <sup>t</sup>Bu(Ph)PCl **45** was tested with all of the heterocarbenes (Scheme 57). Additionally, to gain cursory

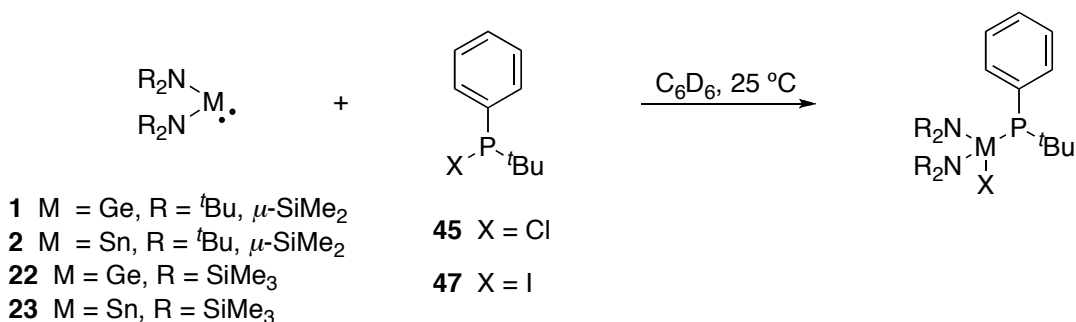


knowledge of any leaving group effect, the iodo analogue of **45**, **47**, was prepared by halide replacement using a modified literature procedure (Scheme 56).<sup>107</sup>



Scheme 56. Synthesis of *tert*-butyliodophenylphosphine **47** from its chloro analogue **45**.

The small amount of kinetic data that has been collected appears to rule out the radical pathway. First, and foremost, reactions of stannylenes proceeded significantly faster than those of germylenes. Computational studies have shown that germylenes require less energy than analogous stannylenes to undergo the transition from the singlet-ground state to the triplet-excited state.<sup>15</sup> This implies that germylenes should react faster (at least to a degree) compared to stannylenes given a radical-based mechanism; however, an opposing trend was observed. Stannylenes react orders of magnitude faster than their germanium analogues. Furthermore, observed leaving group effects show a staggering rate reduction for iodophosphine compared to the chlorophosphine. This would also not be expected for a radical-based mechanism.  $\mu$



Scheme 57. Kinetic experiments for insertions of carbenoids **1**, **2**, **22**, and **23** with chlorophosphine **45** and iodophosphine **47**.

Table 28. Approximate completion times<sup>†</sup> for insertion reactions.

<u>R<sub>2</sub>E</u>	<u>Halophosphine</u>	<u>Temperature (°C)</u>	<u>~ Completion Time (min.)<sup>†</sup></u>
23	45	25	93–98
2	45	25	70–75
1	45	25	> 1288
1	45	50	> 690
1	47	50	< 15
22	47	50	79–94
22	47	25	178–206

<sup>†</sup>Time determined by monitoring reactions using <sup>31</sup>P{<sup>1</sup>H} NMR spectroscopy.

While no insertion products were isolated, NMR data were helpful in ascertaining that the reactivity of this “mixed” chlorophosphine **45** did appear to be intermediate to Ph<sub>2</sub>PCl and <sup>t</sup>Bu<sub>2</sub>PCl. Reaction rates with <sup>t</sup>Bu(Ph)PCl for all carbenoids were found to be intermediate to the homo-substituted monochlorophosphines. In effect, for a given stannylene or germylene, reaction with Ph<sub>2</sub>PCl **11** was faster than with <sup>t</sup>Bu(Ph)PCl **45**, which was faster than with <sup>t</sup>Bu<sub>2</sub>PCl **19**.

Plotted curves (Figure 19) of chlorophosphine concentrations over time, show clear 1<sup>st</sup> order kinetics with respect to the phosphine. Pseudo-first order conditions were used (the [carbenoid] ≈ 10 [chlorophosphine]). Plots of ln[chlorophosphine] versus time give linear best-fit lines with R<sup>2</sup> values greater than 0.99.

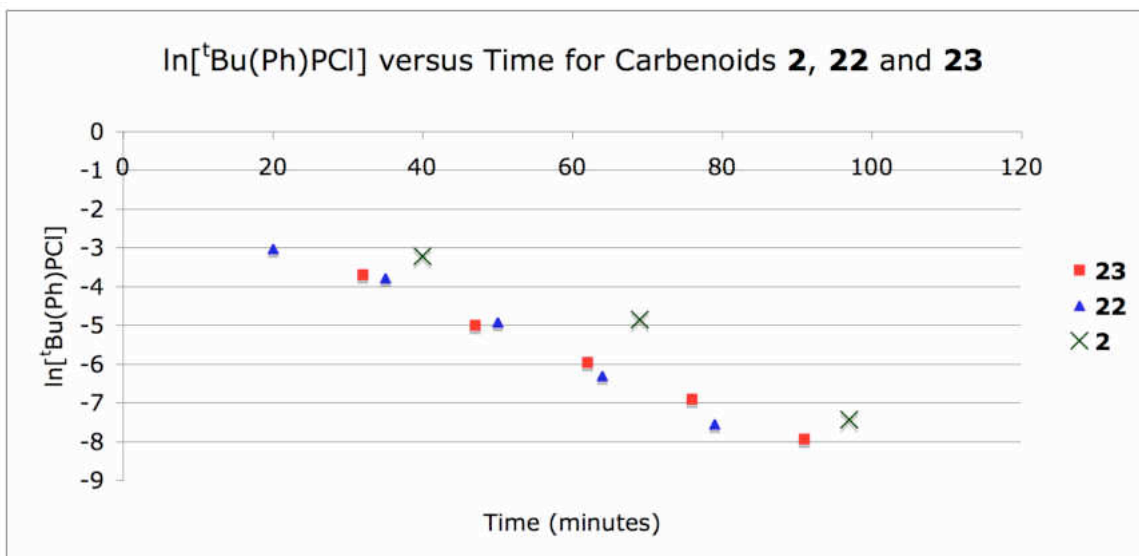
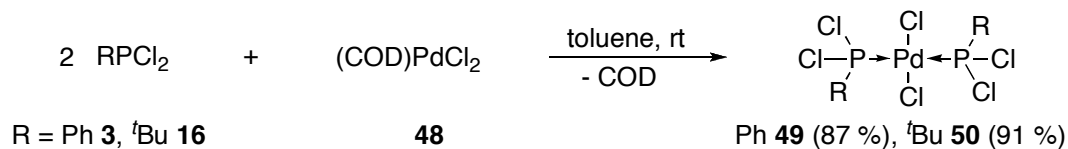


Figure 19. Kinetic data for addition of carbenoids **2**, **22**, and **23** to <sup>t</sup>Bu(Ph)PCl **45**.

In a similar fashion, rates of decomposition (for the cyclic and acyclic stannylenes) followed the same relative rates  $\text{Ph}_2\text{PCl} > {}^t\text{Bu}(\text{Ph})\text{PCl} \gg {}^t\text{Bu}_2\text{PCl}$ . Because the electronic effects of these phosphines are difficult to gauge, we focused on their steric effects. The lone pair on phosphorus should become less available with increasing steric bulk, so it was determined that it was playing a significant role in both the insertion mechanism and the decomposition mechanism.

*P-lone pair “occupation” studies*

Focusing completely on the phosphorus lone pair, we developed several alternative reaction studies to attempt to gauge the role, if any, of phosphorus’s lone pair on the insertion rate. In this vein, we synthesized the previously unreported complexes *trans*-(PhPCl<sub>2</sub>)<sub>2</sub>PdCl<sub>2</sub> **49** and *trans*-(<sup>t</sup>BuPCl<sub>2</sub>)<sub>2</sub>PdCl<sub>2</sub> **50** (Scheme 58).



Scheme 58. Syntheses of *trans*-bisphosphine palladium dichloride complexes **49** and **50**.

The palladium complex **49** crystallized from toluene at 3 °C as orange rods in the triclinic space group  $P\bar{1}$  as a 1:1 toluene solvate with  $Z = 2$ . Additional crystallographic data for **49** can be found in Table 29. The palladium center sits on an inversion center, thus the two phosphine ligands (and their substituents) are crystallographically equivalent, as are the chlorides. Transition metal complexes of halophosphines are a rarity in the literature, and those that have been characterized by single-crystal X-ray analysis only more so. Generally, for trans palladium complexes of the type  $L_2PdCl_2$ , where L = tertiary phosphine, Pd–P bond lengths range from 2.30 to 2.42 Å and Pd–Cl distances from 2.28 to 2.31 Å.<sup>108–113</sup> The P–Pd distances of 2.3041(7) Å are shorter than most for these types of bonds (a list of comparable complexes with pertinent bond lengths is provided in Table 26), as are the Pd–Cl distances of 2.2850(7) Å. Though all ligands on the palladium center are coplanar, the complex does not display ideal square planar geometry with P–Pd–Cl angles of 94.25(3) and 85.75(3)°. No H-bonds are present and van der Waals forces are solely responsible for the intermolecular arrangement of molecules in the unit cell.

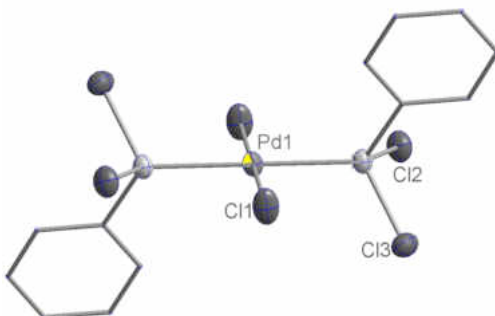


Figure 20. Crystal structure of **49**. Thermal ellipsoids are drawn at 50 % probability. Hydrogen atoms and the toluene solvate molecule are omitted and the phenyl groups are drawn as wireframes for clarity.

Table 29. Crystal data for compound **49**.

Molecular Formula	C <sub>19</sub> H <sub>18</sub> Cl <sub>6</sub> P <sub>2</sub> Pd
Formula Weight (g/mol)	627.37
Crystal System	triclinic
Space Group	<i>P</i> -1 (No. 1)
<i>a</i> , Å	8.1375(13)
<i>b</i> , Å	8.6167(13)
<i>c</i> , Å	9.6102(15)
$\alpha$ , °	80.842(2)
$\beta$ , °	66.100(2)
$\gamma$ , °	71.444(2)
<i>V</i> , Å <sup>3</sup>	583.69(16)
<i>Z</i>	1
F(000)	310
$\rho_{\text{calcd}}$ , g cm <sup>-3</sup>	1.785
$\lambda$ , Å	0.71073
Temperature, K	173
<i>h</i> , min/max	-10/10
<i>k</i> , min/max	-11/11
<i>l</i> , min/max	-12/12
2 $\theta$ maximum, °	56.30
$\mu$ , mm <sup>-1</sup>	1.624
# Reflections Collected	4886
# Unique Reflections ( <i>R</i> <sub>int</sub> )	2568 (0.0165)
<i>R</i> (F) <sup>a</sup>	0.303
<i>R</i> <sub>w</sub> (F <sup>2</sup> ) <sup>b</sup>	0.925
Goof	1.107

$${}^a R = \sum |F_o - F_c| / \sum |F_o| \quad {}^b R_w = \{[\sum w(F_o - F_c)^2 / [\sum w(F_o^2)^2]\}^{1/2}; w = 1/[\sigma^2(F_o)^2 + (xP)^2 + yP],$$

where  $P = (F_o^2 + 2F_c^2)/3$ .

Table 30. Selected bond lengths and angles for compound **49**.

Bond Lengths (Å)			
Pd(1)–Cl(1)	2.2850(7)	P(1)–Cl(2)	2.0136(10)
Pd(1)–P(1)	2.3041(7)	P(1)–Cl(3)	2.0254(10)
P(1)–C(1)	1.793(2)		
Bond Angles (°)			
Cl(1)–Pd(1)–Cl(1)	180.000(1)*	C(1)–P(1)–Cl(3)	103.86(8)
Cl(1)–Pd(1)–P(1)	85.75(3)	Cl(2)–P(1)–Cl(3)	100.97(4)
Cl(1)–Pd(1)–P(1)	94.25(3)	C(1)–P(1)–Pd(1)	117.18(8)
P(1)–Pd(1)–Pd(1)	180.0*	Cl(2)–P(1)–Pd(1)	115.10(4)
C(1)–P(1)–Cl(2)	103.82(9)	Cl(3)–P(1)–Pd(1)	113.96(4)

\* symmetry generated

Table 31. Comparison of Pd–P and Pd–Cl bond lengths for various trans bis(phosphine)palladium dichloride complexes.

<u>L</u>	<u>Pd–P</u> (Å)	<u>Pd–Cl</u> (Å)	<u>Ref.</u>
P( <i>m</i> -tol) <sub>3</sub>	2.3289(4)	2.2897(4)	108
PPh <sub>3</sub>	2.337(1)	2.290(1)	109
P <sup><i>i</i></sup> Pr <sub>2</sub> ( <i>o</i> -tol)	2.3373(4)	2.3065(4)	110
P <sup><i>i</i></sup> Bu <sub>2</sub> <sup><i>i</i></sup> Pr	2.410(2)	2.307(2)	111
PCy <sub>3</sub>	2.3628(9)	2.3012(9)	112
P <sup><i>i</i></sup> Pr <sub>3</sub>	2.3603(6)	2.3030(6)	113
PPh <sub>2</sub> Me	2.3306(12)	2.3045(9)	114

The palladium complex **50** crystallized from toluene at 3 °C as large bright orange blocks in the monoclinic space group  $P2_1/n$  with  $Z = 2$ . Additional crystallographic data

for **50** can be found in Table 32. Similar to **49**, the palladium is located on an inversion center, rendering the phosphine ligands (and associated substituents) and chlorides crystallographically equivalent. The Pd–P bonds are slightly longer than their phenyl counterpart at 2.3121(4) Å. However, the Pd–Cl length of 2.2807(5) Å and P–Cl distances of 2.0136(6) and 2.0145(6) Å are slightly shorter. Compared to **49**, complex **50** is much closer to an ideal square planar geometry with P–Pd–Cl angles of 90.263(15) and 89.737(15)°. No H-bonds are present and van der Waals forces are solely responsible for the intermolecular arrangement of molecules in the unit cell.

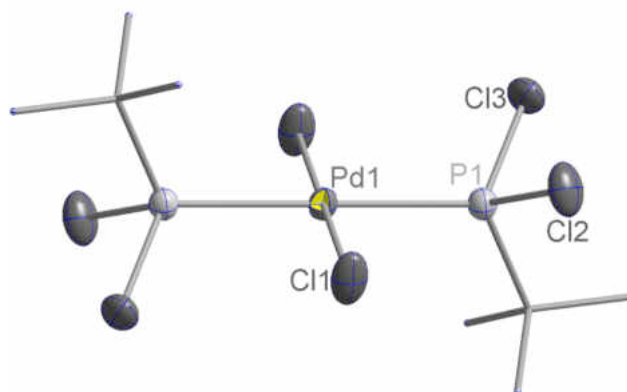


Figure 21. Crystal structure of **50**. Thermal ellipsoids are drawn at 50 % probability. Hydrogen atoms are omitted and the *tert*-butyl groups are drawn as wireframes for clarity.

Table 32. Crystal data for compound **50**.

Molecular Formula	C <sub>8</sub> H <sub>18</sub> Cl <sub>6</sub> P <sub>2</sub> Pd
Formula Weight (g/mol)	495.26
Crystal System	triclinic
Space Group	<i>P</i> 2 <sub>1</sub> / <i>n</i> (No. 14)
<i>a</i> , Å	7.0107(7)
<i>b</i> , Å	10.2125(10)
<i>c</i> , Å	12.5278(13)
$\alpha$ , °	90
$\beta$ , °	98.206(2)
$\gamma$ , °	90
<i>V</i> , Å <sup>3</sup>	887.77(15)
<i>Z</i>	2
F(000)	488
$\rho_{\text{calcd}}$ , g cm <sup>-3</sup>	1.853
$\lambda$ , Å	0.71073
Temperature, K	173
<i>h</i> , min/max	-9/8
<i>k</i> , min/max	-13/11
<i>l</i> , min/max	-16/16
2 $\theta$ maximum, °	56.36
$\mu$ , mm <sup>-1</sup>	2.107
# Reflections Collected	7334
# Unique Reflections ( <i>R</i> <sub>int</sub> )	2058 (0.0160)
<i>R</i> (F) <sup>a</sup>	0.0193
<i>R</i> <sub>w</sub> (F <sup>2</sup> ) <sup>b</sup>	0.0514
Goof	1.021

$${}^a R = \sum |F_o - F_c| / \sum |F_o| \quad {}^b R_w = \{[\sum w(F_o - F_c)^2 / [\sum w(F_o^2)^2]\}^{1/2}; w = 1/[\sigma^2(F_o)^2 + (xP)^2 + yP],$$

where  $P = (F_o^2 + 2F_c^2)/3$ .

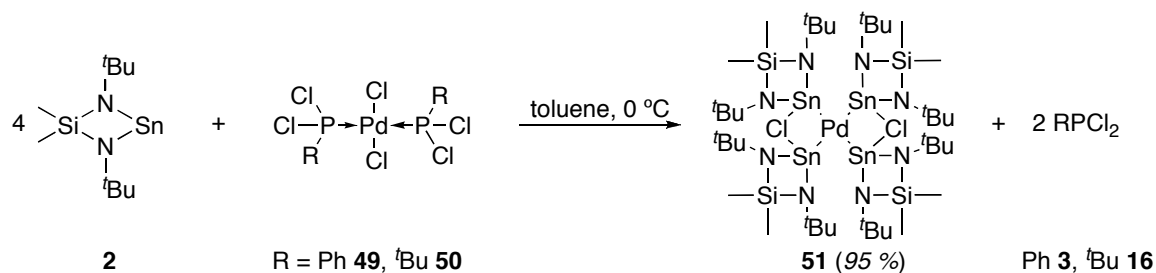


Table 33. Selected bond lengths and angles for compound **50**.

Bond Lengths (Å)			
Pd(1)–Cl(1)	2.2807(5)	P(1)–Cl(2)	2.0136(6)
Pd(1)–P(1)	2.3121(4)	P(1)–Cl(3)	2.0145(6)
P(1)–C(1)	1.8481(16)		
Bond Angles (°)			
Cl(1)–Pd(1)–Cl(1)	180.0*	C(1)–P(1)–Cl(3)	104.31(6)
Cl(1)–Pd(1)–P(1)	90.263(15)	Cl(2)–P(1)–Cl(3)	101.28(3)
Cl(1)–Pd(1)–P(1)	89.737(15)	C(1)–P(1)–Pd(1)	115.95(6)
P(1)–Pd(1)–Pd(1)	180.0*	Cl(2)–P(1)–Pd(1)	114.22(2)
C(1)–P(1)–Cl(2)	104.39(6)	Cl(3)–P(1)–Pd(1)	115.00(2)

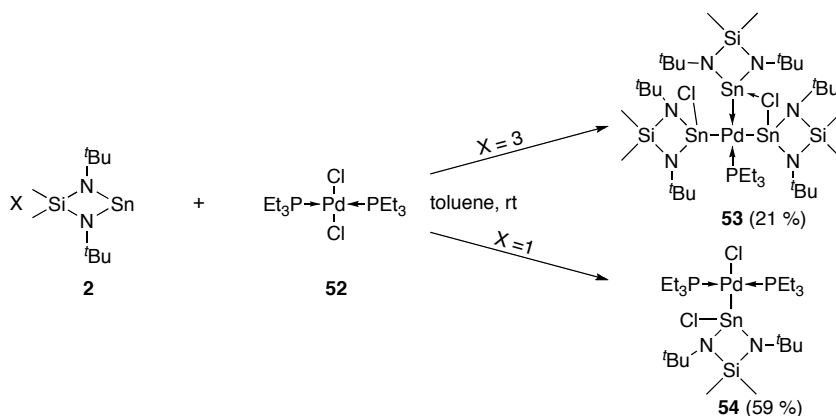
\* symmetry generated

In these complexes the lone pairs of the phosphorus atoms are occupied as bonds to the Pd<sup>II</sup> center. Addition of the cyclic stannylene **2**, in a 4:1 ratio, to each of these complexes had the same net effect (Scheme 59). The stannylene, apparently being a preferred ligand, displaced the dichlorophosphines yielding the previously reported tetrastannyl palladium complex **51**.<sup>115</sup> This was confirmed by the appearance of the <sup>31</sup>P NMR signal associated with the free phosphine. Appearance of reported <sup>1</sup>H NMR signals for the palladium complex, and a solution color change from orange to deep, opaque red (consistent with formation of the palladium complex **51**) were also helpful in determining the reactions' outcomes.



Scheme 59. Reactions of cyclic stannylene **2** with Pd<sup>II</sup> complexes **49** and **50**.

To confirm the validity of our method, we decided to similarly test the addition of stannylene **2** to the previously reported *trans*-(PEt<sub>3</sub>)<sub>2</sub>PdCl<sub>2</sub> **52** (Scheme 60).<sup>116,117</sup> The 1:1 and 3:1 addition products, **54** and **53**, respectively, were obtained in modest yields. With triethylphosphine as a ligand, a change was observed with the stannylene first preferring to displace a chloride, then a phosphine, and lastly the other chloride.



Scheme 60. Reaction of stannylene **2** with Pd<sup>II</sup> complex **52** to give 3:1 and 1:1 addition products **53** and **54**.

The palladium complex **53** crystallized from toluene as deep red blocks in the orthorhombic space group *Pna*2 with *Z* = 4. Additional crystallographic data for **53** can be found in Table 34. Two stannylenes are seen to have formally inserted into the Pd–Cl bonds, while one stannylene coordinated to the metal as a “free” moiety *trans* from the triethylphosphine. The Sn–Pd bond lengths are all nearly equivalent ranging from

2.5545(5) to 2.5880(4) Å and they are slightly longer than the Sn–P bonds in the comparable complex **51** with average bond lengths of 2.544 Å.<sup>115</sup> This lengthening could be due to increased steric congestion around the Pd center or due to increased electron density on Pd from the attached triethylphosphine ligand. The Sn–Cl bonds are significantly different at 2.4384(10) Å for Sn(1)–Cl(1) and 2.5419(9) for Sn(3)–Cl(2). This stark difference is due the formation of an adduct between Sn(2) and Cl(2) with a bond length of 2.8854(10) Å. In contrast, the distance between Sn(2) and Cl(1), in which there is no adduct formation, is 3.4187(10) Å; the distance is longer than would be considered for a bonding interaction.

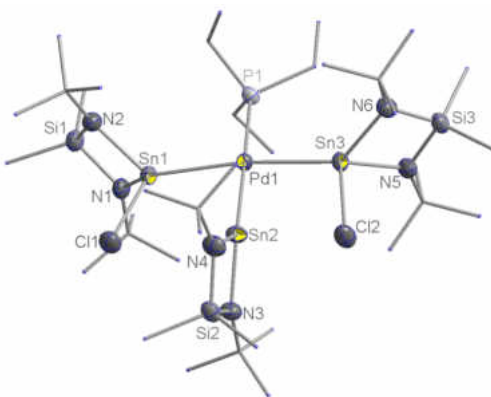


Figure 22. Crystal structure of **53**. Thermal ellipsoids are drawn at 50 % probability. Hydrogen atoms are omitted and the *tert*-butyl, ethyl, and methyl groups are drawn as wireframes for clarity.

Table 34. Crystal data for compound **53**.

Molecular Formula	C <sub>36</sub> H <sub>87</sub> Cl <sub>2</sub> N <sub>6</sub> PPdSi <sub>3</sub> Sn <sub>3</sub>
Formula Weight (g/mol)	1252.73
Crystal System	orthorhombic
Space Group	<i>Pna</i> 2 (No. 33)
<i>a</i> , Å	16.467(2)
<i>b</i> , Å	17.029(2)
<i>c</i> , Å	20.090(3)
$\alpha$ , °	90
$\beta$ , °	90
$\gamma$ , °	90
<i>V</i> , Å <sup>3</sup>	5633.6(14)
<i>Z</i>	4
F(000)	2528
$\rho_{\text{calcd}}$ , g cm <sup>-3</sup>	1.477
$\lambda$ , Å	0.71073
Temperature, K	173
<i>h</i> , min/max	-21/20
<i>k</i> , min/max	-22/22
<i>l</i> , min/max	-25/26
2 $\theta$ maximum, °	56.60
$\mu$ , mm <sup>-1</sup>	1.844
# Reflections Collected	45906
# Unique Reflections ( <i>R</i> <sub>int</sub> )	13018 (0.0243)
<i>R</i> (F) <sup>a</sup>	0.0299
<i>R</i> <sub>w</sub> (F <sup>2</sup> ) <sup>b</sup>	0.0666
Goof	1.073

$${}^a R = \sum |F_o - F_c| / \sum |F_o| \quad {}^b R_w = \{[\sum w(F_o - F_c)^2 / [\sum w(F_o^2)^2]\}^{1/2}; w = 1/[\sigma^2(F_o)^2 + (xP)^2 + yP],$$

where  $P = (F_o^2 + 2F_c^2)/3$ .

Table 35. Selected bond lengths and angles for compound **53**.

Bond Lengths (Å)			
Pd(1)–P(1)	2.3296(9)	Sn(3)–Si(3)	2.8005(10)*
Pd(1)–Sn(3)	2.5545(5)	Sn(2)–N(3)	2.021(3)
Pd(1)–Sn(2)	2.5763(4)	Sn(2)–N(4)	2.030(3)
Pd(1)–Sn(1)	2.5880(4)	Sn(2)–Si(2)	2.7804(10)*
Sn(1)–N(2)	2.046(3)	Sn(2)–Cl(2)	2.8854(10)
Sn(1)–N(1)	2.065(3)	Si(1)–N(1)	1.732(3)
Sn(1)–Cl(1)	2.4384(10)	Si(1)–N(2)	1.741(3)
Sn(1)–Si(1)	2.8087(10)*	Si(2)–N(3)	1.726(3)
Sn(3)–N(5)	2.041(3)	Si(2)–N(4)	1.732(3)
Sn(3)–N(6)	2.048(3)	Si(3)–N(5)	1.730(3)
Sn(3)–Cl(2)	2.5419(9)	Si(3)–N(6)	1.734(3)
Bond Angles (°)			
P(1)–Pd(1)–Sn(2)	178.99(3)	N(5)–Sn(3)–Cl(2)	102.56(9)
P(1)–Pd(1)–Sn(3)	95.17(2)	N(6)–Sn(3)–Cl(2)	103.68(9)
P(1)–Pd(1)–Sn(1)	91.78(2)	N(5)–Sn(3)–Pd(1)	135.39(9)
Sn(2)–Pd(1)–Sn(3)	85.352(13)	N(6)–Sn(3)–Pd(1)	132.52(9)
Sn(2)–Pd(1)–Sn(1)	87.754(12)	Cl(2)–Sn(3)–Pd(1)	101.60(2)
Sn(3)–Pd(1)–Sn(1)	172.216(12)	N(3)–Sn(2)–N(4)	76.53(13)
N(2)–Sn(1)–N(1)	75.99(12)	N(3)–Sn(2)–Pd(1)	141.73(9)
N(2)–Sn(1)–Cl(1)	105.00(9)	N(4)–Sn(2)–Pd(1)	140.10(9)
N(1)–Sn(1)–Cl(1)	105.12(9)	N(3)–Sn(2)–Cl(2)	92.35(9)
N(2)–Sn(1)–Pd(1)	129.14(9)	N(4)–Sn(2)–Cl(2)	95.89(10)
N(1)–Sn(1)–Pd(1)	123.23(9)	Pd(1)–Sn(2)–Cl(2)	93.43(2)
Cl(1)–Sn(1)–Pd(1)	112.11(3)	Sn(3)–Cl(2)–Sn(2)	79.43(3)
N(5)–Sn(3)–N(6)	75.90(13)		

\* non-bonding distance

The palladium complex **54** crystallized from toluene at 3 °C as red blocks in the monoclinic space group  $P2_1/n$  with  $Z = 4$ . Additional crystallographic data for **54** can be found in Table 36. The lone Sn–P bond, at 2.5507(2) Å, is slightly shorter than those in **53**, although it is still longer than those reported for **51** at an average distance of 2.544 Å. This decreased length could be purely due to the reduced congestion around the Pd center or to being located in a trans position to a chloride ligand. In contrast, the Pd–P bond showed a slight lengthening with a distance of 2.3486(6) Å versus the 2.3296(6) Å observed in **53**. The complex does not possess ideal square planar geometry as the angles around the palladium center are 84.20(2), 90.48(2), 92.386(16), and 93.771(16) Å, the smallest being the P(2)–Pd(1)–Cl(2) angle and the largest being P(1)–Pd(1)–Sn(1) angle.

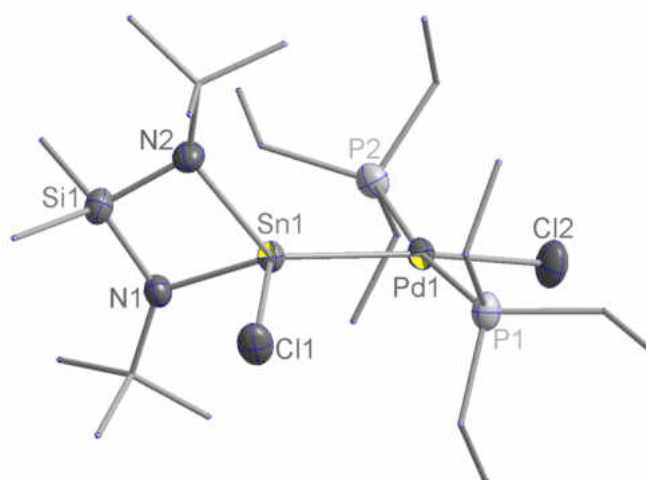


Figure 23. Crystal structure of **54**. Thermal ellipsoids are drawn at 50 % probability. Hydrogen atoms are omitted and the *tert*-butyl, ethyl and methyl groups are drawn as wireframes for clarity.

Table 36. Crystal data for compound **54**.

Molecular formula	C <sub>22</sub> H <sub>54</sub> Cl <sub>2</sub> N <sub>2</sub> P <sub>2</sub> PdSiSn
Formula Weight (g/mol)	732.69
Crystal System	monoclinic
Space Group	<i>P</i> 2 <sub>1</sub> / <i>c</i> (No. 14)
<i>a</i> , Å	10.9080(9)
<i>b</i> , Å	14.4948(12)
<i>c</i> , Å	20.8918(17)
$\alpha$ , °	90
$\beta$ , °	91.1490(10)
$\gamma$ , °	90
<i>V</i> , Å <sup>3</sup>	3302.5(5)
<i>Z</i>	4
F(000)	1496
$\rho_{\text{calcd}}$ , g cm <sup>-3</sup>	1.474
$\lambda$ , Å	0.71073
Temperature, K	173
<i>h</i> , min/max	-13/14
<i>k</i> , min/max	-19/18
<i>l</i> , min/max	-27/27
2 $\theta$ maximum, °	56.48
$\mu$ , mm <sup>-1</sup>	1.609
# Reflections Collected	27899
# Unique Reflections ( <i>R</i> <sub>int</sub> )	7679 (0.0169)
<i>R</i> (F) <sup>a</sup>	0.0272
<i>R</i> <sub>w</sub> (F <sup>2</sup> ) <sup>b</sup>	0.0725
Goof	1.006

$${}^a R = \sum |F_o - F_c| / \sum |F_o| \quad {}^b R_w = \{[\sum w(F_o - F_c)^2 / [\sum w(F_o^2)^2]\}^{1/2}; w = 1/[\sigma^2(F_o)^2 + (xP)^2 + yP],$$

where  $P = (F_o^2 + 2F_c^2)/3$ .

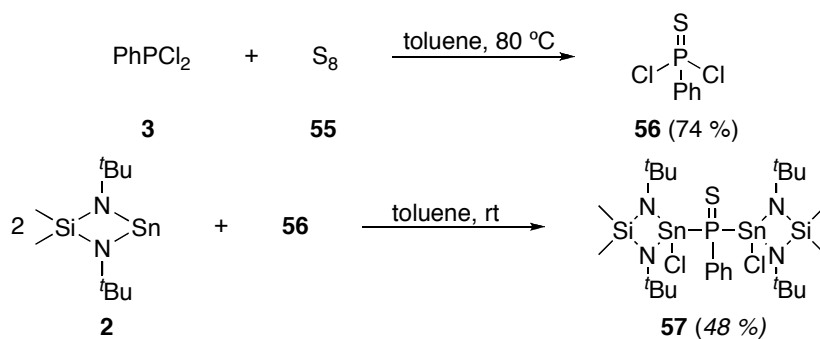
Table 37. Selected bond lengths and angles for compound **54**.

Bond Lengths (Å)			
Sn(1)–N(2)	2.0538(18)	Pd(1)–P(2)	2.3486(6)
Sn(1)–N(1)	2.0564(17)	Pd(1)–Cl(2)	2.3600(6)
Sn(1)–Cl(1)	2.4673(6)	Si(1)–N(1)	1.7289(19)
Sn(1)–Pd(1)	2.5507(2)	Si(1)–N(2)	1.732(2)
Pd(1)–P(1)	2.3390(6)		
Bond Angles (°)			
N(2)–Sn(1)–N(1)	75.41(7)	P(1)–Pd(1)–Cl(2)	90.48(2)
N(2)–Sn(1)–Cl(1)	100.86(6)	P(2)–Pd(1)–Cl(2)	84.20(2)
N(1)–Sn(1)–Cl(1)	98.29(5)	P(1)–Pd(1)–Sn(1)	93.771(16)
N(2)–Sn(1)–Pd(1)	129.75(5)	P(2)–Pd(1)–Sn(1)	92.386(16)
N(1)–Sn(1)–Pd(1)	127.50(5)	Cl(2)–Pd(1)–Sn(1)	171.809(19)
Cl(1)–Sn(1)–Pd(1)	115.676(15)	N(1)–Si(1)–N(2)	93.14(9)
P(1)–Pd(1)–P(2)	171.23(2)		

These results indicated that our previous experiment was slightly flawed. Displacement of the phosphine took place in the cases of  $(R_2PCl)_2PdCl_2$  because: 1) these phosphines are poor donors, 2) the stannylene is a considerably better donor, and 3) the stannylene is also fairly nucleophilic. Most likely the open coordination sites on the  $Pd^{II}$  center disrupted our experiment more than anything. While we can say that no insertion occurred and that the lone pairs of the phosphines were occupied, we cannot justifiably connect these two facts. The open Lewis-acidic sites on the palladium center allowed for an alternative reaction pathway to come into play and we cannot say that insertion would not have occurred if these sites were not available.

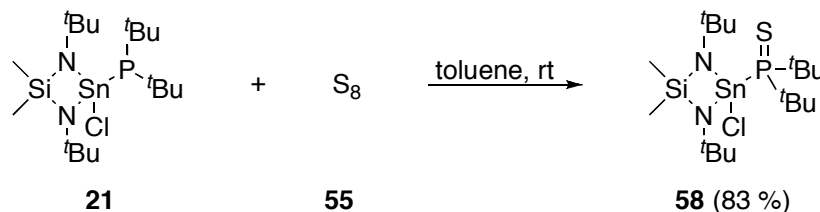


Due to the inconclusive results with the palladium complexes, we took a new approach. The lone pair on phosphorus would be “occupied” through oxidation. The thiophosphine  $\text{Ph(S)PCl}_2$  **56** was synthesized from the oxidation of  $\text{PhPCl}_2$  **3** by  $\text{S}_8$  **55** (Scheme 61).<sup>118</sup> The subsequent addition of the cyclic stannylene **2**, in a 2:1 ratio, did show a diinsertion product in the  $^{31}\text{P}\{^1\text{H}\}$  NMR spectrum, but the rate of reaction was approximately 100-fold slower. This staggering change suggested that likely the insertion for this phosphine sulfide is likely proceeding through a different mechanism from its related phosphine, and, more importantly, that the lone pair of phosphorus is likely playing a crucial role in the insertion mechanism.



Scheme 61. Preparation of thiophosphine **56** and its reaction with stannylene **2**.

Using an alternative approach, the stability of stannyl-substituted thiophosphines was determined by oxidizing  $[\text{Me}_2\text{Si}(\mu\text{-N}^t\text{Bu})_2\text{Sn}(\text{Cl})]\text{P}^t\text{Bu}$  **21** with elemental sulfur **55**. The resulting phosphine **58** (Scheme 62) was found to be stable and X-ray quality crystals were grown from toluene at room temperature.

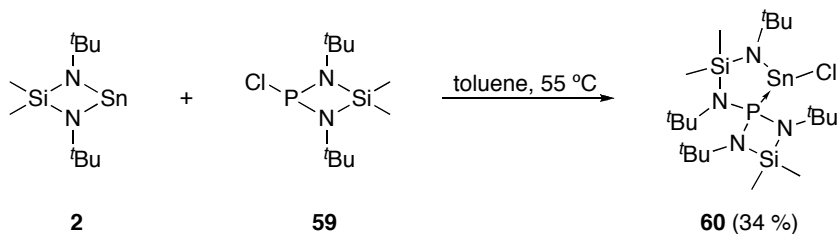


Scheme 62. Sulfur oxidation of **21** providing thiophosphine **58**.

### Reactions of amino(chloro)phosphines

What started as a study investigating the effects of heteroatom substituents on these insertion reactions led to significant evidence towards an insertion mechanism. The addition of the cyclic stannylene and germylene to the aminochlorophosphines  $\text{Me}_2\text{Si}(\mu\text{-N}^t\text{Bu})_2\text{PCl}$  **59**,  $(\text{NEt}_2)_2\text{PCl}$  **61**, and  $\text{NEt}_2\text{PCl}_2$  **64** led to the isolation and structural determination of four new compounds.

The reaction of the cyclic germylene **1** and stannylene **2** with  $\text{Me}_2\text{Si}(\mu\text{-N}^t\text{Bu})_2\text{PCl}$  **59** resulted in a previously unobserved product type. For the stannylene reaction, a “half-ligand-exchange” product was produced (Scheme 63). In contrast, the germylene reaction provided numerous unisolable compounds indicated by a  $^{31}\text{P}\{^1\text{H}\}$  NMR spectrum containing numerous peaks.



Scheme 63. Reaction of stannylene **2** with cyclic bis(amino)chlorophosphine **59**.

The intramolecular P–Sn adduct **60** crystallized as nearly colorless irregularly-shaped crystals from toluene at room temperature as a 1:1 toluene solvate in the orthorhombic space group  $P2_12_12_1$  with  $Z = 4$ . No intermolecular H-bonding is observed and van der Waals forces are primarily responsible for the molecular packing arrangement in the unit cell. Additional crystallographic data for **60** can be found in Table 38. The Sn–P distance of 2.6194(4) Å is longer than the previously discussed regular Sn–P bonds including the 2.5706(6) Å observed in the Sn–P–P–Sn complex **26**. At this time, only one other structurally characterized compound containing an

intramolecular P–Sn dative bond could be found in the literature. A considerably longer Sn–P distance of 2.8400(4) Å was observed for the Sn<sup>II</sup> amide, phenoxide complex.<sup>119</sup> An increase in the Sn–N bond of **60** is observed compared to previous insertion products. Generally, these Sn–N bonds range from 2.00 to 2.07 Å, the longest of which are found in the chlorostannyl palladium complexes **53** and **54**. At 2.105(2) Å, the Sn–N bond in **60** is significantly longer, likely due to the increased electron-density on tin due to the donation from the phosphine. This same bond lengthening effect can also be observed in the Sn–Cl bond. The observed 2.5109(9) Å is again considerably longer and is nearly identical to the elongated Sn(3)–Cl(2) bond of the tristannyl palladium complex **53**. However, the bond elongation observed in **53** was due to the formation of an intramolecular adduct between Cl(2) and a neighboring tin atom. The Sn–Cl bond is still less than the Sn(2)–Cl(2) dative bond in **53** at 2.8854(10) Å. The five-membered ring, formed by the insertion of the phosphorus heterocycle into the Sn(1)–N(3) bond is not planar, but it displays an envelope conformation with an angle of ring by 10.9(1)° between the P(1)Sn(1)N(4) plane and the P(1)N(3)N(4) plane.

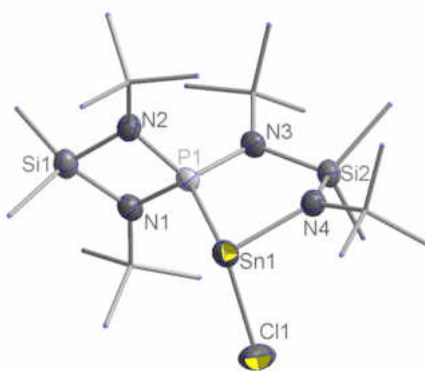


Figure 24. Crystal structure of **60**. Thermal ellipsoids are drawn at 50 % probability. Hydrogen atoms are omitted and the *tert*-butyl, methyl and ethyl groups are drawn as wireframes for clarity.

Table 38. Crystal data for compound **60**.

Molecular Formula	C <sub>27</sub> H <sub>56</sub> ClN <sub>4</sub> PSi <sub>2</sub> Sn
Formula Weight (g/mol)	678.05
Crystal System	orthorhombic
Space Group	<i>P</i> 2 <sub>1</sub> 2 <sub>1</sub> 2 <sub>1</sub> (No. 19)
<i>a</i> , Å	9.3395(7)
<i>b</i> , Å	17.1578(13)
<i>c</i> , Å	21.4239(16)
$\alpha$ , °	90
$\beta$ , °	90
$\gamma$ , °	90
<i>V</i> , Å <sup>3</sup>	3433.1(4)
<i>Z</i>	4
F(000)	1424
$\rho_{\text{calcd}}$ , g cm <sup>-3</sup>	1.312
$\lambda$ , Å	0.71073
Temperature, K	173
<i>h</i> , min/max	-12/12
<i>k</i> , min/max	-21/21
<i>l</i> , min/max	-24/27
2 $\theta$ maximum, °	56.42
$\mu$ , mm <sup>-1</sup>	0.960
# Reflections Collected	29297
# Unique Reflections ( <i>R</i> <sub>int</sub> )	7935 (0.0195)
<i>R</i> (F) <sup>a</sup>	0.0332
<i>R</i> <sub>w</sub> (F <sup>2</sup> ) <sup>b</sup>	0.0864
Goof	1.085

$${}^a R = \sum |F_o - F_c| / \sum |F_o| \quad {}^b R_w = \{[\sum w(F_o - F_c)^2 / [\sum w(F_o^2)^2]\}^{1/2}; w = 1/[\sigma^2(F_o)^2 + (xP)^2 + yP],$$

where  $P = (F_o^2 + 2F_c^2)/3$ .

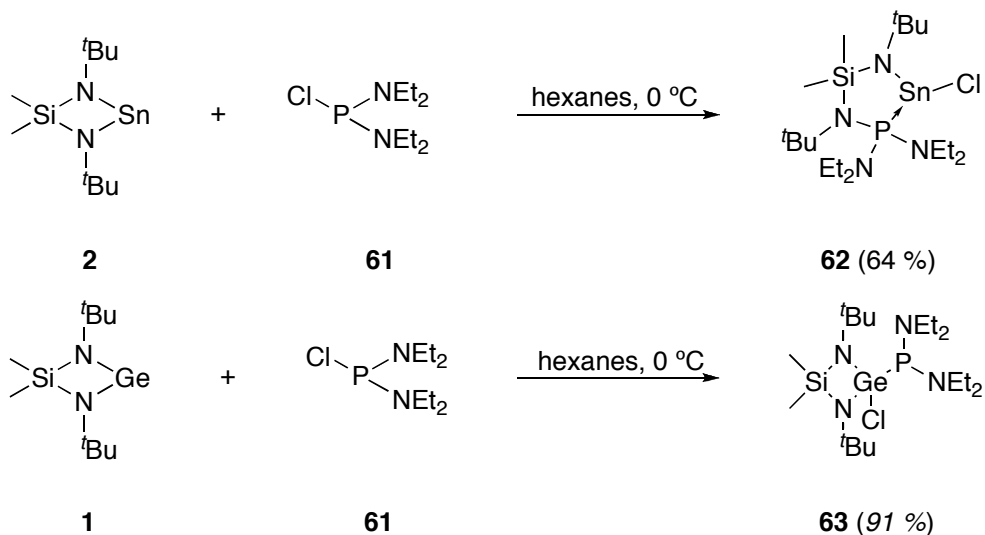
Table 39. Selected bond lengths and angles for compound **60**.

Bond Lengths (Å)			
Sn(1)–N(4)	2.105(2)	P(1)–N(2)	1.698(2)
Sn(1)–Cl(1)	2.5109(9)	Si(1)–N(1)	1.748(2)
Sn(1)–P(1)	2.6322(7)	Si(1)–N(2)	1.750(2)
P(1)–N(3)	1.653(2)	Si(2)–N(3)	1.720(2)
P(1)–N(1)	1.689(2)	Si(2)–N(4)	1.820(2)
Bond Angles (°)			
N(4)–Sn(1)–Cl(1)	96.93(6)	N(1)–P(1)–Sn(1)	119.13(8)
N(4)–Sn(1)–P(1)	81.12(6)	N(2)–P(1)–Sn(1)	108.50(9)
Cl(1)–Sn(1)–P(1)	101.87(3)	N(1)–Si(1)–N(2)	82.41(11)
N(3)–P(1)–N(1)	117.95(11)	P(1)–N(1)–Si(1)	95.54(12)
N(3)–P(1)–N(2)	115.77(12)	P(1)–N(2)–Si(1)	95.16(12)
N(1)–P(1)–N(2)	85.75(11)	N(4)–Si(2)–N(3)	109.09(11)
N(3)–P(1)–Sn(1)	108.02(8)		

The lack of an isolable germylene insertion product was assumed to be caused either by 1) a lack of access to the chloride-opposite side of the phosphorus or 2) from a combination of the rings' bulk and small size of germanium, thus prohibiting the formation of a possible P→Ge initiating complex. Given the results of the previous experiment involving Ph(S)PCl<sub>2</sub> **56**, we heavily favored the latter scenario.

Another aminochlorophosphine, (Et<sub>2</sub>N)<sub>2</sub>PCl **61**, with similar electronic effects, but drastically different geometric constraints was employed to test the validity of the aforementioned hypothesis. Addition of the stannylenes **2** to (Et<sub>2</sub>N)<sub>2</sub>PCl **61**, shown in Scheme 64, yielded an analogous compound to **60**. Addition of germylene **1** to (Et<sub>2</sub>N)<sub>2</sub>PCl **61** confirmed our suspicions by providing the monoinsertion product **63**

nearly quantitatively. However, no crystalline sample of this material could be obtained, and while  $^1\text{H}$  NMR spectrum appeared to indicate a “standard” (i.e. not a “half-ligand-exchange”) product, this could not be verified.



Scheme 64. Reactions of carbenoids **1** and **2** with bis(amido)chlorophosphine **61**.

The intramolecular P–Sn adduct **62** crystallized from hexanes at 3 °C in the monoclinic space group  $P2_1/c$  with  $Z = 4$ . No intermolecular H-bonding is observed nor are any solvent molecules present in the crystal lattice. Van der Waals forces are solely responsible for the molecular arrangement in the unit cell. Additional crystallographic data for **62** can be found in Table 40. This second “non-standard” insertion product shares many similarities with its closely related analogue **60**. The Sn–P bond of **62**, at 2.6194(4) Å, is slightly shorter than the observed 2.6322(7) Å in **60**. This may simply be due to the reduced bulk and greater substituent flexibility for the phosphorus atom in **62** versus its counterpart in **60**. As in **60**, an elongation of the Sn–N and Sn–Cl bonds was observed. However, the effect is slightly more pronounced in **62** with Sn–N and Sn–Cl distances of 2.1137(12) and 2.5156(6) Å, respectively, versus the 2.105(2) and 2.5109(9) Å observed in **60**. The most significant difference between **60** and **62** is the ring shape.

While both display an envelope conformation, the angle between the P(1)Sn(1)N(4) and P(1)N(3)N(4) planes in **62** is drastically larger at  $39.022(60)^\circ$ , versus the  $10.900(98)^\circ$  in **60**. This stark difference is likely caused by the freedom given to the phosphorus atom in **62**. With no constraint from its substituents to adhere to a separate ring structure (as is the case in **60**), the phosphorus atom can adopt a more ideal tetrahedral electronic geometry, with more angles nearer the ideal  $109.5^\circ$ . Indeed, this can be observed in the three angles N(1)–P(1)–Sn(1), N(3)–P(1)–Sn(1), and N(2)–P(1)–Sn(1) measuring  $113.69(5)$ ,  $105.36(4)$ , and  $111.14(5)^\circ$ , respectively. By contrast, the equivalent angles in **62** measure  $119.13(8)$ ,  $108.50(9)$ , and  $119.13(8)^\circ$ , respectively.

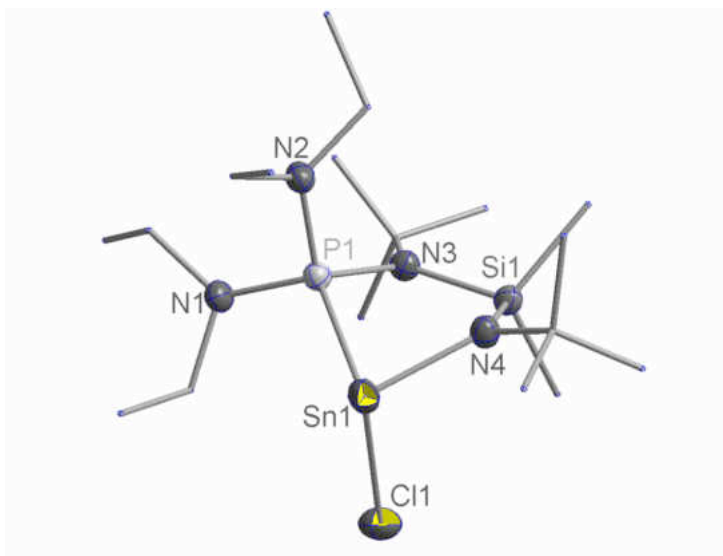


Figure 25. Crystal structure of **62**. Thermal ellipsoids are drawn at 50 % probability. Hydrogen atoms are omitted and the *tert*-butyl, methyl and ethyl groups are drawn as wireframes for clarity.

Table 40. Crystal data for compound **62**.

Molecular Formula	C <sub>18</sub> H <sub>44</sub> ClN <sub>4</sub> PSiSn
Formula Weight (g/mol)	529.77
Crystal System	monoclinic
Space Group	<i>P</i> 2 <sub>1</sub> / <i>c</i> (No. 14)
<i>a</i> , Å	8.9746(13)
<i>b</i> , Å	15.731(2)
<i>c</i> , Å	18.404(3)
$\alpha$ , °	90
$\beta$ , °	92.131(2)
$\gamma$ , °	90
<i>V</i> , Å <sup>3</sup>	2596.4(6)
<i>Z</i>	4
F(000)	1104
$\rho_{\text{calcd}}$ , g cm <sup>-3</sup>	1.355
$\lambda$ , Å	0.71073
Temperature, K	173
<i>h</i> , min/max	-11/11
<i>k</i> , min/max	-19/20
<i>l</i> , min/max	-24/24
2 $\theta$ maximum, °	56.42
$\mu$ , mm <sup>-1</sup>	1.205
# Reflections Collected	21831
# Unique Reflections ( <i>R</i> <sub>int</sub> )	6072 (0.0199)
<i>R</i> (F) <sup>a</sup>	0.0226
<i>R</i> <sub>w</sub> (F <sup>2</sup> ) <sup>b</sup>	0.0621
Goof	0.993

$${}^a R = \sum |F_o - F_c| / \sum |F_o| \quad {}^b R_w = \{[\sum w(F_o - F_c)^2 / [\sum w(F_o^2)^2]\}^{1/2}; w = 1/[\sigma^2(F_o)^2 + (xP)^2 + yP],$$

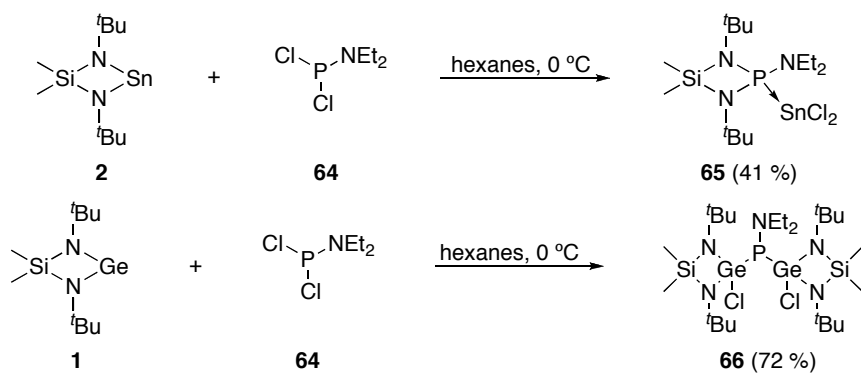
where  $P = (F_o^2 + 2F_c^2)/3$ .



Table 41. Selected bond lengths and angles for compound **62**.

Bond Lengths (Å)			
Sn(1)–N(4)	2.1137(12)	P(1)–N(1)	1.6673(12)
Sn(1)–Cl(1)	2.5156(6)	P(1)–N(2)	1.6791(12)
Sn(1)–P(1)	2.6194(4)	Si(1)–N(4)	1.7279(13)
P(1)–N(3)	1.6769(12)	Si(1)–N(3)	1.8052(12)
Bond Angles (°)			
N(4)–Sn(1)–Cl(1)	97.98(4)	N(3)–P(1)–N(2)	107.35(6)
N(4)–Sn(1)–P(1)	77.44(3)	N(1)–P(1)–Sn(1)	113.69(5)
Cl(1)–Sn(1)–P(1)	96.991(16)	N(3)–P(1)–Sn(1)	105.36(4)
N(3)–P(1)–N(1)	117.00(6)	N(2)–P(1)–Sn(1)	111.14(5)
N(1)–P(1)–N(2)	102.19(6)	N(4)–Si(2)–N(3)	106.89(6)

To verify the ligand-exchange observations for the stannylene additions to these aminochlorophosphines and to attempt to determine the nature of the germylene products, both of the cyclic heterocarbenes were added to Et<sub>2</sub>NPCl<sub>2</sub> **64**. Addition of stannylene **2**, as predicted, caused a full-ligand exchange resulting in the isolation of the phosphine-tin dichloride complex, [Me<sub>2</sub>Si(*μ*-N<sup>t</sup>Bu)<sub>2</sub>P(NEt<sub>2</sub>)]SnCl<sub>2</sub> **65** (Scheme 65). The germylene diinsertion product, [Me<sub>2</sub>Si(*μ*-N<sup>t</sup>Bu)<sub>2</sub>Ge(Cl)]<sub>2</sub>PNEt<sub>2</sub> **66**, was obtained as well, and a single crystal was subjected to X-ray analysis, confirming that ligand-exchange did not take place.



Scheme 65. Reactions of carbenoids **1** and **2** with aminodichlorophosphine **64**.

The Lewis acid-base complex **65** crystallized as colorless rods from hexanes at room temperature in the space group  $P-1$  with  $Z = 2$ . No intermolecular H-bonding is observed, nor are any solvent molecules present in the crystal lattice. Van der Waals forces are solely responsible for the molecular arrangement in the unit cell. Additional crystallographic data for **65** can be found in Table 42. The four-membered ring, with P–N bond lengths of 1.6855(14) and 1.6928(13) Å and Si–N bond lengths of 1.7509(15) and 1.7509(15) Å, is metrically similar to the same ring structure seen in the bisphosphine nickel(II) chloride complex, reported by Schranz *et al.*,<sup>120</sup> with average P–N and Si–N distances of 1.688 and 1.742 Å, respectively. For comparison, in the few reports detailing structural analyses of the diazasilaphosphetidine rings, a wide range of 1.62–1.74 Å for P–N bonds and a predictable range of 1.71–1.76 Å for Si–N distances have been observed.<sup>120–123</sup> The Sn–P distance of 2.7273(4) Å is significantly longer than the previously described intramolecular Sn–P dative bonds of 2.6322(7) Å in **60** and 2.6194(4) Å in **62**. This is likely due to the lack of ring strain to force the tin and phosphorus atoms into closer proximity. No previous examples could be found for phosphine-ligated tin(II) halide complexes. The effect of the longer, and hence weaker,

Sn–P bond can be seen in the shorter Sn–Cl distances of 2.4520(6) and 2.4593(5) Å versus the 2.5109(9) and 2.5156(6) Å observed in **60** and **62**, respectively.

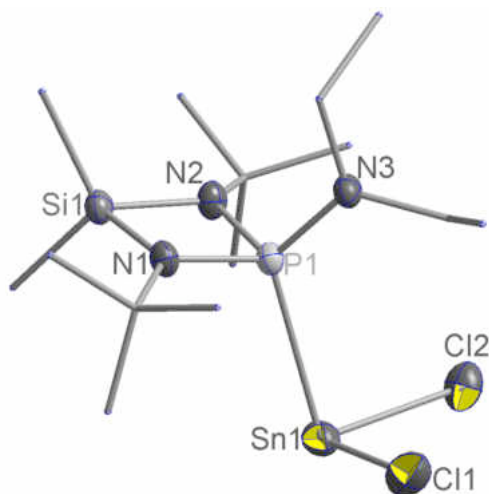


Figure 26. Crystal structure of **65**. Thermal ellipsoids are drawn at 50 % probability. Hydrogen atoms are omitted and the *tert*-butyl, methyl and ethyl groups are drawn as wireframes for clarity.

Table 42. Crystal data for compound **65**.

Molecular Formula	C <sub>28</sub> H <sub>68</sub> Cl <sub>4</sub> N <sub>6</sub> P <sub>2</sub> Si <sub>2</sub> Sn <sub>2</sub>
Formula Weight (g/mol)	986.18
Crystal System	triclinic
Space Group	<i>P</i> -1 (No. 2)
<i>a</i> , Å	8.4019(7)
<i>b</i> , Å	9.6452(8)
<i>c</i> , Å	14.9492(13)
$\alpha$ , °	89.0520(10)
$\beta$ , °	77.8720(10)
$\gamma$ , °	72.3010(10)
<i>V</i> , Å <sup>3</sup>	1126.90(16)
<i>Z</i>	2
F(000)	504
$\rho_{\text{calcd}}$ , g cm <sup>-3</sup>	1.453
$\lambda$ , Å	0.71073
Temperature, K	173
<i>h</i> , min/max	-10/10
<i>k</i> , min/max	-12/12
<i>l</i> , min/max	-19/19
2 $\theta$ maximum, °	56.50
$\mu$ , mm <sup>-1</sup>	1.496
# Reflections Collected	9716
# Unique Reflections ( <i>R</i> <sub>int</sub> )	5008 (0.0139)
<i>R</i> (F) <sup>a</sup>	0.0239
<i>R</i> <sub>w</sub> (F <sup>2</sup> ) <sup>b</sup>	0.0628
Goof	1.004

$${}^a R = \sum |F_o - F_c| / \sum |F_o| \quad {}^b R_w = \{[\sum w(F_o - F_c)^2 / [\sum w(F_o^2)^2]\}^{1/2}; w = 1/[\sigma^2(F_o)^2 + (xP)^2 + yP],$$

where  $P = (F_o^2 + 2F_c^2)/3$ .

Table 43. Selected bond lengths and angles for compound **65**.

Bond Lengths (Å)			
Sn(1)–Cl(1)	2.4520(6)	P(1)–N(1)	1.6855(14)
Sn(1)–Cl(2)	2.4593(5)	P(1)–N(2)	1.6928(13)
Sn(1)–P(1)	2.7273(4)	Si(1)–N(1)	1.7486(14)
P(1)–Si(1)	2.5545(6)*	Si(1)–N(2)	1.7509(15)
P(1)–N(3)	1.6449(14)		
Bond Angles (°)			
Cl(1)–Sn(1)–Cl(2)	94.415(17)	N(3)–P(1)–Sn(1)	119.75(5)
Cl(1)–Sn(1)–P(1)	95.011(16)	N(1)–P(1)–Sn(1)	111.14(5)
Cl(2)–Sn(1)–P(1)	94.282(16)	N(2)–P(1)–Sn(1)	111.93(5)
N(3)–P(1)–N(1)	110.78(7)	N(1)–Si(1)–N(2)	82.08(6)
N(3)–P(1)–N(2)	112.47(7)	P(1)–N(1)–Si(1)	96.11(7)
N(1)–P(1)–N(2)	85.71(7)	P(1)–N(2)–Si(1)	95.76(7)

\* nonbonding distance

The diinsertion product **66** crystallized as colorless, irregularly shaped crystals from hexanes at 3 °C in the monoclinic space group  $P2_1/c$  with  $Z = 4$ . Additional crystallographic data for **66** can be found in Table 44. This structure is nearly identical to compounds **4** and **17** described earlier, only differing in the substituent on phosphorus: phenyl for **4**, *tert*-butyl for **17**, and diethylamino for **66**. The Ge–P bond distances of 2.3526(7) and 2.3336(7) Å are only very slightly longer than the 2.3320 and 2.3325 Å averages observed in **4** and **17**, respectively. Based on these analogous structures, the bulk of the diethylamino group can be estimated to be intermediate in size to the phenyl and *tert*-butyl groups, but much closer to the *tert*-butyl group. This assignment can be made based upon the total angle sums around phosphorus of 324.35(22)° for the

diethylamino-substituted **66**,  $325.51(16)^\circ$  for the *tert*-butyl-substituted **17**, and  $317.92(24)^\circ$  for the phenyl-substituted **4**.

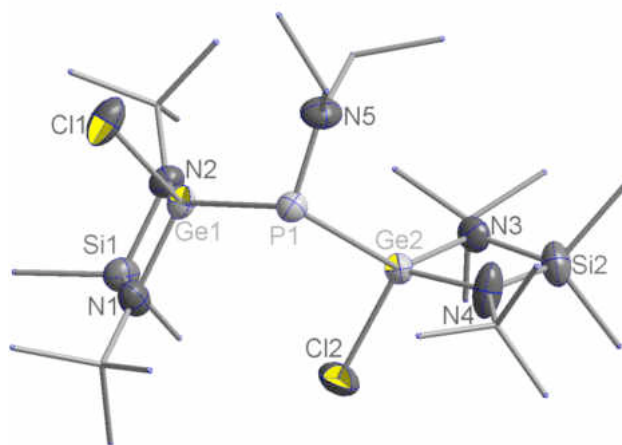


Figure 27. Crystal structure of **66**. Thermal ellipsoids are drawn at 50 % probability.

Hydrogen atoms are omitted and *tert*-butyl, methyl and ethyl groups are drawn as wireframes for clarity.

Table 44. Crystal data for compound **66**.

Molecular Formula	C <sub>24</sub> H <sub>58</sub> Cl <sub>2</sub> Ge <sub>2</sub> N <sub>5</sub> PSi <sub>2</sub>
Formula Weight (g/mol)	719.98
Crystal System	monoclinic
Space Group	<i>P</i> 2 <sub>1</sub> / <i>c</i> (No. 14)
<i>a</i> , Å	16.8501(16)
<i>b</i> , Å	18.6929(18)
<i>c</i> , Å	11.9622(12)
$\alpha$ , °	90
$\beta$ , °	100.568(2)
$\gamma$ , °	90
<i>V</i> , Å <sup>3</sup>	3703.9(6)
<i>Z</i>	4
F(000)	1512
$\rho_{\text{calcd}}$ , g cm <sup>-3</sup>	1.291
$\lambda$ , Å	0.71073
Temperature, K	173
<i>h</i> , min/max	-22/21
<i>k</i> , min/max	-24/24
<i>l</i> , min/max	-15/15
2 $\theta$ maximum, °	56.58
$\mu$ , mm <sup>-1</sup>	1.896
# Reflections Collected	31313
# Unique Reflections ( <i>R</i> <sub>int</sub> )	8609 (0.0234)
<i>R</i> (F) <sup>a</sup>	0.0521
<i>R</i> <sub>w</sub> (F <sup>2</sup> ) <sup>b</sup>	0.1289
Goof	1.039

$${}^a R = \sum |F_o - F_c| / \sum |F_o| \quad {}^b R_w = \{[\sum w(F_o - F_c)^2 / [\sum w(F_o^2)^2]\}^{1/2}; w = 1/[\sigma^2(F_o)^2 + (xP)^2 + yP],$$

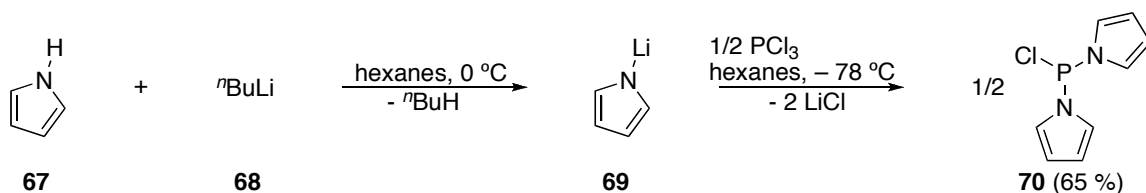
where P = (F<sub>o</sub><sup>2</sup> + 2F<sub>c</sub><sup>2</sup>)/3.

Table 45. Selected bond lengths and angles for compound **65**.

Bond Lengths (Å)			
Ge(1)–N(1)	1.831(2)	Ge(2)–P(1)	2.3336(7)
Ge(1)–N(2)	1.843(2)	P(1)–N(5)	1.671(2)
Ge(1)–Cl(1)	2.2102(8)	Si(1)–N(1)	1.736(2)
Ge(1)–P(1)	2.3526(7)	Si(1)–N(2)	1.747(2)
Ge(2)–N(4)	1.831(3)	Si(2)–N(4)	1.731(3)
Ge(2)–N(3)	1.835(2)	Si(2)–N(3)	1.769(3)
Ge(2)–Cl(2)	2.1969(8)		
Bond Angles (°)			
N(1)–Ge(1)–N(2)	83.46(10)	Cl(2)–Ge(2)–P(1)	100.09(3)
N(1)–Ge(1)–Cl(1)	114.81(8)	N(5)–P(1)–Ge(2)	107.17(10)
N(2)–Ge(1)–Cl(1)	110.81(8)	N(5)–P(1)–Ge(1)	109.19(9)
N(1)–Ge(1)–P(1)	116.57(8)	Ge(2)–P(1)–Ge(1)	107.99(3)
N(2)–Ge(1)–P(1)	135.57(8)	N(1)–Si(1)–N(2)	89.20(11)
Cl(1)–Ge(1)–P(1)	96.52(3)	N(3)–Si(2)–N(4)	88.45(12)
N(4)–Ge(2)–N(3)	83.50(11)	Si(1)–N(1)–Ge(1)	94.06(11)
N(4)–Ge(2)–Cl(2)	111.96(12)	Si(1)–N(2)–Ge(1)	93.75(8)
N(3)–Ge(2)–Cl(2)	111.09(8)	Si(2)–N(3)–Ge(1)	93.18(11)
N(4)–Ge(2)–P(1)	115.47(9)	Si(2)–N(4)–Ge(1)	94.59(13)
N(3)–Ge(2)–P(1)	134.10(8)		

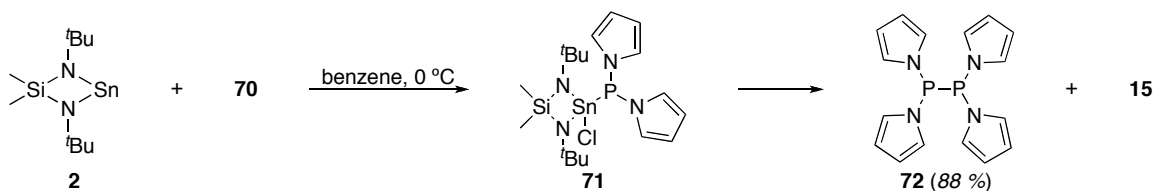
To test a chlorophosphine with electron-withdrawing, N-based substituents, the previously reported<sup>124</sup> chloro-bis(pyrrolyl)phosphine was synthesized by lithiation of pyrrole **67** and subsequent addition to  $\text{PCl}_3$  **39** (Scheme 66) .





Scheme 66. Synthesis of chlorobis(pyrrolyl)phosphine **70**.

Addition of **70** to the cyclic stannylene **2** provided a single Sn–P product. This insertion product was found to be unstable leading to tetrapyrrolyldiphosphine.



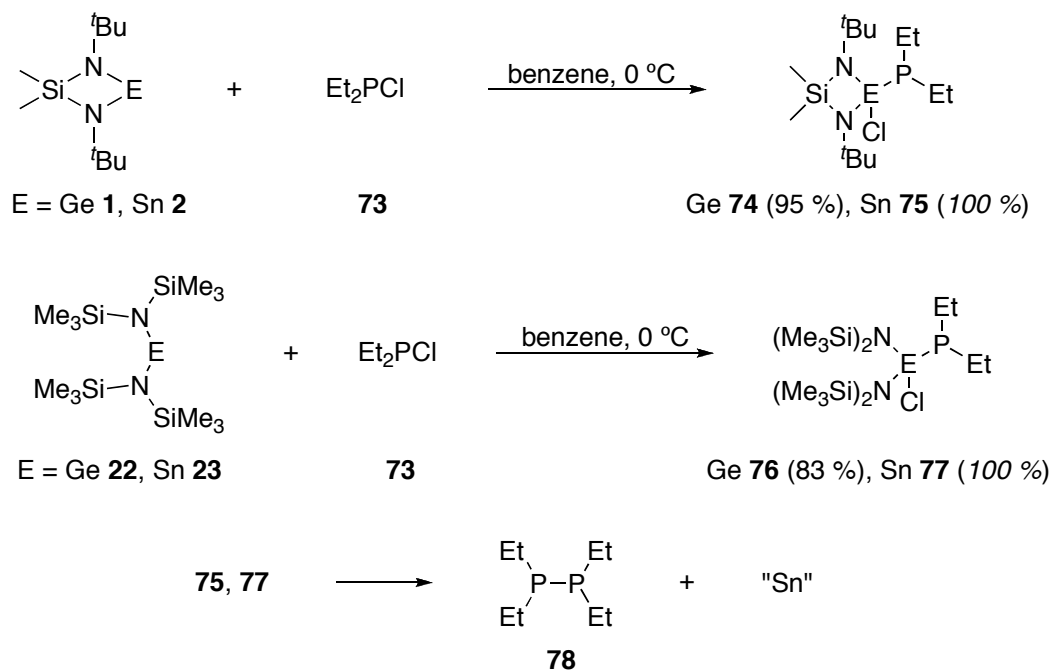
Scheme 67. Reaction of stannylene **2** with monochlorophosphine **70**.

This assignment of the structure in compound **71**, versus a structure resembling compounds **60** and **62**, was made based on the  $^1J_{119/117\text{SnP}}$  coupling constant of 1275/1225 Hz. As we have observed with our structures,  $^1J_{119\text{SnP}}$  values lower than 1700 Hz indicate “standard”-type insertion products. This suggests that either the availability of the nitrogen lone pair or the presence of electron-withdrawing amino groups on phosphorus, is required to cause formal insertion of the phosphine into the Sn–N bond. The diphosphine end-product displays one useful outcome of these reactions, synthesis of diphosphines via metal reduction. However, magnesium would likely be a preferable alternative as it is cheaper, easier to separate from the product, and it should be nearly as effective.

#### *Steric effects of non-halide substituents on phosphorus*

As the likely mechanisms seemed to become better defined, we felt that we had to return to our previous approach with alkyl- and arylchlorophosphines. Our first objective

was to test a monochlorophosphine containing substituents with similar electronic effects to a *tert*-butyl group but with significantly less bulk. To this effect, we tested both cyclic and acyclic germylenes and stannylene with Et<sub>2</sub>P(Ph)Cl **73**. Supporting our belief that steric effects are crucial in determining insertion rates, we observed that relative rates of insertion for all heterocarbenes with Et<sub>2</sub>P(Ph)Cl **73** are significantly faster than even those with Ph<sub>2</sub>P(Ph)Cl **11**. An updated relative rates of insertion ranking would be: Et<sub>2</sub>P(Ph)Cl **73** > Ph<sub>2</sub>P(Ph)Cl **11** > *t*Bu(Ph)P(Ph)Cl **45** >> *t*Bu<sub>2</sub>P(Ph)Cl **17**. Standard insertion products were obtained with an important finding that stannylene insertion products were unstable, providing tetraethyldiphosphine **78** as the end product (Scheme 68).



Scheme 68. Reactions of carbenoids **1**, **2**, **22**, and **23** with chlorodiethylphosphine **73**.

Not only were the stannylene insertion products **75** and **77** unstable, but they appeared to break down more quickly than those of the chlorophenylphosphines. This observation suggests that the stability of the stannylene insertion products is connected

primarily to the steric shielding around Sn, P, or both and not the electron-withdrawing or -donating ability of the phosphorus substituents.

Close monitoring of reaction mixtures by  $^{31}\text{P}\{^1\text{H}\}$  NMR spectroscopy allowed the observation of intermediates between the insertion product and the final cyclic, oligophosphine products. The ability to observe these transient species suggests that it is unlikely that these insertions decompose via a radical pathway. The same spectral pattern (exact chemical shift of the signal varied based on the identity of the phosphine) has been observed while monitoring the breakdown of the insertion products obtained from the addition of the cyclic stannylene **2** to  $\text{PhPCl}_2$  **3**,  $\text{Et}_2\text{PCl}$  **73** and  $\text{PCl}_3$  **39**. The resulting spectra show complex coupling patterns indicating multiple types of Sn atoms with respect to each phosphorus atom as shown in Figure 28.

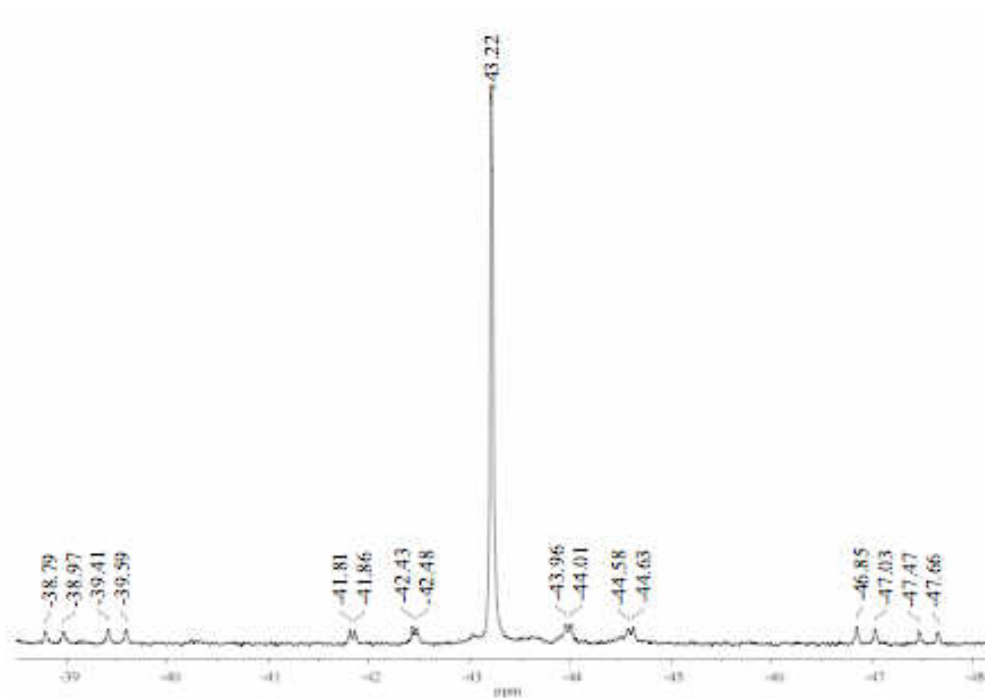
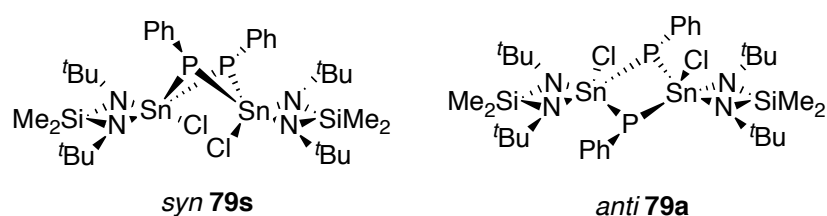


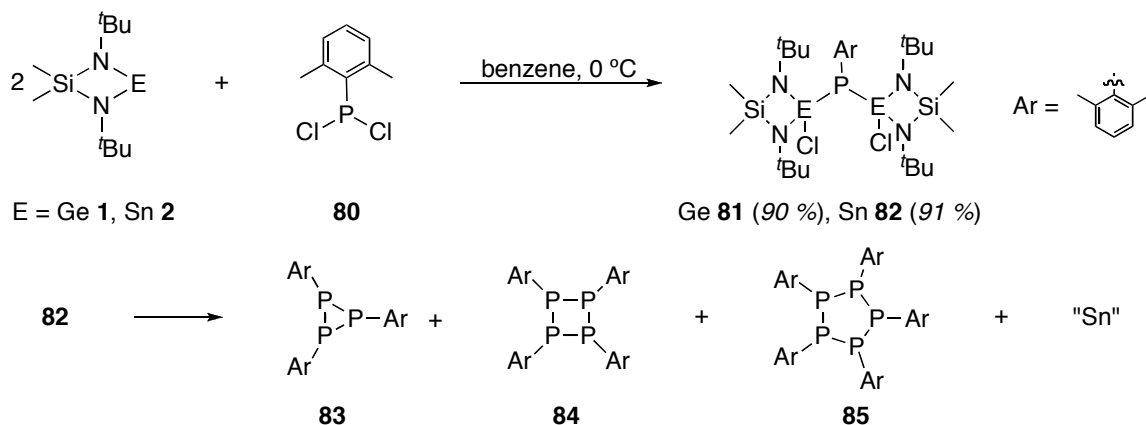
Figure 28.  $^{31}\text{P}\{^1\text{H}\}$  NMR spectrum of the reaction mixture containing cyclic stannylene **2** and dichlorophenylphosphine **3** (see Scheme 43 for reaction).

This signal in the  $^{31}\text{P}\{^1\text{H}\}$  NMR spectrum (shown in Figure 28) of the reaction mixtures can be seen alongside signals for the diinsertion product as well as the phosphacycle end products. While it possesses multiple Sn–P couplings ( $\delta -43.22$ ,  $J_{119/117\text{SnP}} = 1796/1721$  Hz,  $1543/1470$  Hz,  $571/551$  Hz,  $320/300$  Hz), each satellite pair comes to half of the expected integration value (with respect to the center signal). This can be explained by the *syn* **79s** and *anti* **79a** conformations of the complex,  $\{[\text{Me}_2\text{Si}(\mu\text{-N}^t\text{Bu})_2\text{Sn}(\text{Cl})]_2\text{PPh}\}_2$  **79** (Scheme 68). This signal appears in the spectra not long after combination of the reactants but does not continue to grow. Instead, its strength (i.e. the concentration of the complex) reaches an equilibrium point and remains there until the reaction reaches its end and then the signal disappears.



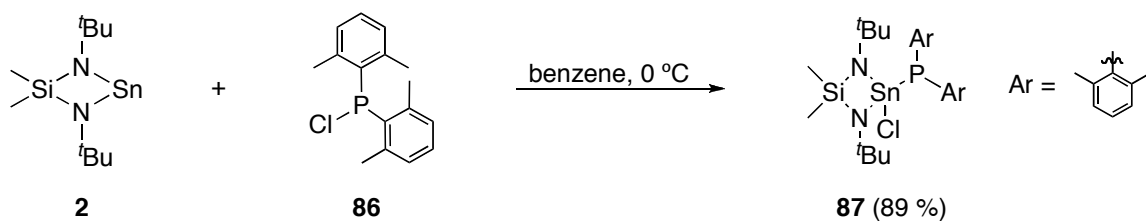
Scheme 69. Two conformations, *syn* **s** and *anti* **a**, of dimeric **79**.

The next objective was to test ortho-substituted phenylchlorophosphines. This would provide similar EW/ED properties while providing more shielding around phosphorus. First, (2,6-Me<sub>2</sub>Ph)PCl<sub>2</sub> **80** was tested with the cyclic germylene **1** and stannylene **2** (Scheme 70). As with the unsubstituted PhPCl<sub>2</sub>, the germylene product **81** was found to be stable and the stannylene product **82** was not. However, in contrast to  $[\text{Me}_2\text{Si}(\mu\text{-N}^t\text{Bu})_2\text{Sn}(\text{Cl})]_2\text{PPh}$  **5**,  $[\text{Me}_2\text{Si}(\mu\text{-N}^t\text{Bu})_2\text{Sn}(\text{Cl})]_2\text{P}(2,6\text{-Me}_2\text{Ph})$  **82** was converted to the cyclic oligophosphines at a significantly slower rate. Moreover, the ratio of (ArP)<sub>3</sub> **83**: (ArP)<sub>4</sub> **84**: (ArP)<sub>5</sub> **85** shifted significantly in favor of the smaller ring sizes indicating that this too is connected to the steric environment of the phosphorus centers.



Scheme 70. Reactions of cyclic carbenoids **1** and **2** with aryldichlorophosphine **80**.

Subsequently, the related monochlorophosphine **86** was treated with stannylene **2** to test the stability of its addition product (Scheme 71).



Scheme 71. Reaction of cyclic stannylene **2** with chlorodiarylpophosphine **86**.

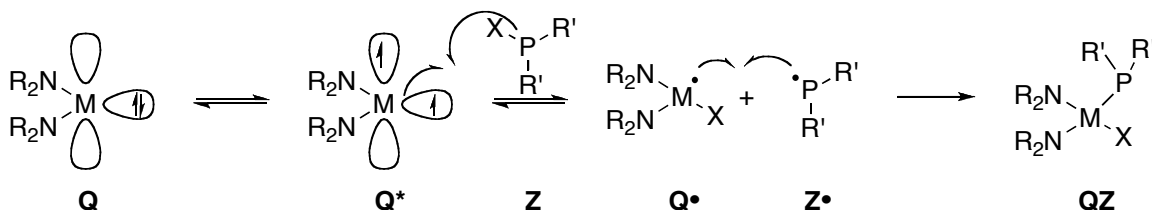
A startling breakthrough was the determination that the insertion product **87** resulting from this combination is stable and isolable. Crystals of the chlorostannylphosphine **87** were isolated and the drawn structure has been assigned based on  $^{31}\text{P}\{^1\text{H}\}$  and  $^1\text{H}$  NMR spectra. The phosphorus signal appears at  $\delta -26.6$  ppm with a Sn–P coupling constants of 1803 and 1725 Hz for  $^{119}\text{Sn}$  and  $^{117}\text{Sn}$  nuclei, respectively. The  $^1\text{H}$  spectrum shows a splitting of the silylmethyl peaks (consistent with the difference in environment above and below the four-membered ring), and other expected features, i.e., a singlet for the *tert*-butyl protons and a singlet for the *ortho*-methyl substituents on each phenyl ring.

### II.3. Mechanistic Hypotheses

#### *Proposed insertion mechanisms*

Several hypotheses have been proposed concerning mechanistic pathways by which insertion takes place: radical (singlet-triplet),  $S_NP$  nucleophilic substitution, P–M coordination-initiated, and phosphonium ion formation/stabilization (related to halide abstraction proposed by Lappert<sup>62</sup> for Si–X insertions, Scheme 28, page 25). The latter two were published during the investigation of these reactions.

The radical mechanism begins with the excitation of the singlet ground state **Q** of the carbenoid to the diradical triplet state **Q\***. This triplet species is assumed to extract a halide radical from a halophosphine **Z** providing a phosphorus-centered radical **Z•**. Subsequently, the phosphorus radical combines with the remaining metal-centered radical species **Q•** providing the insertion product **QZ** (Scheme 72).

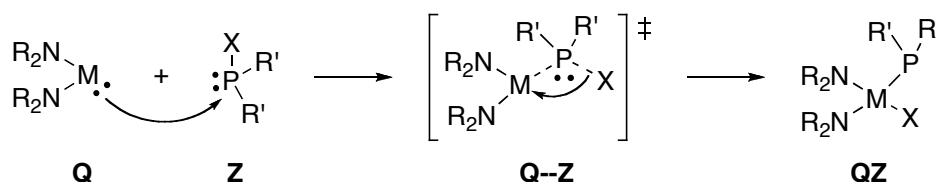


Scheme 72. Radical-based mechanism for insertion of carbenoid **Q** into phosphine **Z**.

The rate-limiting step for this process would presumably be the excitation equilibrium in which the singlet species is excited to the triplet state. This could potentially be initiated by heat or light. Computational studies led by Su<sup>125</sup> have shown that for analogous germynes and stannynes, the singlet-triplet energy gap (barrier to excitation) is greater for stannynes. Based on this, reactions with stannynes should proceed more slowly than with their germanium counterparts. However, the opposite is observed, with germynes reacting magnitudes slower than the analogous stannynes.

Reaction rates are therefore primarily dependent on the heterocarbene (i.e., stannylene or germylene), though they would also be influenced by the substituents on phosphorus. Bulky electron-donating groups should speed the reaction progress while smaller electron-withdrawing groups should hinder it.

$S_NP$  nucleophilic substitution (Scheme 73) is similar to the well-known  $S_N2$  mechanism, but phosphorus, being able to expand its octet, does not require the “leaving” group to actually leave.<sup>126</sup> As applied to these reactions, the pathway would begin with an attack at the phosphorus center **Z** by the nucleophilic carbenoid **Q**, the rate-limiting step. Little is known regarding the relative nucleophilicities of  $M^{II}$  ( $M = \text{Group 14 metal}$ ) species, but it is presumed that the  $\text{Sn}^{II}$  compound would be a stronger nucleophile than the  $\text{Ge}^{II}$  species due to its higher singlet-triplet gap energy and lower electronegativity. As discussed above, this trend is observed (stannylenes react faster than equivalent germylenes). Also, for an  $S_N2$ -like mechanism, leaving group effects should be significant. This was also observed as the rate of insertion of stannylene **1** into the P–X bond of  ${}^t\text{Bu}(\text{Ph})\text{PI}$  **47** was much faster than for  ${}^t\text{Bu}(\text{Ph})\text{PCl}$  **45** as shown in Table 2.



Scheme 73.  $S_NP$  mechanism for halide substitution by a metal fragment.

Steric and electronic effects would be expected to be significant as well. As the bulk of substituents on phosphorus increases, the rate should decrease, and more electron-withdrawing groups should increase the rate. For the halophosphines investigated, these two effects are constantly competing.

A comparison of reactions rates of stannylene **2** with various chlorophosphines, summarized in Table 46, has aided in the investigation of this mechanism. The extremely bulky <sup>t</sup>Bu<sub>2</sub>PCl **11** exhibits a slower reaction rate than any other phosphine, requiring approximately two weeks at 70 °C to reach completion. The isolated mono-insertion product  $\{[(\text{Me}_3\text{Si})_2\text{N}]_2\text{Ge}(\text{Cl})\}\text{P}(\text{tBu})\text{Cl}$  **29**, when combined with stannylene **2**, reacts very slowly at room temperature, the time to completion being estimated at 3–4 weeks. Attempts at higher temperatures (> 55 °C) are complicated by the fact that the insertion product decomposes at accelerated rates with increasing temperature.

Table 46. Summary of relative completion times of stannylene **2** with monochlorophosphines.

<u>Halophosphine</u>	<u>Temp. (°C)</u>	<u>Solvent</u>	<u>~ Completion Time</u>
Ph <sub>2</sub> PCl <b>11</b>	– 78	toluene	< 30 min.
Et <sub>2</sub> PCl <b>73</b>	– 78	benzene	< 30 min.
<sup>t</sup> Bu <sub>2</sub> PCl <b>17</b>	70	toluene	2 weeks
$\{[(\text{Me}_3\text{Si})_2\text{N}]_2\text{Ge}(\text{Cl})\}\text{P}(\text{tBu})\text{Cl}$ <b>29</b>	25	benzene	3–4 weeks
<sup>t</sup> Bu(Ph)PCl <b>45</b>	25	toluene	70–75 min.
<sup>t</sup> Bu(Ph)PI <b>47</b>	25	toluene	< 20 min.

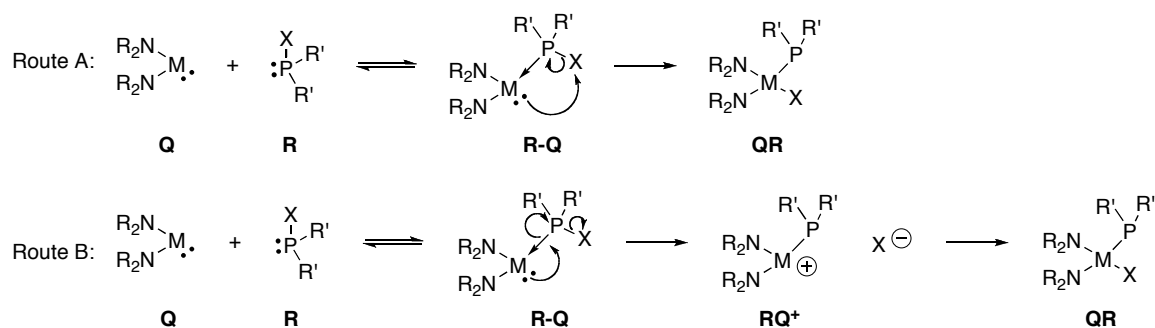
The reaction of **2** with <sup>t</sup>Bu(Ph)PCl **45** was monitored by NMR at room temperature and was complete in 70–75 minutes. Addition of **2** to Ph<sub>2</sub>PCl **11** could not be well monitored by NMR spectroscopy. After one completed data collection (~ 12 minutes), approximately 95 % conversion of **11** to the insertion product **13** was observed. Reaction with Et<sub>2</sub>PCl **73** is too fast to be monitored by NMR at room temperature. Both



reactions appear to be completed within 30 minutes at  $-78$  °C. On the basis of the observed result that germylene **1** reacts with **73** faster than **11** (the corresponding transformations with **1** are significantly slower and thus more easily monitored by  $^{31}\text{P}\{^1\text{H}\}$  NMR spectroscopy) it stands to reason that the stannylene **2** should do so as well.

The additional electron density on phosphorus, from its alkyl substituents, would be expected to inhibit nucleophilic attack by the carbenoid. Accordingly, a slow reaction rate is observed for the addition of any carbenoid to  $t\text{Bu}_2\text{PCl}$  **17**.  $\text{Et}_2\text{PCl}$  **73** shows the electron-rich phosphorus (without steric encumbrance) reacting at a drastically faster rate. The likelihood that  $\text{Et}_2\text{PCl}$  **73** reacts faster than  $\text{Ph}_2\text{PCl}$  **11** for stannylene **2** is based on the rate increase observed for the reaction with germylene **1**. When combined with **1**,  $\text{Ph}_2\text{PCl}$  **11** is fully converted in approximately 1 h at  $0$  °C while  $\text{Et}_2\text{PCl}$  **73** is fully converted before a single spectrum can be collected ( $\sim 20$  min.) given the same conditions. This suggests that the increased electron density on phosphorus has either no effect or the opposite effect. This, however, assumes that the steric difference between the ethyl and phenyl groups is not sufficient to explain the rate reduction.  $(2,6\text{-Me}_2\text{C}_6\text{H}_3)\text{PCl}_2$  **80** has been used as a more encumbered, yet electronically similar analogue to  $\text{PhPCl}_2$  **3**. Stannylene **2** reacts with **73** so quickly, even at reduced temperatures, that it is impossible to monitor the reaction using NMR spectroscopy. In stark contrast, reaction of stannylene **2** with **17** takes weeks at room temperature to reach completion. This demonstrates the large steric effects on the reaction rate compared to electronic effects.

The two aforementioned mechanisms are those that had been put forth previously to attempt to explain these reactions. An alternative mechanism, which we propose here, is a P→M coordination-initiated pathway (Scheme 74). This mechanism has many similarities with nucleophilic substitution. If this is so, steric effects shall play a large role in determining reaction rate, but the role of electronic effects should be opposite from the S<sub>N</sub>P mechanism because of their impact on the donor strength of phosphorus. The rate-limiting step would be the formation of a Lewis acid-base pair **R-Q** between the halophosphine **R** and the carbenoid **Q**. Being a singlet carbenoid, the M<sup>II</sup> center possesses an empty p orbital, allowing it to act as Lewis acid, albeit a weak one. Once the adduct has been formed, the halide can either undergo a 1,2-migration providing the insertion product **QR** (Route A) or the halide can dissociate from phosphorus (Route B), generating a metal cation **RQ<sup>+</sup>**, and then coordinate to the metal center to give the final product **QR**.

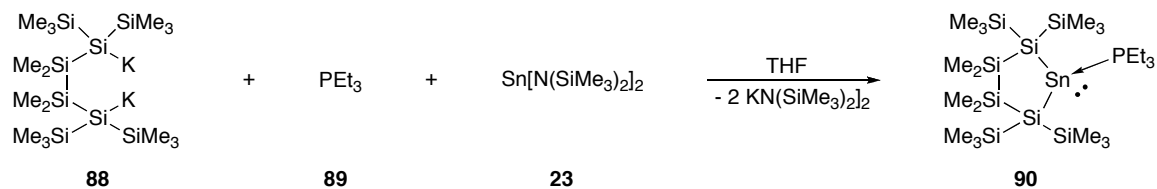


Scheme 74. Two alternative routes for P→M coordination-initiated mechanistic hypothesis.

In order to test this hypothesis, halophosphines with unavailable lone pairs were investigated. The complexes *trans*-(PhPCl<sub>2</sub>)<sub>2</sub>PdCl<sub>2</sub> **49** and *trans*-(<sup>t</sup>BuPCl<sub>2</sub>)<sub>2</sub>PdCl<sub>2</sub> **50** contain halophosphines which have been tested on their own with stannylene **2**, yet the lone pair is now occupied with the more Lewis acidic PdCl<sub>2</sub> moiety. If these reactions

proceed via a nucleophilic substitution route, removal of electron density from phosphorus should theoretically increase the rate of reaction. Many examples have been reported of phosphines being activated towards nucleophilic attack by coordination to a metal center (including Pd<sup>II</sup>).<sup>127</sup> As it was shown in Scheme 59 (page 90), however, these tests did not provide insertion products (instead yielding the tetrastannylpalladium complex **51**). Reactions of stannylene **2** with PdCl<sub>2</sub> species were more complex than we anticipated and formal insertion into Pd–Cl bonds (via an associative mechanism) is a viable option and perhaps even competitive with insertion into P–Cl bonds. This would render the results of these tests not useful for the focus of this investigation.

Phosphine coordination to stannylenes is not without precedent, though it is rather rare. In a recent example<sup>128</sup> a disilylated stannylene–triethylphosphine complex was prepared (Scheme 75).



Scheme 75. Synthesis of the stannylene-phosphine adduct **90**.

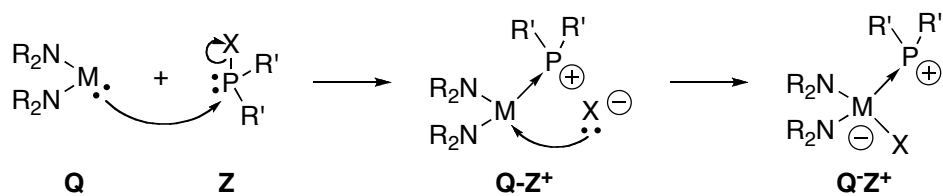
Utilizing a different method to “occupy” the lone pair of phosphorus, the thiophosphine PhP(S)Cl<sub>2</sub> **56** was synthesized. When combined with stannylene **2** an insertion product was observed; however, the change in rate was so drastic as to suggest that an alternative pathway was in play. Addition of two equivalents of stannylene **2** to PhP(S)Cl<sub>2</sub> **56** provides the diinsertion product **57** but this process was extremely slow compared to the same reaction with PhPCl<sub>2</sub> **11** (Scheme 61, page 97). [(Me<sub>2</sub>Si(μ-N<sup>t</sup>Bu)<sub>2</sub>Sn(Cl))<sub>2</sub>PPh] **5** is produced at –78 °C in ~30 minutes (by best estimate), but

reaction with the analogous thiophosphine required approximately one week at room temperature.

Because the lone pair has been removed, an  $S_NP$  mechanism may takeover. This result lends support to the hypothesis that this reaction proceeds via a P–M coordination-initiated pathway. If it were proceeding by an  $S_NP$  mechanism, oxidation by a chalcogen should decrease the electron density on phosphorus making it more susceptible to nucleophilic attack while only adding a limited amount of extra steric interference.

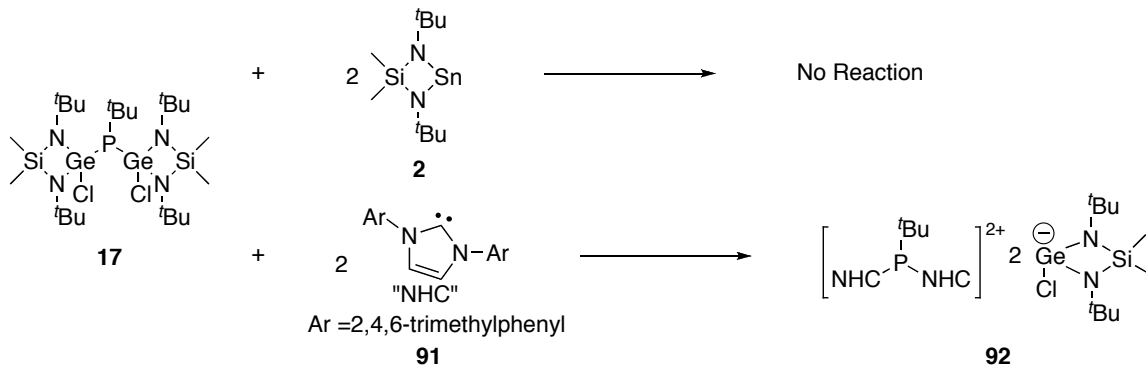
The final possibility for a potential insertion mechanism is to treat instead the heterocarbene and halide (on P) as ligands and to view the process as displacement of a more labile ligand. This approach is based on results reported by MacDonald and coworkers and a follow-up by Weigand showing the action of *N*-heterocyclic carbenes on chlorophosphines, especially  $PCl_3$  (Scheme 38, page 32).<sup>98,99</sup> Addition of the *N*-heterocyclic carbene to  $PCl_3$  resulted in the displacement of two chlorides to give a chlorophosphenium cation. The remaining chloride, having nowhere else to go, becomes a counter ion in the outer coordination sphere.

As applied to the reactions studied in this investigation (Scheme 76), the halide on halophosphine **Z** is displaced by the less labile carbenoid **Q** generating the cationic Lewis adduct **Q-Z<sup>+</sup>**. Following this, the empty p orbital on the metal center is a reasonable place for the chloride to coordinate providing complex **Q<sup>+</sup>Z<sup>-</sup>** (structurally identical to **QZ**, but taken from a different electronic perspective) rather than remain outside the inner coordination sphere.



Scheme 76. Phosphenium ion generation  $Q-Z^+$  and stabilization  $Q^+Z^+$  by carbenoid species  $Q$ .

It has been determined experimentally and supported with calculation-based results that germylenes are stronger donors than analogous stannylenes.<sup>129–131</sup> This can be used to explain the observation that complexes containing germylenes are more stable (compared to analogous stannylene complexes) and generally do not undergo any reactions with other phosphorus centers to produce diphosphines or cyclic oligophosphines. However, stannylenes are significantly weaker donors and are not able to stabilize all phosphenium ions, only  ${}^t\text{Bu}_2\text{P}^+$  and  ${}^t\text{BuP}^{2+}$  as of yet. In an attempt to determine the likelihood of this pathway,  $[\text{Me}_2\text{Si}(\mu\text{-N}^t\text{Bu})_2\text{Ge}(\text{Cl})]_2\text{P}^t\text{Bu}$  **17** was separately reacted with two equivalents of stannylene **2** and the NHC  $N,N'$ -bis(2,4,6-trimethylphenyl)imidazol-2-ylidene **88** (Scheme 77). The structure of the NHC-stabilized phosphenium ion **89** with chlorogermanate counter ion was determined on the basis of  ${}^{31}\text{P}\{^1\text{H}\}$  and  ${}^1\text{H}$  NMR spectra.



Scheme 77. Attempted reactions of **17** with stannylene **2** and NHC **88**.

The stannylene, being a more weakly coordinating ligand, was unable to displace the chlorogermyl moiety, while the NHC displaced, although slowly, the germanium providing [(NHC)<sub>2</sub>P<sup>t</sup>Bu][ClGe( $\mu$ -N<sup>t</sup>Bu)<sub>2</sub>SiMe<sub>2</sub>] **89**. Carbenes are known as powerful stabilizers due to their strong binding to acceptors and their ability to displace other relatively strong ligands (e.g. phosphines). The data support the belief that donor ability drops upon descending the group, i.e. carbenes are stronger donors than germylenes, which are in turn stronger than stannylenes.<sup>129–132</sup>

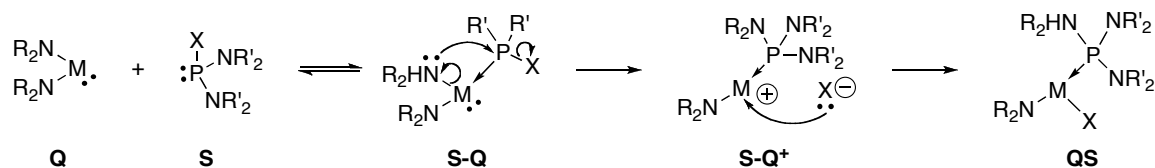
Given the four potential routes, by which these insertions can take place, it is the reactions with the aminochlorophosphines that have given the most important insight. The chlorophosphines Me<sub>2</sub>Si( $\mu$ -N<sup>t</sup>Bu)<sub>2</sub>PCl **59**, (Et<sub>2</sub>N)<sub>2</sub>PCl **61**, Et<sub>2</sub>NPCl<sub>2</sub> **64**, and chlorobis(pyrrolyl)phosphine **70** provided different product types when combined with **1** and **2**. Stannylene **2** does not insert into **59**, **61**, and **64**, but instead reacts by ligand exchange yielding products **60**, **62**, and **65** (Schemes 63–65, pages 98, 102, and 106). However, for germylene **1**, insertion products **63** and **66** are obtained from its addition to **61** and **64**, respectively.

Isolation of this new type of products appears to rule out both the radical and S<sub>N</sub>P mechanisms. If these insertions did proceed by a radical pathway, it is difficult to understand why only now would this alternative product form be found and why not as a mixture with the “standard” insertion product (e.g. **5**). Since by this mechanism the reaction itself should mostly be dictated by the heterocarbene, there appears to be no reason for this change in reaction outcome when viewed within the confines of this mechanism.

The  $S_{NP}$  mechanism, similar to the radical mechanism, has a reaction initiation step that is strongly dependent on the carbenoid in play. The amide substituents would possibly create a stronger partial positive charge on phosphorus (N is more electronegative than C), but this would only suggest that the reaction rate should increase, and not promote an alternative product. Moreover, reactions with  $PCl_3$  **39**, possessing much more electronegative substituents, do not give this type of outcome. When combined with **39**, germylene **1** yielded only the triinsertion product **40**, stannylene **2** provided as of yet undetermined phosphacycles (Scheme 54, page 77), and the acyclic germylene **22** and stannylene **23** gave the stable and meta-stable diinsertion products, **40** and **41**, respectively (Scheme 55, page 78). Based on this, the outcomes of reactions with amidophosphines point to either the coordination-initiated or phosphonium ion mechanisms.

If insertion is initiated by coordination of the halophosphine **C** to the metal center in **S**, as shown in Scheme 78, then at this point phosphorus has a larger partial positive charge in the complex **S-Q**. The weak Sn-N bond **Q** breaks to form a favored P-N bond with  $X^-$  acting as a leaving group providing a phosphine-coordinated, cationic metal center **S-Q<sup>+</sup>**. The free halide then attaches to the metal yielding the  $P^{III} \rightarrow M^{II}$  product **QS**. The reason germylenes do not display this reactivity can be explained in two ways: 1) the strength of the Ge-N bond (compared to the Sn-N bond)<sup>133</sup> does not allow for its cleavage and 2) the smaller size of Ge (van der Waals radii of Ge = 2.00 and Sn = 2.17)<sup>105</sup> does not offer the flexibility necessary to align the phosphine properly to allow for nucleophilic attack by the metal-attached amide. One or both of these effects could be

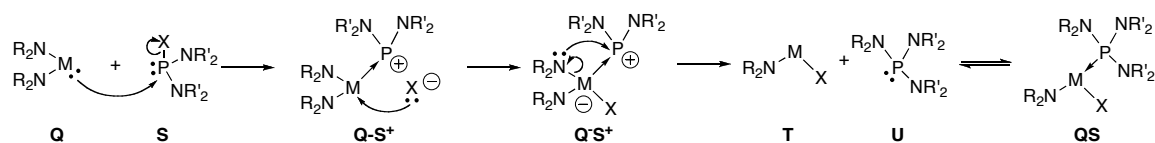
contributing to the isolation of a “standard” diinsertion product for the addition of germylene **1** to **64**.



Scheme 78. Coordination-initiated pathway for the reaction of carbenoid **Q** with bis(amido)chlorophosphine **S** resulting in the ligand-exchange product **QS**.

This type of nucleophilic attack on a metal-coordinated phosphine by a metal-attached nucleophile is not without precedent. It is a common problem in homogenous catalyst systems (more examples for Rh<sup>I</sup> and Pd<sup>II</sup> systems) as it destroys catalysts by phosphine decomposition.<sup>122</sup>

Alternatively, formation and stabilization of a phosphonium ion could also be used to explain the compounds produced from the combination of stannylene **2** and the aminophosphines (Scheme 79). Formation of the phosphonium ion **Q-S<sup>+</sup>**, initiated by the carbenoid **Q** displacing the halide on phosphine **S**, provides an electron-poor phosphorus center that is susceptible to attack by Lewis bases. After the halide attaches to the metal center, providing **Q<sup>-</sup>S<sup>+</sup>**, the M–N bond will be more easily cleaved to allow the amide to attack the phosphonium ion. This exchange provides the triaminophosphine **U** and a metal amide/halide **T**. These species form the Lewis acid-base pair **QS** with ease, especially when held in proximity by a bridging diamide ligand.



Scheme 79. Phosphonium ion pathway for formation of complex **QS**.



Again, since germylenes do not display this reactivity, possible explanations for this phenomenon are the following: 1) as in the coordination-initiated approach the greater strength of the Ge–N bond (compared to the Sn–N bond)<sup>133</sup> may disallow this alternative outcome and 2) the acid-base pair of the phosphonium ion and the germylene may be too strong and stable to make the phosphorus susceptible to nucleophilic attack. Also, as stated before, one or both of these effects may play some role in affecting the observed outcome.

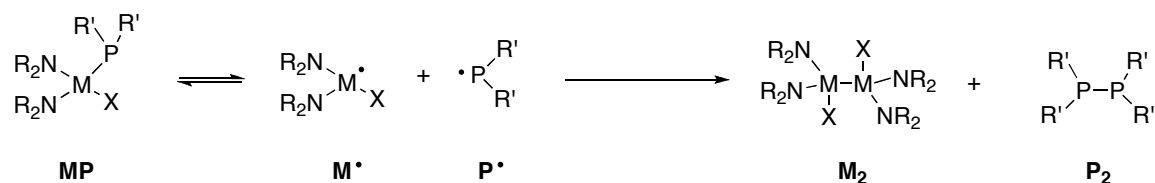
*Mechanistic hypotheses for the decomposition of insertion products*

A major portion of the aforementioned insertion products are not thermally stable. Nearly all germylene insertions are stable and do not undergo further reaction while nearly all stannylene insertions can be seen as intermediates to the eventual formation of P–P bonds.

The two possible mechanisms identified for these decomposition processes are homolytic cleavage of the P–M bond (i.e. radical mechanism with eventual intramolecular termination) and intermolecular complexation/elimination (similar to reductive elimination). The radical mechanism was put forth by Veith *et al.* when they first investigated these types of reactions,<sup>76</sup> whereas the elimination route is an alternative that we are proposing and which appears to explain the same results better than the radical mechanism.

The radical pathway is initiated by homolytic cleavage of the P–M bond in **MP**, either thermally or from incident light, yielding the radicals **M•** and **P•** (Scheme 80). For monochlorophosphines the newly formed chlorostannyl/germyl radical and dialkyl/diaryl

phosphine radical can either recombine (equilibrium exchange) or “dimerize” to form a  $M^{III}$  digermene or distannane  $M_2$  and a diphosphine  $P_2$  (formally  $P^{II}$ ).

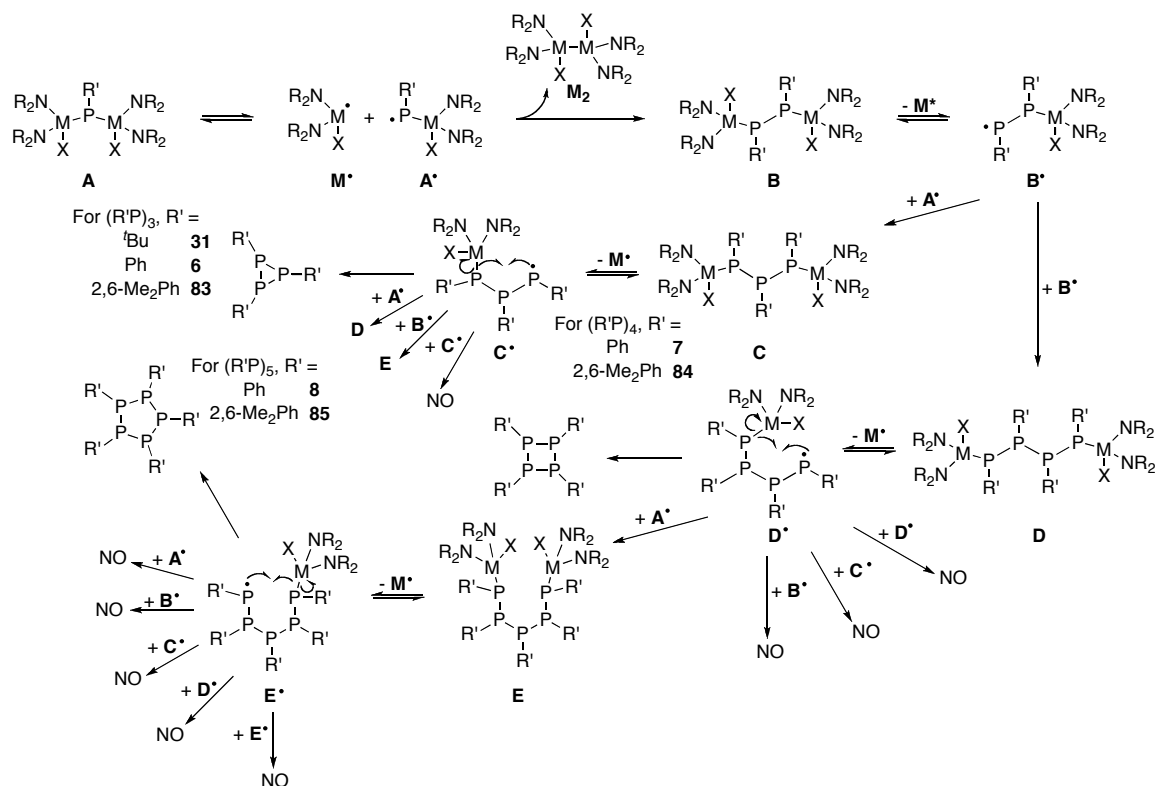


Scheme 80. Breakdown of insertion product **MP** by homolytic cleavage (radical mechanism).

In the case of dichlorophosphines, the same stannyl or germyl radical is formed although the phosphorus species is more uncertain. Potentially a phosphinidene (diradical  $P^I$ ) could be formed by nearly simultaneous cleavage of both P–M bonds or an alkyl/aryl chlorostannyl/germyl phosphorus radical could be formed. The stannyl/germyl radicals could dimerize as before but the potential intermediates for the phosphorus radicals are more numerous. A dimerized phosphinidene would create a diphosphene (containing a P–P double bond) which could then dimerize (2+2 cycloaddition) or combine with a free phosphinidene (2+1 cycloaddition), both being terminating steps. These steps involving phosphinidenes are left out for clarity and, although their presence would be appealing, they are likely not generated.

As shown in Scheme 81, diinsertion product **A** undergoes radical cleavage to produce the metal-centered radical  $M^\bullet$  and the phosphorus-centered radical  $A^\bullet$ . The phosphorus radical can react with another one to give a bis(chlorostannyl/germyl)diphosphine **B** which can undergo further homolytic cleavage to form phosphacycles ranging from 3- to 6-membered rings. The isolated product  $[(Me_3Si)_2N)_2Sn(Cl)PPh]_2$  **26**, resulting from the 2:1 addition of the acyclic stannylene **23** to  $PhPCl_2$  **3** is a direct example of the structural type **B**, and appears to be a stable

intermediate in this process. Why it does not undergo further cleavage cannot be explained using this mechanistic paradigm. Heating **26** (Scheme 47, page 59) to reflux in toluene has proven insufficient to cause further breakdown to phosphacycle products.



Scheme 81. Radical-based mechanism for the breakdown of diinsertion products **A** eventually yielding phosphacycles **6–8**, **31**, and **83–85** (NO = “not observed”).

The ring sizes of these phosphacycles appears to be primarily determined by the size of the substituent on phosphorus. Large *tert*-butyl groups favor smaller three-membered rings **31** while the smaller Ph groups favor formation of four- and five-membered rings **7** and **8**, respectively, the bulkier 2,6-dimethylphenyl group also favors smaller ring sizes **84** and **85**.

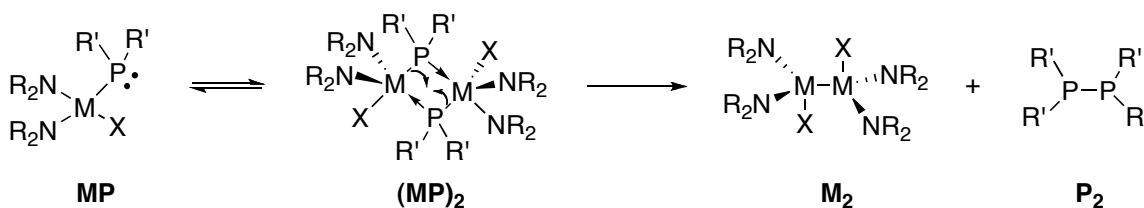
Ge–P bonds are stronger than Sn–P bonds.<sup>133</sup> Since the observed relative stabilities of these compounds show that Ge-containing molecules are much more likely

to remain intact than their Sn counterparts, the data seems to suggest that this radical pathway is plausible. Favoring the idea that thermal decomposition is the primary source for radical formation is the fact that numerous Sn-containing insertion products are unstable even at  $-15\text{ }^{\circ}\text{C}$  with a complete absence of light.

Despite the few consistencies, the radical mechanism does not appear to be the best fit to explain the decomposition of these insertion products, both in terms of predicting relative stabilities of products and in the distribution of phosphacycle ring sizes. In general, stabilization of the phosphorus radical would be expected to happen by two methods, electronically and sterically. Since the radical is an electron-deficient species, electron-donating groups would be expected to favor radical formation. There have been no studies reported analyzing substituents effects on  $\text{P}^{\text{III}}$ -centered radicals. However, in the recent literature an important trend is observable, the use of large substituents, which shield the radical from interacting with other molecules, extending the lifetime of these species.<sup>134-137</sup> Applying this, it would be expected that the trend for ease of phosphorus radical formation would be as follows:  $\bullet\text{P}^t\text{Bu}_2 > \bullet\text{P}(^t\text{Bu})\text{Ph} > \bullet\text{PPh}_2 \approx \bullet\text{PEt}_2$ . However the observed trend for disappearance of insertion product is completely opposite:  $\text{MPEt}_2 > \text{MPPH}_2 > \text{MP}(^t\text{Bu})\text{Ph} > \text{MP}^t\text{Bu}_2$ ,  $\text{M} = (\text{Me}_2\text{Si}(\mu\text{-N}^t\text{Bu})_2\text{Sn}(\text{Cl}))$ . Moreover, these insertions and decompositions, proceed fairly cleanly with all phosphorus-containing products identifiable by  $^{31}\text{P}$  NMR spectroscopy. A lack of side products seems unlikely given the number of radicals potentially present in the reaction mixture. Finally, the only reason why ring sizes abruptly stop at five atoms can only be attributed to the ever increasing likelihood of an intramolecular reaction with increasing

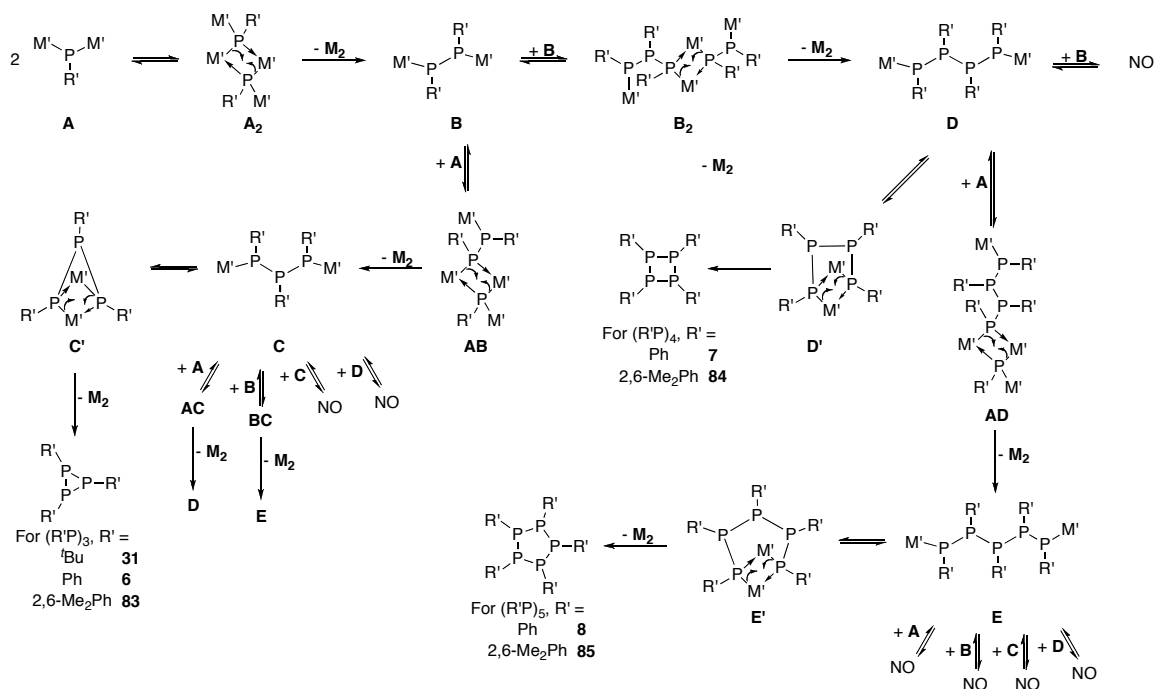
chain size, although statistically, with so many potential species present one would expect to see some larger rings, even if in small quantities.

To explain these discrepancies, we have developed the complexation/elimination hypothesis (Scheme 82). The initiating step in this mechanism is the formation of a dimeric Lewis acid-base adduct  $(\text{MP})_2$  between the metal-bound phosphine and metal atom of an identical molecule  $\text{MP}$ . Forming this adduct allows for subsequent reductive elimination of the P-moieties and M-moieties providing a formal  $\text{P}^{\text{II}}$  diphosphine  $\text{P}_2$  and formal  $\text{M}^{\text{III}}$  dimetalane  $\text{M}_2$ .



Scheme 82. Complexation-elimination route for decomposition of monoinsertion  $\text{MP}$  yielding  $\text{M}_2$  and  $\text{P}_2$ .

For diinsertions (Scheme 83), this first step yields a diphosphine with Ge- or Sn-based substituents  $\text{B}$  and would undergo successive complexation-elimination steps eventually forming phosphacycles **6–8**, **31**, and **83–85** in terminating steps. Dimer  $\text{A}_2$  is the form we believe we have witnessed spectroscopically as the dimers **79a** and **79s** (Scheme 67, spectrum in Figure 28). While other complexes (e.g.  $\text{B}_2$ ) should theoretically be present, they may be in small enough quantities to disallow their identification by NMR. The formation of diphosphines  $\{[(\text{Me}_3\text{Si})_2\text{N}]_2\text{Sn}(\text{Cl})\text{PPh}\}_2$  **26** and  $\{[(\text{Me}_3\text{Si})_2\text{N}]_2\text{Ge}(\text{Cl})\text{PCl}\}_2$  **44** can also be viewed as forms of  $\text{B}$  that are too bulky to allow for the formation of the dimeric  $\text{B}_2$ .



Scheme 83. Complexation-elimination mechanism for the decomposition of diinsertion product **A** eventually yielding phosphacycles (NO = “not observed”).

The plausibility of this mechanism is evidenced primarily by the fact that the trend for decomposition unwaveringly follows the trend of steric bulk i.e., the bulkier the substituents on phosphorus the slower the decomposition takes place. In the extreme case of  $(\text{Me}_2\text{Si}(\mu\text{-N}^t\text{Bu})_2\text{Sn}(\text{Cl}))\text{P}^t\text{Bu}_2$  **21**, the insertion product is stable and does not undergo any kind of decomposition even with heating to reflux in toluene. Only one Ge-containing insertion product has been shown to be unstable at room temperature, namely  $[(\text{Me}_3\text{Si})\text{N}]_2\text{Ge}(\text{Cl})\text{P}(\text{Ph})\text{Cl}$  **24**. Given the smaller size of Ge compared to Sn (van der Waals radii of 2.00 and 2.17 Å, respectively), it is not surprising that formation of the penta-coordinated intermediate is generally not achieved.

The major detriment to either of these decomposition mechanisms is the form of the metal-containing by-product. While we have found the dimetallane form **M<sub>2</sub>**, produced in the reaction of cyclic stannylene **2** with chlorodiphenylphosphine **11** and

shown in Scheme 43 as  $[\text{Me}_2\text{Si}(\mu\text{-N}^t\text{Bu})_2\text{Sn}(\text{Cl})]$  **15**, Veith *et al.* reported the dichlorostannane  $\text{Me}_2\text{Si}(\mu\text{-N}^t\text{Bu})_2\text{SnCl}_2$  **10** produced in reactions of **2** with both  $\text{PCl}_3$  **39** and  $\text{PhPCl}_2$  **3**. In our investigation, we have yet to determine the forms of any of these tin-containing by-products, and their identification may be necessary to confirm the decomposition pathway.

#### II.4. Conclusions

The insertion reactions of Group 14 carbenoids of the form  $(\text{R}_2\text{N})_2\text{E}$  (E = Ge and Sn) into P–halogen bonds were investigated. Numerous new compounds were obtained and subsequently characterized by  $^{31}\text{P}\{^1\text{H}\}$  and  $^1\text{H}$  NMR spectroscopic methods and, in some cases, single-crystal X-ray diffraction. A few of these compounds, specifically  $[\text{Me}_2\text{Si}(\mu\text{-N}^t\text{Bu})_2\text{SnCl}]_2\text{P}^t\text{Bu}$  **18**,  $\text{Me}_2\text{Si}(\mu\text{-N}^t\text{Bu})_2\text{Sn}(\text{Cl})\text{P}^t\text{Bu}_2$  **21**, and  $\text{Me}_2\text{Si}(\mu\text{-N}^t\text{Bu})_2\text{Sn}(\text{Cl})\text{P}(2,6\text{-Me}_2\text{Ph})_2$  **87**, are unprecedented, inasmuch as they contain a non-dative Sn–P bond resulting from an insertion reaction and have been characterized by X-ray crystallography (for **18** and **21**).

Reactions of the same carbenoids with aminochlorophosphines have resulted in the isolation of a new type of “non-standard” insertion product. Compounds **60**, **62**, and **65** are the result of a ligand exchange reaction between the cyclic diaminostannylene **2** and the aminochlorophosphines **59**, **61**, and **64**. In contrast, addition of the analogous germylene **1** to **61** and **64** resulted in the “standard” insertion products **63** and **66**.

A combination of kinetic studies and observed products’ stabilities and distributions were employed to discuss the possible insertion mechanisms and their likelihoods. It was previously believed that a radical-based mechanism was most likely. Our results indicate that more likely the mechanistic pathway is initiated by the formation

of a phosphine-carbenoid adduct, dubbed the “coordination-initiated” mechanism. The alternative  $S_NP$  and phosphonium ion formation mechanisms were also discussed and deemed as possible.

Many of the insertion products, primarily those resulting from the addition of a stannylene to a chlorophosphine, were observed to be unstable. The mechanism of decomposition for these unstable insertion products was also addressed. A radical-based pathway, initiated by homolytic cleavage of the Sn–P bond and a complexation-elimination route, initiated by the formation of a  $P^{III} \rightarrow M^{IV}$  ( $M = \text{Ge}$  and  $\text{Sn}$ ) adduct, were discussed in detail. It was deemed that the latter was more probable.

Based on the obtained results, potential applications have been identified: first, the controlled and selective synthesis of cyclic polyphosphines, second, the synthesis of diphosphines and diphosphenes, and third, the formation of P–C bonds from halophosphines and alkyl and aryl halides. Future research in this area would benefit from a specially designed ligand structure to aid in stabilization of the M–P bond. Additionally, confirmation of the decomposition pathway would have great impact on the viability of the proposed applications.



## CHAPTER III

### EXPERIMENTAL

#### III.1. Starting Materials and General Procedures

All manipulations and reactions were carried out under an inert atmosphere of argon gas using standard Schlenk techniques. Solvents were dried over and distilled from Na/benzophenone (toluene), K/benzophenone (THF, hexanes and pentane) or CaH<sub>2</sub> (methylene chloride). <sup>n</sup>BuLi, <sup>t</sup>BuLi, 1,3-bis(2,4,6-trimethylphenyl)imidazol-2-ylidene and 2,6-Me<sub>2</sub>C<sub>6</sub>H<sub>3</sub>MgBr were purchased from Aldrich Chemical Co. and used as received. PhPCl<sub>2</sub> **3**, Ph<sub>2</sub>PCl **11**, and CH<sub>2</sub>(PCl<sub>2</sub>)<sub>2</sub> **32** were purchased from Aldrich Chemical Co. and distilled prior to use. Sodium iodide was purchased from Fischer Scientific and dried using heat and vacuum prior to use. Elemental sulfur was purchased from Eastman Kodak Co. and purified by sublimation under an inert atmosphere prior to use. Phosphorus trichloride **39** was purchased from Alfa Aesar and distilled prior to use. The aliphatic phosphine <sup>t</sup>Bu<sub>2</sub>PCl **19** was synthesized using a published procedure,<sup>138</sup> and <sup>t</sup>BuPCl<sub>2</sub> **16** and <sup>t</sup>Bu(Ph)PCl **45** were prepared similarly using only one equivalent of <sup>t</sup>BuLi. The heterocarbenoids Me<sub>2</sub>Si( $\mu$ -N<sup>t</sup>Bu)<sub>2</sub>E (E = Ge **1**, Sn **2**) and [(Me<sub>3</sub>Si)<sub>2</sub>N]<sub>2</sub>E (E = Ge **22**, Sn **23**),<sup>139-142</sup> the aminochlorophosphines Me<sub>2</sub>Si( $\mu$ -N<sup>t</sup>Bu)<sub>2</sub>PCl **59**, (Et<sub>2</sub>N)<sub>2</sub>PCl **61**, and Et<sub>2</sub>NPCl<sub>2</sub> **64**,<sup>75,143,144</sup> and the palladium complex *trans*-(PEt<sub>3</sub>)<sub>2</sub>PdCl<sub>2</sub> **52**,<sup>145</sup> were synthesized according to literature procedures. Elemental analyses were conducted by Desert Analytics, Midwest Microlabs, and Columbia Analytical Services. All <sup>1</sup>H, <sup>13</sup>C,

and  $^{31}\text{P}$  NMR spectra were recorded on a Bruker Avance 500 NMR spectrometer and collected at 25 °C. Coupling constant values ( $J$ ) are given in Hz. The NMR spectra were recorded in  $\text{C}_6\text{D}_6$ ,  $\text{THF-}d_8$ , and  $\text{CD}_2\text{Cl}_2$  (all purchased from Cambridge Isotope Laboratories and distilled prior to use), and the chemical shifts,  $\delta$ , are relative to the solvent peak(s) (e.g.  $\text{C}_6\text{HD}_5$ ) for  $^1\text{H}$  and  $^{13}\text{C}$  spectra, and the external standard  $\text{P}(\text{OEt})_3$  for  $^{31}\text{P}$  spectra. Melting points were obtained on a Mel-Temp apparatus; they are uncorrected.

### III.2. Syntheses

#### *[Me<sub>2</sub>Si( $\mu$ -N<sup>t</sup>Bu)<sub>2</sub>GeCl]<sub>2</sub>PPh 4:*

In a 50 mL flask,  $\text{PhPCl}_2$  (0.27 mL, 2.0 mmol) was stirred in pentane (4 mL) at 0 °C. A 2.0 M toluene solution of  $\text{Me}_2\text{Si}(\mu\text{-}^t\text{BuN})_2\text{Ge}$  (2.0 mL, 4.0 mmol) was added by syringe over 15 min. After 2 h the reaction mixture was removed from the cold bath and allowed to stir at rt overnight. Colorless crystals were obtained in an almost quantitative yield from a pentane/toluene solution at 3 °C. Yield 1.39 g (96 %). Mp: 112–114 °C. Anal. Calcd. for  $\text{C}_{26}\text{H}_{53}\text{Cl}_2\text{Ge}_2\text{N}_4\text{PSi}_2$  (725.06) C 43.07; H 7.37; N 7.73; found C 43.10; H 7.30; N 7.67.  $^1\text{H}$  NMR (500 MHz,  $\text{CD}_2\text{Cl}_2$ , 25 °C):  $\delta$  0.35 (s, 6 H, SiMe), 0.44 (s, 6 H, SiMe), 1.19 (s, 36 H, N<sup>t</sup>Bu), 7.34 (m, 1 H, *p*-C<sub>6</sub>H<sub>5</sub>), 7.36 (m, 2 H, *m*-C<sub>6</sub>H<sub>5</sub>), 7.94 (m, 2 H, *o*-C<sub>6</sub>H<sub>5</sub>).  $^{13}\text{C}\{^1\text{H}\}$  NMR (125.8 MHz,  $\text{CD}_2\text{Cl}_2$ ):  $\delta$  5.43 (s, SiMe), 6.87 (s, SiMe), 34.5 (s,  $\text{NCMe}_3$ ), 52.8 (s,  $\text{NCMe}_3$ ), 128.6 (d,  $^1J_{\text{PC}} = 13.8$ , PC) 128.9 (d,  $^3J_{\text{PC}} = 8.8$ , *m*-C<sub>6</sub>H<sub>5</sub>), 129.9 (s, *p*-C<sub>6</sub>H<sub>5</sub>), 137.2 (d,  $^2J_{\text{PC}} = 17.6$ , *o*-C<sub>6</sub>H<sub>5</sub>).  $^{31}\text{P}\{^1\text{H}\}$  NMR (202.5 MHz,  $\text{CD}_2\text{Cl}_2$ ):  $\delta$  -55.2.

*Me<sub>2</sub>Si(μ-<sup>n</sup>Bu)<sub>2</sub>Ge(Cl)PPh<sub>2</sub> 12*

In a 25 mL two-neck flask, a 1.0 M toluene solution of PhPCl<sub>2</sub> (3.0 mL, 3.0 mmol) was stirred at -78 °C. A 1.0 M toluene solution of Me<sub>2</sub>Si(μ-<sup>1</sup>BuN)<sub>2</sub>Ge (6.0 mL, 6.0 mmol) was added dropwise by syringe over 45 min. The solution was warmed to rt and stirred overnight. The solvent was removed *in vacuo* with minor heating and the product was washed with a small amount (~ 1 mL) of cold hexanes. Product was determined to be ~98 % pure by NMR. Yield 1.979 g (91 %). Mp 132–134 °C. Anal. Calcd. for C<sub>26</sub>H<sub>53</sub>Cl<sub>2</sub>Ge<sub>2</sub>N<sub>4</sub>PSi<sub>2</sub> (725.06): C 43.07; H 7.37; N 7.73; found, C 43.21; H 7.20; N 7.50. <sup>1</sup>H NMR (500 MHz, C<sub>6</sub>D<sub>6</sub>): δ 0.42 (s, 6H), 0.46 (s, 6 H), 1.41 (s, 36H), 7.01–7.07 (m, 8H, *o*- and *m*-Ph), 7.74–7.80 (m, 2H, *p*-Ph). <sup>13</sup>C{<sup>1</sup>H} (125.8 MHz, C<sub>6</sub>D<sub>6</sub>): δ 5.73 (s, SiMe), 7.69 (s, SiMe), 34.92 (s, NC(CH<sub>3</sub>)<sub>3</sub>), 53.97 (s, NC(CH<sub>3</sub>)<sub>3</sub>), 129.21 (d, <sup>2</sup>J<sub>PC</sub> = 83, *o*-C<sub>6</sub>H<sub>5</sub>), 135.20 (d, <sup>3</sup>J<sub>PC</sub> = 25, *m*-C<sub>6</sub>H<sub>5</sub>), 137.43 (d, <sup>4</sup>J<sub>PC</sub> = 22, *p*-C<sub>6</sub>H<sub>5</sub>). <sup>31</sup>P{<sup>1</sup>H} NMR (202.5 MHz, C<sub>6</sub>D<sub>6</sub>): δ -5.9.

*[Me<sub>2</sub>Si(μ-<sup>n</sup>Bu)<sub>2</sub>GeCl]<sub>2</sub>P<sup>t</sup>Bu 17:*

In a 25 mL two-neck flask, a 1.0 M toluene solution of <sup>t</sup>BuPCl<sub>2</sub> (2.0 mL, 2.0 mmol) was stirred at 0 °C. A 1.0 M toluene solution of Me<sub>2</sub>Si(μ-<sup>1</sup>BuN)<sub>2</sub>Ge (4.0 mL, 4.0 mmol) was added dropwise by syringe over 30 min. The solution was warmed to rt and stirred for 3 d. The product was isolated as clear, colorless crystals in several fractions from toluene at 3 °C. Yield 0.813 g (58 %). Mp: 117–119 °C. Anal. Calcd. for C<sub>24</sub>H<sub>57</sub>Cl<sub>2</sub>Ge<sub>2</sub>N<sub>4</sub>PSi<sub>2</sub> (705.07): C 40.88; H 8.15; N 7.95; found, C 40.52; H 7.98; N 7.81. <sup>1</sup>H NMR (500 MHz, C<sub>6</sub>D<sub>6</sub>): δ 0.41 (s, 6 H), 0.46 (s, 6 H), 1.42 (s, 36 H), 1.68 (d, 9 H, <sup>3</sup>J<sub>HP</sub> = 14.9). <sup>13</sup>C{<sup>1</sup>H} (125.8 MHz, C<sub>6</sub>D<sub>6</sub>): δ 5.83 (s, SiMe), 7.59 (s, SiMe), 34.99 (d, <sup>2</sup>J<sub>PC</sub>

= 12.5, P<sup>t</sup>Bu), 35.06 (s, NC(CH<sub>3</sub>)<sub>3</sub>), 38.78 (d, <sup>1</sup>J<sub>PC</sub> = 32.6, PC), 53.41 (s, NC(CH<sub>3</sub>)<sub>3</sub>).  
<sup>31</sup>P{<sup>1</sup>H} NMR (202.5 MHz, C<sub>6</sub>D<sub>6</sub>): δ 3.2.

*[Me<sub>2</sub>Si(μ-N<sup>t</sup>Bu)<sub>2</sub>SnCl]<sub>2</sub>P<sup>t</sup>Bu* **18**:

In a 50 mL two-neck flask, <sup>t</sup>BuPCl<sub>2</sub> (0.467 g, 2.94 mmol) was stirred in 10 mL of hexanes at 0 °C. Me<sub>2</sub>Si(μ-<sup>t</sup>BuN)<sub>2</sub>Sn (1.875 g, 5.87 mmol) was added dropwise by syringe over 1.5 minutes. The solution became yellow-orange during the addition. The flask was removed from the cold bath after 40 min. of stirring at 0 °C. Yellow crystals of X-ray quality were obtained in multiple fractions from the reaction solution at 3 °C after several days. Yield = 1.351 g (58 %). Mp: 112–116 °C. Anal. Calcd. for C<sub>24</sub>H<sub>57</sub>Cl<sub>2</sub>N<sub>4</sub>PSi<sub>2</sub>Sn<sub>2</sub> (797.21): C 36.16; H 7.21; N 7.03; found, C 36.10; H 7.22; N 6.78. <sup>1</sup>H NMR (500 MHz, C<sub>6</sub>D<sub>6</sub>): δ 0.41 (s, 6 H, SiMe), 0.48 (s, 6 H, SiMe), 1.36 (s, 36 H, N<sup>t</sup>Bu), 1.61 (d, 9 H, <sup>3</sup>J<sub>PH</sub> = 15, <sup>4</sup>J<sub>SnH</sub> = 10, P<sup>t</sup>Bu). <sup>13</sup>C{<sup>1</sup>H} (125.8 MHz, C<sub>6</sub>D<sub>6</sub>): δ 6.9 (s, <sup>3</sup>J<sub>SnC</sub> = 50, SiMe), 7.9 (s, <sup>3</sup>J<sub>SnC</sub> = 50, SiMe), 35.9 (d, <sup>3</sup>J<sub>SnC</sub> = 41.5, <sup>2</sup>J<sub>PC</sub> = 12.6, PCMe<sub>3</sub>), 36.5 (s, <sup>3</sup>J<sub>SnC</sub> = 34.0, NCMe<sub>3</sub>), 38.9 (d, <sup>1</sup>J<sub>PC</sub> = 37.7, <sup>2</sup>J<sub>SnC</sub> = 31.5, PCMe<sub>3</sub>), 53.6 (s, <sup>2</sup>J<sub>SnC</sub> = 20.6, NCMe<sub>3</sub>). <sup>31</sup>P{<sup>1</sup>H} NMR (202.5 MHz, C<sub>6</sub>D<sub>6</sub>): δ 7.1 (<sup>1</sup>J<sub>119,117SnP</sub> = 1616, 1543 Hz).

*Me<sub>2</sub>Si(μ-N<sup>t</sup>Bu)<sub>2</sub>Ge(Cl)P<sup>t</sup>Bu<sub>2</sub>* **20**

In a 50 mL two-neck flask, a 1.0 M toluene solution of Me<sub>2</sub>Si(μ-<sup>t</sup>BuN)<sub>2</sub>Ge (5.0 mL, 5.0 mmol) was treated dropwise at rt with a 0.67 M toluene solution of <sup>t</sup>Bu<sub>2</sub>PCl (7.46 mL, 5.0 mmol), which was added by syringe over 20 minutes. The solution was kept stirring at 70 °C for 39 d. The product was isolated as colorless crystals from hexanes at –8 °C. Yield of 0.431 g (19%). Mp: 130–132 °C. Anal. Calcd. for C<sub>18</sub>H<sub>42</sub>ClGeN<sub>2</sub>PSi (453.69): C 47.65; H 9.33; N 6.17; found, C 47.24; H 9.36; N 6.02. <sup>1</sup>H NMR (500 MHz,

C<sub>6</sub>D<sub>6</sub>):  $\delta$  0.41 (s, 3 H, SiMe), 0.50 (s, 3 H, SiMe), 1.19 (s, 18 H, N<sup>t</sup>Bu), 1.23 (d, 18 H, <sup>3</sup>J<sub>PH</sub> = 12.5, P<sup>t</sup>Bu). <sup>13</sup>C{<sup>1</sup>H} (125.8 MHz, C<sub>6</sub>D<sub>6</sub>)  $\delta$  7.4 (s, SiMe), 8.4 (s, SiMe), 33.3 (d, P<sup>t</sup>Bu<sub>2</sub>, <sup>2</sup>J<sub>PC</sub> = 13.6), 35.8 (s, N<sup>t</sup>Bu), 36.3 (d, <sup>1</sup>J<sub>PC</sub> = 37.3, PC), 53.02 (s, NC). <sup>31</sup>P{<sup>1</sup>H} NMR (202 MHz, C<sub>6</sub>D<sub>6</sub>):  $\delta$  63.5.

*Me<sub>2</sub>Si( $\mu$ -N<sup>t</sup>Bu)<sub>2</sub>Sn(Cl)P<sup>t</sup>Bu<sub>2</sub> 21:*

In a 50 mL two-neck flask, a 1.0 M toluene solution of Me<sub>2</sub>Si(<sup>t</sup>BuN)<sub>2</sub>Sn (6.0 mL, 6.0 mmol) was stirred at 0 °C. A 0.67 M toluene solution of (<sup>t</sup>Bu)<sub>2</sub>PCl (4.0 mL, 9.0 mmol) was added dropwise by syringe over 25 minutes. The solution was heated to 60 °C and stirred for 17 d. The product was isolated as yellow crystals from toluene at 3 °C. Yield 2.645 g (88%). Mp: 128–129 °C. Anal. Calcd. for C<sub>18</sub>H<sub>42</sub>ClN<sub>2</sub>PSiSn (499.76): C 43.26; H 8.47; N 5.61; found, C 43.05; H 8.20; N 5.61. <sup>1</sup>H NMR (500 MHz, C<sub>6</sub>D<sub>6</sub>):  $\delta$  0.35 (s, 3 H, SiMe), 0.54 (s, 3 H, SiMe), 1.38 (s, 18 H, N<sup>t</sup>Bu), 1.39 (d, 18 H, <sup>3</sup>J<sub>PH</sub> = 12.4, P<sup>t</sup>Bu). <sup>13</sup>C{<sup>1</sup>H} (125.8 MHz, C<sub>6</sub>D<sub>6</sub>):  $\delta$  7.2 (s, SiMe), 8.5 (s, SiMe), 33.7 (d, P<sup>t</sup>Bu<sub>2</sub>, <sup>2</sup>J<sub>PC</sub> = 13.5), 36.5 (s, N<sup>t</sup>Bu), 36.8 (d, <sup>1</sup>J<sub>PC</sub> = 37.3, PC), 53.3 (s, NC). <sup>31</sup>P{<sup>1</sup>H} NMR (202 MHz, C<sub>6</sub>D<sub>6</sub>):  $\delta$  92.8 (<sup>1</sup>J<sub>119,117SnP</sub> = 1734, 1657).

*{[(Me<sub>3</sub>Si)<sub>2</sub>N]<sub>2</sub>Sn(Cl)P(Ph)}<sub>2</sub> 26:*

In a 100 mL flask, [(Me<sub>3</sub>Si)<sub>2</sub>N]<sub>2</sub>Sn (2.79 g, 6.24 mmol) was stirred in 10 mL of hexanes at 0 °C. Exactly 1.56 mL of a 2.0 M toluene solution of PhPCl<sub>2</sub> (3.12 mmol) was added by syringe over 20 min, producing a yellow solution with a significant amount of a yellow precipitate. Bright yellow crystals were obtained in several fractions from a concentrated THF solution at 3 °C. Yield 2.62 g (72 %). Mp: 220–221 °C. Anal. Calcd. for C<sub>36</sub>H<sub>82</sub>Cl<sub>2</sub>N<sub>4</sub>P<sub>2</sub>Si<sub>8</sub>Sn<sub>2</sub> (1166.02): C 37.08; H 7.09; N 4.80; found C 37.05; H 6.81; N

4.97.  $^1\text{H}$  NMR (500 MHz,  $\text{C}_6\text{D}_6$ ):  $\delta$  0.11 (s, 72 H, SiMe), 7.47 (m, 2 H, *m*- $\text{C}_6\text{H}_5$ ), 7.52 (m, 2 H,  $^3J_{\text{PH}} = 1.9$ , *o*- $\text{C}_6\text{H}_5$ ), 7.98 (m, 1 H, *p*- $\text{C}_6\text{H}_5$ ).  $^{13}\text{C}\{^1\text{H}\}$  (125.8 MHz,  $\text{C}_6\text{D}_6$ ):  $\delta$  1.5, (s, SiMe), 130.3 (s, *m*- $\text{C}_6\text{H}_5$ ), 130.7 (s, *o*- $\text{C}_6\text{H}_5$ ), 131.8 (s, *p*- $\text{C}_6\text{H}_5$ ).  $^{31}\text{P}\{^1\text{H}\}$  NMR (202.5 MHz,  $\text{C}_6\text{D}_6$ ):  $\delta$  -28.5 ( $^1J_{^{119,117}\text{SnP}} = 1470, 1404$ ).

*[(Me<sub>3</sub>Si)<sub>2</sub>N]<sub>2</sub>Ge(Cl)PPh<sub>2</sub> 27:*

In a 25 mL, two-neck flask, a 2.0 M toluene solution of  $[(\text{Me}_3\text{Si})_2\text{N}]_2\text{Ge}$  (1.0 mL, 2.0 mmol) was stirred at 0 °C. A 2.67 M toluene solution of  $\text{Ph}_2\text{PCl}$  (0.75 mL, 2.0 mmol) was added dropwise by syringe over 30 min. The product was isolated as colorless crystals from toluene at 3 °C. Yield 1.15 g (94 %). Mp: 126–128 °C. Anal. Calcd. for  $\text{C}_{24}\text{H}_{46}\text{ClGeN}_2\text{PSi}_4$  (614.04): C 46.94; H 7.55; N 4.56; found, C 46.54; H 7.29; N 4.34.  $^1\text{H}$  NMR (500 MHz,  $\text{C}_6\text{D}_6$ ):  $\delta$  0.30 (s, 36 H, SiMe<sub>3</sub>), 7.01–7.08 (m, 6 H, *o*, *m*- $\text{P-C}_6\text{H}_5$ ), 7.75–7.78 (m, 4 H, *p*- $\text{P-C}_6\text{H}_5$ ).  $^{13}\text{C}\{^1\text{H}\}$  (125.8 MHz,  $\text{C}_6\text{D}_6$ ):  $\delta$  7.18 (s, SiMe<sub>3</sub>), 129.34 (d,  $^2J_{\text{PC}} = 84.3$ , *o*- $\text{C}_6\text{H}_5$ ), 134.88 (d,  $^3J_{\text{PC}} = 22.6$ , *m*- $\text{C}_6\text{H}_5$ ), 136.91 (d,  $^4J_{\text{PC}} = 21.4$ , *p*- $\text{C}_6\text{H}_5$ ).  $^{31}\text{P}\{^1\text{H}\}$  NMR (202.5 MHz,  $\text{C}_6\text{D}_6$ ):  $\delta$  -16.0.

*[(Me<sub>3</sub>Si)<sub>2</sub>N]<sub>2</sub>Ge(Cl)P(Cl)<sup>t</sup>Bu 29:*

In a 50 mL, two-neck flask, <sup>t</sup>BuPCl<sub>2</sub> (0.692 g, 4.35 mmol) was stirred at rt in benzene (5 mL). A sample of  $[(\text{Me}_3\text{Si})_2\text{N}]_2\text{Ge}$  (1.712 g, 4.35 mmol) was added all at once and the ensuing solution was stirred for 5 d. The solvent was removed *in vacuo*, leaving a pale yellow solid. This was redissolved in a minimal amount of hexanes, affording X-ray quality crystals overnight at rt. Yield 1.36 g (56 %). Mp: 151–153 °C. Anal. Calcd. for  $\text{C}_{16}\text{H}_{45}\text{Cl}_2\text{GeN}_2\text{PSi}_4$  (552.40): C 34.79; H 8.21; N 5.07; found, C 35.00; H 8.08; N 4.96.  $^1\text{H}$  NMR (500 MHz,  $\text{C}_6\text{D}_6$ ):  $\delta$  0.47 (s, 36 H, SiMe<sub>3</sub>), 1.36 (d, 9 H,  $^3J_{\text{PH}} = 14.7$ , P<sup>t</sup>Bu).

$^{13}\text{C}\{^1\text{H}\}$  (125.8 MHz,  $\text{C}_6\text{D}_6$ ):  $\delta$  7.25 (s,  $\text{SiMe}_3$ ), 28.8 (d,  $^2J_{\text{PC}} = 17.6$ ,  $\text{PC}(\text{CH}_3)_3$ ), 39.9 (d,  $^1J_{\text{PC}} = 45.3$  Hz,  $\text{PC}(\text{CH}_3)_3$ ).  $^{31}\text{P}\{^1\text{H}\}$  NMR (202.5 MHz,  $\text{C}_6\text{D}_6$ ):  $\delta$  117.5.

*{[Me<sub>2</sub>Si( $\mu$ -N<sup>t</sup>Bu)<sub>2</sub>Ge(Cl)]<sub>2</sub>P}<sub>2</sub>CH<sub>2</sub> 32:*

In a 50 mL three-neck flask,  $\text{Me}_2\text{Si}(\mu\text{-}^t\text{BuN})_2\text{Ge}$  (0.557 g, 2.04 mmol) was stirred in hexanes at  $-78$  °C. Via syringe  $\text{CH}_2(\text{PCl}_2)_2$  (0.069 mL, 0.51 mmol) was added dropwise over 9 min. The reaction solution changed from pale yellow to colorless. After warming to rt a white precipitate appeared. All solvent was removed and the solid was redissolved in toluene. Clear, colorless, X-ray quality crystals were obtained from toluene at  $\sim 3$  °C after a few days. Yield 0.350 g (52 %). Mp: 188 °C (dec). Anal. Calcd. for  $\text{C}_{41}\text{H}_{98}\text{Cl}_4\text{Ge}_4\text{N}_8\text{P}_2\text{Si}_4$  (1309.93): C 37.59; H 7.54; N 8.55; found, C 37.80; H 7.39; N 8.44.  $^1\text{H}$  NMR (500 MHz,  $\text{C}_6\text{D}_6$ ):  $\delta$  0.46 (s, 12H,  $\text{SiMe}$ ), 0.54 (s, 12H,  $\text{SiMe}$ ), 1.44 (s, 72H,  $\text{N}^t\text{Bu}$ ), 3.62 (t, 2H,  $\text{PCH}_2\text{P}$ ,  $^2J_{\text{PH}} = 3.2$ ).  $^{13}\text{C}\{^1\text{H}\}$  (125.8 MHz,  $\text{C}_6\text{D}_6$ ):  $\delta$  6.2 (s,  $\text{SiMe}$ ), 7.2 (s,  $\text{SiMe}$ ), 12.1 (t,  $\text{PCH}_2\text{P}$ ,  $^1J_{\text{PC}} = 157$ ), 35.2 (s,  $\text{NCCH}_3$ ), 53.0 (s,  $\text{NCCH}_3$ ).  $^{31}\text{P}\{^1\text{H}\}$  NMR (202.5 MHz,  $\text{C}_6\text{D}_6$ ):  $\delta$   $-51.9$ .

*[Me<sub>2</sub>Si( $\mu$ -N<sup>t</sup>Bu)<sub>2</sub>GeCl]<sub>3</sub>P 40:*

In a 50 mL two-neck flask,  $\text{Me}_2\text{Si}(\mu\text{-}^t\text{BuN})_2\text{Ge}$  (0.603 g, 2.21 mmol) was stirred in hexanes at 0 °C. Via syringe,  $\text{PCl}_3$  (0.064 mL, 0.74 mmol) was added dropwise over 11 min. The reaction solution changed from pale yellow to colorless and became very cloudy. All solvent was removed and the solid was redissolved in toluene ( $\sim 75$  mL). Clear, colorless, needle crystals were obtained from toluene at  $-3$  °C after a few days. Yield 0.410 g (58 %).  $^1\text{H}$  NMR (500 MHz,  $\text{C}_6\text{D}_6$ ):  $\delta$  0.50 (s, 9H,  $\text{SiMe}$ ), 0.55 (s, 9H,  $\text{SiMe}$ ), 1.45 (s, 54H,  $\text{N}^t\text{Bu}$ ).  $^{31}\text{P}\{^1\text{H}\}$  NMR (202.5 MHz,  $\text{C}_6\text{D}_6$ ):  $\delta$   $-78.0$ .

$\{[(Me_3Si)_2N]_2Ge(Cl)P(Cl)\}_2$  **44**:

In a 50 mL two-neck flask,  $[(Me_3Si)_2N]_2Ge$  (651 mg, 1.66 mmol) was stirred at 0 °C in hexanes (16 mL). A 1.0 M hexanes solution of  $PCl_3$  (0.827 mL, 0.827 mmol) was added at once. After 1 h the reaction mixture was warmed to rt. The solution was initially bright yellow or amber but changed to bright pink after 3.5–4 h. Solution was concentrated and pale pink crystals were grown as a 1:1 hexane solvate at 3 °C. Yield 937 mg (57 %). Mp 150 °C (dec.). Anal. Calcd. for  $C_{24}H_{72}Cl_4Ge_2N_4P_2Si_8$  (990.58): C 29.10; H 7.33; N 5.66; found, C 30.27; H 7.33; N 5.44.  $^1H$  NMR (500 MHz,  $C_6D_6$ ):  $\delta$  0.48 (s, SiMe).  $^{13}C\{^1H\}$  (125.8 MHz,  $C_6D_6$ ):  $\delta$  7.1 (s, SiMe).  $^{31}P\{^1H\}$  NMR (202.5 MHz,  $C_6D_6$ ):  $\delta$  62.6.

$tBu(Ph)PI$  **47**:

In a 250 mL three-neck flask,  $tBu(Ph)PCl$  (4.71 mL, 25.0 mmol) and sodium iodide (14.99 g, 100 mmol) were stirred in refluxing toluene for 8 h. The reaction solution changed from colorless to pale yellow. All solvent was removed *in vacuo*. This crude product was found to be sufficient for all studies. Purity was determined by  $^1H$  NMR to be > 95 %. Yield 5.232 g (72 %).  $^1H$  NMR (500 MHz,  $C_6D_6$ ):  $\delta$  1.01 (d, 9H,  $tBu$ ,  $^3J_{PH} = 15.0$ ), 7.02–7.81 (m, 5H, Ph).  $^{31}P\{^1H\}$  NMR (202.5 MHz,  $C_6D_6$ ):  $\delta$  106.1.

*trans*-( $PhPCl_2$ ) $_2PdCl_2$  **49**:

In a 50 mL two-neck flask, (1,5-cyclooctadiene) $PdCl_2$  (108 mg, 0.378 mmol) was stirred in toluene at rt.  $PhPCl_2$  was added as a 2.0 M toluene solution (0.40 mL, 0.80 mmol). After several minutes the solution became orange, with all turbidity cleared. The



complex was isolated as large, orange crystals from toluene at 3 °C in the form of a 1:1 toluene solvate. Yield 0.206 g (87 %). Mp 153–156 °C. Anal. Calcd. for C<sub>12</sub>H<sub>10</sub>Cl<sub>6</sub>P<sub>2</sub>Pd (535.29): C 26.93; H 1.88; found, C 27.46; H 1.56. <sup>1</sup>H NMR (500 MHz, CDCl<sub>3</sub>): δ 7.60 (t, 2 H, *o*-C<sub>6</sub>H<sub>5</sub>, <sup>2</sup>J<sub>HH</sub> = 15.0), 7.66 (t, 1 H, *p*-C<sub>6</sub>H<sub>5</sub>, 14.5), 8.14 (s, 2 H, *m*-C<sub>6</sub>H<sub>5</sub>). <sup>13</sup>C{<sup>1</sup>H} (125.8 MHz, CDCl<sub>3</sub>): δ 129.1 (s, *o*-C<sub>6</sub>H<sub>5</sub>), 131.3 (s, *p*-C<sub>6</sub>H<sub>5</sub>), 134.2 (s, *m*-C<sub>6</sub>H<sub>5</sub>). <sup>31</sup>P{<sup>1</sup>H} NMR (202.5 MHz, CDCl<sub>3</sub>): δ 115.8.

*trans*-(<sup>t</sup>BuPCL<sub>2</sub>)<sub>2</sub>PdCl<sub>2</sub> **50**:

In a 50 mL two-neck flask, (1,5-cyclooctadiene)PdCl<sub>2</sub> (69 mg, 0.242 mmol) was stirred in toluene at rt. <sup>t</sup>BuPCL<sub>2</sub> was added as a 1.0 M toluene solution (0.50 mL, 0.50 mmol). After several minutes the solution became orange, with all turbidity cleared. The complex was isolated as orange crystals in several fractions from toluene at 3°C. Yield 0.109 g (91 %). Mp 190 °C (dec.). Anal. Calcd. for C<sub>8</sub>H<sub>18</sub>Cl<sub>6</sub>P<sub>2</sub>Pd (495.31): C 19.40; H 3.66; found, C 19.53; H 3.76. <sup>1</sup>H NMR (500 MHz, CDCl<sub>3</sub>): δ 1.52 (*pseudo*-t, *J* = 21.8). <sup>13</sup>C{<sup>1</sup>H} (125.8 MHz, CDCl<sub>3</sub>): δ 25.5 (s, CCH<sub>3</sub>), 47.0 (s, CCH<sub>3</sub>). <sup>31</sup>P{<sup>1</sup>H} NMR (202.5 MHz, CDCl<sub>3</sub>): δ 160.1.

*trans*-[Me<sub>2</sub>Si(μ-<sup>t</sup>Bu)<sub>2</sub>Sn(Cl)]<sub>2</sub>Pd(PEt<sub>3</sub>)[Sn(μ-<sup>t</sup>Bu)<sub>2</sub>SiMe<sub>2</sub>] **53**:

In a 25 mL two-neck flask, (PEt<sub>3</sub>)<sub>2</sub>PdCl<sub>2</sub> (156 mg, 0.377 mmol) was stirred in toluene (2 mL) at rt. Me<sub>2</sub>Si(μ-<sup>t</sup>Bu)<sub>2</sub>Sn (0.565 mL, 1.13 mmol) was added by syringe over 3 min. Solution promptly changed from bright yellow to dark red. Solution was stirred overnight at rt. X-ray quality crystals were grown from toluene at 3 °C. Yield 97 mg (21 %). Mp 190 °C (dec.). Anal. Calcd. for C<sub>36</sub>H<sub>87</sub>Cl<sub>2</sub>N<sub>6</sub>PPdSi<sub>3</sub>Sn<sub>3</sub> (1252.80): C 34.51; H 7.00; N 6.71; found, C 34.69; H 6.89; N 6.20. <sup>1</sup>H NMR (500 MHz, C<sub>6</sub>D<sub>6</sub>, 25

°C):  $\delta$  0.79 (s, 12 H, SiMe), 1.03 (m, 9 H, PCH<sub>2</sub>CH<sub>3</sub>), 1.21 (d, 6H, SiMe,  $J_{PH} = 170$ ), 1.50 (s, 18 H, N<sup>t</sup>Bu), 1.54 (s, 36H, N<sup>t</sup>Bu), 2.12 (m, 6H, PCH<sub>2</sub>). <sup>13</sup>C{<sup>1</sup>H} (125.8 MHz, C<sub>6</sub>D<sub>6</sub>):  $\delta$  9.8 (d, PCH<sub>2</sub>CH<sub>3</sub>,  $^2J_{PC} = 30$ ), 17.0 (d, PCH<sub>2</sub>CH<sub>3</sub>,  $^1J_{PC} = 35$ ), 31.8 (s, SiMe), 34.3 (d, SiMe,  $J_{PC} = 415$ ), 36.8 (s, NCCH<sub>3</sub>,  $^3J_{SnC} = 28$ ), 37.5 (s, NCCH<sub>3</sub>,  $^3J_{SnC} = 36$ ), 52.0 (s, NCCH<sub>3</sub>), 54.1 (s, NCCH<sub>3</sub>). <sup>31</sup>P{<sup>1</sup>H} NMR (202.5 MHz, C<sub>6</sub>D<sub>6</sub>, 25 °C):  $\delta$  12.6 ( $^2J_{SnP} = 138$  Hz).

*trans*-(Et<sub>3</sub>P)<sub>2</sub>Pd(Cl)[(Cl)Sn( $\mu$ -N<sup>t</sup>Bu)<sub>2</sub>SiMe<sub>2</sub>] **54**:

In a 25 mL two-neck flask, (PEt<sub>3</sub>)<sub>2</sub>PdCl<sub>2</sub> (290 mg, 0.702 mmol) was stirred in toluene (2 mL) at rt. Me<sub>2</sub>Si( $\mu$ -<sup>t</sup>BuN)<sub>2</sub>Sn (0.351 mL, 0.702 mmol) was added by syringe over 3 min. Solution promptly changed from bright yellow to dark red. Solution was stirred overnight at rt. X-ray quality crystals were grown from toluene at 3 °C. Yield 303 mg (59 %). Mp 144–146 °C (dec.). Anal. Calcd. for C<sub>22</sub>H<sub>54</sub>Cl<sub>2</sub>N<sub>2</sub>P<sub>2</sub>PdSiSn (732.75): C 36.06; H 7.43; N 3.82; found, C 35.72; H 7.13; N 3.79. <sup>1</sup>H NMR (500 MHz, C<sub>6</sub>D<sub>6</sub>):  $\delta$  0.98 (m, 18 H, PCH<sub>2</sub>CH<sub>3</sub>), 1.14 (dd, 6H, SiMe,  $J_{PH} = 418$  Hz,  $J_{PH} = 185$  Hz), 1.43 (s, 18 H, N<sup>t</sup>Bu), 2.17 (m, 12H, PCH<sub>2</sub>). <sup>13</sup>C{<sup>1</sup>H} (125.8 MHz, C<sub>6</sub>D<sub>6</sub>):  $\delta$  9.2 (d, PCH<sub>2</sub>CH<sub>3</sub>,  $^2J_{PC} = 25$  Hz), 17.1 (d, PCH<sub>2</sub>CH<sub>3</sub>,  $^1J_{PC} = 26$  Hz), 32.3 (d, SiMe,  $J_{PC} = 479$  Hz), 36.6 (s, NCCH<sub>3</sub>,  $^3J_{SnC} = 29$  Hz), 52.9 (s, NCCH<sub>3</sub>). <sup>31</sup>P{<sup>1</sup>H} NMR (202.5 MHz, C<sub>6</sub>D<sub>6</sub>):  $\delta$  11.5 (d,  $^2J_{PP} = 399$ ,  $^2J_{SnP} = 194$ ), 20.9 (d,  $^2J_{PP} = 399$ ,  $^2J_{SnP} = 107$ ).

*PhP(S)Cl*<sub>2</sub> **56**:

In a 250 mL three-neck flask PhPCl<sub>2</sub> (3.30 mL, 24.3 mmol) and elemental sulfur (0.820 g, 25.6 mmol) were stirred in refluxing toluene for 55 h. Solvent was removed leaving an oily, yellow residue. The residue was distilled under vacuum. The first

fraction, which distilled at 65 °C (1 mbar) was discarded. The second fraction, which distilled at 79–80 °C (1 mbar), contained the product. Yield 2.55 g (50 %).  $^1\text{H}$  NMR (500 MHz,  $\text{CDCl}_3$ ):  $\delta$  7.05–7.85 (m, Ph).  $^{31}\text{P}\{^1\text{H}\}$  NMR (202.5 MHz,  $\text{CDCl}_3$ ):  $\delta$  73.0.

*Me<sub>2</sub>Si( $\mu$ -N<sup>t</sup>Bu)<sub>2</sub>Sn(Cl)P(S)<sup>t</sup>Bu<sub>2</sub>* **58**:

In a 25 mL two-neck flask, a 2.0 M solution of  $\text{Me}_2\text{Si}(\mu\text{-N}^t\text{Bu})_2\text{Sn}$  (0.50 mL, 1.0 mmol), elemental sulfur (33 mg, 1.03 mmol), and toluene were stirred (5 mL) at rt. After 2 d of stirring at rt, the solution was concentrated. Crystals were grown as bright orange blocks at 3 °C. Yield 441 mg (83 %).  $^1\text{H}$  NMR (500 MHz,  $\text{C}_6\text{D}_6$ ):  $\delta$  0.52 (s, 3H, SiMe), 0.53 (s, 3H, SiMe), 1.19 (d, 18H, P<sup>t</sup>Bu,  $^3J_{\text{PH}} = 18.0$ ), 1.49 (s, 18H, N<sup>t</sup>Bu).  $^{31}\text{P}\{^1\text{H}\}$  NMR (202 MHz,  $\text{C}_6\text{D}_6$ ):  $\delta$  92.1 ( $^1J_{\text{SnP}} = 57$ ).

*[Me<sub>2</sub>Si( $\mu$ -N<sup>t</sup>BuSnCl)( $\mu$ -N<sup>t</sup>Bu(P( $\mu$ -N<sup>t</sup>Bu)<sub>2</sub>SiMe<sub>2</sub>))] ]* **60**:

In a 50 mL two-neck flask, 7.5 mL of a 1.0 M toluene solution of  $\text{Me}_2\text{Si}(\mu\text{-N}^t\text{Bu})_2\text{SnCl}$  (7.5 mmol) was stirred at 0°C. 7.5 mL of a 1.0M toluene solution of  $\text{Me}_2\text{Si}(\mu\text{-N}^t\text{Bu})_2\text{Sn}$  (7.5 mmol) was added dropwise by syringe over 40 min. Immediately following the addition, the reaction was stirred at 60 °C for 15 d. The product was collected as transparent colorless to light yellow-brown crystals directly from the reaction solution by cooling to –15°C. Several crystal fractions were collected to give an overall yield of 1.493 g (34 %). Mp 159–160 °C. Anal. Calcd. for  $\text{C}_{20}\text{H}_{48}\text{ClN}_4\text{PSi}_2\text{Sn}$  (585.93): C 41.00; H 8.26; N 9.56; found, C 40.74; H 8.11; N 9.18.  $^1\text{H}$  NMR (500 MHz,  $\text{C}_6\text{D}_6$ ):  $\delta$  0.17 (s, 3H, SiMe), 0.24 (s, 3H, SiMe), 0.77 (s, 6H, SiMe<sub>2</sub>), 1.33 (s, 18H, *exo*-PN<sup>t</sup>Bu), 1.49 (s, 9H, *endo*-PN<sup>t</sup>Bu), 1.55 (s, 9H, SnN<sup>t</sup>Bu).  $^{13}\text{C}\{^1\text{H}\}$  (125.8 MHz,  $\text{C}_6\text{D}_6$ )  $\delta$  7.2

(SiMe), 8.5 (SiMe), 33.7 (P<sup>t</sup>Bu<sub>2</sub>, <sup>2</sup>J<sub>PC</sub> = 13.5), 36.5 (N<sup>t</sup>Bu), 36.8 (PC, <sup>1</sup>J<sub>PC</sub> = 37.3), 53.3 (NC). <sup>31</sup>P{<sup>1</sup>H} NMR (202 MHz, C<sub>6</sub>D<sub>6</sub>): δ 86.0 (<sup>1</sup>J<sub>119,117SnP</sub> = 2022, 1932).

*[Me<sub>2</sub>Si(μ-N<sup>t</sup>BuSnCl)(μ-N<sup>t</sup>Bu(P(NEt<sub>2</sub>)<sub>2</sub>)]* **62**:

In a 100 mL single-neck flask, Me<sub>2</sub>Si(μ-N<sup>t</sup>Bu)<sub>2</sub>Sn (0.720 g, 2.26 mmol) was stirred at 0 °C in 35 mL of hexanes. (Et<sub>2</sub>N)<sub>2</sub>PCL (0.474 mL, 2.26 mmol) was added neat by syringe over 6 min. The solution turned from orange to yellow after the addition of phosphine. After 60 min. the flask was removed from the cold bath and was allowed to warm and stir overnight at rt. Large, clear, colorless crystals suitable for X-ray analysis were obtained in a few hours from hexanes at 3 °C. Yield 0.770 g (64 %). Mp 91–93 °C . Anal. Calcd. for C<sub>18</sub>H<sub>44</sub>ClN<sub>4</sub>PSiSn (529.79): C 40.81; H 8.37; N 10.58; found, C 40.51; H 7.99; N 10.71. <sup>1</sup>H NMR (500 MHz, C<sub>6</sub>D<sub>6</sub>): δ 0.74 (s, 6H, SiMe), 0.93 (t, 12H, NCH<sub>2</sub>CH<sub>3</sub>, <sup>3</sup>J<sub>HH</sub> = 15), 1.26 (s, 9H, PN<sup>t</sup>Bu), 1.53 (s, 9H, SnN<sup>t</sup>Bu), 2.83 (m, 8H, NCH<sub>2</sub>). <sup>13</sup>C{<sup>1</sup>H} (125.8 MHz, C<sub>6</sub>D<sub>6</sub>): δ 12.1 (SiMe), 13.9 (NCH<sub>2</sub>CH<sub>3</sub>), 33.3 (PNCCH<sub>3</sub>), 37.4 (SnNCCH<sub>3</sub>, <sup>3</sup>J<sub>SnC</sub> = 52), 39.0 (NCH<sub>2</sub>), 55.2 (d, PNCCH<sub>3</sub>, <sup>2</sup>J<sub>PC</sub> = 14), 56.6 (d, SnNCCH<sub>3</sub>, <sup>3</sup>J<sub>PC</sub> = 11). <sup>31</sup>P{<sup>1</sup>H} NMR (202 MHz, C<sub>6</sub>D<sub>6</sub>): δ 96.1 (<sup>1</sup>J<sub>119,117SnP</sub> = 2057, 1966).

*[Me<sub>2</sub>Si(μ-N<sup>t</sup>Bu)<sub>2</sub>P(NEt<sub>2</sub>)]SnCl<sub>2</sub>* **65**:

In a 25 mL two-neck flask, Me<sub>2</sub>Si(μ-N<sup>t</sup>Bu)<sub>2</sub>Sn (150 mg, 0.470 mmol) was stirred at –78 °C in hexanes (5 mL). Et<sub>2</sub>NPCL<sub>2</sub> (0.94 mL, 0.47 mmol) was added over 15 minutes. After several minutes the flask was removed from the cold bath. As the solution warmed a white precipitate slowly formed in the yellow solution. The solution was filtered and crystals suitable for X-ray analysis were grown from the hexanes reaction solution. Yield 95 mg (41 %). Mp 161 °C (dec). Anal. Calcd. for C<sub>14</sub>H<sub>34</sub>Cl<sub>2</sub>N<sub>3</sub>PSiSn

(493.12): C 34.10; H 6.95; N 8.52; found, C 34.28; H 7.09; N 8.79.  $^1\text{H}$  NMR (500 MHz,  $\text{C}_6\text{D}_6$ ):  $\delta$  0.32 (d, 6H, SiMe,  $J_{\text{PH}} = 215$ ), 0.91 (dt, 6H,  $\text{NCH}_2\text{CH}_3$ ,  $^3J_{\text{PH}} = 60$ ,  $^3J_{\text{HH}} = 9$ ), 1.18 (s,  $\text{N}^t\text{Bu}$ ), 2.97 (dq, 4H,  $\text{NCH}_2\text{CH}_3$ ,  $^2J_{\text{PH}} = 165$ ,  $^3J_{\text{HH}} = 9$ ).  $^{31}\text{P}\{^1\text{H}\}$  NMR (202 MHz,  $\text{C}_6\text{D}_6$ ):  $\delta$  105.0.

*[(Me<sub>2</sub>Si)( $\mu$ -N<sup>t</sup>Bu)<sub>2</sub>Ge(Cl)]<sub>2</sub>PNEt<sub>2</sub> 66:*

In a 25 mL two-neck flask,  $\text{Me}_2\text{Si}(\mu\text{-N}^t\text{Bu})_2\text{Ge}$  (0.622 g, 2.28 mmol) was stirred in 1 mL of hexanes at 0 °C.  $\text{Et}_2\text{NPCI}_2$  (0.166 mL, 1.14 mmol) was added dropwise by syringe over ~1 min. Approximately 2 mL of hexanes were added to dissolve the small amount of precipitate which appeared. X-ray quality crystals were obtained from hexanes at rt with a yield of 0.367 g (72 %). Mp 106–107 °C. Anal. calcd. for  $\text{C}_{24}\text{H}_{58}\text{Cl}_2\text{Ge}_2\text{N}_5\text{PSi}_2$  (720.08): C 40.03; H 8.12; N 9.73; found, C 40.24; H 7.89; N 9.54.  $^1\text{H}$  NMR (500 MHz,  $\text{C}_6\text{D}_6$ ):  $\delta$  0.41 (s, 3H, SiMe<sub>3</sub>),  $\delta$  0.48 (s, 3H, SiMe<sub>3</sub>),  $\delta$  1.12 (t, 6H,  $\text{NCH}_2\text{CH}_3$ ,  $^3J_{\text{HH}} = 14.4$ ),  $\delta$  1.41 (s, 36H,  $\text{N}^t\text{Bu}$ ),  $\delta$  3.28 (dq, 4H,  $\text{NCH}_2\text{CH}_3$ ,  $^3J_{\text{HH}} = 14.4$ ,  $^3J_{\text{PH}} = 2.3$ ).  $^{13}\text{C}\{^1\text{H}\}$  (125.8 MHz,  $\text{C}_6\text{D}_6$ ):  $\delta$  6.03 (s, SiMe<sub>3</sub>),  $\delta$  7.32 (s, SiMe<sub>3</sub>),  $\delta$  15.2 (d,  $\text{NCH}_2\text{CH}_3$ ,  $^3J_{\text{PC}} = 5.0$ ),  $\delta$  35.1 (s,  $\text{NC}(\text{CH}_3)_3$ ),  $\delta$  57.6 (d,  $\text{NCH}_2\text{CH}_3$ ,  $^2J_{\text{PC}} = 10.1$ ),  $\delta$  53.0 (s,  $\text{NC}(\text{CH}_3)_3$ ).  $^{31}\text{P}\{^1\text{H}\}$  NMR (202.5 MHz,  $\text{C}_6\text{D}_6$ ):  $\delta$  66.3.

*(C<sub>4</sub>H<sub>4</sub>N)<sub>2</sub>PCl 70:*

In a 250 mL three-neck flask,  $\text{PCl}_3$  (3.02 mL, 34.7 mmol) was stirred in THF (60 mL) at –78 °C. Triethylamine (11.5 mL, 82.5 mmol) was dissolved in THF (10 mL) and slowly added dropwise by addition funnel to the reaction mixture. After completion, the addition funnel was charged with pyrrole (2.00 mL, 34.7 mmol) in THF (25 mL). This pyrrole solution was added very slowly over 70 minutes. After 30 min. of stirring, a

second, identical pyrrole solution was added to the addition funnel and its addition was completed after 45 min. After 30 min. the flask was removed from the cold bath and allowed to warm to rt. After additions and warming, a large amount of yellow precipitate was present. Solution was filtered and distilled. The first fraction distilled at 68 °C (1 mbar) and was discarded. The second fraction distilled at 69–71°C (1 mbar) and contained the product as a hazy, colorless oil. Yield 2.171 g (32 %).  $^{31}\text{P}\{^1\text{H}\}$  NMR (202.5 MHz,  $\text{C}_6\text{D}_6$ ):  $\delta$  102.2.

*[(Me<sub>3</sub>Si)<sub>2</sub>N]<sub>2</sub>Ge(Cl)PEt<sub>2</sub> 76:*

In a 50 mL two-neck flask, [(Me<sub>3</sub>Si)<sub>2</sub>N]<sub>2</sub>Ge (389 mg, 0.989 mmol) was stirred at 0 °C in hexanes (10 mL). Et<sub>2</sub>PCL in a 1.0 M hexanes solution (0.99 mL, 0.99 mmol) was added over a few minutes. After 10 min., the flask was removed from the cold bath and the reaction mixture was stirred at rt for 7.5 h. All volatiles were removed *in vacuo* leaving a pale orange-yellow solid. This was redissolved in a minimal amount of hexanes. Crystals formed at rt after several days. Yield 221 mg (43 %). Mp 102–105 °C.  $^1\text{H}$  NMR (500 MHz,  $\text{C}_6\text{D}_6$ ):  $\delta$  0.50 (s, 36H, SiMe), 0.85 (t, 6H, PCH<sub>2</sub>CH<sub>3</sub>,  $^3J_{\text{HH}} = 14$ ), 2.563 (m, 4H, PCH<sub>2</sub>).  $^{31}\text{P}\{^1\text{H}\}$  NMR (202.5 MHz,  $\text{C}_6\text{D}_6$ ):  $\delta$  20.4.

*(2,6-Me<sub>2</sub>C<sub>6</sub>H<sub>3</sub>)PCL<sub>2</sub> 80:*

In a 250 mL three-neck fitted with an addition funnel, (Et<sub>2</sub>N)<sub>2</sub>PCL (1.31 mL, 9.00 mmol) was stirred in hexanes (24 mL) at 0 °C. A 1.0 M THF solution of 2,6-Me<sub>2</sub>C<sub>6</sub>H<sub>3</sub>MgBr (18.0 mL, 18.0 mmol) was added over 1 h. After 40 min., the flask was removed from the bath and allowed to warm to rt. Volatiles were removed *in vacuo*. The solid residue was redissolved in hexanes and filtered. Dry HCl<sub>(g)</sub> was bubbled through

this solution over ~90 min. Solution was filtered to remove the ammonium salt by-product and crystals were grown at rt. Yield 1.98 g (80 %).  $^{31}\text{P}\{^1\text{H}\}$  NMR (202.5 MHz,  $\text{C}_6\text{D}_6$ ):  $\delta$  151.8.

*(2,6-Me<sub>2</sub>C<sub>6</sub>H<sub>3</sub>)<sub>2</sub>PCl* **86**:

In a 250 mL three-neck fitted with an addition funnel,  $\text{Et}_2\text{NPCl}_2$  (1.31 mL, 9.00 mmol) was stirred in hexanes (24 mL) at 0 °C. A 1.0 M THF solution of 2,6-Me<sub>2</sub>C<sub>6</sub>H<sub>3</sub>MgBr (18.0 mL, 18.0 mmol) was added over 1 h. After 40 min., the flask was removed from the bath and allowed to warm to rt. Volatiles were removed *in vacuo*. The solid residue was redissolved in hexanes and filtered. Dry  $\text{HCl}_{(\text{g})}$  was bubbled through this solution over ~30 minutes. The solution was filtered to remove ammonium salt by-product and crystals were grown from at rt. Yield 1.98 g (80 %). Mp 57–59 °C.  $^1\text{H}$  NMR (500 MHz,  $\text{C}_6\text{D}_6$ ):  $\delta$  2.35 (s, 12H, *o*-MePh), 6.86 (m, 4H, *m*-Ph), 7.04 (t, 2H, *p*-Ph,  $^3J_{\text{HH}} = 15$ ).  $^{31}\text{P}\{^1\text{H}\}$  NMR (202.5 MHz,  $\text{C}_6\text{D}_6$ ):  $\delta$  82.2.

*Me<sub>2</sub>Si( $\mu$ -N<sup>t</sup>Bu)<sub>2</sub>Sn(Cl)P(2,6-Me<sub>2</sub>C<sub>6</sub>H<sub>3</sub>)<sub>2</sub>* **87**:

In a 50 mL two-neck flask,  $(2,6\text{-Me}_2\text{C}_6\text{H}_3)_2\text{PCl}$  (130 mg, 0.469 mmol) was stirred in benzene (5 mL) at 0 °C. A 1.0 M solution of  $\text{Me}_2\text{Si}(\mu\text{-N}^t\text{Bu})_2\text{Sn}$  (0.47 mL, 0.47 mmol) was added dropwise over 5 min. After 30 min, the reaction mixture was warmed to rt and all volatiles were removed *in vacuo*. The residue was redissolved in a minimal amount of toluene. Orange, chunk crystals were grown at 3 °C from toluene. Yield 249 mg (89 %).  $^1\text{H}$  NMR (500 MHz,  $\text{C}_6\text{D}_6$ ):  $\delta$  0.29 (s, 3H, SiMe), 0.50 (s, 3H, SiMe), 1.27 (s, 18H, N<sup>t</sup>Bu), 2.44 (s, 12H, *o*-MePh), 6.84 (m, 4H, *m*-Ph), 6.94 (t, 2H, *p*-Ph,  $^3J_{\text{HH}} = 15$ ).  $^{31}\text{P}\{^1\text{H}\}$  NMR (202.5 MHz,  $\text{C}_6\text{D}_6$ ):  $\delta$  -26.6 ( $^1J_{119/117\text{SnP}} = 1803/1725$ ).

### III.3. X-ray Crystallography

Suitable single crystals of were coated with Paratone N oil or Fomblin Y, affixed to Mitegen or Litholoop crystal holders and centered on the diffractometer in a stream of cold nitrogen. Reflection intensities were collected with a Bruker Apex diffractometer, equipped with an Oxford Cryosystems 700 Series Cryostream cooler, operating at 173 K. Data were measured with  $\omega$  scans of  $0.3^\circ$  per frame for 20 s until complete hemispheres of data had been collected. Cell parameters were retrieved using SMART software and reduced with *SAINt-plus*,<sup>146</sup> which corrects for Lorentz and polarization effects and crystal decay. Empirical absorption corrections were applied with *SADABS*.<sup>147</sup> The structures were solved by direct methods and refined by full-matrix least-squares methods on  $F^2$  with *SHELXL-97* incorporated into *SHELXTL*, version 6.14.<sup>148</sup>



## REFERENCES

1. Al-Ktaifani, M. M.; Hitchcock, P. B.; Lappert, M. F.; Nixon, J. F. Uiterweerd, P. *Dalton Trans.* **2008**, 2825–2831.
2. Poremba, P.; Brüser, W.; Edelmann, F. T. *J. Fluorine Chem.* **1997**, *82*, 43–46.
3. Veith, M.; Stahl, L.; Huch, V. *Organometallics* **1993**, *12*, 1914–1920.
4. Gynane, M. J. S.; Lappert, M. F.; Miles, S. J.; Power, P. P. *J. Chem. Soc., Chem. Comm.* **1976**, 256–257.
5. Gynane, M. J. S.; Lappert, M. F.; Miles, S. J.; Carty, A. J.; Taylor, N. J. *J. Chem. Soc., Dalton Trans.* **1977**, 2009–2015.
6. Lappert, M. F.; Misra, M. C.; Onyszchuk, M.; Rowe, R. S.; Power, P. P.; Slade, M. J. *J. Organomet. Chem.* **1987**, *330*, 31–46.
7. Braunschweig, H.; Chorley, R. W.; Hitchcock, P. B.; Lappert, M. F. *J. Chem. Soc., Chem. Commun.* **1992**, 1311–1313.
8. Schmidpeter, A.; Schrödel, H.-P.; Knizek, J. *Heteroatom Chem.* **1998**, *9*, 103–108.
9. Jana, A.; Objartel, I.; Roesky, H. W.; Stalke, D. *Inorg. Chem.* **2009**, *48*, 798–800.
10. Jana, A.; Schulzke, C.; Roesky, H. W. *J. Am. Chem. Soc.* **2009**, *131*, 4600–4601.
11. Peng, Y.; Ellis, B. D.; Wang, X.; Power, P. P. *J. Am. Chem. Soc.* **2008**, *130*, 12268–12269.
12. Kuchen, W.; Buchwald, H. *Angew. Chem.* **1957**, *69*, 307–308.
13. Pass, F.; Schindlbauer, H. I. *Mitt. Monatsh. Chem.* **1959**, *90*, 148–156.

14. Horner, L.; Beck, P.; Hoffmann, H. *Chem. Ber.* **1959**, *92*, 2088–2094.
15. Bloomfield, P. R.; Parvin, K. *Chem. Ind.* **1959**, 541–5422.
16. Henderson, W. A.; Epstein, M.; Seichter, F. S. *J. Am. Chem. Soc.* **1963**, *85*, 2462–2466.
17. Issleib, K.; Fluck, E. *Angew. Chem. Int. Ed., Engl.* **1966**, *5*, 587–588.
18. Hoffman, P. R.; Caulton, K. G. *J. Am. Chem. Soc.* **1975**, *97*, 6370–6374.
19. Baudler, M.; Koch, D. *Z. Anorg. Allg. Chem.* **1976**, *425*, 227–285.
20. Baudler, M.; Koch, D.; Tolls, E.; Diedrich, K. M.; Kloth, B. *Z. Anorg. Allg. Chem.* **1976**, *420*, 146–154.
21. Yoshifuji, M.; Shima, I.; Inamoto, N. *J. Am. Chem. Soc.* **1981**, *103*, 4587–4589.
22. Hinke, A.; Kuchen, W. *Chem. Ber.* **1983**, *116*, 3003–3010.
23. Veith, M.; Huch, V.; Majoral, J.-P.; Bertrand, G.; Manuel, G. *Tetrahedron Lett.* **1983**, *24*, 4219–4222.
24. Cowley, A.; Kilduff, J. E.; Lasch, J. G.; Mehrotra, S. K.; Norman, N. C.; Pakulski, M.; Whittlesey, B. R.; Atwood, J. L.; Hunter, W. E. *Inorg. Chem.* **1984**, *23*, 2582–2593.
25. Couret, C.; Escudie, J.; Satge, J. *Tetrahedron Lett.* **1982**, *23*, 4941–4942.
26. Flynn, K. M.; Olmstead, M. M.; Power, P. P. *J. Am. Chem. Soc.* **1983**, *105*, 2085–2086.
27. Flynn, K. M.; Murray, B. D.; Olmstead, M. M.; Power, P. P. *J. Am. Chem. Soc.* **1983**, *105*, 7460–7461.
28. Flynn, K. M.; Hope, H.; Murray, B. D.; Olmstead, M. M.; Power, P. P. *J. Am. Chem. Soc.* **1983**, *105*, 7750–7751.

29. Bartlett, R. A.; Rasika Dias, H. V.; Flynn, K. M.; Hope, H.; Murray, B. D.; Olmstead, M. M.; Power, P. P. *J. Am. Chem. Soc.* **1987**, *109*, 5693–5698.
30. Bartlett, R. A.; Rasika Dias, H. V.; Flynn, K. M.; Olmstead, M. M.; Power, P. P. *J. Am. Chem. Soc.* **1987**, *109*, 5699–5703.
31. Borm, J.; Huttner, G.; Zsolnai, L.; Evertz, K.; Berke, H. *J. Organomet. Chem.* **1987**, *327*, 223–235.
32. Bock, H.; Bankmann, M. *J. Chem. Soc., Chem. Commun.* **1989**, 1130–1132.
33. Aitken, R. A.; Masamba, W.; Wilson, N. J. *Tetrahedron Lett.* **1997**, *38*, 8417–8420.
34. Twamley, B.; Sofield, C. D.; Olmstead, M. M.; Power, P. P. *J. Am. Chem. Soc.* **1999**, *121*, 3357–3367.
35. Urnézius, E.; Protasiewicz, J. D. *Main Group Chem.* **1996**, *1*, 369–372.
36. Smith, R. C.; Shah, S.; Protasiewicz, J. D. *J. Organomet. Chem.* **2002**, *646*, 255–261.
37. Kawashima, M. *Nip. Kag. Kaishi* **1999**, 359–361.
38. Schisler, A.; Lönnecke, P.; Huniar, U.; Ahlrichs, R.; Hey-Hawkins, E. *Angew. Chem. Int. Ed.* **2001**, *40*, 4217–4219.
39. Geier, J.; Rügger, H.; Wörle, M.; Grützmacher, H. *Angew. Chem. Int. Ed.* **2003**, *42*, 3951–3954.
40. Wolf, R.; Schisler, A.; Lönnecke, P.; Jones, C.; Hey-Hawkins, E. *Eur. J. Inorg. Chem.* **2004**, 3277–3286.
41. Wolf, R.; Hey-Hawkins, E. *Z. Anorg. Allg. Chem.* **2006**, *632*, 727–734.

42. Stein, D.; Dransfeld, A.; Flock, M.; Rügger, H.; Grützmacher, H. *Eur. J. Inorg. Chem.* **2006**, 4157–4167.
43. Gómez-Ruiz, S.; Gallego, B.; Hey-Hawkins, E. *Dalton Trans.* **2009**, 2915–2920.
44. Herrero, R.; Gómez-Ruiz, S.; Dávalos, J. Z.; Hey-Hawkins, E. *Comptes Rend. Chim.* **2010**, *13*, 1185–1190.
45. Schaffrath, M.; Villinger, A.; Michalik, D.; Rosenthal, U.; Schulz, A. *Organometallics* **2008**, *27*, 1393–1398.
46. Bos, K. D.; Bulten, E. J.; Noltes, J. G. *J. Organomet. Chem.* **1974**, *67*, C13–C15.
47. Denk, M.; Lennon, R.; Hayashi, R.; West, R.; Belyakova, A. V.; Verne, H. P.; Haaland, A.; Wagner, M.; Metzler, N. *J. Am. Chem. Soc.* **1994**, *116*, 2691–2692.
48. Gehrhus, B.; Lappert, M. F.; Heinicke, J.; Boese, R.; Bläser, D. *J. Chem. Soc., Chem. Commun.* **1995**, 1931–1932.
49. Gehrhus, B.; Hitchcock, P. B.; Lappert, M. F.; Heinicke, J.; Boese, R.; Bläser, D. *J. Organomet. Chem.* **1996**, *521*, 211–220.
50. Moser, D. F.; Bosse, T.; Olson, J.; Moser, J. L.; Guzei, I. A.; West, R. *J. Am. Chem. Soc.* **2002**, *124*, 4186–4187.
51. Su, M.-D. *J. Am. Chem. Soc.* **2003**, *125*, 1714–1715.
52. Delawar, M.; Gehrhus, B.; Hitchcock, P. B. *Dalton Trans.* **2005**, 2945–2953.
53. Hill, N. J.; West, R. *J. Organomet. Chem.* **2004**, *689*, 4165–4183.
54. Miller, K. A.; Bartolin, J. W.; O'Neill, R. M.; Sweeder, R. D.; Owens, T. M.; Kampf, J. W.; Banaszak Holl, M. M.; Wells, N. J. *J. Am. Chem. Soc.* **2003**, *125*, 8986–8987.

55. Fouquet, E.; Pereyre, M.; Rodriguez, A. L.; Roulet, T. *Bull. Chem. Soc. Fr.* **1997**, *134*, 959–967.
56. Bartolin, J. M.; Kavara, A.; Kampf, J.; Banaszak Holl, M. M. *Organometallics* **2006**, *25*, 4738–4740.
57. Kavara, A.; Cousineau, K. D.; Rohr, A. D.; Kampf, J. W.; Banaszak Holl, M. M. *Organometallics* **2008**, *27*, 1041–1043.
58. Dickie, D. A.; Lee, P. T. K.; Labeodan, O. A.; Schatte, G.; Weinberg, N.; Lewis, A. R.; Bernard, G. M.; Wasylshen, R. E.; Clyburne, J. A. C. *Dalton Trans.* **2007**, 2862–2869.
59. Wetherby Jr., A. E.; Samanamu, C. R.; Schrick, A. C.; DiPasquale, A.; Golen, J. A.; Rheingold, A. L.; Weinert, C. S. *Inorg. Chim. Acta* **2010**, *364*, 89–95.
60. Wills, C.; Izod, K.; Clegg, W.; Harrington, R. W. *Dalton Trans.* **2010**, *39*, 2379–2384.
61. Sen, S. S.; Hey, J.; Kratzert, D.; Roesky, H. W.; Stalke, D. *Organometallics* **2012**, *31*, 435–439.
62. Drost, C.; Hitchcock, P. B.; Lappert, M. F. *Organometallics* **2002**, *21*, 2095–2100.
63. Ishida, S.; Iwamoto, T.; Kabuto, C.; Kira, M. *Silicon Chem.* **2003**, *2*, 137–140.
64. du Mont, W.-W.; Schumann, H. *Angew. Chem.* **1975**, *87*, 354–355.
65. du Mont, W.-W.; Schumann, H. *J. Organomet. Chem.* **1975**, *84*, C45–C47.
66. du Mont, W.-W.; Neudert, B.; Schumann, H. *Angew. Chem.* **1976**, *88*, 304–305.
67. Schumann, H.; du Mont, W.-W.; Kroth, H.-J. *Chem. Ber.* **1976**, *109*, 237–245.
68. Schumann, H.; du Mont, W.-W.; Wöbke, B. *Chem. Ber.* **1976**, *109*, 1017–1022.

69. du Mont, W.-W.; Kroth, H.-J.; Schumann, H. *Chem. Ber.* **1976**, *109*, 3017–3024.
70. du Mont, W.-W.; Neudert, B. *Z. Anorg. Allg. Chem.* **1977**, *436*, 270–276.
71. du Mont, W.-W.; Neudert, B. *Chem. Ber.* **1978**, *111*, 2267–2272.
72. Karnop, M.; du Mont, W.-W.; Jones, P. G.; Jeske, J. *Chem. Ber./Recueil* **1997**, *130*, 1611–1618.
73. du Mont, W.-W.; Karnop, M.; Mahnke, J.; Martens, R.; Druckenbrodt, C.; Jeske, J.; Jones, P. G. *Chem. Ber./Recueil* **1997**, *130*, 1619–1623.
74. Zanin, A.; Karnop, M.; Jeske, J.; Jones, P. G.; du Mont, W.-W. *J. Organomet. Chem.* **1994**, *475*, 95–98.
75. Veith, M.; Grosser, M.; Huch, V. *Z. Anorg. Allg. Chem.* **1984**, *513*, 89–102.
76. Veith, M.; Gouygou, M.; Detemple, A. *Phosphorus, Sulfur Silicon Relat. Elem.* **1993**, *75*, 183–186.
77. Fauré, J.-L.; Gornitzka, H.; Réau, R.; Stalke, D.; Bertrand G. *Eur. J. Inorg. Chem.* **1999**, 2295–2299.
78. Carmalt, C. J.; Lomeli, V.; McBurnett, B. G.; Cowley, A. H. *Chem. Commun.* **1997**, 2095–2096.
79. Reeske, G.; Hoberg, C. R.; Hill, N. J.; Cowley, A. H. A case of intramolecular charge transfer. *J. Am. Chem. Soc.* **2006**, *128*, 2800–2801.
80. Dube, J. W.; Farrar, G. J.; Norton, E. L.; Szelesky, K. L. S.; Cooper, B. F. T.; Macdonald, C. L. B. *Organometallics* **2009**, *28*, 4377–4384.
81. Fleming, S.; Lupton, M. K.; Jekot, K. *Inorg. Chem.* **1972**, *11*, 2534–2540.
82. Maryanoff, B. E.; Hutchins, R. O. *J. Org. Chem.* **1972**, *37*, 3475–3480.
83. Kopp, R. W.; Bond, A. C.; Parry, R. W. *Inorg. Chem.* **1976**, *15*, 3042–3046.

84. Schultz, C. W.; Parry, R. W. *Inorg. Chem.* **1976**, *15*, 3046–3050.
85. Schmidpeter, A.; Lochschmidt, S.; Sheldrick, W. S. *Angew. Chem. Int. Ed., Engl.* **1982**, *21*, 63–64.
86. Schmidpeter, A.; Lochschmidt, S.; Burget, G.; Sheldrick, W. S. *Phosphorus, Sulfur Relat. Elem.* **1983**, *18*, 23–26.
87. Cowley, A.; Kemp, R. A. *Chem. Rev.* **1985**, *85*, 367–382.
88. Kaukoat, T.; Neda, I.; Schmutzler, R. *Coord. Chem. Rev.* **1994**, *137*, 53–107.
89. Burford, N.; Losier, P.; Bakshi, P. K.; Cameron, T. S. *Chem. Commun.* **1996**, 307–308.
90. Burford, P.; Ragona, P. J. *J. Chem. Soc., Dalton Trans.* **2002**, 4307–4315.
91. Spinney, H. A.; Yap, G. A. P.; Korobkov, I.; DiLabio, G.; Richeson, D. S. *Organometallics* **2006**, *25*, 3541–3543.
92. Reeske, G.; Cowley, A. H. *Inorg. Chem.* **2007**, *46*, 1426–1430.
93. Dillon, K. B.; Goeta, A. E.; Howard, J. A. K.; Monks, P. K.; Shepherd, H. J.; Thompson, A. L. *Dalton Trans.* **2008**, 1144–1149.
94. Weigand, J. J.; Burford, N.; Decken, A. *Eur. J. Inorg. Chem.* **2008**, 4343–4347.
95. Arduengo III, A. J.; Calabrese, J. C.; Cowley, A. H.; Rasika Dias, H. V.; Goerlich, J. R.; Marshall, W. J.; Riegel, B. *Inorg. Chem.* **1997**, *36*, 2151–2158.
96. Arduengo III, A. J.; Carmalt, C. J.; Clyburne, J. A. C.; Cowley, A. H.; Pyati, R. *Chem. Commun.* **1997**, 981–982.
97. Kuhn, N.; Fahl, J.; Bläser, D.; Boese, R. *Z. Anorg. Allg. Chem.* **1999**, *625*, 729–734.

98. Ellis, B. D.; Dyker, C. A.; Decken, A.; Macdonald, C. L. B. *Chem. Commun.* **2005**, 1965–1967.
99. Weigand, J.; Feldmann, K.-O.; Henne, F. D. *J. Am. Chem. Soc.* **2010**, *132*, 16321–16323.
100. Abdellah, I.; Lepetit, C.; Canac, Y.; Duhayon, C.; Chauvin, R. *Chem. Eur. J.* **2010**, *16*, 13095–13108.
101. Wang, Y.; Robinson, G. H. *Inorg. Chem.* **2011**, *50*, 12327–12337.
102. Canac, Y.; Maaliki, C.; Abdellah, I.; Chauvin, R. *New J. Chem.* **2012**, *36*, 17–27.
103. Petuskova, J.; Patil, M.; Holle, S.; Lehmann, C. W.; Thiel, W.; Alcarazo, M. *J. Am. Chem. Soc.* **2011**, *135*, 20758–20760.
104. Schmidpeter, A.; Günther, B. *Phosphorus, Sulfur Relat. Elem.* **1985**, *22*, 323–325.
105. Pauling, L. *The Nature of the Chemical Bond*, 3<sup>rd</sup> ed.; Cornell University Press: Ithaca, NY, 1960.
106. Schranz, I.; Lief, G. R.; Midstokke, S. J.; Stahl, L. *Inorg. Chem.* **2002**, *41*, 6919–6927.
107. Humbel, S.; Bertrand, C.; Darcel, C.; Baudin, C.; Jugé, S. *Inorg. Chem.* **2003**, *42*, 420–427.
108. Meijboom, R.; Muller, A.; Roodt, A. *Acta Crystallogr., Sect. E* **2006**, *62*, m1603–m1605.
109. Ferguson, G.; McCrindle, R.; McAlees, A. J.; Parvez, M. *Acta Crystallogr., Sect. B* **1982**, *38*, 2679–2681.



110. Vuoto, S.; Autio, J.; Laitila, M.; Haukka, M.; Pursianen, J. *Eur. J. Inorg. Chem.* **2008**, 397–407.
111. DeMeglio, C. M.; Ahmed, K. J.; Luck, L. A.; Weltin, E. E.; Rheingold, A. L.; Bushweller, C. H. *J. Phys. Chem.* **1992**, *96*, 8765–8777.
112. Grushin, V. V.; Bensimon, C.; Alper, H. *Inorg. Chem.* **1994**, *33*, 4804–4806.
113. Wisniewska, A.; Baranowska, K.; Pikies, J. *Acta Crystallogr., Sect. E* **2008**, *64*, m967.
114. Guzman-Jimenez, I. Y.; Whitmire, K. A. *Acta Crystallogr., Sect. C* **1999**, *55*, IUC9900028.
115. Veith, M.; Müller, A.; Stahl, L.; Nötzel, M.; Jarczyk, M.; Huch, V. *Inorg. Chem.* **1996**, *35*, 3848–3855.
116. Turco, A.; Giacometti, G. *Ricerca sci.* **1960**, *30*, 1051–1055.
117. Woisetschlager, O. E.; Beck, W.; Polborn, K. *Private Communication* **2005**.
118. Wang, L-S. *Phosphorus, Sulfur Silicon Relat. Elem.* **2007**, *182*, 227–236.
119. Nimistsiriwat, N.; Marshall, E. L.; Gibson, V. C.; Elsegood, M. R. J.; Dale, S. H. *J. Am. Chem. Soc.* **2004**, *126*, 13598–13599.
120. Schranz, I.; Lief, G. R.; Midstokke, S. J.; Stahl, L. *Inorg. Chem.* **2002**, *41*, 6919–6927.
121. Nieger, M.; Niecke, E.; Detsch, R. *Private Communication* **2002**.
122. Eichorn, B.; Noth, H. *Z. Naturforsch. B* **2000**, *55b*, 352–360.
123. Gau, D.; Kato, T.; Saffon-Merceron, N.; De Cozar, A.; Cossio, F. P.; Baceiredo, A. *Angew. Chem. Int. Ed.* **2010**, *49*, 6585–6588.
124. Moloy, K. G.; Petersen, J. L. *J. Am. Chem. Soc.* **1995**, *117*, 7696–7710.

125. Chen, J.-Y.; Su, M.-D. *Dalton Trans.* **2011**, *40*, 7898–7907.
126. Kyba, E. P. *J. Am. Chem. Soc.* **1976**, *98*, 4805–4809.
127. van Leeuwen, P. W. N. M. *Homogenous Catalysis*. Kluwer Academic Publishers. Dordrecht, The Netherlands. **2004**, 52–54.
128. Arp, H.; Baumgartner, J.; Marschner, C.; Müller, T. *J. Am. Chem. Soc.* **2011**, *133*, 5632–5635.
129. Lein, M.; Szabó, A.; Kovács, A.; Frenking, G. *Faraday Discuss.* **2003**, *24*, 365–378.
130. Hahn, F. E.; Zabula, A. V.; Pape, T.; Hepp, A.; Tonner, R.; Haunschild, R.; Frenking G. *Chem. Eur. J.* **2008**, *14*, 10716–10721.
131. Portnyagin, I. A.; Nechaev, M. S. *J. Organomet. Chem.* **2009**, *694*, 3149–3153.
132. Schoeller, W. W.; Schneider, R. *Chem. Ber./Recueil* **1997**, *130*, 1013–1020.
133. No firm data comparing Sn–P and Ge–P nor Sn–N and Ge–N bond enthalpies/bond dissociation energies could be found in the literature. However, there is a consistent periodic trend that for a given E–A bond (E = Ge, Sn; A = any other atom), the Ge–A bond will be stronger than the Sn–A bond. Data to this effect can be found in: Sanderson, R. T. *Chemical Bonds and Bond Energy* 2<sup>nd</sup> ed.; University Press: New York, NY, 1976.
134. Dumitrescu, A.; Rudzevich, V. L.; Romanenko, V. D.; Mari, A.; Scheller, W. W.; Bourissou, D.; Bertrand, G. *Inorg. Chem.* **2004**, *43*, 6546–6548.
135. Ndiaye, B.; Bhat, S.; Jouaiti, A.; Berclaz, T.; Bernardinelli, G.; Geoffroy, M. J. *Phys. Chem. A* **2006**, *110*, 9736–9742.

136. Back, O.; Celik, M. A.; Frenking, G.; Melaimi, Donnadiou, B.; Bertrand, G. *J. Am. Chem. Soc.* **2010**, *132*, 10262–10263.
137. Ishida, S.; Hirakawa, F.; Iwamoto, T. *J. Am. Chem. Soc.* **2011**, *133*, 12968–12971.
138. Schweizer, S.; Becht, J-M.; Le Drian, C. *Org. Lett.* **2007**, *9*, 3777–3780.
139. Veith, M. *Angew. Chem.* **1975**, *87*, 287–288.
140. Veith, M. *Z. Naturforsch. B* **1978**, *33b*, 1–6.
141. Veith, M.; Grosser, M. *Z. Naturforsch. B* **1982**, *32b*, 1375–1381.
142. Gynane, M. J. S.; Harris, D. H.; Lappert, M. F.; Power, P. P. Rivière, P.; Rivière-Baudet, M. *Chem. Soc., Dalton Trans.* **1977**, 2004–2009.
143. Pudovik, M. A.; Mikhailov, Y. B.; Pudovik, A. N. *Zhurn. Obsch. Khim.* **1985**, *55*, 1475–1479.
144. Amigues, E. J.; Hardacre, C.; Keane, G.; Migaud, M. E. *Green Chem.* **2008**, *10*, 660–669.
145. Hartley, F. R. *Organomet. Chem. Rev. A* **1970**, *6*, 119–137.
146. *SAINt-plus*; Siemens Analytical X-ray Systems, Madison, WI, 1995.
147. SADABS program for absorption correction using the Bruker CCD Detector System. Based on: Blessing, R. H. *Acta Crystallogr., Sect. A* **1995**, *51*, 33–38.
148. Sheldrick, G. M. A short history of SHELX. *Acta Crystallogr., Sect. A* **2008**, *64*, 112–122.